Original Copy

NDOT Research Report

Report No: RDT-01-002

Shake Table Testing of Flared Bridge Columns with Steel Jacket Retrofit

NEVADA
DEPARTMENT OF
TRANSPORTATION

April 11, 2001

TECHNICAL REPORT DOCUMENTATION PAGE

1. Report No. RDT-01-002	2. Government Accession No.	3. Recipient's Catalog No.
4. Title and Subtitle **Shake Table Testing of Flared Bridge Columns with Steel Jacket Retrofit**	5. Report Date **January 2000** 6. Performing Organization Code	
7. Author(s) **B. McElhaney, M. Saiidi, and S. Sanders**	8. Performing Organization Report No. **CCEER-00-3**	
9. Performing Organization Name and Address **Center for Civil Engineering Earthquake Research** **Department of Civil Engineering/258** **University of Nevada, Reno** **Reno, NV 89557**	10. Work Unit No. 11. Contract or Grant No.	
12. Sponsoring Agency Name and Address **Nevada Department of Transportation** **1263 S. Stewart** **Carson City, NV 89712**	13. Type or Report and Period Covered 14. Sponsoring Agency Code	
15. Supplementary Notes		

16. Abstract

A study incorporating experimental and analytical investigations was performed. The objective of the experimental research was to evaluate the seismic performance of reinforced concrete bridge columns with structural flares and a steel jacket retrofit design for these columns. The objectives of the analytical portion of the study were to: 1) explain the behavior of the column observed during testing; 2) evaluate the validity of the analytical methods by comparing the calculated results to the measured data; and 3) assess the effect of the steel jacket retrofit by comparing experimental data from as-built and retrofitted test specimens.

The prototype column was from a viaduct located on US 395 in Reno, Nevada. It was designed in 1979 in accordance with the 1977 AASHTO Standard Specifications and the 1978 Interim Specifications. Two thirty-percent scale models were constructed and dynamically tested on one of the shake tables at the University of Nevada, Reno. One specimen represented the as-built details and one was outfitted with a steel jacket incorporating an intermediate gap. The two columns were subjected to the Sylmar record of the January 17, 1994 Northridge earthquake. The testing program consisted of multiple motions with gradually increasing intensity of shaking. Testing was performed in the strong direction under nominally constant axial load.

The analysis included: estimating lateral load-deflection relationships, calculating displacement histories and hysteretic responses, and performing a shear analysis using various methods of calculating shear capacity. Also, tie bar strains and other aspects of column behavior observed in the as-built and retrofitted specimens during testing were compared and discussed.

17. Key Words earthquakes, column flare, reinforced concrete, retrofit, steel jacket		18. Distribution Statement **Unrestricted. This document is available through the National Technical Information Service, Springfield, VA 21161**	
19. Security Classif. (of this report) Unclassified	20. Security Classif. (of this page) Unclassified	21. No. Of Pages **178**	22. Price

ACKNOWLEDGMENTS

The study presented in this report was funded by the Nevada Department of Transportation (NDOT) under Agreement P497-94-803. However, the opinions and comments expressed in the report are those of the authors and do not necessarily reflect the views of NDOT. The support and comments of Mr. Bill Crawford, Chief Bridge Engineer at NDOT and other Bridge Division staff members are appreciated. The authors are also thankful to Mr. Mike Mayberry and Ms. Catherine French, undergraduate research assistants at the University of Nevada, Reno, for their dedicated work in the course of this project.

Abstract

A study incorporating experimental and analytical investigations was performed. The objective of the experimental research was to evaluate the seismic performance of reinforced concrete bridge columns with structural flares and a steel jacket retrofit design for these columns. The objectives of the analytical portion of the study were to: 1) explain the behavior of the column observed during testing, 2) evaluate the validity of the analytical methods by comparing the calculated results to the measured data, and 3) assess the effect of the steel jacket retrofit by comparing experimental data from as-built and retrofitted test specimens.

The prototype column was from a viaduct located on U.S. 395 in Reno, Nevada. It was designed in 1979 in accordance with the 1977 AASHTO Standard Specifications and the 1978 Interim Specifications. Two thirty-percent scale models were constructed and dynamically tested on one of the shake tables at the University of Nevada, Reno. One specimen represented the as-built details and one was outfitted with a steel jacket incorporating an intermediate gap. The two columns were subjected to the Sylmar record of the January 17, 1994 Northridge earthquake. The testing program consisted of multiple motions with gradually increasing intensity of shaking. Testing was performed in the strong direction under nominally constant axial load.

The analysis included: estimating lateral load-deflection relationships, calculating displacement histories and hysteretic responses, and performing a shear analysis using various methods of calculating shear capacity. Also, tie bar strains and other aspects of column behavior observed in the as-built and retrofitted specimens during testing were compared and discussed.

TABLE OF CONTENTS

SECTION PAGE

CHAPTER 1: INTRODUCTION

CHAPTER 2: EXPERIMENTAL METHOD AND TEST SETUP

CHAPTER 3: EXPERIMENTAL RESULTS

CHAPTER 4: ANALYSIS OF TEST RESULTS

CHAPTER 5: SUMMARY AND CONCLUSIONS

LIST OF TABLES

LIST OF FIGURES

FIGURE PAGE

Chapter 1

Introduction

1.1 Background

One of the fundamental principles of contemporary seismic design philosophy is that structures should not collapse even in severe earthquakes. This requires that either the response of the structure remain entirely elastic or that inelastic deformations occur without an associated degradation of the ability to carry gravity loads. Since the dynamic forces associated with an elastic response may be considerably higher than the forces of an inelastic response, it is often uneconomical to design for the elastic response. Consequently, structures are generally not designed to remain elastic under severe loading conditions. Instead, structures are typically designed for an inelastic response to severe loads. To assure that the structure will maintain its strength under large inelastic deformations, a ductile mode of failure is necessary. This requires proper detailing of the member in which the plastic deformations will occur.

In bridges, the superstructure generally remains elastic under earthquake loads and inelastic deformations are accommodated through the formation of plastic hinges in the columns. This is because the superstructure design is controlled by gravity loads, and that the need to accommodate traffic lanes leads to large superstructure cross sections with high capacity. In reinforced concrete bridge columns, it is necessary to provide relatively large ductilities without shear failure or significant strength degradation. This is accomplished by providing adequate confinement through lateral reinforcement in areas of expected plastic hinging. When properly detailed, lateral confinement steel can provide high concrete strain capacity, prevent premature buckling of main reinforcement, and avert shear failure. When lateral reinforcement is insufficient, added confinement and shear strength may be provided by a jacket.

During the January 17, 1994 Northridge earthquake, several flared, reinforced concrete bridge columns supporting the Mission-Gothic undercrossing of SR-118 failed in a non-ductile shear mode. These columns had parabolic flares over the upper part of the column. The column main reinforcement was placed in a circular pattern inside a prismatic core and extended over the entire height of the column. The flares were moderately reinforced with longitudinal steel that terminated at the bottom of the flared segment and were considered to be non-structural (architectural). Studies[1,2] conducted after the Northridge earthquake concluded that the flare actually enhanced the flexural strength of the column in the flared region and consequently forced the plastic hinge to form outside of the flared segment. This caused a reduction in the column shear span and an associated increase in the shear demand. Additionally, the degradation of concrete under inelastic cyclic loading reduced the shear capacity in the plastic hinge region. This combination of factors resulted in a shear failure in the columns.

After the Northridge earthquake revealed seismic performance problems inherent in flared bridge columns, an assessment of the seismic vulnerability of bridge columns with structural flares in northern Nevada was undertaken[3]. Subsequently, analytical[4] and experimental[5,6] studies were performed. The experimental studies focused on verification and remediation of the seismic performance problems. As-built and retrofitted specimens were tested.

The experimental research program presented in this paper followed the two previous studies[5,6] on the as-built and retrofitted behavior of flared bridge columns. The previous program used slow, cyclic tests. The program described in this document consisted of analyzing and dynamically testing one as-built specimen and one steel-jacketed specimen.

1.2 Previous Studies

A review of previous research regarding the effects of confinement and flares on reinforced concrete columns was conducted in this study. There is an abundance of studies in the literature documenting confinement effects on the seismic behavior of reinforced concrete columns, in order to avoid duplication only a limited selection is presented for this study. A more extensive review can be found in Reference 5. There is a relatively limited amount of research work in general, and experimental investigation in particular, concerning the effects of flares on the seismic performance of reinforced concrete bridge columns. The available research data on flared columns are reviewed in this study in their entirety.

1.2.1 Confinement

There is an extensive amount of research on confinement and its effects on ductility. In this document a summary of two selected studies concerning the effect of confinement on ductility is presented. The first study pertained to the behavior of columns provided with moderate confinement in which four rectangular specimens were tested. The second study included six circular specimens and evaluated the behavior of circular reinforced concrete columns retrofitted with steel jackets.

Wehbe et al.[5] tested two groups of rectangular reinforced concrete bridge columns; each group contained two specimens. The purpose of the study was to determine the required amount of transverse reinforcement for areas of moderate seismicity where ductility demand may not be as high as in areas of high seismicity. The axial load and the amount of transverse reinforcement were varied among the specimens. The first group contained 46 percent of the transverse steel required by the American Association of State Highway and Transportation Officials (AASHTO). The second group contained 60 percent of that required by AASHTO. Within each group, the axial loads were varied, representing typical values found in bridge columns. For the first group, the axial loads were 0.10 f'_cA_g (where f'_c = measured concrete compressive strength and A_g = gross cross-sectional area of the section) and 0.24 f'_cA_g. For the second group the axial loads were 0.09 f'_cA_g and 0.23 f'_cA_g. It was found that the displacement ductilities of the first group of columns were 5.2 and 5.3 depending on the axial load. The displacement ductilities of the second group ranged from 6.1 to 6.7, also depending on the axial load. Equations were developed that related confining steel to ductility. The study concluded that for areas of moderate seismicity, where ductility demand is less, a more practical and economical design can be achieved by providing less confinement steel.

Chai et al.[7] tested six circular reinforced concrete bridge columns. The specimens were designed to incorporate deficiencies associated with columns built prior to the 1970's. One of the deficiencies addressed in the study was short lap splices. Two of the specimens were constructed as reference columns, and the remaining four represented different retrofit designs using steel jackets. Results from the test data indicated that for the retrofitted specimen with the inadequate lap splices, the jacket confined the concrete and was successful in allowing the lap-spliced bars to yield. Failure occurred for this specimen at a displacement ductility of 7, and was due to low-cycle fatigue in the main reinforcement.

1.2.2 Effects of Flares on Reinforced Concrete Bridge Columns

Prior to the Northridge earthquake of January 1994, research on flared reinforced concrete columns was practically non-existent. Failure of the flared columns supporting the Mission-Gothic undercrossing during the earthquake instigated the study of such columns in order to evaluate their seismic vulnerability and to find the cause of failure. Following the Northridge earthquake, preliminary analytical studies were done by the

National Institute of Standards and Technology[2] (NIST) and the University of California at San Diego[1] (UCSD) on the flared columns of the Mission-Gothic undercrossing. Both studies generally agreed in their findings regarding the cause of failure. They concluded that the flares did not spall as expected, thus increasing the flexural capacity of the column flared segment. The plastic hinge was forced to form at the bottom of the flares, causing a reduction in the shear span. The shear failure scenario was presented in section 1.1.

The first experimental research on the effects of flares was conducted by Sanchez et al.[8]. The test specimens represented 40 percent scale models of two types of prototype bridge columns with architectural flares. The first group consisted of four specimens representing the Mission-Gothic flared columns. The second group was comprised of six specimens representing a standard flared column type that is used in California. Both groups contained circular spirals of reinforcement with a minimal amount of longitudinal reinforcement placed along the flare. Within each group, one reference column representing the column core without the flares and at least one column representing the as-built condition were tested. The remaining specimens were retrofitted versions of the as-built columns. The experimental results from these tests confirmed the analytical prediction that architectural flares increase the flexural capacity of the column flared segment. It was concluded that an economical and effective retrofitting scheme for columns with architectural flares would be to separate the flare from the core at the bridge soffit. It was recommended that the flare steel and concrete be cut to provide a 50-mm vertical gap at the flare-soffit interface. The gap would extend through the flare to the column core and be filled with Styrofoam. The discontinuity between the flare and the soffit would eliminate the contribution of the flare to the flexural strength.

Wehbe et al.[4] analytically investigated the behavior of four bridges with flared columns in northern Nevada. The columns on these bridges had structural flares with the main reinforcement extending into the flare. There were two general types of reinforcement details incorporated in the columns of these bridges. The first detail contained circular transverse reinforcement along the core with additional main reinforcement extending into the flare. The second detail had the main reinforcement extending into the flare, with only rectilinear transverse reinforcement and no vertical steel in the core. The "limit state" method of analysis was used to determine the location of plastic hinges and the corresponding shear demands. It was found that the columns detailed with the inner core reinforcement had adequate shear capacity. The columns with only longitudinal reinforcement extending into the flare did not possess adequate shear capacity.

The results of the analytical study on flared bridge columns in northern Nevada prompted an experimental investigation into the as-built behavior of the columns that were found to have inadequate shear capacity. Two specimens representing the prototype as-built columns were tested. The experimental results verified that the shear capacity was inadequate. Although neither specimen failed in shear, the factor of safety for shear failure was determined to be inadequate. Thus, a retrofit was necessary.

Subsequently, a study by Caywood et al.[6] evaluated two potential retrofit designs for these columns using steel jackets. Two columns representing the prototype columns were retrofitted and tested. One retrofit design incorporated a space filled with polystyrene between the column and the jacket to reduce the passive confinement. The other design had a horizontal gap along the height of the jacket creating a discontinuity. Based on the experimental results the optimum design was the latter. Additionally, it was analytically determined that changing the location of the gap and thus controlling the plastic hinge location could increase the ductility.

1.3 Objective and Scope

The primary objective of this study was to evaluate: 1) the seismic vulnerability of reinforced concrete bridge columns with structural flares and 2) a steel jacket seismic retrofit design of these columns. An experimental study was conducted, in which two 30 percent scale specimens were dynamically tested on one of the University of Nevada, Reno shake tables. The prototype columns were from a viaduct located in Reno, Nevada. The first specimen represented the as-built condition while the second was an identical column retrofitted with a steel jacket. The as-built specimen established the seismic response of the prototype columns and acted as a control with which to compare the retrofitted specimen. Representative material properties and axial loads were used. The specimens were tested in the strong direction because the loading would lead to higher shear demand on the column. Some of the criteria used to judge the retrofit were shear capacity, ductility, and ease of construction.

In addition to the experimental portion of the study, analytical studies were performed to: 1) explain the behavior of the column observed during testing, 2) evaluate the validity of the analytical procedures, and 3) assess the effect of the steel jacket. The analysis included: estimating lateral load-deflection relationships, calculating displacement histories and hysteretic responses, and performing a shear analysis.

Chapter 2

Experimental Method and Test Setup

2.1 Introductory Remarks

The purpose of this experimental study was twofold. The primary purpose was to evaluate the seismic performance of as-built, flared bridge columns from bridge I-1250 located on U.S. 395 in Reno, Nevada and a steel jacket retrofit of these columns using a state-of-the-art shake table. The secondary purpose was to compare the results of these dynamic tests to previous cyclic, quasi-static tests on models of the same flared bridge columns[5,6].

The purpose of this chapter is to describe: (1) the selection of the test specimens, (2) the design and details of the test specimens, (3) the materials and construction, (4) instrumentation and data collection, and (5) the test setup and procedure.

2.2 Selection of Test Specimens

This study was the third in a series of four studies conducted at the University of Nevada, Reno on reinforced concrete bridge columns with structural flares[5,6]. The fourth study in the series is in progress. The studies are in response to a request by the Nevada Department of Transportation (NDOT). Because flared bridge columns have been used in Nevada since the 1970's, NDOT developed an interest after the January 17, 1994 Northridge earthquake revealed some seismic performance problems inherent in flared bridge columns. During the Northridge earthquake, several flared, reinforced concrete columns supporting the Mission-Gothic undercrossing failed in non-ductile modes. Some columns suffered brittle shear failures while others failed with limited ductility due to plastic hinges forming at the start of the column flare rather than at the column top, thus decreasing the column's shear span and consequently increasing its shear demand. Also, shear capacity in the hinge zone was decreased by degradation of concrete under inelastic cyclic loading.

Subsequently, an analytical study was done on the seismic vulnerability of flared bridge columns in northern Nevada[3]. The study concluded that columns detailed with inner core, vertical reinforcement in addition to flare reinforcement have adequate shear capacity. However, columns with all longitudinal reinforcement located along the flares and none in the core do not possess sufficient shear strength and could fail in shear under large seismic loads. The study also identified material overstrength as exacerbating the problem by increasing the shear demand without a significant, corresponding increase in shear capacity.

Bridge I-1250, designed in 1979-80, and constructed in 1980, was identified as a prototype for this study. The bridge is in a moderate to high seismic risk zone, and it incorporates structural flares in the columns.

There are a total of ninety-four columns in this bridge with either six or seven columns per bent. The columns are fixed at the top and pinned at the base with a two-way hinge detail. They are flared in the strong direction and have a constant width in the weak direction, with the largest sections being at the top. All the columns from this bridge are similar. The differences are: their height and that the amount and distribution of longitudinal steel varies among bents. The heights of the prototype columns vary from 6096 mm to 7010 mm. The experimental studies focused on the shortest columns, because with the shortest shear span they would develop the largest shear forces in order to develop a plastic hinge. There are three different longitudinal steel configurations: low, medium and high steel ratios (1.0, 1.4, and 1.8 percent at the largest section, respectively). The first two tests (References 1 and 2) focused on the high and low steel ratios. Based on the test results, conclusions about the medium steel ratio columns were determined. These two tests showed the seismic performance of the columns with the low steel ratio to be adequate. Therefore, this study was focused on the columns with the high steel ratio. Two columns, one representing the as-built details and one outfitted with a steel jacket retrofit were built and tested.

2.3 Design and Details of Shake Table Specimens

2.3.1 Column

The specimens that had been tested under quasi-static loads were of 40 percent scale. The scale of the models tested on the shake table had to be reduced because of the limitation of the shake table. The goal was to build and test the largest scale model possible, without exceeding the capacity of the table. Forty percent, thirty-three percent, and thirty-one percent scales were first considered and found to exceed certain limitations of the shake table.

The method of arriving at the appropriate scale model involved modeling the column seismic response using the non-linear, dynamic simulation program RC-Shake[9]. The idealized column was subjected to several ground motions of record. The ground motion peak accelerations were scaled up until the column reached an expected failure ductility indicated by the previous two tests. Then, several table parameters including: table acceleration, actuator capacity, table displacement, cumulative stroke, and table velocity were checked to ensure that the table limitations had not been exceeded. Based on the analysis, it was decided that the largest scale model of this column that could be tested to its full capacity without exceeding the capacity of the table was thirty percent.

Before the RC-Shake analysis could be performed, an idealized load-deflection relationship for the column had to be derived. Specifically, RC-Shake required input of the yield force and deflection, and the inelastic slope beyond that. Since the flexural capacity varied along the height of the column, determination of the critical section, and the associated yield and ultimate forces, necessitated the evaluation of the theoretical moment-curvature relationships at different cross-sections. Flexural demand and capacity profiles along the column height were found, and their point of tangency corresponded to the critical section. The yield and ultimate forces corresponding to that critical section were the yield and ultimate forces of the column. See sections 4.2 and 4.3 for more details on this process.

Before the design of the test specimens began, details of the prototype columns were considered (Fig. 2-1). In the prototype column, the main reinforcement is placed along the flare only and consists of 44 ϕ36 mm (#11) bars at the top of the column, reducing gradually to 24 ϕ36 mm (#11) bars within the non-flared segment. The longitudinal steel varies between 1.79 percent at the top of the column to 2.13 percent for cross sections located at 3.66 m from the top of the column. The lateral ties and cross-ties consist of ϕ13 mm (#4) bars placed at 102-mm vertical spacing throughout the entire column height. However, the tie set arrangement used in the upper 1.83-m flared segment has one cross tie in the short direction more than the tie set arrangement used elsewhere in the column.

For ease of construction and testing, the specimens were constructed and tested in an upside-down position, with the pinned connection at the top and the fixed connection at the bottom. The columns were labeled FA (flared, as-built) and FR (flared, retrofitted). Both columns had the same dimensions (Fig. 2-2). The only difference between the two models was the retrofit (Fig. 2-3). The height from the top of the footing to the point of lateral loading is 1778 mm, which corresponds to the scaled clear height of the prototype columns. The top of the models is a pinned connection since the prototype has a two-way hinge at the base. The flare is parabolic and extends from the top of the footing to 1422 mm above the footing. The column width in the strong (flared) direction ranges from 711 mm at the footing, to 400 mm at the termination of the flare. The width in the weak direction is constant at 356 mm.

There are four typical cross-sections along the height of the column as indicated in Fig. 2-1. The differences among these sections are due to the termination of transverse and longitudinal steel reinforcing bars. These bar cutoffs correspond to the scaled locations in the prototype column. There are also four typical cross-section for the retrofit. These are due to fabrication of the jacket in four half-shells before welding.

The size of the longitudinal reinforcement is ϕ13 mm (#4). These bars achieve the desired steel ratio of 1.8% at the largest section. Of the four typical cross-sections shown Fig. 2-2, starting from the largest section at top of the footing, there are 28, 24, 20, and 20 longitudinal bars in the sections, respectively. The transverse reinforcement was scaled as closely as possible to the prototype column. First, a ϕ6 mm (#2) deformed bar was tried but the spacing required to achieve the desired volumetric ratio violated the six longitudinal bar diameter limit to avoid longitudinal bar buckling. It was decided to use a ϕ4.5 mm (7 gage) smooth wire. A 51-mm spacing would achieve the desired volumetric ratio. Two issues had to be addressed: (1) to find a supplier that could provide the wire with the needed 414 MPa (Grade 60) yield strength, and (2) to account for the smoothness of the wire in bonding. The first problem was solved by obtaining 7 gage galvanized wire. The yield stress for the wire was in the required strength range. The zinc galvanization was removed with a 0.1 Molar sodium hydroxide bath to expose the steel underneath, and, therefore, more accurately model a steel-concrete bond rather than a zinc-concrete bond. The second issue, the development length arising from the smoothness of the wire was dealt with by increasing the cross tie lap length (Fig. 2-2) and hook length (in terms of bar diameters) of the prototype column by a factor to arrive at the lap and hook lengths (in terms of bar diameters) for the scale model. References and guiding documents to arrive at this factor were the 1963 ACI code[10] (which directly took into consideration bond strength) and a 1976 University of Illinois study[11] on bond stresses and pullout of smooth wire. As a result, the lap lengths were increased from $36d_b$ in the prototype to $45d_b$ in the model, and hook extensions were increased from $18d_b$ in the prototype to $22.6d_b$ in the model.

At the top of the column there is an integral concrete block for applying the lateral and axial loads (Figs. 2-2 and 2-4). The mid-height of the block corresponds to the location of the pinned connection at the footing of the prototype columns. This is where the center of lateral loading was applied. A steel I-beam was placed across the top of the loading block to apply the axial load via two Dywidag prestressing bars. Each bar was anchored at the top of the beam, passed through the footing, and was attached to a coupler and plate that was anchored at the bottom of the footing (Fig. 2-4).

2.3.2 Footing

Only the behavior of the column was of interest. Therefore, footing damage was avoided by overdesigning the footing.

The footing dimensions were 2438 mm long by 1829 mm wide by 762 mm high (Figs. 2-2 and 2-5). There were both top and bottom mats of steel consisting of ϕ25 mm (#8) bars in both directions. For shear reinforcement, there were vertical ϕ9 mm (#3) cross ties at each intersection of the longitudinal reinforcement. To fix the footing to the table, ten Dywidag prestressing bars were used. The bars were passed through ϕ89 mm vertical holes in the footings aligned with the threaded anchor holes of the table.

2.3.3 Retrofit

In designing the retrofit, the method and procedures established by the author of the previous static test done on these columns were used[6]. Shear strength, ductility, lateral load capacity, and constructability were considered.

A steel jacket retrofit was the only alternative considered in this phase of the study. The steel jacket consists of two sections along the height of the column; a top piece and a bottom piece, with a gap in between. The gap prevents the jacket from acting as longitudinal reinforcement and increasing the flexural capacity of the column. The gap location was chosen to coincide with the hinge location providing maximum ductility as indicated by results that were verified in the previous static tests[6]. The gap width was large enough to prevent closing of the gap before failure and small enough to prevent longitudinal bar buckling. Elliptical cross-sections were used because this shape follows most closely the shape of the column. The jacket width in the weak direction is constant, as is the column width. The jacket dimension in the strong direction varies, as does the column dimension. The jacket was constructed in four half-shells. The dimension in the strong direction varies linearly along the height of each half-shell. Two of the four sections were welded to form two half-shells for the top portion of the retrofit and the remaining two sections constituted the bottom portion. The half-shells were placed around the column and welded along the height of the jacket on the non-flared sides. The space between the jacket and the column face was filled with grout. The grout thickness varies from 38 mm to 64 mm. Refer to Fig. 2-3.

The design of the jacket thickness was done according to the provisions of the FHWA[12] retrofit design method with an assumed crack inclination, θ, of 45 degrees. The lateral load required to form a plastic hinge at the gap was considered to be the column shear demand. A factor of safety of two was applied to this value and it was then compared to the shear capacity, V_n, of the column at the hinge calculated as the sum of the capacity of the column concrete and the transverse steel. This nominal shear capacity, V_n, was calculated according to the provisions of the California Department of Transportation (CALTRANS) method[13]. The CALTRANS method was used because it addresses the reduced shear capacity of concrete in the plastic hinge region. The shear capacity of the steel is dependent on the area of the steel, the yield stress, the distance from the extreme concrete compression fiber to the centroid of tension reinforcement, and the spacing. Considered in the shear capacity of the concrete is: the level of confinement, the applied compressive axial stress, and the strength of the concrete. The thickness of the jacket was designed to account for this deficit of column capacity as compared to demand. The required jacket thickness was found to be less than 2 mm. However, the logistics of fabrication, transportation, placement, and welding required a larger, more practical thickness. A 3.2-mm jacket thickness was selected. This corresponds to an approximately 11-mm jacket thickness in the prototype column.

An important consideration in this retrofit design is that the flexural enhancement of the column be minimized. A significant increase in the flexural capacity of the column could force the failure to occur in adjacent members, including bridge superstructure and footings. Therefore, two factors influencing flexural enhancement of the column are purposely avoided in the retrofit design: increased cross-section and the jacket acting as longitudinal steel reinforcement. These are both dealt with by making the jacket discontinuous at the desired hinge location (i.e. a gap along the height of the jacket). The center of the gap is located at 441 mm above the footing and is 32-mm wide. The location of the gap corresponds to the hinge location providing maximum ductility as indicated by the analysis done as part of a previous study[6]. The gap width is sufficiently small to prevent longitudinal bar buckling.

2.4 Materials and Construction

Materials used in the model columns were chosen to most accurately match those of the prototype columns. The prototype columns have grade 60 steel for both longitudinal and transverse reinforcement. Tension tests were performed on the steel prior to use in the models to verify that their material properties corresponded to those of the prototype. The measured average steel yield stress in the prototype columns was 484.0 MPa (with a specified yield stress of 413.7 MPa). The results for the reinforcement in the specimens are summarized in Table 2-1. The jacket was made from A36 steel, commonly used in column retrofits. Table 2-1 also lists the measured properties of the steel jacket.

Footings were cast separately from the column. A 28-day strength of 34.5 MPa was specified with a maximum aggregate size of 13 mm. A plasticizer was added to increase the workability. Standard 150 X 300 mm cylinders were tested at 7, 14, 21, and 28 days. The results are shown in Table 2-2.

The specified concrete strength of the prototype columns was 27.6 MPa and the measured average strength in 28 days was 40.3 MPa. The columns and loading blocks for the models were cast monolithically. The specified strength was 27.7 MPa and the measured strength on the day of testing was 37.6 MPa and 39.6 MPa for the as-built (FA) and retrofitted (FR) models, respectively. A maximum aggregate size of 9.5 mm was specified because of congestion of reinforcement in the column. The mix was done with warm water because of the winter conditions existing during casting. A plasticizer was added to increase the workability of the concrete. Standard 150 X 300 mm cylinders were taken and tested at 7, 14, 21, and 28 days as well as on the column test days. These values are reported in Table 2-2.

The steel jacket was ordered in half-shells. The half-shells were placed around the column and welded on the flat sides. The top and bottom openings of the jacket were sealed and the void between the column face and the steel jacket was pressure-grouted through 25.4 mm threaded holes on both sides near the tops of the jacket sections. The grout strength was 65.0 MPa on test day.

2.5 Instrumentation and Data Collection

Data from strain gages, displacement transducers, accelerometers, and load cells were recorded on a *Pacific* data collection system. The rate of recording was set at 250 Hz.

Twenty-nine strain gages were used in specimen FA and forty-four in specimen FR, to measure strain in the column longitudinal and transverse reinforcement as well as in the steel jacket. The gages were manufactured by Tokyo Sokki Kenkyujo Co., Ltd. of Japan. Three different types of gages were used: 10 mm (YL-10-3L) on the longitudinal steel (Figs. 2-6 and 2-7), 2 mm (YFLA-2-3L) on the transverse steel (Figs. 2-8 and 2-9), and both 10 mm unidirectional (YL-10-3L) and 10 mm rosette (YRS-10-5L) on the jacket (Fig.2-10). Push and pull directions indicated on the figures refer to the force applied by the link to the loading head. The locations shown under different sections are measured from the top of the footing. A negative sign in the locations indicates gages installed below the top of the footing to monitor possible yield spread into the footing.

Ten *novotechnik* transducers, with a displacement range of ±25.4 mm, were used to measure the curvature at five locations along the height of specimen FA (Fig. 2-11). The top layer of transducers was omitted from the retrofitted column to allow for more of the available channels to be used for strain gages on the steel jacket. Transducers were mounted on 9.5-mm threaded rods that ran horizontally through the column. On the retrofitted specimen, 38-mm holes through the grout and jacket were placed around the threaded rods to assure that the curvature of only the core portion of the column and not the grout or jacket was being measured.

The lateral and axial loads applied to the column were measured in different ways. The lateral load transmitted to the column was measured by an accelerometer fixed to the link that connects the column to the mass rig (Fig. 2-11). This acceleration was multiplied by the inertial mass on the other end of the link to determine the force. The axial load was measured by two load cells placed between the vertical hydraulic actuators and the I-beam (Fig. 2-4).

A displacement transducer attached to the top of the column (at the center of the loading block) was used to measure the combined deflection of the column and the table (Fig. 2-11). Table deflection, measured by a displacement transducer internal to the table, was used to find column deflection relative to the table.

2.6 Test Setup and Procedure

The columns were tested on a 4267 X 3658 mm shake table. The lateral load was applied via a steel link attached to the loading block at the top of the column and to four 89 kN concrete blocks used as inertial mass. The blocks were situated atop a mechanism (referred to as the mass rig) consisting of four steel beams attached to the floor with pin connections and a platform to which the blocks are attached (Fig. 2-11).

After the specimen was tied down to the table and attached to the mass rig, an axial load of 286.9 kN was applied through the vertical actuators (Fig. 2-4). An accumulator was used in the hydraulic line to minimize fluctuation of axial loads. The axial load was determined by matching the axial load index (defined as the ratio of axial load to the product of the cross-sectional area and the concrete compressive strength) of the specimens to that of the prototype columns. The cross-sectional areas of the columns ranged from 205 X 10^3 mm^2 at the base to 109 X 10^3 mm^2 at the top. Based on measured concrete compressive strength, the axial load index for the as-built specimen was 0.037 at the base and 0.070 at the top and, the axial load index for the retrofitted specimen was 0.035 at the base and 0.066 at the top. These indices corresponded very closely to those of the prototype columns with the axial load calculated as the tributary weight of the bridge superstructure and the column weight. Before application of the axial load, all instrument readings were set to zero.

The axial load and the inertial mass on the mass rig were not the same. The inertial mass was increased to allow testing of the columns to their full capacity. The axial load was 286.9 kN, the inertial mass (including the effective mass of the mass rig) was 444.8 kN. Since the oscillating mass (on the mass rig) was more than the tributary mass on the column (axial load), the natural period of vibration was longer than would be expected had the oscillating mass and the tributary mass been identical. The frequency content of the earthquake motion was adjusted to account for this variation. The time scale of the motion was decreased by the ratio of the period of the scaled model (due to the mass on the mass rig) to the period of the prototype column. If the inertial and axial masses had been identical, the time scaling factor would be solely a function of the model scale. That factor was 0.54. Due to the inertial and axial mass discrepancy another time scaling factor had to be introduced. This factor increased the time scaling of the input motion to account for the increase in the model column period (due to increased oscillating mass). This value was 1.245. The end result, the time scaling factor due to the combination of the model scale effect and to mass discrepancy effect (on the period) was 0.672.

The test setup and procedure were identical for both columns. Initially, a decision had to be made as to which ground motion would be used. The field of prospective ground motions was narrowed down to two, from a list of ten, in the process of finding the largest scale model that the table could handle (Section 2.3). There were only two ground motions that could fail the column without exceeding the capabilities of the table. They were the Osa record of the Kobe, Japan 1995 earthquake and the Sylmar record of the Northridge, California 1994 earthquake. The Sylmar record of the Northridge earthquake was chosen because it is more representative of earthquakes in the western United States.

The second consideration was to make a decision concerning the testing program in terms of the input motion intensity. The general choices were to apply a strong earthquake record or to apply multiple motions with gradually increasing intensity of shaking. The latter was selected (Table 2-3). This is not a sequence of ground motions that would normally be expected to occur in nature; it was selected because the actual ductility capacity of the specimen was uncertain, and motions with a fine amplitude increment would allow for a more accurate determination of column capacity. It was decided to initially subject the column to a one-fifth scale version of the Sylmar record. This corresponded to a pre-yield run as indicated by dynamic modeling. Next, a two-fifths version of the earthquake was to be run, which corresponded to first yielding in the longitudinal bars. After that, a three-quarters version was run with subsequent runs increasing by one-quarter (of the original full-scale motion) until failure. See Table 2-3 for complete testing schedules of the two specimens. Also, some quick-release tests consisting of pulling the column with a cable to cause a small deflection then cutting the cable and recording the free-vibration were performed. The purpose was to provide some estimate of changes in column period and damping.

Chapter 3

Experimental Results

3.1 Introductory Remarks

This chapter presents the experimental results for the as-built specimen (FA) and the retrofitted specimen (FR). The results for the test specimens include: forces, displacements, strains, curvatures, and other aspects of behavior observed during testing. Peak strains are tabulated for all runs, and whenever possible figures for strains and curvatures are presented as envelopes plotted along the height of the column to facilitate visualization of the variation of these parameters. This chapter also presents target and achieved shake table accelerations and acceleration spectra.

3.2 Shake Table

The specimens were subjected to earthquake records listed in Table 2-3. The original measured accelerations at Sylmar during the 1994 Northridge earthquake is shown in Fig. 3-1. Due to dynamic interaction between the shake table and the test specimen, there are usually differences between the achieved and target table accelerations.

Because the primary objective of the study was to compare the response of the retrofitted and as-built specimens, it was important to determine if the two specimens were subjected to similar demand. Therefore, the target and achieved table acceleration records and spectra were compared.

Target table accelerations for all runs are shown in Fig. 3-2. Table accelerations, in terms of target, achieved for Specimen FA, and achieved for Specimen FR, for run 4 are presented in Fig. 3-3 as a representative sample. A zoomed-in view is presented in Fig. 3-4. Accelerations for all runs are shown in Figs. 3-5 and 3-6. Generally, the control system seems to have overcompensated for the dynamic interaction between the shake table and the test specimen. Recorded peaks are generally higher than the target peaks. This can be accounted for by considering two factors: 1) the progressive damage incurred on the test specimens during testing and the associated degradation of stiffness, and 2) the way in which the control system compensates for the aforementioned dynamic interaction between table and specimen. Prior to testing, the table was tuned to the column by running 'white noise' (random, small amplitude accelerations). This allowed the control system of the table to adjust to the resistance that had to be overcome in order to achieve the target accelerations. As the stiffness of the column decreased over the course of testing, this resistance became less. The control system was compensating based on the previous stiffness of the column and accounted for more resistance to acceleration than was actually encountered. Therefore, it typically overshot the peaks.

Peak accelerations and peak "effective" accelerations are tabulated in Tables 3-1 and 3-2, respectively. Peak "effective" acceleration is defined as the peak acceleration from the table record multiplied by the ratio of the inertial mass (concrete blocks and mass rig, 444.8 kN) to the tributary mass corresponding to the axial load (286.9 kN). Although, in general, most of the target accelerations were overshot by the table, the measured absolute peak was often less than the target. This was the case for all of the runs for specimen FR; the measured accelerations were typically about eighty percent of the target. For specimen FA, for the first two runs the peaks were about ninety percent of target. Runs three and four were ninety-five and ninety-seven percent of target, respectively. The peaks during the last three runs, five through seven, were greater than target. They increased from eight percent above target for run five, to fifteen percent above target for run seven. Since, for the prototype column in the actual bridge, the inertial mass and the tributary mass corresponding to the axial load were the same, peak "effective" accelerations are a useful parameter relating the experimental loading conditions of the model to the field conditions of the prototype. Peak "effective" accelerations are simply the acceleration that would be required to achieve a given inertial force had the inertial mass been equal to the tributary mass.

To further quantify the comparison between FA and FR, the frequency content of the achieved input motions was analyzed using the computer program *Spect*[14]. Spectral accelerations for run 4 are shown in Fig. 3-7. Spectral accelerations for all runs are shown in Figs. 3-8 and 3-9.

Two estimates of the periods of both specimens during the course of testing are shown in Table 3-3. Although the periods were not constant within each run due to progressive damage incurred during testing, some estimate of the effective period was necessary. By having an estimate of the effective period of the column and the acceleration spectra of the achieved input motions, an approximate comparison could be made between loading demand for the two specimens. It was desired to subject both columns to exactly the same input motion. However this is not possible nor is it necessary. A comparison of the spectral accelerations from the two achieved input motions for the relevant periods would give a quantifiable comparison of the two input motions. The two methods used in period estimation are referred to as 'Method A' and 'Method B'. 'Method A' is based on spectral acceleration data obtained from the computer program *Spect*[14]. Spectral analysis of the measured acceleration record at the top of the column indicated a dominant period of the column. Figure 3-10 shows a sample. The period for 'Method B' was found from the achieved table acceleration spectra. The measured peak acceleration at the top of the column was matched with the corresponding period on the graph.

From the spectral analysis (Figs. 3-8 and 3-9), it was seen that the dominant period of the achieved acceleration records was nearly identical to that of the target acceleration record. The dominant period of the target motion was 0.25 seconds, similarly the dominant period of the achieved motions was 0.25 seconds. Considering the spectral accelerations of the achieved motions in the vicinity of the relevant periods from Method B (0.61 seconds to 0.68 seconds for specimen FA and 0.33 seconds to 0.65 seconds for specimen FR) the input motion was essentially the same for both specimens. Run one is an exception to this where the spectral accelerations for FR were substantially lower than for FA.

3.3 Summary of Test Results for Static Tests

A secondary purpose of this study was to compare the results to previous static tests done on the same prototype columns. The static tests included a high steel ratio specimen (HS for as-built, high steel and R-HS for retrofitted, high steel) and a low steel ratio specimen (LS for as-built, low steel and R-LS for retrofitted, low steel). Only columns with high steel ratio (HS and R-HS) pertain to this study. This section provides a brief summary of the test results for the as-built and retrofitted columns (HS and R-HS) that were tested under cyclic static loads at the University of Nevada, Reno[5,6]. Specimens HS and R-HS modeled the same prototype as was used in this dynamic test, but their scale was forty percent as opposed to thirty percent, which was the scale of the shake table specimens.

3.3.1 As-Built Specimen

The as-built specimen, called HS, exhibited wide and stable hysteretic load-displacement loops until failure. The yield deflection was 26.6 mm and the ultimate deflection was 160 mm. From these values, the measured displacement ductility factor was 6.0.

Spalling of concrete cover was observed and recorded to give an indication of the heights and lengths of plastic hinging. Spalling initiated at

740 mm above the footing. The spalling was well-spread at failure, and ranged from 410 mm to 1300 mm above the footing. Failure occurred in the area of plastic hinging and was due to longitudinal bar fracture caused by low-cycle fatigue. The fracture occurred at 740 mm.

The strains in the transverse steel of the as-built specimen remained elastic until high displacements were applied. No ties yielded up to a displacement ductility of four , two ties yielded at $\mu_\Delta = 5$, and seven ties yielded at $\mu_\Delta = 6$. All yielding of shear reinforcement occurred within the observed plastic hinge region.

The shear cracks in the as-built specimen indicated the amount of shear demand placed on the concrete. Although the specimen did not fail in shear, the shear cracks in the plastic hinge region were profound.

3.3.2 Retrofitted Specimen

The retrofitted specimen, called R-HS, was identical to the as-built specimen except that it was outfitted with a steel jacket that included a 38 mm gap centered at 762 mm above the footing. The location of the gap was chosen such that the lateral load to cause flexural yielding was minimum. The hysteretic load-displacement loops were stable until failure at a displacement ductility of 6. The measured yield deflection was 26.7 mm and the ultimate deflection was 160 mm.

After testing and removal of the steel jacket plastic hinging was observed to be confined to a relatively small area in the vicinity of the gap. The spalling ranged from 710 mm to 890 mm and one side and 680 mm to 890 mm on the other. As compared to the as-built specimen, the placement of the jacket prevented shear damage. The strains in the transverse steel of the retrofitted specimen were significantly lower than those in the as-built specimen. The maximum strain in the transverse reinforcement occurred at 737 mm above the footing and was 1900 microstrain, which is 87 percent of yielding. The failure occurred due to longitudinal bar fracture.

Strains in the steel jacket remained essentially elastic, with one area of localized yielding. A maximum horizontal strain of 1310 microstrain occurred at 660 mm above the footing on the non-flared side, next to the vertical weld. The maximum measured vertical strain was 881 microstrain and occurred at the same location. These values correspond to 124 and 71 percent of yield, respectively. These maximum stresses occurred at 82.5

mm below the gap in the jacket and seemed to be isolated to this location. At other locations, horizontal and vertical strains were consistently lower.

3.4 Specimen FA: As-built

3.4.1 General Observations

During the first run flexural cracks were observed from 216 mm to 1181 mm above the footing (refer to Table 2-3). During the second run more flexural cracks were seen and they extended from 114 mm to 1334 mm (Fig. 3-11). Shear cracks began to appear from 256 mm to 576 mm. More flexural cracks were observed between 114 mm and 1334 mm after run three. Also, during run three more shear cracks appeared ranging from 256 mm to 1168 mm. Some minimal spalling, at 457 mm and 559 mm, began to occur on this run (Fig. 3-12). Significant spalling, as well as propagation of flexural and shear cracks was observed after run four. Also, after run four, a significant permanent offset of 24 mm was observed in the westward direction. This side was the dominant compression side and spalling of concrete cover had occurred from 394 mm to 737 mm above the footing on this side. After run five, the permanent offset had increased to 40 mm. Spalling of concrete cover had begun to extend around the sides of the column. Spalling continued and the permanent offset increased to 70 mm after run six. During run seven, the three extreme bars on the west side of the column buckled and fractured. Figures 3-13 and 3-14 show the column after failure. The fractures were at 394 mm, 419 mm, and 533 mm. In addition, four of the perimeter ties fractured due to longitudinal bar buckling: at 483 mm, 533 mm, 584 mm, and 635 mm. Also, the hook of the cross tie at 432 mm opened. Crushing of core concrete was also observed during run seven.

3.4.2 Forces

The lateral loading history for all runs, for specimen FA, is presented in Fig. 3-15. These were the total forces taken as the combination of the inertial forces and P-delta forces. Inertial forces were taken directly from the link accelerometer readings and the effective inertial mass (mass rig and inertial blocks). Since damping is a dynamic property it is implicitly included in this force. However the P-delta force (due to geometrical properties of the mass rig) is a function of absolute displacement and is not a dynamic parameter.

So the inertial force, taken directly from the acceleration data, is lower than the total force, which includes the P-delta effect. The force associated with the P-delta effect was calculated from geometrical properties of the mass rig and the weight of the mass rig. Since the mass rig was pinned at the base, any displacement from the vertical position created an overturning moment that had to be resisted by a lateral force in the column applied through the link (refer to Fig. 2-11). Since the link was rigid, the overturning moment applied to the mass rig was equal to the product of the weight of the mass rig and the absolute displacement at the top of the column. The resisting moment was equal to the product of the force in the link and the moment arm from the pin connection at the base of the mass rig to the pin connection at the platform supporting the inertial mass. Equating the overturning and resisting moments yielded the P-delta force applied through the link as a lateral force to the column. This P-delta force combined with the dynamic force from the accelerometer on the link comprised the total force. The P-delta force comprised 0.8%, 2.2%, 4.1%, 5.2%, 6.8%, 8.6%, and 13.6% of the total force for runs one through seven, respectively.

The P-delta effect due to the axial load applied directly on the column was neglected because the prestressing rod that applied the axial load passed through a point near the mid-depth of the column critical section.

The total peak lateral force, including the P-delta effect, increased steadily from 97.5 kN for run 1 to 262.9 kN for run four. The peak lateral force for all runs occurred during run four. The peak lateral force decreased from 254.1 kN for run five to 200.4 kN recorded during run seven when longitudinal bars buckled and fractured.

The axial forces are presented in Fig. 3-16. Prior to testing, an axial load of 286.9 kN was applied. At high drift levels, however, the measured axial load varied from 156.0 kN to 453.3 kN. An accumulator had been connected to the hydraulic line for the actuators applying the axial load to control the load fluctuation. However, this system was not sufficiently responsive to rapid changes in displacements. The effect of this variation will be discussed in more detail in Chapter 4.

3.4.3 Displacements

The displacement history for all runs for specimen FA is shown in Fig. 3-17. Displacement histories for each of the individual runs are presented in Figs. 3-18 and 3-19. A permanent offset from the datum position of the column top was observed after run three. It increased from 7 mm at the end of run three to 67 mm at the end of run six. The offset increased to nearly 200 mm at failure in run seven.

Lateral load-displacement hysteresis relationships are shown in Figs. 3-20 and 3-21. Column behavior remained essentially in the elastic range for the first two runs, and hysteretic energy dissipation began to occur in run three. The outer curves indicated a relatively large dissipation of energy. Lateral load-displacement envelopes are shown in Fig. 3-22. There are two curves, referred to as coincident and non-coincident. Lateral loads for both are the same. Displacements differ in the following way: the non-coincident curve contains peak displacements for that run regardless of when they occur during the run, while the coincident curve contains only those displacements that occurred at the same instant in time when the peak load occurred. As expected during small amplitude runs, the two curves were the same. As more yielding developed and strength degradation occurred, the peak displacement increased beyond the displacement that corresponded to the peak force. The coincident lateral load-deflection curve was used for the analysis.

3.4.4 Strains

Measured peak strains for all the runs are tabulated in Tables 3-4 and 3-5. Strain gage numbers are marked in Figs. 2-6 and 2-8. Table 3-4 lists data for the longitudinal reinforcement and Table 3-5 presents data for the transverse reinforcement. The peak lateral force recorded during that run is indicated along with the run number. Also, peak strains are indicated for both tension and compression. A dash indicates that no data were recorded for that particular run. Note that the yield strain was 2290 microstrain for longitudinal bars and 2240 microstrain for ties (Table 2-1). The strain value of 42,000 was a limit of the data acquisition system.

Measured tensile and compressive strain envelope profiles along the height of the column for extreme longitudinal bar layers are shown in Figs. 3-23 through 3-26. The gage at 533 mm, generally recorded the highest strain for extreme longitudinal bars. Strain history for gage seven, located on an extreme east longitudinal bar at 279 mm above the footing is shown in Fig. 3-27. The strain history for this longitudinal bar provides some measurement of the spread of yielding in longitudinal bars. It is on an extreme layer of bars so yielding would be seen here first, as opposed to other bar layers. The plot indicates that yielding at this location first occurred in run two. By run four strains at this location were well over 10,000 microstrain, indicating that yielding was well-spread. This plot is in agreement with the hysteresis loops shown in Figs. 3-20 and 3-21 in supporting the assertion that yielding first began to occur during run two and was well-spread by run four. Hysteretic energy dissipation was first observed beginning to occur during the same runs that significant yielding was first observed to occur in the extreme longitudinal bar. As longitudinal bar yielding became more extensive, hysteretic energy dissipation seen in Figs. 3-20 and 3-21 became more pronounced.

Measured tensile strain envelopes for cross ties and perimeter ties are shown in Figs. 3-28 and 3-29. Generally, the highest strains for lateral steel were also recorded at the 533 mm level. The extremely high strains in run seven were due to the outward buckling of longitudinal bars. Even during run six, several of the ties yielded. Strain history for gage twenty-four, located on a perimeter tie at 660 mm above the footing is shown in Fig. 3-30. The plot shows that the bar yielded in run four. Perimeter and cross tie bar strain envelopes plotted as a function of peak effective table acceleration are shown in Figs. 3-31 through 3-35. Yielding occurred at the following locations during the indicated runs: perimeter tie at 279 mm above the footing (run six), cross tie at 533 mm (run four), perimeter tie at 533 mm (run six), cross tie at 660 mm (run seven), perimeter tie at 660 mm (run three), perimeter_tie at 800 mm (run seven), and cross tie at 1092 mm (run seven). Generally, a lag between strains in perimeter ties and strains in cross ties was observed. This can be attributed to deterioration of the concrete over the lap splice in the cross ties. The perimeter ties registered high strains associated with high drifts, whereas the cross ties experienced some bond slippage and had lower strains.

3.4.5 Curvatures

Average curvature was measured across the gage length and plotted at the center of the gage length. This measured value was not necessarily the curvature value at that specific location, rather it was the average across the gage length.

The curvature envelopes along the height of the column are shown in Fig. 3-36. The greatest curvatures were seen in the 584-737 span. This is the span that included most of the plastic hinging as indicated by spalling of concrete (see section 3.4.1). Run two corresponded to the onset of yielding. Significant yielding and hysteretic energy dissipation began to occur in run three. Also in run three, a significant concentration of curvature developed in the 483-584 mm (above footing) and 584-737 mm spans, indicating the formation of a plastic hinge. In runs four through seven the greatest curvatures were concentrated in the 483-584 mm span.

3.5 Specimen FR: Retrofitted

3.5.1 General Observations

The steel jacket precluded any observations about concrete cracking or spalling being made during the course of testing, except where the concrete was exposed at the gap. At the gap, flexural and shear cracks were first observed after run eight (Fig. 3-37). Existing cracks were highlighted by hand due to lack of clarity in the photograph. Also, first spalling was observed after run eight (Fig. 3-38). Failure occurred after run ten, and was due to longitudinal bar fracture at the gap (Fig. 3-39). Fracture occurred in the fifteen bars in the seven easternmost layers of longitudinal steel (from the extreme layer through the middle layer on the non-flared side of the column). No buckling of longitudinal bars was observed. Upon removal of the jacket (Figs. 3-40 and 3-41), after testing, spalling was observed to be very isolated to the vicinity of the gap. The gap was from 425 mm to 457 mm above the footing, and spalling was observed from 393 mm to 483 mm. There were flexural cracks from 64 mm to 1232 mm. Also, there was a concentration of shear cracks from 330 mm to 813 mm. Two shear cracks were seen extending from 991 mm to the top of the column at 1461 mm.

3.5.2 Forces

The lateral loading history for all the runs for specimen FR is presented in Fig. 3-42. As for specimen FA, these forces were the total forces taken as the combination of the inertial and P-delta forces. Inertial forces were calculated by multiplying the link accelerometer readings by the effective inertial mass. This force is the dynamic force and is lower than the total force derived from both the dynamic and geometric (P-delta) forces.

The force associated with the P-delta effect was calculated from geometrical properties of the mass rig and the weight of the mass rig. Since the mass rig was pinned at the base, any displacement from the vertical position created an overturning moment that had to be resisted by a lateral force in the column applied through the link (refer to Fig. 2-11). Since the link was rigid, the overturning moment applied to the mass rig was equal to the product of the weight of the mass rig and the absolute displacement at the top of the column. The resisting moment was equal to the product of the force in the link and the moment arm from the pin connection at the base of the mass rig to the pin connection at the base of the platform supporting the inertial mass. Equating the overturning and resisting moments yielded the P-delta force applied through the link as a lateral force to the column. This P-delta force combined with the dynamic force from the accelerometer on the link comprised the total force. The P-delta force comprised 1.4%, 1.9%, 2.2%, 2.7%, 4.3%, 4.9%, 5.8%, 6.7%, 7.9%, and 10.4% of the total force for runs one through ten, respectively.

As for specimen FA, the P-delta effect due to the axial load applied directly on the column was neglected because the prestressing rod that applied the axial load passed through a point near the mid-depth of the column critical section.

The total peak lateral force, including the P-delta effect, increased steadily from 103.0 kN recorded during run one to 359.0 kN recorded during run six. The peak lateral force was recorded during run six. The peak lateral force steadily decreased from 350.1 kN during run seven, to 284.7 kN during run ten when longitudinal bars fractured.

The axial forces are presented in Fig. 3-43. Specimen FR was also subjected to an axial force of 286.9 kN prior to testing. However, as was seen in specimen FA, at high drift levels, the axial load varied. The measured variation was from 199.9 kN to 600.3 kN. The effect of this variation will be discussed in more detail in Chapter 4.

3.5.3 Displacements

The displacement history for all runs is presented in Fig. 3-44. Displacement histories for each of the individual runs are presented in Figs. 3-45 and 3-46. A significant permanent offset was observed after run five. It increased from about 10 mm at the end of run five to 73 mm at the end of run nine. The offset increased to nearly 176 mm at failure in run ten.

Lateral load-displacement hysteresis relationships are shown in Figs. 3-47 and 3-48. Behavior remained essentially elastic for the first two runs, and hysteretic energy dissipation began to occur in run three. Lateral load-displacement envelopes are shown in Fig. 3-49. As with specimen FA, there are two curves, referred to as coincident and non-coincident. Explanations for coincident and non-coincident curves are the same as they were for specimen FA. Lateral loads for both are the same. Displacements differ in the following way: the non-coincident curve shows peak displacements for that run regardless of when they occur during the run, while the coincident curve contains only those displacements that occurred at the same instant in time when the peak load occurred. As was seen with specimen FA, during small amplitude runs the curves were the same. As more yielding developed and strength degradation occurred, the peak displacement increased beyond the displacement that corresponded to the peak force.

3.5.4 Strains

Measured peak strains for all the runs are tabulated in Tables 3-6, 3-7, and 3-8. Strain gage numbers are marked in Figs. 2-7, 2-9, and 2-10. Table 3-6 lists data for the longitudinal reinforcement, Table 3-7 presents data for the transverse reinforcement, and Table 3-8 contains data for the steel jacket. The peak lateral force recorded during that run is indicated along with the run number. Also, peak strains are indicated for both tension and compression. A dash indicates that no data was recorded for that particular run. Note that the measured yield strain was 2290 microstrain for longitudinal bars and 2240 microstrain for ties (Table 2-1). The measured yield strain for the jacket was 1920 microstrain.

Measured tensile and compressive strain envelope profiles along the height of the column for extreme longitudinal bar layers are shown in Figs. 3-50 through 3-53. The entire strain history for strain gage seven (located on the extreme longitudinal bar at 279 mm above the footing) is shown in Fig. 3-54. As was indicated in section 3.4.4 for specimen FA this plot provides some indication of the extent of yielding in the longitudinal bars. Also, used in conjunction with the hysteresis plots of Figs. 3-20 and 3-21 it provides some collaborative evidence of when hysteretic energy dissipation began to occur. Hysteretic energy dissipation is seen in Fig. 3-20 on run three and significant yielding is seen on Fig. 3-54 on run three.

Measured tensile strain envelopes for cross ties and perimeter ties are shown in Figs. 3-55 and 3-56. Strain history for gage twenty-four, located on a perimeter tie at 660 mm above the footing, is shown in Fig. 3-57. The plot shows that this bar remained well below yielding prior to failure of the column. Perimeter and cross tie bar strains plotted as a function of peak effective table acceleration are shown in Figs. 3-58 through 3-61. The retrofitted specimen had generally lower strains in the lateral reinforcement than the as-built specimen especially at large accelerations. This trend will be discussed further in section 4.4. Also, the slippage observed in the cross ties of specimen FA was not observed in the cross ties of specimen FR. The cross ties registered strains comparable to the perimeter ties and there was no lag in strains. In some cases, the cross ties registered higher strains than the perimeter ties. It appeared that the added confinement provided by the steel jacket prevented slippage. The constraint provided to the core concrete may have been sufficient to prevent the deterioration that caused cross tie slippage in FA.

Measured horizontal tensile strain envelopes along the height of the jacket are shown in Figs. 3-62 through 3-65. Measured vertical tensile strain envelopes are shown in Figs. 3-66 and 3-67. The jacket remained essentially elastic prior to failure, with the exception of one area of localized yielding slightly above the gap. Strain gage thirty-six, a horizontal gage located 76 mm above the top of the gap, registered strains that were 148 percent of yield.

3.5.5 Curvatures

The curvature envelopes along the height of the column are shown in Fig. 3-68. They represent the average curvature along the span being measured and not necessarily the curvature at that location. Initially, the greatest curvatures were seen in the 483-584 mm span, which spanned the gap in the jacket. First yielding was observed during run two and the curvature envelope began to show a curvature concentration in the span including the gap. This indicates the initiation of plastic hinging at the gap. After run seven, the curvatures of the 0-152 mm span slightly surpassed those of the 483-584 mm span. This was because one of the *novotechnik* transducers spanning the jacket gap exceeded its limit. Visual inspection during the course of testing clearly indicated more curvature at the gap than that at the base. The high degree of curvature observed in the 0-152 mm span of the column can be attributed to the 19 mm gap in the jacket at the base of the column (Fig. 2-3). Because there was a gap in the jacket, there was no increased section size and no composite action with the jacket as there was with other sections where the jacket was continuous. Also, the base of the column was under the greatest flexural demand because it had the largest moment arm to the point of loading. The added confinement of the jacket allowed the section to reach high curvatures without failure.

3.6 Concluding Remarks

The placement of the steel jacket retrofit significantly altered the seismic response of the column. It drastically reduced tie strains as well as changing the mode of failure. In the as-built specimen, four ties yielded prior to failure. In the retrofitted specimen, no ties yielded prior to failure. Upon failure of the column, some yielding of ties did occur. But this was after the column had lost over twenty percent of its lateral load capacity and the fracture of all longitudinal bars on one half of the column and a large flexural crack made half of the column discontinuous in the longitudinal direction (Fig. 3-39). After that, the shear forces had to be transferred through half of the column concrete and half as many longitudinal bars. Consequently, the transverse steel in the vicinity of the gap registered a jump in strains. The mode of failure in the as-built specimen could be characterized as flexure-shear. Longitudinal bars buckled and fractured due to low-cycle fatigue and there was extensive yielding of the ties. In the retrofitted specimen bar buckling was prevented by the added confinement of the jacket. Longitudinal bars fractured on the tension side of the column.

Spalling of concrete was well-spread in the as-built column, whereas spalling in the retrofitted specimen was confined to the vicinity of the gap. Insofar as spalling is indicative of plastic hinging, the hinging in the retrofitted specimen was confined to a relatively small area in the vicinity of the gap. It is evident that the placement of the retrofit decreased the length of damage, and did not allow the spread of plastic hinging.

The placement of the steel jacket did seem to significantly affect the displacement ductility of the column calculated as the ultimate displacement divided by the yield displacement. The displacements were those that were coincident to the peak forces (see Figs. 3-22 and 3-49) for each run. The ultimate displacement was taken as the displacement corresponding to the run that had a peak lateral load that had dropped by at least twenty percent of the peak lateral load for all runs. This was run seven for specimen FA. For specimen FR, the lateral load had dropped by nearly ten percent for run nine and twenty-two percent for run ten. However, the displacement coincident to the peak force for run ten was less than that for run nine. Since the column had already reached the displacement of run nine without losing enough lateral load capacity to consider the column failed, the displacement of run nine was considered a conservative estimate of the ultimate displacement. The yield displacement was taken as the displacement associated with the peak lateral force of the run in which onset of significant yielding occurred. This was run two for both specimen FA and specimen FR. According to this method, the displacement ductility for specimen FA was 6.0 and the displacement ductility of specimen FR was 9.7.

The results of this study (the comparison between the as-built and retrofitted specimens) generally support and collaborate the results of the static tests. For the as-built specimens, HS[5] and FA, it was shown that when all or a high percentage of the main reinforcement is placed along the flare, the plastic hinge may form along the flare at a section which does not necessarily coincide with the location of maximum bending moment.

This is due to the fact that parabolic flares increase the effective depth of the flare reinforcement at a rate that is higher than the rate of moment increase. Also, as evidenced by longitudinal bar buckling and yielding of ties, the confinement and shear steel of the as-built specimens was inadequate. For the retrofitted specimens, R-HS[6] and FR, it was demonstrated that the retrofit provided the necessary shear capacity to avoid shear failure. The maximum hoop strains in the steel jacket were significantly below yielding, indicating that there was an acceptable reserve of shear capacity. Also, the retrofit drastically reduced strains in the column transverse reinforcement when compared to the as-built results (refer to section 4.4). In addition, in both static and dynamic tests the retrofit appeared to have prevented or delayed longitudinal bar buckling as well as prevented spread of plastic hinging. Longer plastic hinge lengths can help spread energy dissipation over a larger area. However, repair of long plastic hinges is more costly. The steel jacket retrofit allowed for sufficient energy dissipation while preventing spread of damage.

In contrast to the static tests, the dynamic loading seems to have affected the shear response more adversely than the slow cyclic loading. Shear cracks were more pronounced and more widely distributed. In addition, yielding of ties in the statically-tested specimen was limited to the plastic hinge region. In the dynamically-tested specimen, yielding was more spread along the length of the column. The primary factor for the difference between the response of HS and FA is believed to be the differences in the loading histories that the two specimens experienced. A detailed study of the reasons for the difference in the static and dynamic behavior is beyond the scope of the current study.

Chapter 4

Analysis of Test Results

4.1 Introductory Remarks

This chapter presents the analytical procedures and results for specimens FA and FR. The objectives of this chapter are to describe: 1) the evaluation of the validity of the analytical procedures by comparing the calculated results to the measured data, and 2) the assessment of the effect of the steel jacket retrofit by comparing experimental data from the two specimens.

Various aspects of column behavior are analyzed in this chapter. A discussion of the effect of variation of the measured axial load on the axial load-moment interaction diagrams is included. A moment-curvature analysis of several sections along the height of the column is also included. Lateral load-deflection relationships are calculated and plotted against measured values. Calculated displacement histories and hysteretic responses are compared with the recorded measurements. Also, a shear analysis using various methods of calculating shear capacity is presented and compared to shear demands recorded during testing.

Finally, the effect of the steel jacket is evaluated by comparing experimental data, including tie bar strains and other aspects of column behavior, observed in FA and FR during testing

Some prefatory remarks about the strain rates observed during testing are included for the purpose of improving the analysis.

4.2 Analysis of Specimen FA

4.2.1 Effect of Strain Rate

Table 4-1 shows the measured peak strain rates and the corresponding increases in material strength for the pre-yield run, the yield run, and the run that included the peak lateral force for all runs. Strain rates were calculated as the slope of the strain history diagram for the extreme longitudinal bar at a location near the hinge. The correlation of strain rate and increase in material strength came from empirical data presented in references 15 through 17. The maximum strain rate recorded for pre-yield and yield runs was 0.012 sec^{-1} and 0.019 sec^{-1}, respectively. Strain rates were relatively low and the increase in steel yield for the pre-yield and yield runs was below four percent. The increase in concrete strength was below fifteen percent for the pre-yield and yield runs. The peak strain rate recorded during the run of peak lateral load (run four) was 0.085 sec^{-1}. The increase in concrete strength at that instant was twenty percent. Because the impact of the increased strain rates was relatively small on the overall behavior of the column, especially prior to yield, and the impact of concrete overstrength was minimal compared to that of steel, it was deemed acceptable to use measured material properties in calculations. Values for material strengths were taken directly from tension tests on the steel, and compression tests on the concrete (Tables 2-1 and 2-2, respectively).

4.2.2 Effect of Axial Load Variation

Because the accumulator in the hydraulic line connected to the actuators that applied the axial load was not sufficiently responsive to rapid changes in displacements, there was axial load fluctuation during testing. The target axial load was 286.9 kN. However, the axial load varied between a minimum of 155.7 kN (during run seven) and a maximum of 453.7 kN (during run five) (Fig. 3-16). The axial load-moment interaction diagram was calculated for the critical section (635 mm above the footing) to determine the effect of a varying axial load (Figs. 4-1 and 4-2). The location of the critical section was determined using measured material properties according to the method described in section 4.2.3.1. Figure 4-1 shows the complete interaction diagram with the recorded range of axial loads indicated. Figure 4-2 covers the range of axial load recorded during testing (with the target axial load indicated). The peak axial load recorded during testing led to a five percent increase in moment capacity, as compared to the moment capacity corresponding to the target axial load. The minimum axial load recorded corresponded to a four-and-a-half percent decrease in moment capacity. Considering the fact that the maximum discrepancy from target axial load did not occur on every run and that the effect on moment capacity and ultimate deflection was small (five percent or less), the variation was deemed negligible and all the subsequent calculations were done assuming target axial load.

4.2.3 Load-Deflection Envelopes

4.2.3.1 Analytical Methods

The total lateral deflection at the center of loading was calculated as the sum of deflections due to flexure, shear, and bond slip, represented by:

$$\Delta_{tot} = \Delta_{flex} + \Delta_{sh} + \Delta_{bs} \qquad (4\text{-}1)$$

where:

Δ_{tot} = total deflection,
Δ_{flex} = deflection due to flexure,
Δ_{sh} = deflection due to shear
Δ_{bs} = deflection due to bond slip.

Each component of the deflection was calculated independently and then combined according to Eq. 4-1. The components of the calculated lateral deflections for specimen FA, according to Eq. 4-1, at yield and ultimate, are shown in Table 4-2 .

Flexural Deflection

Since the flexural capacity varied along the height of the column, determination of the critical section and the associated yield and ultimate forces necessitated the evaluation of the theoretical moment-curvature relationships at different cross-sections (Fig. 4-3). No overstrength effect due to strain rate was included. As expected, the smaller sections toward the top of the column had lower flexural capacities and were more ductile as evidenced by higher ultimate curvatures. As the cross-sectional area of the column became smaller toward the top of the column, the level of confinement became greater. This is because the same amount of lateral steel was confining a lessening amount of core concrete. Higher levels of confinement allowed greater ultimate curvatures to be reached.

For analysis, the confined concrete properties were calculated according to the modified Mander et al. model[18] using measured, unconfined material properties (Table 2-2). A trilinear model, based on the measured properties, was used for steel (Table 2-1). The computer program RCMC[5] was used to calculate moment-curvature relationships. The moment-curvature relationships were developed for an axial load of 286.9 kN, which was the target value.

The critical section was determined by constructing a flexural capacity profile along the height of the column based on flexural capacities determined from the RCMC analysis (Fig. 4-4). Next, a flexure demand profile along the height of the column (assuming fixed connection at bottom and pinned connection at top) was found until it was tangent to the capacity profile. The point of tangency was the critical section and the yield and ultimate loads corresponding to that critical section were the yield and ultimate loads of the column. The critical section was found to be at 635 mm above the footing. Figure 4-5 shows the theoretical moment-curvature relationship for the critical section. The middle curve is for the target axial load and the upper and lower bound curves correspond to the maximum and minimum axial loads measured during testing, respectively. In calculating the flexural behavior of this section, the two layers of longitudinal bars that terminated at 800 mm above the footing (see Fig. 2-2) were neglected due to insufficient development length. From this plot, it can be observed that flexural capacity is directly proportional to the applied axial load and that ductility (maximum curvature) varies inversely with the applied axial load. The assumed yield point is shown on the curve. The yield moments corresponding to the minimum and maximum axial loads are within eight percent of the assumed yield moment. The ultimate moments corresponding to the maximum and minimum axial loads are within five percent of the of the assumed ultimate moment and the ultimate curvatures are within ten percent.

The flexural deflection, Δ_{flex}, at the top of the column was calculated using the moment area theorem as follows:

$$\Delta_{flex} = \int_0^l \varphi \, x dx \qquad (4\text{-}2)$$

where:

φ = curvature
x = vertical distance to the center of lateral load
l = length of specimen from the top of the footing to center of lateral load.

This is the static moment of the area under the curvature profile taken about the column free end.

The curvature profiles along the column height were constructed by dividing the column into ten segments. For a given lateral load, the bending moments were evaluated at the ends of each segment. The corresponding curvatures were obtained from the calculated moment-curvature relationships (Fig. 4-3). The curvature profile along the height of each segment was assumed to vary linearly between the curvature values at the segment ends. Thus, the curvature profile of each segment represented a trapezoidal shape. The theoretical curvatures along the column height, for yield and ultimate loads, are shown in Figs. 4-6 and 4-7.

Shear Deflection

Thin shear cracks introduce added flexibility into the system that cannot be accounted for in equations that assume uncracked members. Shear deflections were found according to the shear stiffness equation developed by Park and Paulay[19] using a truss analogy. For assumed 45° shear cracks, the shear stiffness may be expressed as:

$$K_{v,45} = \frac{\rho_v}{1+4n\rho_v} E_s b_w d \qquad (4\text{-}3)$$

where:

$K_{v,45}$ = shear stiffness for an element with unit length
E_s = elastic modulus of shear reinforcement
b_w = section width perpendicular to applied shear
d = effective section depth parallel to applied shear
n = E_s/E_c (modular ratio)
E_c = elastic modulus of concrete
ρ_v = A_v/sb_w (shear reinforcement ratio)
A_v = area of shear reinforcement
s = spacing of shear reinforcement along longitudinal axis

This expression is empirical and includes the effects of shear cracks throughout the member.

Having the shear stiffness along the height, the total shear deflection, Δ_{sh}, would be:

$$\Delta_{sh} = \sum_{i=1}^{i=m} \left[\frac{L_i}{(K_{v,45})_i} \right] \qquad (4\text{-}4)$$

where m is the total number of column segments with different shear stiffnesses, and L_i and $(K_{v,45})_i$ are the length and stiffness of segment i, respectively.

Bond Slip Deflection

For the moment connection at the column-footing interface of the model, longitudinal bars must be sufficiently developed. Strains associated with stresses along tensile bar development length create additional elongation of the tensile bar at the connection interface. To calculate deflections due to bond slip, the method developed by Wehbe[5] was used. The method is based on compatibility and equilibrium of the tensile bars.

The method is applicable to reinforced concrete connections with adequate anchorage. The deformation due to bond slip, Δ_{bs}, can be found as

$$\Delta_{bs} = \theta_s L \tag{4-5}$$

where:

θ_s = bond slip rotation at the pivot point, normally the base
L = specimen length from the footing to center of loading

The bond slip rotation, θ_s, is calculated as the longitudinal bar extension of the extreme tensile bar, divided by the distance to the neutral axis. The distance to the neutral axis is determined from the moment-curvature analysis at the base of the member.

To determine the bar extension, the bond stress of reinforcing bars in tension is considered. From the 1963 American Concrete Institute code[5], the bond stress can be determined as:

$$u = \frac{20\sqrt{f'_c}}{d_b} \quad \text{(MPa)} \tag{4-6}$$

where:

u = bond stress
f'_c = concrete compressive strength, MPa
d_b = longitudinal bar diameter

For cases where the calculated steel strain is less than or equal to strain at strain hardening, the development length is:

$$l = \frac{f_s d_b}{4u} \tag{4-7}$$

where:

l = development length of extreme tensile reinforcement
f_s = calculated steel stress in extreme tensile reinforcement

The bar extension is determined as

$$\delta l = \frac{\varepsilon_s l}{2} \tag{4-8}$$

where :

δl = bar extension of extreme tensile reinforcement
ε_s = steel strain in extreme tensile reinforcement, determined from moment-curvature analysis

For cases where the strain is greater than the strain hardening, the development lengths can be found from:

$$l_1 = \frac{(f_s - f_y)d_b}{4u} \qquad (4\text{-}9)$$

$$l_2 = \frac{f_y d_b}{4u} \qquad (4\text{-}10)$$

and the bar extension is determined from:

$$\delta l = \frac{\varepsilon_y l_2}{2} + \frac{(\varepsilon_s + \varepsilon_y) l_1}{2} \qquad (4\text{-}11)$$

4.2.3.2 Results

The calculated load-deflection diagrams are shown in Figs. 4-8 and 4-9. Figure 4-8 is from a moment-curvature analysis using the program RCMC[5]. Figure 4-9 is from the non-linear dynamic simulation program RC-Shake[9]. The load-deflection relationship observed during testing is indicated on each of the graphs as a series of dots corresponding to runs one through six. Measured forces are the total peak forces (including geometrical effects of the mass rig, refer to section 3.4.2) and the corresponding displacements are the displacements that occur at the time the peak forces are recorded during different runs.

RCMC[5]

The calculated bilinear load-deflection diagram, based on a moment-curvature analysis, for specimen FA is shown in Fig. 4-8. This relationship was calculated according to Eq. 4-1, described above, for the loads corresponding to yield and ultimate curvatures of the critical section. The method for determining the critical section and the corresponding yield and ultimate loads is described in section 4.2.2.1.

The bilinear load-deflection diagram based on yield and ultimate points from the program RCMC[5] (Fig. 4-8) shows a very good correlation to experimental observations. The peak calculated lateral load was within three percent of the peak measured lateral load. And although the theoretical relationship was bilinear and the measured relationship was curvilinear, the calculated yield and ultimate points fell very close to the measured curve.

RC-Shake[9]

The load-deflection diagram based on the non-linear dynamic simulation program RC-Shake[9] is shown in Fig. 4-9. The load-deflection relationship calculated from the RC-Shake[9] model (Fig. 4-9) showed very good correlation with the measured data for the early runs prior to the development of the permanent offset at the top of the column. As the offset increased, the measured displacement grew further from the calculated displacement; the RC-Shake[9] model did not predict the permanent offset to be as large as was observed during testing. The correlation between calculated and measured lateral loads corresponding to each run was very close.

4.2.4 Displacement Histories

The response of the column was calculated using the computer program RC-Shake[9]. This program is for nonlinear response history analysis of single-degree-of-freedom systems subjected to ground motion. A lumped rotational spring accounts for flexibility of the system. The hysteretic response of the spring is represented by the Q-Hyst model[20] which accounts for stiffness degradation of reinforced concrete members.

The calculated displacement histories for each run, using program RC-Shake[9], are shown superimposed on measured displacement histories in Figs. 4-10 through 4-12. Characteristics of the column that are used as parameters in the RC-Shake analysis include: elastic stiffness, plastic stiffness, yield deflection and damping. The elastic and plastic stiffnesses and yield deflection were taken from the load-displacement relationship described in section 4.2.3. The critical damping ratio used was two percent, a common assumption for member design. The input motions were the achieved acceleration records shown in Figs. 3-5 and 3-6. These records were spliced together in the analysis.

Generally, the displacements calculated using the RC-Shake[9] model showed very good correlation with measured displacements relative to the original datum position (at the beginning of each run). However, as the permanent offset at the top of the column increased during testing, the calculated displacement history deviated from the measured displacement history. The amount of the offset between calculated and measured displacements was roughly equal to the amount of permanent offset recorded during testing. In other words, the displacement history calculated using the RC-Shake[9] model showed very good correlation to the measured displacement history except for the permanent offset at the top of the column observed during testing.

4.2.5 Hysteresis Loops

A comparison of measured and calculated hysteresis loops, for selected runs (three and six) are shown in Figs. 4-13 through 4-16. RC-Shake[9] was used to model the hysteretic behavior of the column. See section 4.2.3 for more details. Figure 4-13 shows the measured hysteresis loop for run three and Fig. 4-14 shows the calculated hysteresis loop for the same run. Run three was selected because it was the first run in which significant hysteretic energy dissipation was observed. As was seen in the load-deflection diagram (Fig. 4-4) and the displacement histories (Figs. 4-10 through 4-12), the measured and calculated loads were rather closely correlated for the RC-Shake[9] model but displacements were off by an amount roughly equal to the measured offset from datum at the column top. This effect was more pronounced in the hysteresis loops for run six (Figs. 4-15 and 4-16) because the offset was more severe.

4.2.6 Shear Capacity

The shear capacity, V_n, of the test specimen was analyzed using two of the most commonly used methods: the CALTRANS[13], and the Federal Highways Administration (FHWA)[12], and an additional method, the Modified CALTRANS developed by Wehbe, et al[5].

Previous studies[21,22] have shown that when plastic hinging occurs, the concrete shear capacity in the plastic hinge region is reduced due to the deterioration of concrete under inelastic cyclic loading. Although the shear capacity varied along the height of the column, the most severe deterioration in the core concrete was assumed to occur at the critical section which was at 635 mm above the footing. The shear capacity of this section using different methods is presented in Table 4-4. Shear demand was considered at the peak lateral force recorded during testing.

The provisions of the CALTRANS[13] method are as follows:

$$V_n = V_c + V_s \tag{4-12}$$

where:

V_c = concrete nominal shear capacity
V_s = steel nominal shear capacity

V_s is given by

$$V_s = \frac{A_v f_y d}{s} \qquad \text{for ties and cross ties} \qquad (4\text{-}13)$$

$$V_s = \frac{\pi}{2}\,\frac{A_v f_y D'}{s} \qquad \text{for spiral reinforcement} \qquad (4\text{-}14)$$

where:

A_v = area of shear reinforcement
f_y = yield strength of shear reinforcement
d = distance from extreme concrete compression fiber to the centroid of tension reinforcement, generally taken as 80% o of the total depth of the section
D' = diameter of concrete within the spiral measured to the spiral bar center
s = spacing of shear reinforcement in the direction parallel to main reinforcement

The method used by CALTRANS relates V_c to the confinement level, the attained ductility ratio, and the applied axial load as follows:

$$V_c = (F_1)(F_2)\sqrt{f'_c}\,A_e \le 0.028\ A_e \qquad \text{(MPa)} \qquad (4\text{-}15)$$

where:

F_1 = factor that depends on the level of confinement and the displacement ductility. F_1 can be found according to Eq. 4-16 but need not be less than 0.3
F_2 = factor that depends on the applied compressive axial stress. It ranges from 1.0 for zero axial stress to 1.5 for a compressive stress of 6.90 MPa
A_e = effective concrete area which is equal to 80% of the gross cross-sectional area of the column

F_1 can be found according to the following equation:

$$F_1 = \frac{\rho'' f_{yt}}{1.03} + 3.67 - \mu_\Delta \le 3.0 \quad \text{(MPa)} \qquad (4\text{-}16)$$

where:

f_{yt} = yield strength of transverse reinforcement

$$\rho'' = \frac{\text{volume of transverse reinforcement}}{\text{volume of core concrete}}$$

The FHWA[12] method is an adaptation of the method proposed by Priestley et al.[23] except that the FHWA method employs a simplified term for the shear capacity component provided by arch action. The provisions of the FHWA method are as follows:

Shear resistance is provided by three components:

$$V_n = V_c + V_t + V_p \qquad (4\text{-}17)$$

where:

V_c = shear force carried by concrete
V_t = shear force carried by truss action (lateral reinforcement)
V_p = lateral component of compression strut in the column due to the applied axial load (arch action)

In this model, the shear capacity of concrete at the critical section depends on the displacement ductility and can be obtained as follows :

$$V_c = v_c A_e = k\sqrt{f'_c}\ A_e \qquad (4\text{-}18)$$

where:

A_e = 80% of the gross cross-sectional area
k = 0.29 in MPa units when $\mu_\Delta \leq 2$, and 0.1 when $\mu_\Delta \geq 4$. Linear interpolation is used for displacement ductilities between 2 and 4.

The equations for the shear resistance provided by truss mechanism are similar to the CALTRANS equations but modified by a factor to reflect the inclination of the shear cracks. Thus, V_t is evaluated as follows:

$$V_t = \frac{A_v f_y D'}{s} \cot\theta \quad \text{for ties and cross ties} \qquad (4\text{-}19)$$

$$V_t = \frac{\pi}{2}\frac{A_v f_y d}{s} \cot\theta \quad \text{for spiral reinforcement} \qquad (4\text{-}20)$$

Priestley recommends a value of 30° for θ whereas CALTRANS equations are based on a more conservative shear crack inclination of 45° as suggested by the ACI[24] code.

The shear resistance due to arch action, V_p, in the Priestley method is found from geometrical consideration of the compression strut that forms between the flexural compression at the top and bottom of the column.

For simplification, in the FHWA method it is recommended that V_p be taken as 20% of the applied axial load.

The modified CALTRANS method[5] developed by Wehbe applies to non-circular reinforced concrete columns. The shear capacity according to the modified CALTRANS method can be calculated as follows:

$$V_n = V_c + V_s + V_p \tag{4-21}$$

where V_p is 20 percent of the applied axial load and V_s and V_c are according to the CALTRANS equations (Eqs. 4-13 and 4-15) as follows:

$$V_s = \frac{A_v f_y d}{s} \tag{4-13}$$

$$V_c = (F_1)(F_2)\sqrt{f'_c}\, A_e \le 0.028 \quad A_e \qquad \text{(MPa)} \tag{4-15}$$

The parameters in Eqs. 4-13 and 4-15 are as described above in the CALTRANS method.

These methods were developed for prismatic columns in which the longitudinal bars are perpendicular to the direction of shear and therefore have no component of force in the direction of shear. For columns with structural flares, the longitudinal steel is not strictly perpendicular to the direction of shear. The longitudinal steel is slightly inclined with respect to the vertical. Therefore, the shear capacity of columns with structural flares has an added term which is the component of the longitudinal steel force. This term is referred to as V_l. A steel stress of $1.1f_y$ was assumed in order to calculate the force in the longitudinal bars. Five extreme bars were considered to be in tension and the component of the force of these bars in the direction of shear was calculated as V_l. This force was 39.1 kN. This value was simply added to the shear capacity calculated using each of the methods described above and reported in Table 4-4.

The data presented in chapter 3 showed that the failure mode for FA was flexure/shear, and that the shear capacity of the column was reached. The measured shear, therefore, was used to evaluate the adequacy of different shear design methods.

The F_1 value from Eq. 4-16, used in the CALTRANS and modified CALTRANS methods was calculated for a displacement ductility ratio of 6.0. The same ratio was used to obtain the k value in Eq. 4-18 of the FHWA method although there is no differentiation for displacement ductilities above six. The calculated shear capacities for the FHWA method and the modified CALTRANS method were greater than the shear demand (Table 4-4), however, the CALTRANS method indicated that the shear capacity was exceeded by the shear demand. In fact, during testing wide shear cracks were observed and the ties yielded, but the failure could not be classified solely as one of shear. Table 4-4 indicates that the CALTRANS method for calculating the shear capacity is more conservative than that recommended by FHWA. For instance, when the minimum shear capacity at the critical section is considered, the calculated shear capacity using the FHWA method and the suggested 30° shear crack inclination, is more than twice the calculated shear capacity using the CALTRANS method.

Shear demand exceed calculated shear capacity by 38 kN according to the CALTRANS method. Shear capacity exceeded shear demand by 68 kN and 189 kN for the FHWA method considering shear crack inclinations of 45 and 30 degrees, respectively. The shear capacity calculated according to the modified CALTRANS method came closest to the measured shear demand on the column. According to the modified CALTRANS method, the shear capacity exceeded the shear demand by only 19 kN.

4.3 Analysis of Specimen FR

4.3.1 Effect of Strain Rate

Table 4-1 shows the measured peak strain rates and the corresponding increases in material strength for the pre-yield run, the yield run, and the run that included the peak lateral force for all runs. The correlation of strain rate and increase in material strength came from empirical data presented in references 15 through 17. The maximum strain rate recorded for pre-yield and yield runs was 0.011 sec^{-1} and 0.017 sec^{-1}, respectively. Strain rates were relatively low and the increase in steel yield for the pre-yield and yield runs was below four percent. The increase in concrete strength was below fifteen percent for the pre-yield and yield runs. The peak strain rate recorded during the run of peak lateral load (run six) was 0.071 sec^{-1}. The increase in concrete strength at that instant was eighteen percent. Because the impact on overall column behavior was small, especially prior to yield, it was deemed acceptable to use measured material properties in calculations. Values for material strengths were taken directly from tension tests on the steel, and compression tests on the concrete (Tables 2-1 and 2-2, respectively).

4.3.2 Effect of Axial Load Variation

As was seen during the testing of specimen FA, the accumulator in the hydraulic line was not sufficiently responsive and an axial load fluctuation was observed during testing of specimen FR. The target axial load was 286.9 kN. The measured variation was between 200.2 kN and 600.5 kN (both during run ten). Refer to Fig. 3-43 for the axial load history of specimen FR. A macroscopic view of the axial load-moment interaction diagram for the critical section (at the gap) of specimen FR is shown in Fig. 4-17. An enlarged view of the same diagram showing the range of axial load observed during testing is shown in Fig. 4-18. The peak axial load recorded during testing corresponded to an eight-and-a-half percent increase in moment capacity, as compared to the target axial load. The minimum axial load recorded during testing corresponded to a two-and-a-half percent decrease in moment capacity. Considering the fact that the maximum discrepancy from target axial load only occurred on the last run and that the effect on moment capacity was relatively small, calculations were done assuming the target axial load.

4.3.3 Load-Deflection Envelopes

4.3.3.1 Analytical Methods

The total lateral deflection at the center of loading was calculated as the sum of deflections due to flexure, shear, and bond slip according to Eq. 4-1. The components of the calculated lateral deflections for specimen FR, according to Eq. 4-1, at yield and ultimate, are shown in Table 4-3.

Flexural Deflection

As was the case with specimen FA, since the flexural capacity varied along the height of the column, determination of the critical section and the associated yield and ultimate forces necessitated the evaluation of the theoretical moment-curvature relationships at different cross-sections (Fig. 4-19). Increased section sizes as well as added confinement, due to grout and jacket were considered for all sections analyzed except the end sections (0 mm and 1461 mm above the footing) and the section at the gap (441 mm above the footing). No section was added at these locations but confinement was added due to the jacket. For the sections that included added section due to grout and steel jacket, the jacket was modeled as discrete longitudinal bars to account for composite action between jacket and concrete. The actual area of the jacket was decreased by a factor to account for the development length of the jacket. Table 4-6 shows the effectiveness of the jacket at various locations along the height of the jacket. In other words, the sections away from the ends of the jacket (towards the middle of the jacket segments) were given more credit (in terms of the area) for the composite action between column and jacket at that section. The sections close to the ends of the jacket were given less credit for composite action at that section. The logic is that the sections toward the ends of the jacket do not have sufficient development length to achieve full composite action. The aforementioned factor that was used to adjust the area of jacket steel was the ratio of developed stress in the jacket at a particular location (based on a 1.38 MPa bond stress between jacket and grout)[7] and the yield stress of the jacket. Because the measured strains in the jacket indicated that a bond stress greater than 1.38 MPa was achieved, this was a conservative factor that assured the contribution of the jacket was not overestimated. As expected, the locations that included added section as well as added confinement achieved greater flexural capacities. However, the locations that did not have the added section, but only had added confinement showed significant increases in ductility (ultimate curvatures). This emphasizes the effect of good confinement on the achievable ductility of a section.

For analysis, the confined concrete properties were calculated according to the modified Mander et al. model[18] using measured, unconfined material properties. A trilinear model, based on the measured properties, was used for the steel of the reinforcing bars as well as the jacket. The computer program RCMC[5] was used to calculate moment-curvature relationships. Refer to Tables 2-1 and 2-2 for material properties. From Table 2-1, the jacket stresses used in the analysis were the measured values of 383 MPa for yield and 591 MPa for ultimate. The moment-curvature relationships were developed for an axial load of 286.9 kN, which was the target axial load.

The critical section was determined by constructing a flexural capacity profile along the height of the column based on flexural capacities determined from the RCMC analysis (Fig. 4-20). Next, a flexure demand profile along the height of the column (assuming fixed connection at bottom and pinned connection at top) was found until it was tangent to the capacity profile. The point of tangency was the critical section and the yield and ultimate loads corresponding to that critical section were the yield and ultimate loads of the column idealized as a whole. As expected, the critical section was found to be at the gap in the jacket (441 mm above the footing). Figure 4-21 shows the theoretical moment-curvature relationship for the critical section. The middle curve is for the target axial load and the upper and lower bound curves correspond to the maximum and minimum axial loads measured during testing, respectively. In calculating the flexural behavior of this section, the two layers of longitudinal bars that were terminated at 533 mm above the footing (see Fig. 2-2) were neglected due to insufficient development length. From Fig 4-21, it can be observed that flexural capacity increases with increasing axial load and that ductility (maximum curvature) varies inversely with the applied axial load. The assumed yield point is shown on the curve. The yield moments corresponding to the minimum and maximum axial loads are within seven percent of the assumed yield moment. The ultimate moments corresponding to the maximum and minimum axial loads are within eight-and-a-half percent of the of the assumed ultimate moment and the ultimate curvatures are within three percent.

The flexural deflection, Δ_{flex}, at the top of the column was calculated using the moment area theorem (Eq. 4-2).

Similar to the analysis of specimen FA, the curvature profiles along the column height were constructed by dividing the column into ten segments. For a given lateral load, the bending moments were evaluated at the ends of each segment. The corresponding curvatures were obtained from the theoretical moment-curvature relationships. The curvature profile along the height of each segment was assumed to vary linearly between the curvature values at the segment ends. Thus, the curvature profile of each segment represented a trapezoidal shape. The theoretical curvatures along the column height, for yield and ultimate loads, are shown in Figs. 4-22 and 4-23.

Shear Deflection

To account for the shear deformations, Eqs. 4-3 and 4-4 presented in section 4.2.2.2 were used. To account for the contribution of the jacket to the shear stiffness, the shear reinforcement ratio in Eq. 4-3 was increased. This equation includes the effects of shear cracks throughout the member. Note in Table 4-3 that shear deformation accounted for twenty-one percent and four percent of total displacement at yield and ultimate, respectively.

Bond Slip Deflection

To account for the elongation of the tensile bars at the column-footing interface equations 4-5 through 4-11 were used. See section 4.2.2.3 for more explanation. Table 4-3 shows that bond slip deformation accounted for five percent and one percent of total displacement at yield and ultimate, respectively.

4.3.3.2 Results

Two calculated load-deflection relationships using RCMC[5] and RC-Shake[9] are shown in Figs. 4-24 and 4-25 respectively. For comparison, the measured load-deflection relationships are shown as a series of points on each of these graphs. The points correspond to each of the runs one through nine. Measured forces are the total peak forces (including geometrical effects of the mass rig, refer to section 3.5.2) and the corresponding displacements are those measured at the time the peak forces occurred.

RCMC[5]

The calculated bilinear load-deflection diagram, based on a moment-curvature analysis, for specimen FR is shown in Fig. 4-24. The two points on this curve that were calculated were the yield and ultimate points that corresponded to the yield and ultimate loads of the critical section. See section 4.2.2.1 for the procedure to determine the critical section and the corresponding yield and ultimate loads.

The bilinear load-deflection diagram, based on yield and ultimate points from the program RCMC[5] (Fig. 4-24), shows a very good correlation to experimental observations for the yield point. The yield point is on the measured curve. The load corresponding to the ultimate point was very close to the measured ultimate load (within one percent), however the ultimate deflection was overestimated considerably.

RC-Shake[9]

The load-deflection diagram based on the non-linear dynamic simulation program RC-Shake[9] is shown in Fig. 4-25. As was the case with the specimen FA, the load-deflection relationship for specimen FR, calculated from the RC-Shake[9] model, showed high correlation to the measured data for the early runs prior to the development of the permanent offset at the top of the column. As the offset increased, the measured displacement grew further from the calculated displacement; the RC-Shake[9] model did not predict the permanent offset to be as large as was observed during testing.

4.3.4 Displacement Histories

The response of the column was calculated using the computer program RC-Shake[9]. This program for calculating nonlinear response history analysis of single-degree-of-freedom systems is described in section 4.2.3.

The calculated displacement histories for each run, using program RC-Shake[9], are shown superimposed on measured displacement histories in Figs. 4-26 through 4-29. Characteristics of the column that are used as parameters in the RC-Shake analysis include: elastic stiffness, plastic stiffness, yield deflection and damping. The elastic and plastic stiffnesses and yield deflection were taken from the load-displacement relationship described above in section 4.3.2. The critical damping ratio used was two percent. The input motions were the achieved acceleration records shown in Figs. 3-5 and 3-6.

For the pre-yield and yield runs (one and two) RC-Shake[9] significantly overestimated the displacements. This is because the curvilinear load-deflection diagram was modeled by a bilinear, elasto-plastic load-deflection diagram. The slope of the elastic portion of the bilinear model was the average slope of the initial portion of the curvilinear load-deflection diagram. Therefore, prior to yielding, the stiffness of the actual column was significantly higher than that of the model. In addition, the damping of the initially uncracked, unyielded column was greater than the assumed two percent of the model. This was expected because the RC-Shake model is designed to model non-linear behavior and is not a model for pre-yield behavior. After yielding, the calculated displacement history correlated very closely to the measured displacement history except for the permanent offset at the column top. This was the same as was seen in specimen FA. As the permanent offset at the top of the column grew, the offset between the calculated and measured displacement histories grew by roughly an equal amount. In summary, the displacement histories calculated using the RC-Shake model showed very good correlation with the measured displacements for post-yield runs, except for the permanent offset observed during testing.

4.3.5 Hysteresis Loops

A comparison of the measured and calculated hysteresis loops, for selected runs (three, six, and nine) are shown in Figs. 4-30 through 4-35. RC-Shake[9] was used to model the hysteretic behavior of the column. See section 4.3.3 for more details. Figure 4-30 shows the measured hysteresis loop for run three and Fig. 4-31 shows the calculated hysteresis loop for the same run. Run three was selected because it was the first run in which significant hysteretic energy dissipation was observed. However, the RC-Shake model did not correlate well with the hysteretic behavior observed during run three. The RC-Shake model indicated some minimal hysteretic energy dissipation beginning to occur, but the curves generally remained very narrow and essentially elastic. As was seen in the load-deflection diagram (Fig. 4-20) and the displacement histories (Figs. 4-26 through 4-29), measured and predicted loads were generally closely correlated for the RC-Shake[9] model but displacements were off by an amount roughly equal to the measured offset from datum at the column top. This effect is more pronounced in the hysteresis loops for runs six and nine (Figs. 4-32 through 4-35) because the offset was more severe. The model for run six showed wide hysteretic loops and significant energy dissipation, but underestimated the measured peak force and displacement by twenty-four and sixteen percent respectively. This may be an indication that the stiffness of the actual column had been significantly degraded by this time. The RC-Shake model showed high correlation for the peak load of run nine. It was within one percent of the peak measured load. However, the peak displacement was underestimated by 46 mm, roughly equal to the permanent offset from datum at the column top at the beginning of run nine which was 49 mm.

4.3.6 Shear Capacity

The shear capacity, V_n, of the test specimen was analyzed using two of the most commonly used methods: the CALTRANS[13], and the Federal Highways Administration (FHWA)[12], and an additional method, the Modified CALTRANS developed by Wehbe et al[5].

The most severe deterioration in the core concrete was assumed to occur at the critical section which was at the gap in the jacket (441 mm above the footing). The shear capacity of this section for the different methods is presented in Table 4-5. Note that specimen FR failed in flexure and that the shear capacity was not reached. Therefore, calculated shear values were compared to an estimated shear capacity of the column. The estimated shear capacity was extrapolated from the peak measured lateral load and a reserve capacity. The reserve capacity was based on average tensile stresses attained in the lateral steel and average horizontal tensile stresses attained in the jacket steel during the run of peak lateral load. Average strains were obtained from recorded strain data in the vicinity of the gap at 533 mm above the footing. These strains (567 microstrain for ties and 643 microstrain for the jacket) were compared to measured yield stresses and their reserve capacity in terms of shear applied to the column was calculated. This extrapolated reserve capacity was added to the peak measured lateral load to obtain the estimated shear capacity of the column.

The provisions of the CALTRANS method are outlined in Eqs. 4-12 through 4-16 in section 4.2.5. The provisions of the FHWA method are outlined in Eqs. 4-17 through 4-20. The provisions of the modified

CALTRANS method are shown in Eqs. 4-12 through 4-15. The component of the longitudinal bar forces in the direction of shear, V_l, was calculated as described in section 4.2.6 for specimen FA. This force was 48.5 kN. F_1 in Eq. 4-16 and k in Eq. 4-18 were calculated for a displacement ductility of 9.7. For all of the methods the calculated shear capacity was greater than the estimated shear capacity. This may have been due to an anomaly in the stress pattern near the edges of the jacket. Recorded jacket stresses at other locations farther away from the edges of the jacket were considerably lower. For this reason, the estimated shear capacity of the column may have been underestimated. The shear capacity calculated according to the FHWA method with a crack inclination of 30 degrees was much more than the shear capacity calculated according to the CALTRANS and modified CALTRANS methods. The FHWA method using a crack inclination of 30 degrees gave a shear capacity comparable to the CALTRANS and modified CALTRANS methods. The FHWA method has no factor that gives credit to the concrete component of shear capacity for high levels of confinement such as those seen in jacketed columns. Some of the added shear capacity comes from the added confinement provided by the jacket. While the CALTRANS and modified CALTRANS methods include the F_1 factor of Eq. 4-15 that takes into account the level of confinement, the FHWA method has no such factor.

4.4 Effect of Steel Jacket

The retrofit appears to have prevented longitudinal bar buckling even though specimen FR was subjected to larger forces and displacements than specimen FA was. Bar fracture in the retrofitted specimen (FR) was observed in fifteen bars on the tension side of the column (Fig. 3-39). They failed due to low-cycle fatigue and no buckling was observed. All bar fractures were within the gap section. In contrast, in the as-built specimen (FA) bar fracture due to buckling was observed in three bars (Fig. 3-13). No bars failed solely due to low-cycle fatigue, all bar fractures were preceded by buckling. In addition, the critical section was shifted down to the gap at 441 mm above the footing in FR. All bar fractures in FR were at the gap. Bar fractures in FA were at 394 mm, 419 mm, and 533 mm above the footing.

In specimen FR, the spalling and plastic hinging was confined to a relatively small area in the vicinity of the gap in the steel jacket. The placement of the jacket decreased the length of damage, and did not allow the spread of plastic hinging. In contrasting the as-built and retrofitted specimens, the plastic hinge lengths were different and the longitudinal bars failed differently.

The main effect of the jacket was that it increased the shear capacity of the column. Fewer shear cracks were observed in the retrofitted specimen, and the strains in the lateral reinforcement were significantly decreased. This is shown in Figs. 4-36 through 4-43, in which the cross tie and perimeter tie strains for FA and FR are plotted against the peak effective table acceleration. These are the tie sets that are from 279 mm to 800 mm above the footing and cover the length of the plastic hinge zone. From these figures, it is evident that the retrofitted specimen had generally lower strains in the lateral reinforcement than the as-built specimen especially at large accelerations. The plots showing perimeter ties show this trend much better than the plots showing the cross ties. This is attributable to the slippage experienced by the cross ties in FA (see section 3.4.4). Due to bond slippage they did not develop the strains that would normally have been expected.

The steel jacket remained nearly elastic. Aside from the localized strain measured near the gap in the retrofit, the maximum measured horizontal strain was 22 percent of yield. As mentioned previously, specimen FR had no ties yield prior to failure whereas in FA four ties yielded prior to failure, and four ties fractured.

To evaluate the effect of the retrofit on the stiffness and other characteristics of the load deflection diagram, the measured peak loads and associated displacements for each run are plotted in Fig. 4-44. The idealized elasto-plastic load-deflection diagrams are shown superimposed on the same plot. It can be seen from the figure that the jacket changed the initial stiffness somewhat. This is due to the increased section sizes because of grout and jacket. Based on the point on Fig. 4-44 that corresponds to run one, the initial stiffness increased by fifty-eight percent for the retrofitted specimen as compared to the as-built. The initial stiffness for FA was 10.83 kN/mm and the initial stiffness for FR was 17.17 kN/mm. Based on the yield point established by the idealized elasto-plastic load-deflection diagram the initial stiffness increased by fifty-nine percent. After yielding, the retrofitted specimen continued to increase in lateral load, whereas the as-built specimen reached a maximum load quickly after yielding. Also, it can be seen that the displacement ductility was significantly altered by the retrofit. Based on the points of the measured load-deflection diagram (Fig. 4-44) established by the peak loads and associated deflections for each run, the displacement ductilities were 6.0 and 9.7 for specimens FA and FR, respectively, as described in section 3.6. This represented an increase of sixty-two percent. Based on the idealized elasto-plastic load deflection diagrams of Fig. 4-44, the displacement ductilities were 4.5 and 6.2 for specimens FA and FR, respectively. This represents an increase of thirty-eight percent. Both specimens began to lose lateral load capacity at a deflection of about 75 mm.

The primary reason for the prevention of longitudinal bar buckling and decrease in lateral steel strains in FR was the added confinement provided by the jacket. To isolate and further evaluate the effect of the added confinement, a moment-curvature analysis was done at the gap section (Fig. 4-45). One curve represents the moment-curvature relationship for the section at the gap considering the added confinement, the other neglects the added confinement. Because the only difference between the two curves is the added confinement of the jacket, changes in the moment-curvature relationship may be attributed to the increase in confinement. It can be seen from the plot that the initial stiffness of the section, prior to yielding was unaltered by the added confinement. After yielding, the inelastic slope of the section with added confinement was greater. The most significant effect of the added confinement was the increase in ductility of the section. Ultimate curvature of the section with increased confinement was 150 percent greater than the section without added confinement.

4.5 Concluding Remarks

As was shown in the presentation and analysis of the data, the steel jacket was effective in preventing shear failure and improving the ductility of the retrofitted column as compared to the as-built specimen. The retrofit caused the initial stiffness to increase due to the added section provided by the grout and jacket. Accompanying an increase in stiffness is an increase in the seismic demand placed on the column. Stiffer members 'attract' more seismic forces. However, the jacket can be designed to resist the added forces. The jacket was designed using FHWA[12] provisions. The satisfactory performance of the retrofit indicates that the FHWA retrofit design method can lead to an improved seismic behavior under strong earthquakes.

Chapter 5

Summary and Conclusions

5.1 Summary

The primary objective of this study was to evaluate the seismic performance of as-built, flared bridge columns from bridge I-1250 located on U.S. 395 in Reno, Nevada and a steel jacket retrofit of these columns.

Many reinforced concrete bridges in the western United States are supported by columns with architectural or structural flares. Flared bridge columns have been used in Nevada since the 1970's. Recent studies[21,22,23] of columns with architectural flares that suffered shear failures in the 1994 Northridge earthquake concluded that architectural flares have adverse effects on the seismic performance of bridge columns. Although structural flares are also commonly used in bridge piers, there was a particular lack of research assessing the vulnerability of such columns to high seismic loading.

In response, analytical studies[3,24] assessing the vulnerability of columns with structural flares were conducted at the University of Nevada, Reno. Four existing bridges, in northern Nevada, supported by parabolic structural flares were studied. Experimental studies[1,2] on verification and remediation of the vulnerability to high seismic loads were conducted on two flared column specimens from one of the prototype bridges. The columns were subjected to static, cyclic loads. The selected bridge (I-1250) had columns with the lowest shear capacity-to-demand ratio (most vulnerable) among the analyzed prototypes. The columns of the selected prototype had identical lateral steel but different longitudinal reinforcement. The specimens represented the prototype columns with the highest and lowest longitudinal steel ratios. These two tests[1,2] showed the seismic performance of the columns with the low steel ratio to be adequate. The test on the high steel ratio columns raised concerns regarding the shear capacity and ductility.

This study was a continuation of the two previous static tests[1,2]. The columns with the high steel ratio were studied using a state-of-the-art shake table at the University of Nevada, Reno. Two 30 percent scale specimens, one representing the as-built details and one outfitted with a steel jacket retrofit were constructed and tested. The steel jacket of the retrofitted specimen incorporated an intermediate gap at a location that was chosen to coincide with the hinge location providing maximum ductility as indicated by results that were verified in the previous static tests[2]. The two columns were subjected to the Sylmar record of the January 17, 1994 Northridge earthquake. The testing program consisted of multiple motions with gradually increasing intensity of shaking. Testing was performed in the strong direction under nominally constant axial load. Test data, including forces, displacements, strains, curvatures, and other aspects of behavior observed during testing, were used to evaluate the performance of the specimens.

In addition to the experimental study, analytical studies were performed to: 1) explain the behavior of the column observed during testing, 2) evaluate the validity of the analytical procedures by comparing the calculated results to the measured data, and 3) assess the effect of the steel jacket retrofit by comparing experimental data from the two specimens. The analysis included: estimating lateral load-deflection relationships, calculating displacement histories and hysteretic responses, and performing a shear analysis using various methods of calculating shear capacity.

Considering the experimental results, the steel jacket was effective in preventing shear failure and improving the ductility of the retrofitted column as compared to the as-built specimen. In addition, the satisfactory performance of the retrofit indicated that the FHWA[7] retrofit design method can lead to an improved seismic behavior under large seismic loads.

5.2 Conclusions

From the testing and analysis of the specimens, the following conclusions were made:

1. For columns with structural parabolic flares (majority of the longitudinal steel is placed along the flare), the plastic hinge may form along the flare at a section which does not necessarily coincide with the location of maximum bending moment. This is due to the fact that parabolic flares increase the effective depth of the flare reinforcement at a rate that is higher than the rate of moment increase.

2. Flared columns with a majority of the longitudinal reinforcement placed along the flare could fail in shear under large seismic loads. The longitudinal bar buckling and yielding and fracture of ties observed in the as-built specimen indicated that the confinement and shear steel was inadequate in the prototype bridge.

3. It was demonstrated that the retrofit provided the necessary shear capacity to avoid shear failure. The maximum hoop strains in the steel jacket were

significantly below yielding, indicating that there was an acceptable reserve of shear capacity.

4. The retrofit drastically reduced stains in the column transverse reinforcement especially at large accelerations. In the as-built specimen there was extensive yielding of the ties. In addition, four ties yielded prior to failure and four ties fractured upon failure. The as-built column failed during earthquake Run 7 (Table 3.1). In the retrofitted specimen there was no yielding of ties prior to failure and no fracture of ties upon failure. This column failed during Run 10 (Table 3.1).

5. The retrofit increased the displacement ductility. Based on the points of the measured load-deflection envelopes, the displacement ductility was increased by over sixty percent, from 6.0 to 9.7, for the retrofitted specimen as compared to the as-built specimen. Based on the idealized elasto-plastic load deflection envelopes, the calculated displacement ductility was increased by thirty-eight percent, from 4.5 to 6.2. In addition, increased ductility associated with shifting the gap in the steel jacket to the location coinciding with the hinge location providing maximum ductility as indicated by the results of previous static tests[1,2] was verified.

6. The placement of the steel jacket retrofit significantly altered the seismic response of the column. It changed the mode of failure from flexure-shear to one of pure flexure. In the as-built specimen, longitudinal bars buckled and fractured due to low-cycle fatigue and there was extensive yielding of ties. In the retrofitted specimen, even though the loads were much higher, longitudinal bar buckling was prevented by the added confinement of the jacket. The gap placed in the jacket was sufficiently small to prevent bar buckling, instead longitudinal bars fractured on the tension side of the column.

7. The retrofit decreased the length of damage and did not allow the spread of plastic hinging. Hinging was well-spread in the as-built column, whereas hinging in the retrofitted column was confined to a relatively small area in the vicinity of the gap in the steel jacket. Longer plastic hinge lengths can help spread energy dissipation over a larger area. However, repair of long plastic hinges is more costly. The steel jacket retrofit allowed for sufficient energy dissipation while preventing spread of damage.

8. The retrofit increased the initial stiffness of the column by sixty percent and increased column forces. However, the reserve capacity of the jacket was more than adequate to resist the added forces.

9. In contrast to the static tests, the dynamic loading seems to have affected the shear response more adversely than the slow cyclic loading. Shear cracks were more pronounced and more widely distributed. In addition, yielding of ties under static loads was limited to the plastic hinge region, whereas yielding of ties under the dynamic loads was more spread along the length of the column.

10. The moment-area theorem used in conjunction with a moment-curvature analysis using the computer program RCMC[1] produced good results for modeling the load-deflection diagram especially for the yield point.
11. The non-linear dynamic simulation program RC-Shake[4] produced good results for modeling post-yield displacement histories. However, it did not accurately model the progressively increasing permanent offset observed at the top of the column during testing. The model generally underestimated measured peak loads.

12. The testing of the as-built specimen showed that the CALTRANS[8] method for calculating the shear capacity of bridge columns that are not jacketed tends to be conservative, generally underestimating the shear capacity. On the other hand, the FHWA[7] method appears to be unconservative because it overestimates the shear capacity of the unjacketed columns. Based on the experimental results, the modified CALTRANS method[1] gives a reasonably accurate estimate of the shear capacity.

5.3 Recommendations

Based on the experimental and analytical results presented in this study, the following recommendations are made:

1. Considering the poor seismic behavior and significant shear distress in the as-built specimen, it is recommended that the shear capacity of the prototype columns be increased.

2. The steel jacket retrofit with an intermediate gap showed good seismic behavior and a substantial increase in ductility. Therefore, a jacket with a gap is recommended for design. The presence of the gap is expected to improve the seismic response in all flared columns that are likely to form plastic hinges away from the column ends. Generally this situation is encountered when the base of the column is detailed to behave as a hinge. In flared columns with moment connections at both ends, plastic hinges form at the ends, and a gap in the jacket is not recommended.

In columns of Bridge 1250, the location of the gap when converted to the full-scale dimensions of the prototype column would be at 1500 mm below the superstructure soffit. The vertical gap length would be 100 mm.

3. Based on the satisfactory performance of the column with the steel jacket, the FHWA[7] method for design of steel jackets is recommended for design.

REFERENCES

1. Priestley, M.J.N., Seible, F., and Uang, C.M., *"The Northridge Earthquake of January 17, 1994 - Damage Analysis of Selected Bridges,"* Report No. SSRP-94/06, Department of Applied Mechanics and Engineering Sciences, University of California, San Diego, La Jolla, California, February,1994.

2. *"1994 Northridge Earthquake: Performance of Structures, Lifelines, and Fire Protection Systems,"* United States Department of Commerce, NIST Special Publication 862, May, 1994.

3. Wehbe, N.I., and Saiidi, M., *"Effects of Confined Core on Seismic Vulnerability of Reinforced Concrete Columns with Structural Flares,"* ACI Special Publication 187, Seismic Response of Concrete Bridges, 1999, pp. 275-298.

4. Wehbe, N., and Saiidi, M., *"Effects of Confined Core on Seismic Vulnerability of Reinforced Concrete Columns with Structural Flares,"* ACI Special Publication, Seismic Response of Concrete Bridges, 1998.

5. Wehbe, N.I., Saiidi, M., and Sanders, D.H., *"Effects of Confinement and Flares on the Seismic Performance of Reinforced Concrete Bridge Columns,"* Report No. 97-2, CCEER. Department of Civil Engineering, University of Nevada, Reno, September, 1997.

6. Caywood, C., Saiidi, M., and Sanders, D.H., *"Seismic Retrofit of Flared Bridge Columns with Steel Jackets,"* Report No. 99-1, CCEER. Department of Civil Engineering, University of Nevada, Reno, June, 1998.

7. Chai, Y.H., *"An Analysis of the Seismic Characteristics of Steel-Jacketed Circular Bridge Columns,"* Earthquake Engineering and Structural Dynamics, Vol. 25, pp. 149-161, 1996.

8. Sanchez, A.V., Seible, F., and Priestley, M.J.N., *"Solutions to Seismic Performance Problems of Flared Bridge Columns,"* Proceedings of the Second Symposium on Practical Solutions for Bridge Strengthening an Rehabilitation, The National Science Foundation, Kansas City, Missouri, March 24-25, 1997, pp. 93-102.

9. Laplace, P., Sanders, D.H., Douglas, B., and Saiidi, M., *"Shake Table Testing of Flexure Dominated Reinforced Concrete Bridge Columns,"* M.S.C.E. Thesis. Department of Civil Engineering, University of Nevada, Reno, August, 1999.

10. American Concrete Institute, *"Building Code Requirements for Structural Concrete,"* Farmington Hills, Michigan, 1963.

11. Gavin, N.L., *"Bond Characteristics of Model Reinforcement,,"* Report No. UILU-ENG-766-2007, Civil Engineering Studies, Structural Research Series No. 427, University of Illinois at Urbana-Champaign, Urbana, Illinois, April, 1976.

12. Federal Highway Administration, *"Seismic Retrofitting Manual for Highway Bridges,"* Publication No. FHWA-RD-94-052, May 1995, Georgetown Pike, Mclean, Virginia 22101-2296.

13. California Department of Transportation, *"Memo to Designers 20-4, Attachment B,"* Sacramento, California, March, 1995, pp. 11-13.

14. *"Spect,"* Computer Subroutine written in FORTRAN, taken from Course Number CE 479/679: Earthquake Engineering, Department of Civil Engineering, University of Nevada, Reno, Spring, 1998.

15. Kulkarni, S.M., and Shah, S.P., *"Response of Reinforced Concrete Beams at High Strain Rates,"* ACI Structural Journal, Vol. 95, No. 6, November-December 1998, pp. 705-715.

16. Shimazaki, Kazushi, and Wada, Akira, *"Dynamic Analysis of a Reinforced Concrete Shear Wall with Strain Rate Effect,"* ACI Structural Journal, Vol. 95, No. 5, September-October 1998, pp. 488-497.

17. Fu, H.C., Erki, M.A., and Seckin, M., *"Review of Effects of Loading Rate on Reinforced Concrete,"* ASCE Journal of Structural Engineering, Vol. 117, October-December 1991, pp. 3660-3679.

18. Mander, J.B., Priestley, M.J.N., and Park, R., *"Theoretical Stress-Strain Model for Confined Concrete Columns,"* ASCE Journal of Structural Engineering, Vol. 114, No. 8, August 1988, pp. 1804-1826.

19. Park, R., and Paulay, T., *"Reinforced Concrete Structures,"* John Wiley & Sons, New York, 1975.

20. Saiidi, M., *"Hysteresis Model for Reinforced Concrete,"* Journal of Structural Division, ASCE, Vol. 108, No. ST5, May 1982, pp. 1077-1085.

21. Ang, B.G., Priestley, M.J.N., and Paulay, T., *"Seismic Shear Strength of Circular Reinforced Concrete Columns,"* ACI Structural Journal, January-February 1989, pp. 45-59.

22. Wong, Y.L., Paulay, T., and Priestley, M.J.N., *"Response of Circular Reinforced Concrete Columns to Multi-Directional Seismic Attack,"* ACI Structural Journal, March-April 1993, pp. 181-191.

23. Priestley, M.J.N., Verma, R., and Xiao, Y., *"Seismic Shear Strength of Reinforced Concrete Columns,"* ASCE Journal of Structural Engineering, Vol. 120, No. 8, August 1994, pp. 2310-2329.

24. American Concrete Institute Committee 318, *"Building Code Requirements for Reinforced Concrete Columns to Multi-Directional Seismic Attack,"* ACI Structural Journal, March-April 1993, pp. 181-191.

TABLES

Table 2-1 Tensile Properties of Steel

Steel Location	Yield Strain	Yield Stress (MPa)	Ultimate Strain	Ultimate Stress (MPa)
Longitudinal	0.0023	459	0.15	716
Transverse	0.0022	447	0.14	517
Jacket	0.0019	383	0.16	591

Table 2-2 Measured Compressive Properties of Concrete

Concrete Location	Compressive Strength (MPa)					
	7-day	14-day	21-day	28-day	FA Test Day	FR Test Day
Footing	22.2	28.9	36.5	42.1	----	----
Column	27.9	31.0	33.6	36.4	37.6	39.6
Grout	----	----	----	----	----	65.0

Table 2-3 Testing Program

Run	FA	FR
A	Quick Release	Quick Release
1	0.20 Scale	0.20 Scale
2	0.40 Scale	0.40 Scale
B	Quick Release	Quick Release
3	0.75 Scale	0.75 Scale
4	1.00 Scale	1.00 Scale
5	1.25 Scale	1.25 Scale
6	1.50 Scale	1.50 Scale
C	Quick Release	Quick Release
7	1.75 Scale	1.75 Scale
8	N/A	2.00 Scale
9	N/A	2.25 Scale
10	N/A	2.50 Scale

Table 3-1 Peak Accelerations (g)

	Run 1	Run 2	Run 3	Run 4	Run 5	Run 6	Run 7	Run 8	Run 9	Run 10
Target	0.121	0.243	0.455	0.607	0.758	0.910	1.062	1.213	1.365	1.517
FA	0.110	0.208	0.431	0.591	0.819	1.013	1.217	n/a	n/a	n/a
FR	0.073	0.167	0.406	0.503	0.630	0.698	0.865	0.997	1.134	1.237

Table 3-2 Peak "Effective" Accelerations (g)

	Run 1	Run 2	Run 3	Run 4	Run 5	Run 6	Run 7	Run 8	Run 9	Run 10
Target	0.188	0.376	0.705	0.941	1.176	1.411	1.646	1.881	2.116	2.352
FA	0.170	0.322	0.668	0.916	1.270	1.571	1.886	n/a	n/a	n/a
FR	0.113	0.259	0.630	0.780	0.976	1.081	1.341	1.545	1.757	1.918

Table 3-3 Frequency Analysis over Course of Testing

	Specimen FA					Specimen FR				
	Period (sec)	Spectral Acceleration, Table (g)		Peak Acc. Recorded (g)	Period (sec)	Period (sec)	Spectral Acceleration, Table (g)		Peak Acc. Recorded (g)	Period (sec)
	Method A	Achieved	Target	Link	Method B	Method A	Achieved	Target	Link	Method B
Snapback 1	0.40	n/a	n/a	n/a	n/a	0.20	n/a	n/a	n/a	n/a
Run 1	0.40	0.24	0.24	0.21	0.61	0.30	0.16	0.26	0.15	0.33
Run 2	0.40	0.45	0.49	0.39	0.58	0.40	0.39	0.49	0.45	0.35
Snapback 2	0.50	n/a	n/a	n/a	n/a	0.30	n/a	n/a	n/a	n/a
Run 3	0.55	0.71	0.95	0.53	0.62	0.40	0.68	0.92	0.62	0.34
Run 4	0.55	0.85	1.27	0.53	0.65	0.55	0.93	1.27	0.65	0.64
Run 5	0.55	1.04	1.58	0.50	0.68	0.55	1.10	1.58	0.70	0.65
Run 6	0.55	1.25	1.90	0.47	1.78	0.55	1.14	1.90	0.73	0.65
Snapback 3	0.50	n/a	n/a	n/a	n/a	0.50	n/a	n/a	n/a	n/a
Run 7	0.55	1.47	2.22	0.36	(a)	0.55	1.28	2.22	0.70	0.67
Run 8	n/a	n/a	n/a	n/a	n/a	0.55	1.42	2.53	0.67	0.69
Run 9	n/a	n/a	n/a	n/a	n/a	0.55	1.56	2.85	0.65	1.75
Run 10	n/a	n/a	n/a	n/a	n/a	0.55	1.74	3.17	0.54	(a)

(a) Period not measured due to deterioration of specimen

Table 3-4 Peak Strains (Specimen FA, longitudinal)

Strain Gage	Run						
	1	2	3	4	5	6	7
	Peak Lateral Force (kN)						
	97.5	180.2	255.3	262.9	254.1	243.3	200.4
	Peak Strain (microstrain)						
1 Tens.	21539	41100	41100	41100	41100	41100	41100
Comp.	-3502	-4290	-3440	-2990	-1710	--	--
2	1380	2300	5090	6040	1390	--	--
	-1030	-2130	-10300	-18900	-31200	-41200	-41200
3	1220	2010	6140	7040	41300	41300	41300
	-842	-1650	-8350	-9650	-8960	-41300	-41300
5	1230	2130	4860	6710	6390	6690	6730
	-1070	-2030	-4700	-5460	-5910	-5650	-4840
6	1140	1900	3670	7480	6110	5370	41300
	-915	-1640	-5240	-6020	-6170	-5180	-3200
7	1590	3630	9160	17900	25300	27700	34300
	-654	-843	-1590	-1740	-7	--	--
8	1430	2450	4820	6130	6280	7220	9750
	-941	-1930	-5560	-6680	-7020	-7640	-6980
9	1100	1880	2700	5760	5460	1620	2060
	-602	-1240	-2290	-3100	-2410	-2740	--
10	1310	2850	8290	2350	40900	40900	40900
	-678	-1070	-2320	-1900	-1150	-6790	-10
13	887	1480	2160	2690	2670	2770	2690
	-506	-1240	-1920	-2140	-2120	-1970	-1570
14	1100	2450	7330	8750	10600	12600	15700
	-285	-687	-761	--	--	--	--
15	912	1510	2160	2560	2510	2570	2460
	-368	-1010	-1510	-1600	-1560	-1470	-1220

* Gages 4, 11, and 12 malfunctioned

Table 3-5 Peak Strains (Specimen FA, transverse)

Strain Gage	Run						
	1	2	3	4	5	6	7
	Peak Lateral Force (kN)						
	97.5	180.2	255.3	262.9	254.1	243.3	200.4
	Peak Strain (microstrain)						
16 Tens.	147	55	764	1070	885	659	576
Comp.	--	-38	--	--	--	--	-494
17	1480	409	988	2030	2170	1620	41700
	--	--	--	--	--	--	-7960
18	294	181	530	1380	1440	2150	41800
	--	-11	-15	-104	-119	-123	-27
19	618	588	576	1490	2180	2560	2370
	--	--	--	--	--	--	--
20	218	179	578	773	866	820	694
	--	--	--	--	--	--	--
21	420	420	924	1300	1300	2250	4010
	--	--	--	--	--	--	--
23	425	446	1020	1510	1560	1900	5870
	--	--	-22	--	--	--	--
24	315	202	1060	2640	3120	6800	41500
	--	--	--	--	--	--	--
25	352	418	276	365	41500	41500	41500
	--	--	--	--	-8580	-8500	-8490
26	387	304	759	887	558	478	901
	--	--	-39	--	--	--	--
27	329	234	712	1050	1190	1450	2140
	--	--	--	--	--	--	--
28	226	176	297	769	1030	1180	41700
	--	--	--	--	--	--	-5520
29	199	176	1030	546	467	439	294
	--	--	-119	-345	-323	-250	-516

* Gage 22 malfunctioned

Table 3-6 Peak Strains (Specimen FR, longitudinal)

Strain Gage	Run									
	1	2	3	4	5	6	7	8	9	10
	Peak Lateral Force (kN)									
	103.0	206.9	289.1	307.4	336.9	359.0	350.1	339.5	334.8	284.7
	Peak Strain (microstrain)									
1 Tens.	596	2859	12655	14526	19869	19900	41413	41413	41413	41413
Comp.	-1130	-1306	-1768	-1529	-287	--	-784	-4813	-41440	-41440
3	1350	2533	10304	11292	11784	15209	16791	18002	19148	41519
	-301	-701	-1982	-2172	-2106	-2433	-2998	-3456	-4266	-16719
5	917	1765	2093	2263	2238	2404	2537	2622	41088	41088
	-204	-496	-1090	-1283	-1596	-1823	-1873	-1898	-8665	-9946
6	195	985	1480	1798	1827	2071	2214	2321	2446	41348
	-724	-938	-1428	-1573	-1826	-1990	-2024	-2036	-2067	-1837
7	1320	2766	10388	10875	15961	18419	16780	18308	41827	41827
	-616	-1196	-817	-881	-758	-1005	-42	--	-1493	-3055
8	116	773	1259	2486	2261	2850	3082	3127	3092	2189
	-825	-1178	-1542	-2467	-3863	-4835	-6093	-8538	-12635	-41290
9	1040	2139	2939	7363	7948	9615	8370	3852	3484	2850
	-326	-631	-1406	-1683	-3022	-4981	-3472	-3074	-2960	-2492
13	882	1726	4699	7296	6936	8025	8679	9307	10147	10371
	-434	-902	-2070	-2727	-3552	-4399	-4826	-5128	-5289	-4100

* Gages 2 and 4 malfunctioned

Table 3-7 Peak Strains (Specimen FR, transverse)

Strain Gage	Run									
	1	2	3	4	5	6	7	8	9	10
	Peak Lateral Force (kN)									
	103.0	206.9	289.1	307.4	336.9	359.0	350.1	339.5	334.8	284.7
	Peak Strain (microstrain)									
16 T	231	783	1161	660	562	594	648	686	41538	41538
C	--	--	--	--	--	--	--	--	-8987	--
17	94	158	103	215	362	571	744	841	930	41838
	--	--	-125	--	--	--	--	--	--	--
18	116	235	86	208	391	535	719	817	950	1275
	--	--	-52	--	--	--	--	--	--	--
20	146	208	15	62	220	523	812	1111	1244	1260
	--	--	-81	-49	--	--	--	--	--	--
21	700	447	700	763	827	890	953	1333	1840	2347
	--	-187	--	--	--	--	--	--	--	-313
22	209	420	469	599	715	866	875	889	987	41763
	--	--	--	--	--	--	--	--	--	--
23	240	501	785	1017	1283	1530	1645	1681	1673	1383
	--	--	--	--	--	--	--	--	--	--
24	129	301	429	532	714	928	1072	1160	1258	41670
	--	--	-7	--	--	--	--	--	--	-8022
26	174	294	520	740	802	900	969	990	997	981
	--	--	--	--	--	--	--	--	--	--
27	102	195	206	236	185	49	13	6	13	41402
	--	--	-66	-164	-284	-376	-375	-381	-370	-6672

* Gages 19 and 25 malfunctioned

Table 3-8 Peak Strains (Specimen FR, jacket)

Strain Gage	Run									
	1	2	3	4	5	6	7	8	9	10
	Peak Lateral Force (kN)									
	103.0	206.9	289.1	307.4	336.9	359.0	350.1	339.5	334.8	284.7
	Peak Strain (microstrain)									
30 T	102	170	--	--	--	9	71	61	67	94
C	--	--	-200	-207	-173	-132	-122	-97	-67	-198
32	--	--	--	--	--	--	--	--	--	--
	-800	-758	-1037	-1025	-1080	-1104	-1054	-1021	-1000	-987
33	142	206	--	38	219	141	194	216	260	313
	--	--	-142	-66	--	-18	-68	-43	--	-87
34	220	508	188	400	603	523	462	474	498	728
	--	--	-154	-113	-79	-37	-32	--	--	--
35	147	296	286	440	559	643	673	714	782	877
	--	--	-76	-37	--	--	--	--	--	--
36	44	160	105	341	349	218	833	1193	2698	3124
	-44	-34	-313	-255	-381	-426	-228	-382	-271	--
38	84	125	--	--	--	--	--	--	--	--
	-31	-175	-495	-541	-581	-831	-892	-600	-655	-510
39	151	206	--	--	--	--	--	--	--	--
	--	-220	-850	-1015	-1314	-1660	-1401	-1548	-1753	-1994
40	--	84	--	--	3	56	89	95	108	109
	-33	--	-171	-144	-123	-93	-57	-41	-31	-27
41	130	264	41	--	160	249	303	331	345	345
	--	--	-120	-87	--	--	--	--	--	--
44	129	320	199	249	287	295	330	330	334	374
	--	--	-115	-99	-71	-30	--	--	--	--
45	136	256	52	100	136	258	381	453	501	427
	--	--	-149	-108	-108	-67	-26	-16	--	--
46	120	240	79	156	199	277	317	325	358	40125
	--	-38	-365	-441	-471	-484	-471	-440	-429	-42134
47	113	285	189	275	300	363	377	405	421	445
	-3	-153	-541	-638	-755	-798	-722	-697	-682	-571
48	96	197	109	146	246	304	281	267	268	172
	--	--	-57	-30	--	--	--	--	--	-10
50	105	153	25	95	206	358	398	391	421	301
	--	--	-109	-82	-53	-11	--	--	--	--
51	104	229	145	179	227	155	143	243	315	305
	--	--	-92	-71	-64	-31	--	--	--	--
52	13	93	--	--	--	71	--	--	--	--
	-21	--	-253	-237	-236	-202	-191	-237	-234	-193
53	135	214	4	59	189	125	41	63	80	131
	--	--	-140	-141	-121	-80	-24	--	--	--
54	64	170	--	--	--	74	173	220	212	374
	--	--	-375	-424	-502	-545	-424	-358	-360	-100

* Gages 31 and 37 malfunctioned

Table 4-1 Measured Peak Strain Rates and Corresponding Increases in Material Strength

	FA			FR		
	Peak Strain Rate	Increase in Steel Yield	Increase in Conc. Strength	Peak Strain Rate	Increase in Steel Yield	Increase in Conc. Strength
Pre-Yield (Run1)	.012 sec^{-1}	3%	14%	.011 sec^{-1}	3%	14%
Yield (Run 2)	.019 sec^{-1}	3%	14%	.017 sec^{-1}	3%	14%
Peak Load	.085 sec^{-1}	8%	20%	.071 sec^{-1}	6%	18%

Table 4-2 Components Of Calculated Lateral Deflections for Specimen FA (mm)

	Flexure	Shear	Bond Slip	Total
Yield (218.7 kN)	17.21	5.31	0.96	23.48
Ultimate (246.8 kN)	76.79	5.99	1.08	83.86

Table 4-3 Components Of Calculated Lateral Deflections for Specimen FR (mm)

	Flexure	Shear	Bond Slip	Total
Yield (262.0 kN)	18.34	5.40	1.19	24.92
Ultimate (360.0 kN)	160.12	7.41	1.78	169.31

Table 4-4 Shear Analysis of Specimen FA

Method	Calculated Shear Capacity (kN)	$V_{calc.}/V_{meas.}$
CALTRANS	224.6	0.85
FHWA (Theta = 45 deg.)	330.5	1.26
FHWA (Theta = 30 deg.)	451.9	1.72
Modified CALTRANS	282.0	1.07

Measured Peak Lateral Force = 262.9 kN

Table 4-5 Shear Analysis of Specimen FR

Method	Calculated Shear Capacity (kN)	$V_{calc.}/V_{extrap.}$
CALTRANS	1442.3	1.38
FHWA (Theta = 45 deg.)	1318.4	1.26
FHWA (Theta = 30 deg.)	2057.3	1.97
Modified CALTRANS	1499.7	1.43

Extrapolated Shear Capacity = 1046.3 kN

Table 4-6 Effectiveness of Steel Jacket as Longitudinal Reinforcement

Height Above Footing (mm	Effectiveness[a] (%)
101.6	1.17
177.8	2.52
279.4	1.8
533.4	1.08
635	2.52
800.1	4.86
939.8	6.83
1092.2	4.95
1244.6	2.79

[a] based on 200 psi bond stress for development

Figures

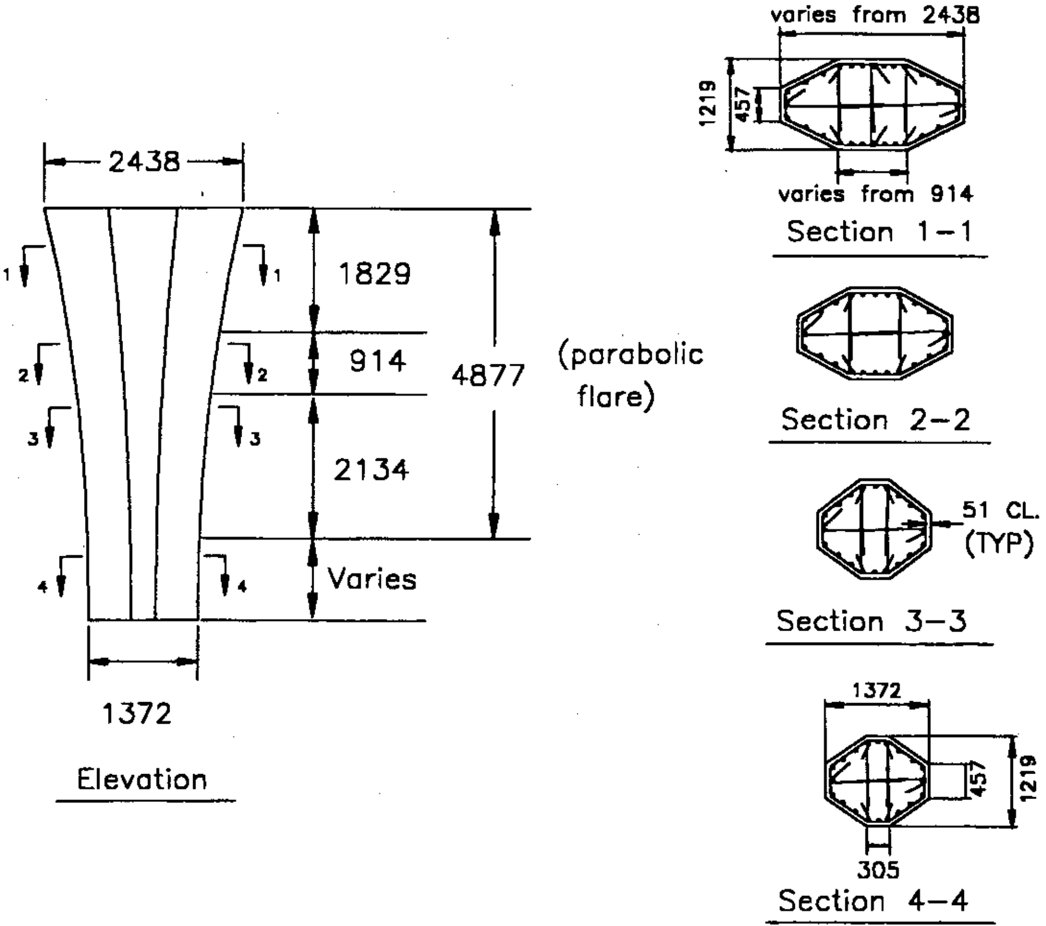

Notes:

All Longitudinal Bars are ϕ35 mm (#11)

All Transverse Bars are ϕ13 mm (#4) at 102 mm

All Dimensions are in mm

Fig. 2-1 Prototype Column Details

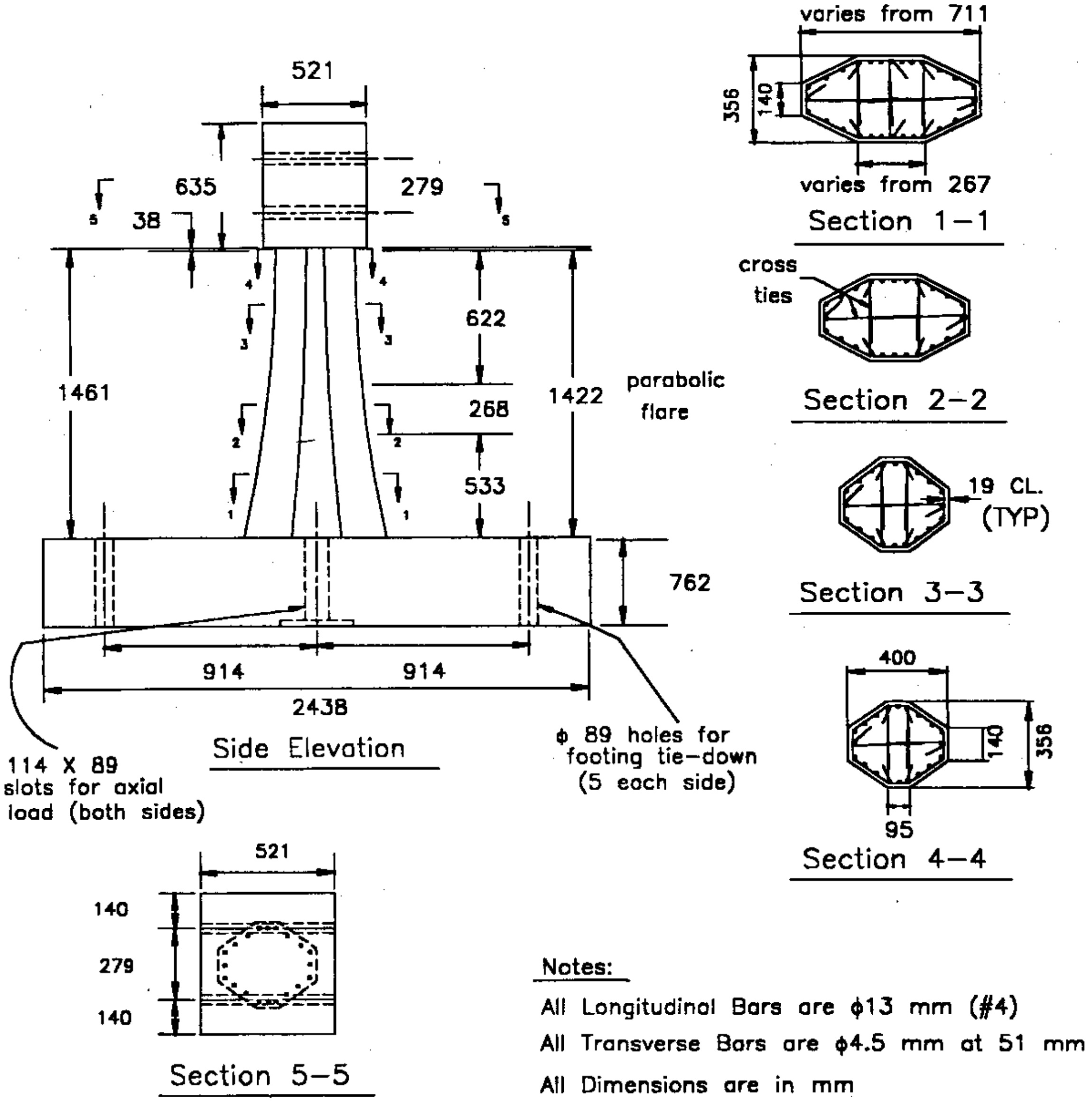

Notes:

All Longitudinal Bars are ϕ13 mm (#4)

All Transverse Bars are ϕ4.5 mm at 51 mm

All Dimensions are in mm

Fig. 2-2 Model Column Details

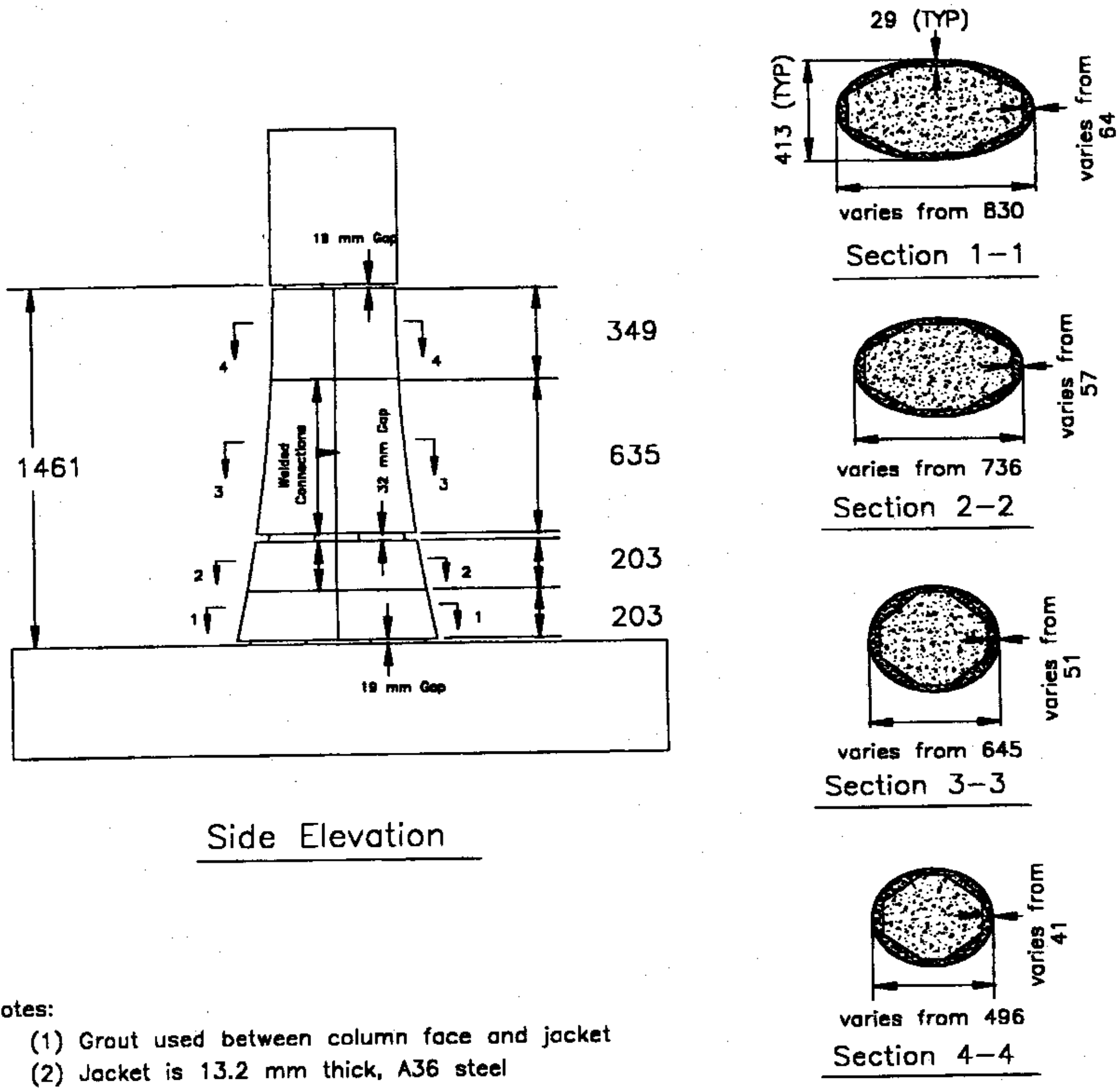

Notes:
(1) Grout used between column face and jacket
(2) Jacket is 13.2 mm thick, A36 steel
(3) Cross-sections are elliptical
(4) All Dimensions are in mm

Fig. 2-3 Retrofit Details

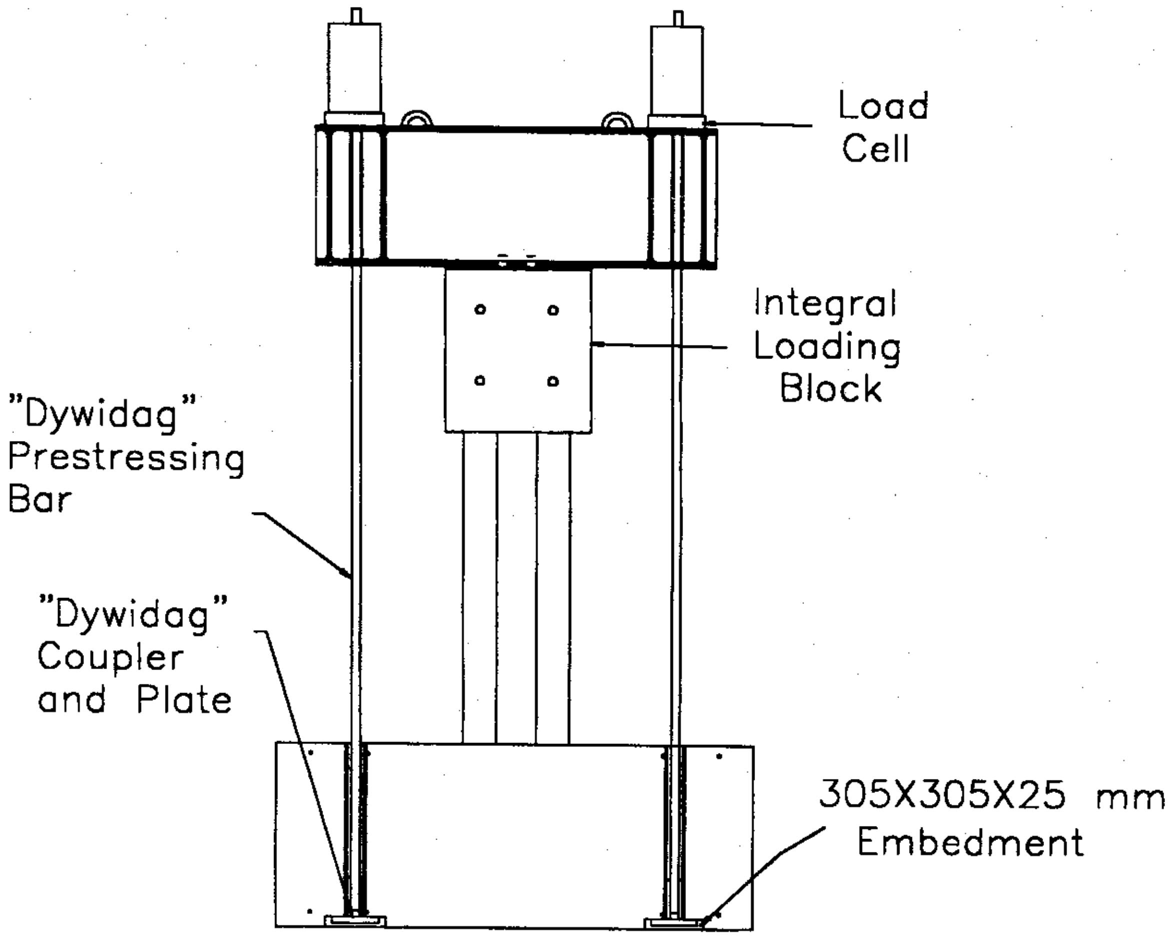

Fig. 2-4 Axial Load Apparatus and Setup

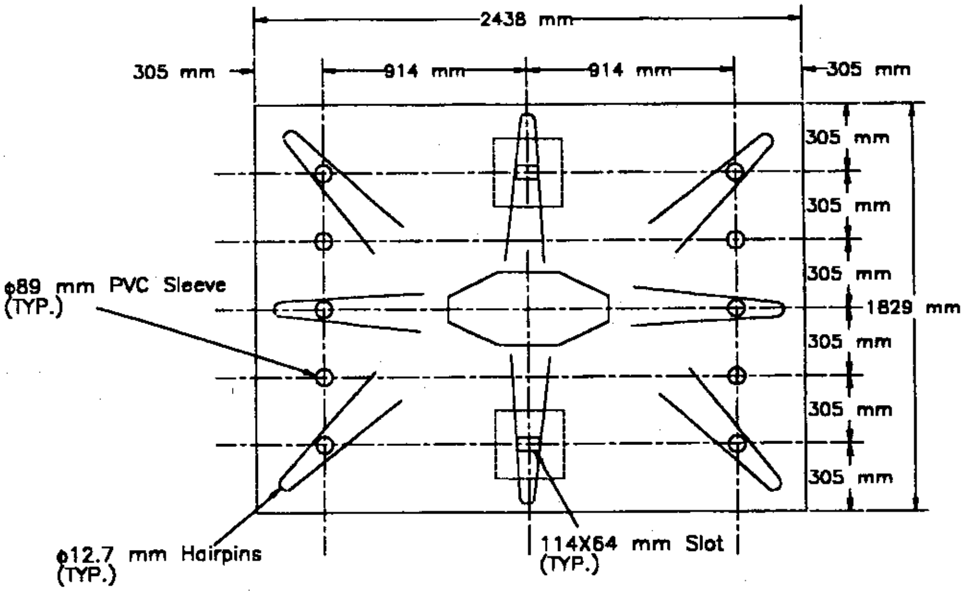

Plan

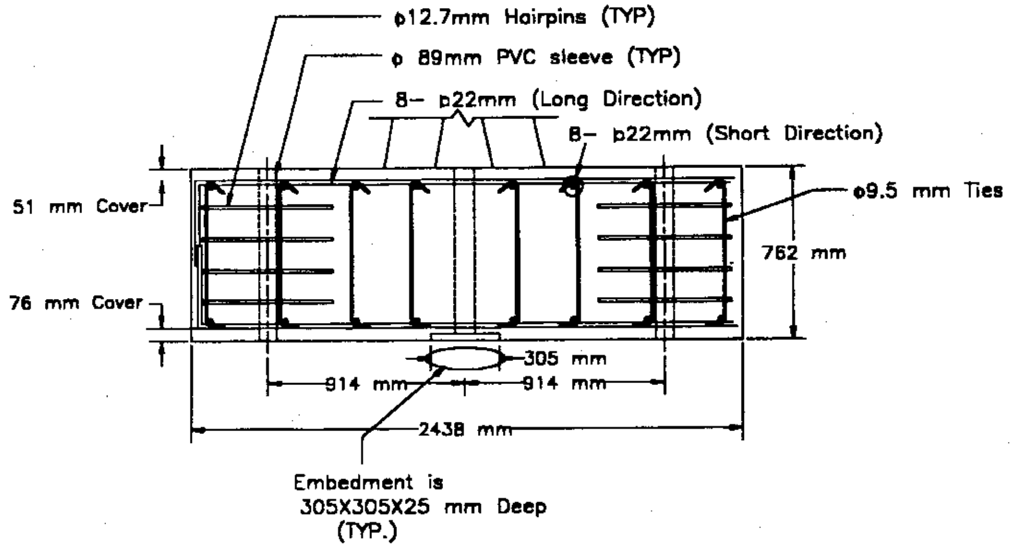

Section

Fig. 2-5 Footing Details

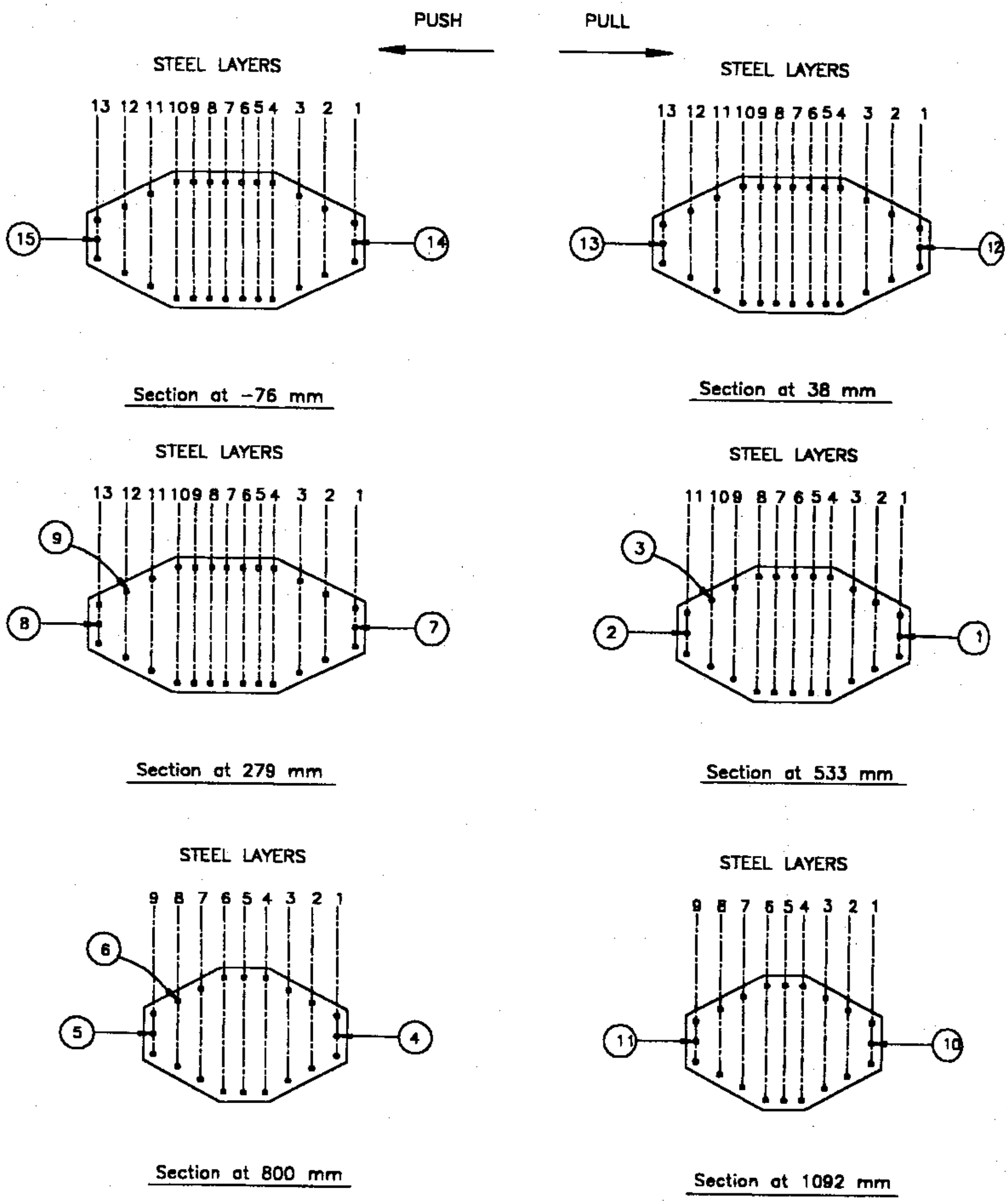

Section at -76 mm

Section at 38 mm

Section at 279 mm

Section at 533 mm

Section at 800 mm

Section at 1092 mm

Fig. 2-6 Strain Gages on Longitudinal Reinforcement of Specimen FA

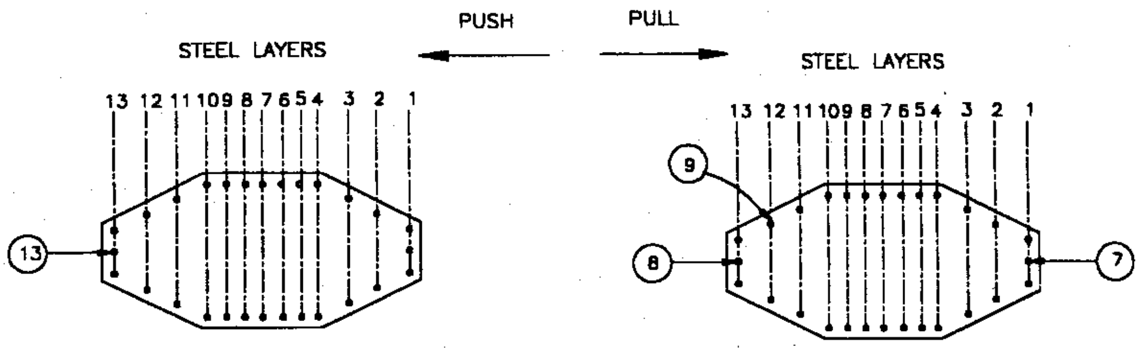

Section at 38 mm

Section at 279 mm

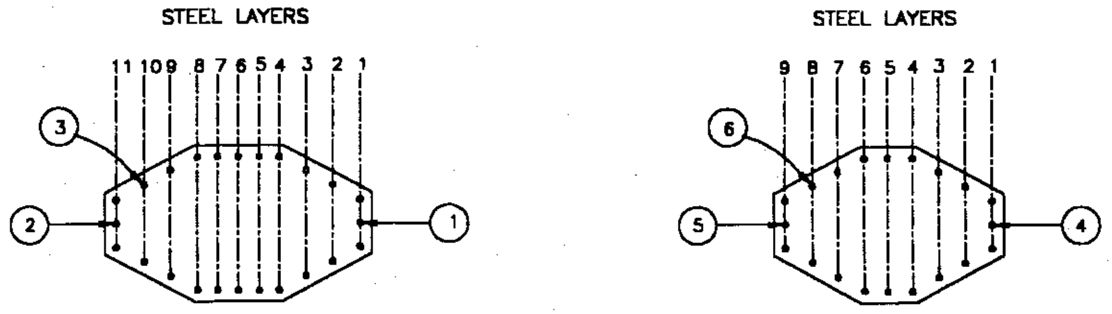

Section at 533 mm

Section at 800 mm

Fig. 2-7 Strain Gages on Longitudinal Reinforcement of Specimen FR

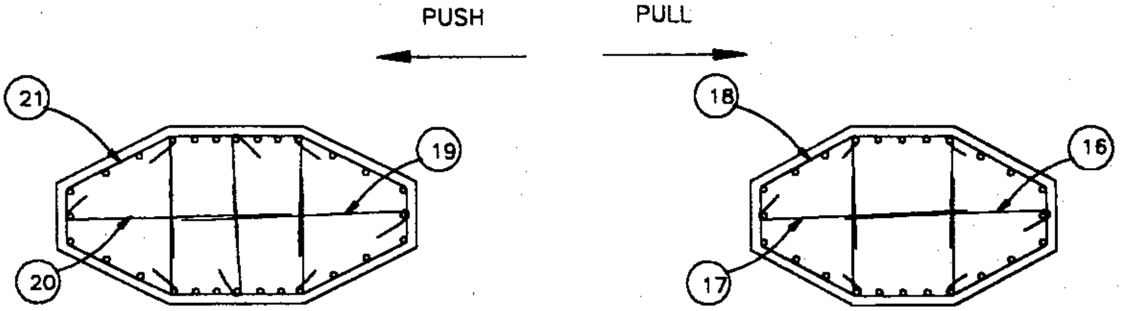

Section at 279 mm

Section at 533 mm

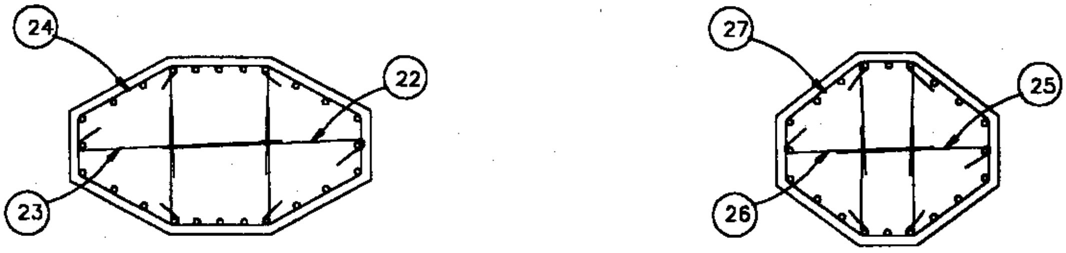

Section at 660 mm

Section at 800 mm

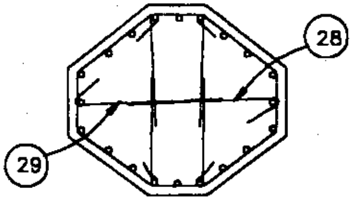

Section at 1092 mm

Fig. 2-8 Strain Gages on Transverse Reinforcement of Specimen FA

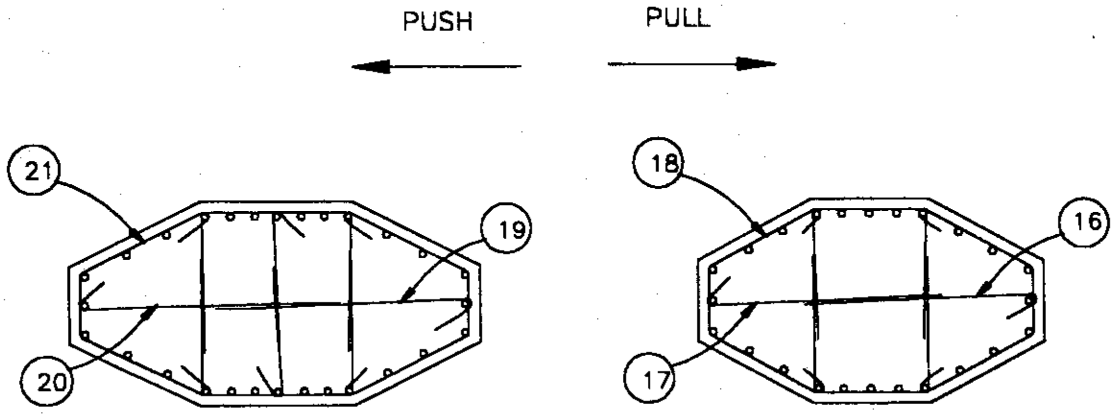

Section at 279 mm

Section at 533 mm

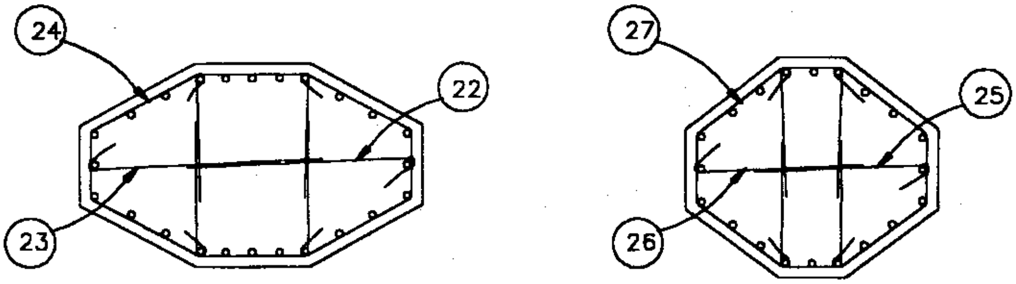

Section at 660 mm

Section at 800 mm

Fig. 2-9 Strain Gages on Transverse Reinforcement of Specimen FR

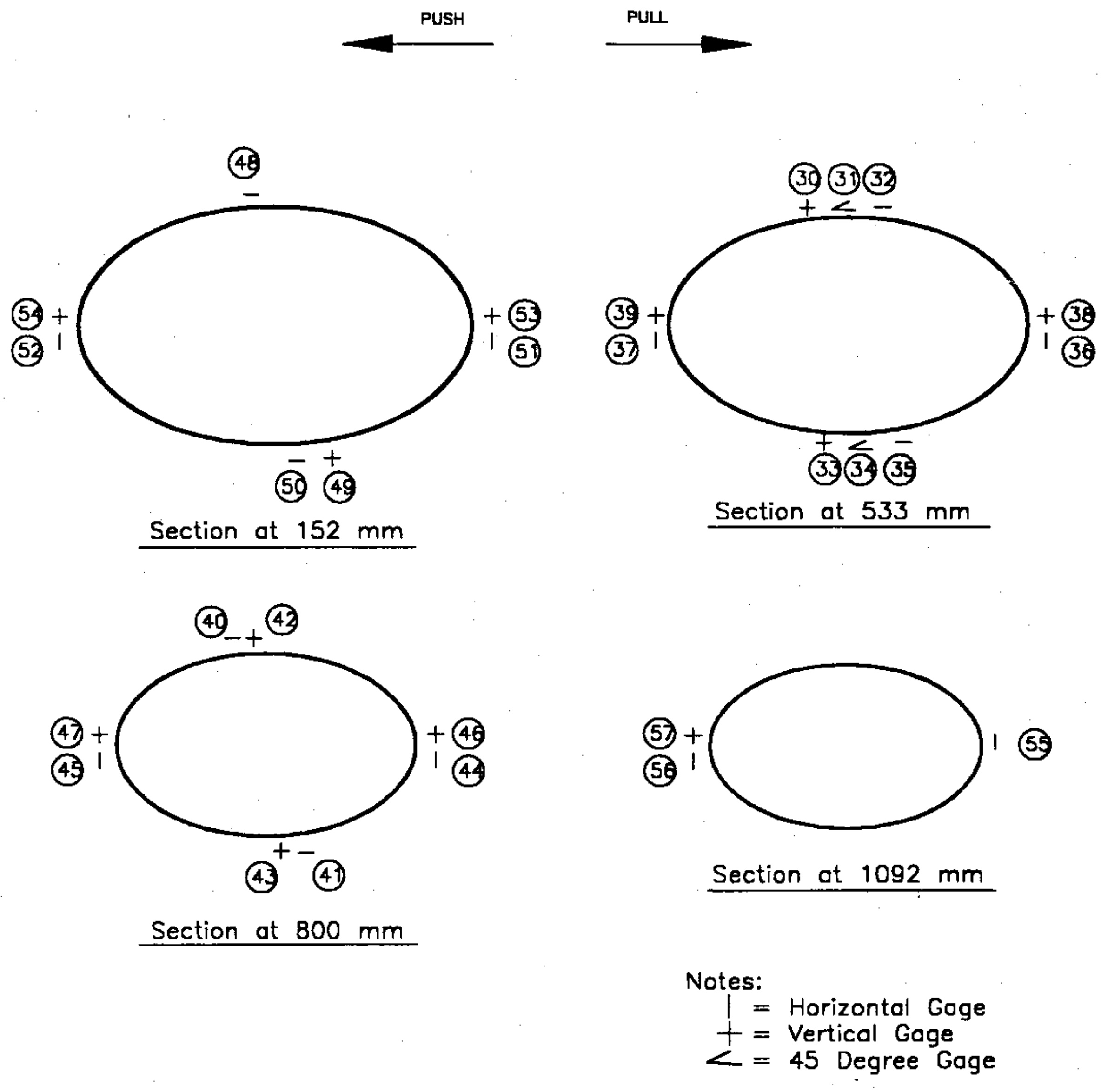

Section at 152 mm

Section at 533 mm

Section at 800 mm

Section at 1092 mm

Fig. 2-10 Strain Gages on Steel Jacket

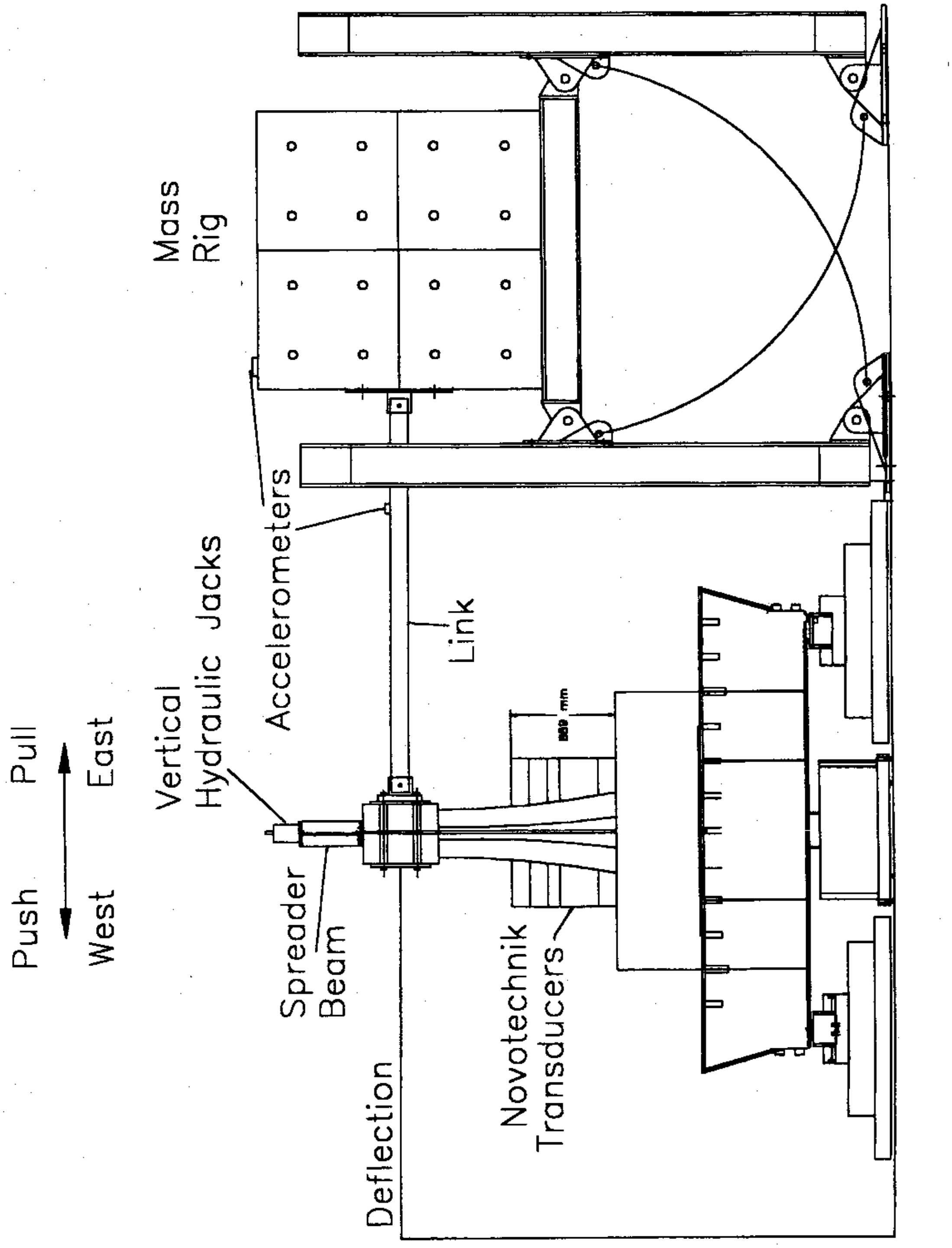

Fig. 2-11 Test Setup

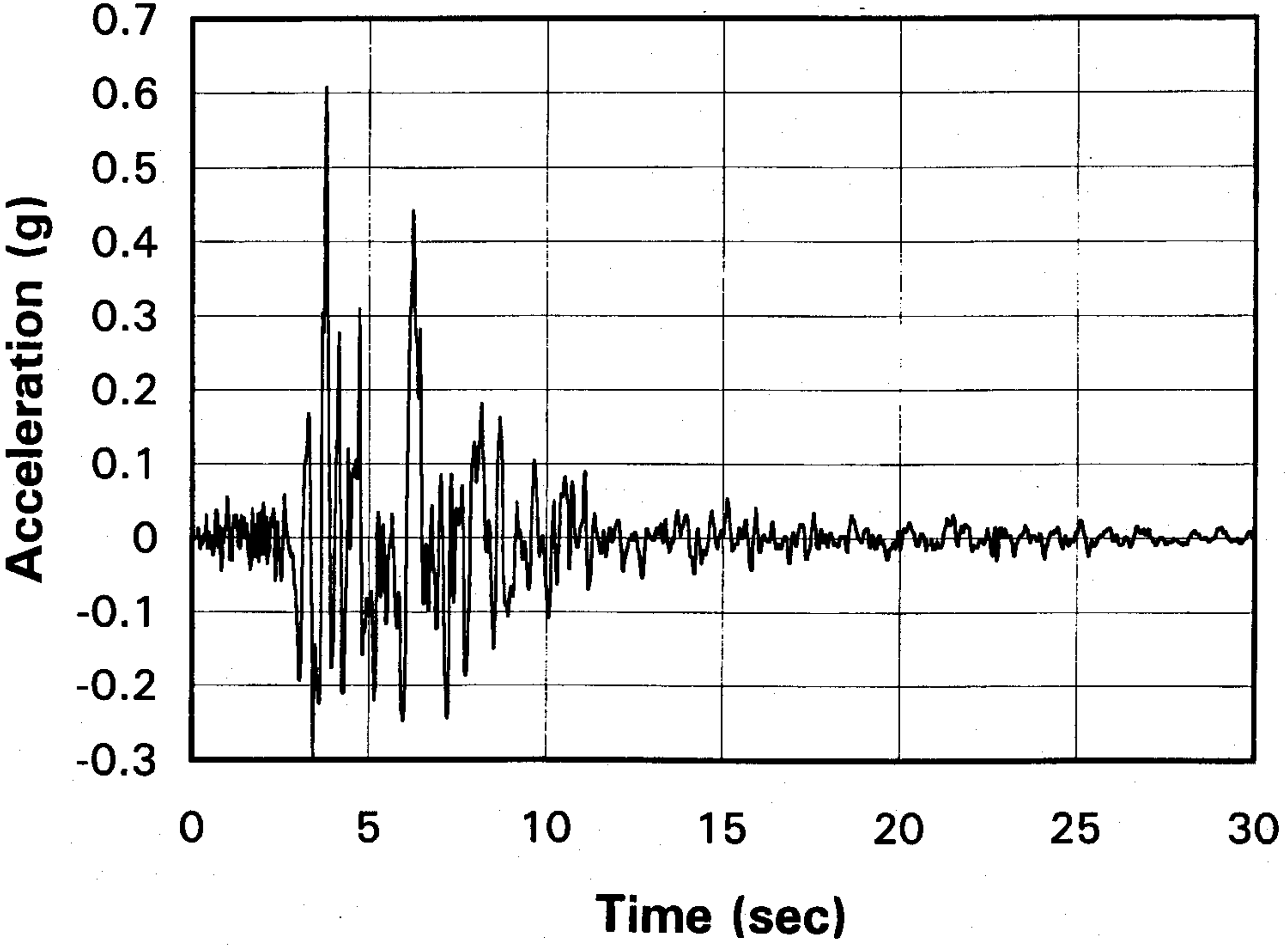

Fig. 3-1 Original Sylmar Record

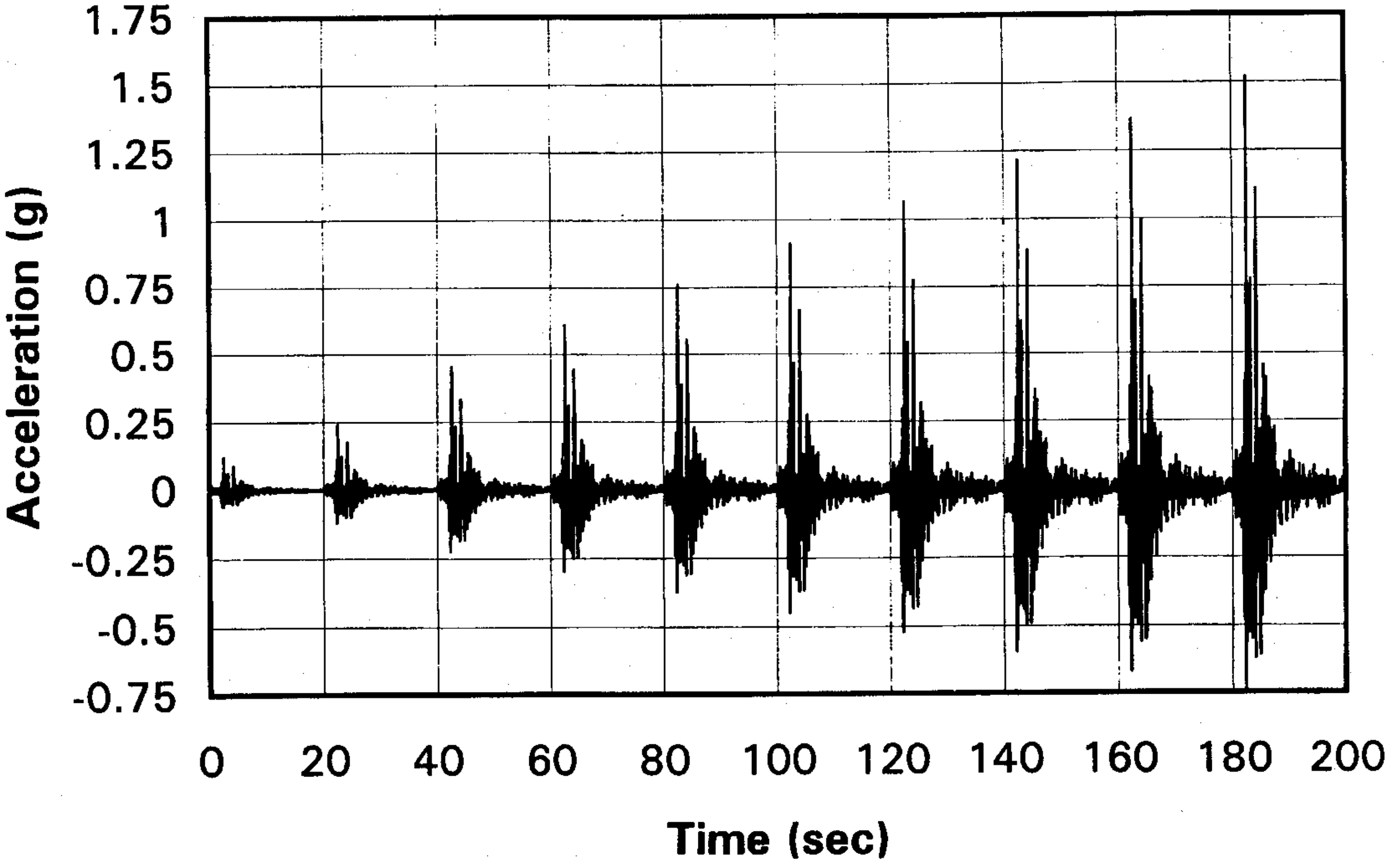

Fig. 3-2 Target Table Accelerations, All Runs

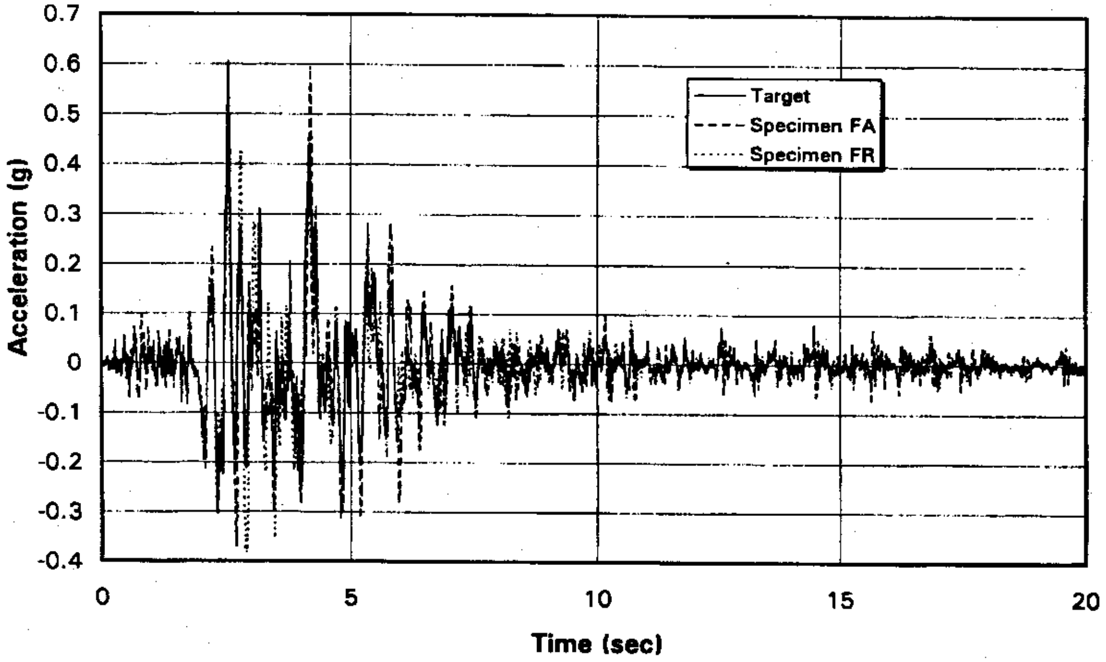

Fig. 3-3 Table Accelerations for Run 4

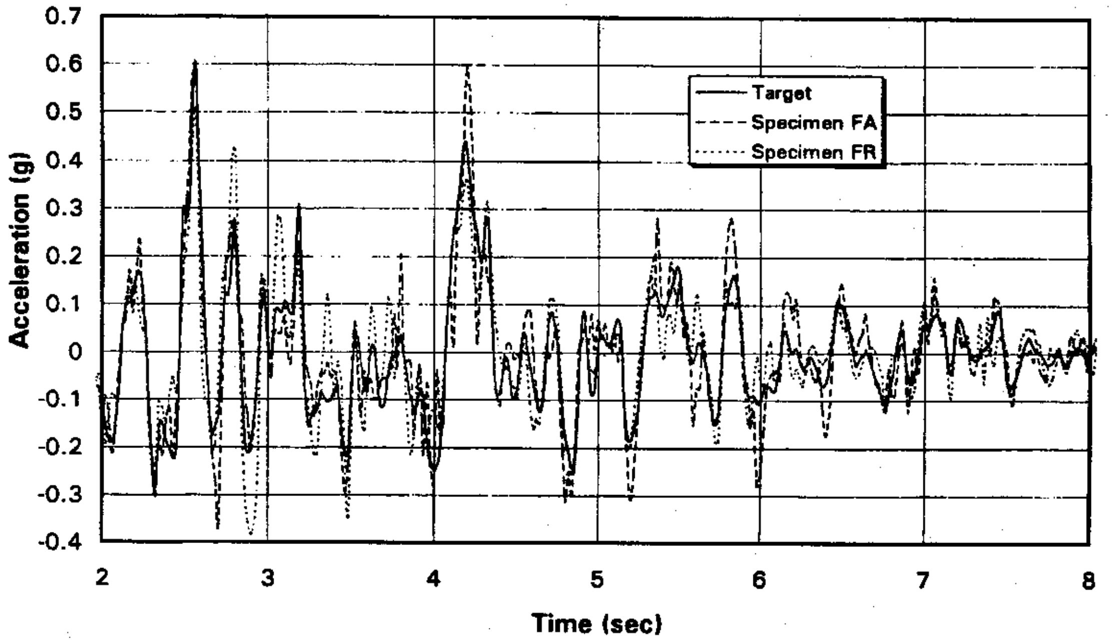

Fig. 3-4 Table Accelerations for Run 4, 2-8 Sec.

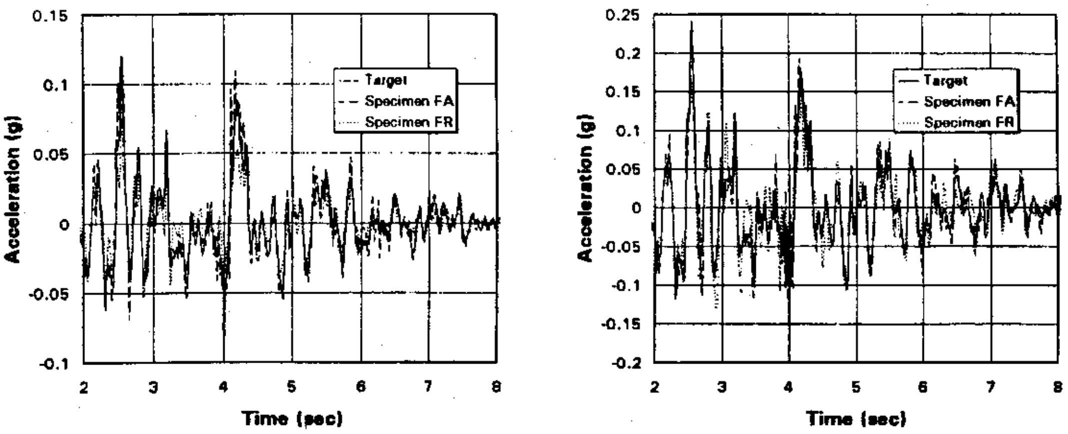

Table Accelerations for Run 1

Table Accelerations for Run 2

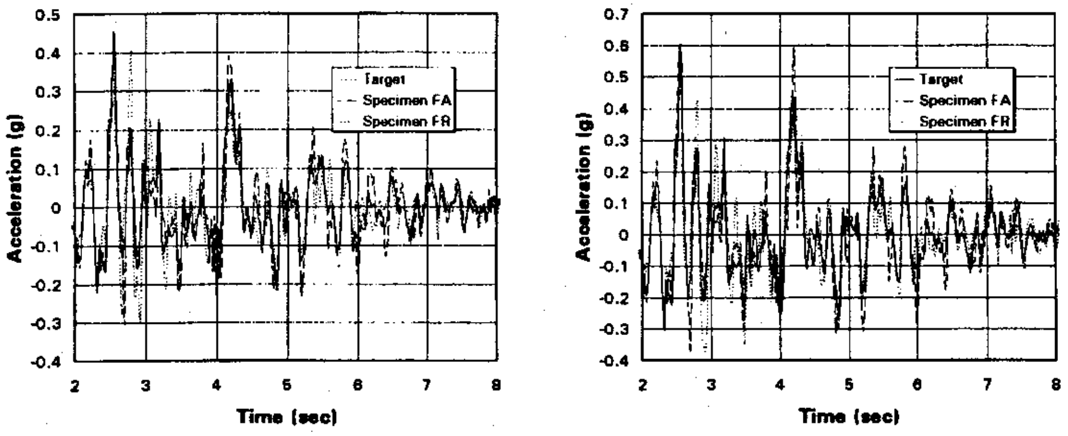

Table Accelerations for Run 3

Table Accelerations for Run 4

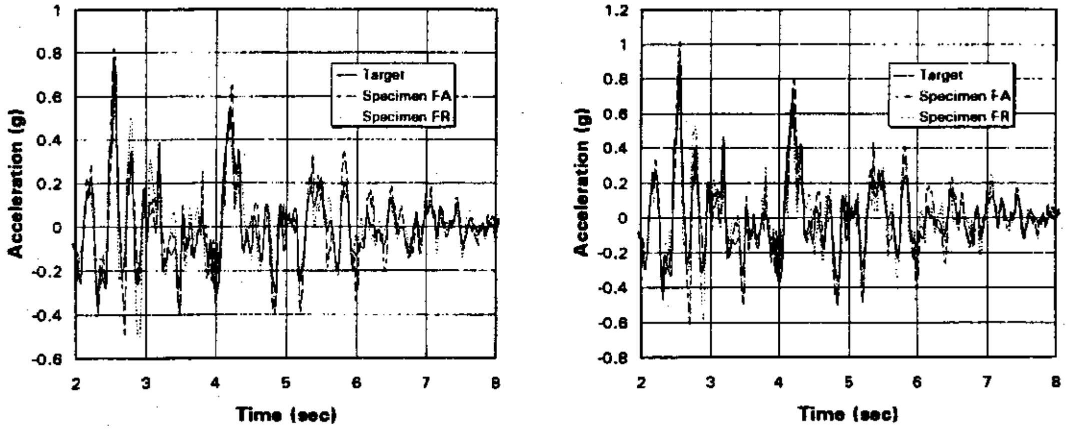

Table Accelerations for Run 5

Table Accelerations for Run 6

Fig. 3-5 Table Accelerations for Runs 1-6

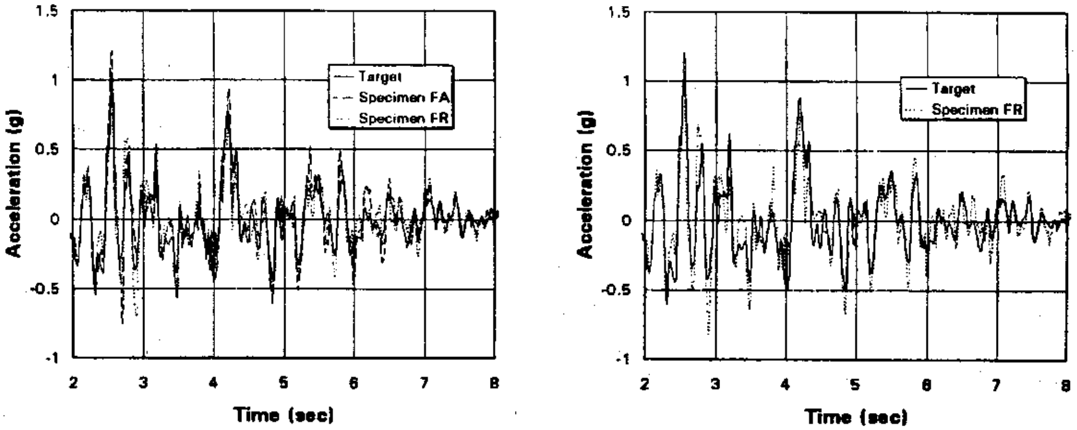

Table Accelerations for Run 7

Table Accelerations for Run 8

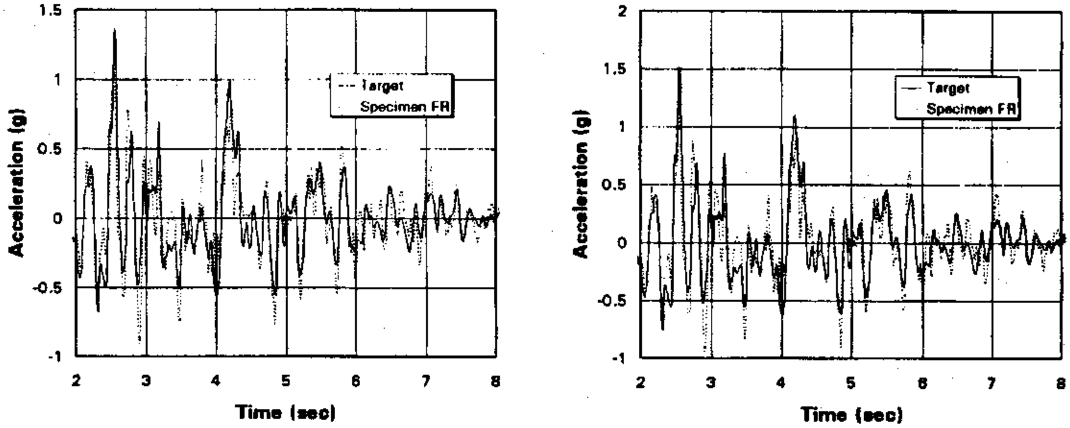

Table Accelerations for Run 9

Table Accelerations for Run 10

Fig. 3-6 Table Accelerations for Runs 7-10

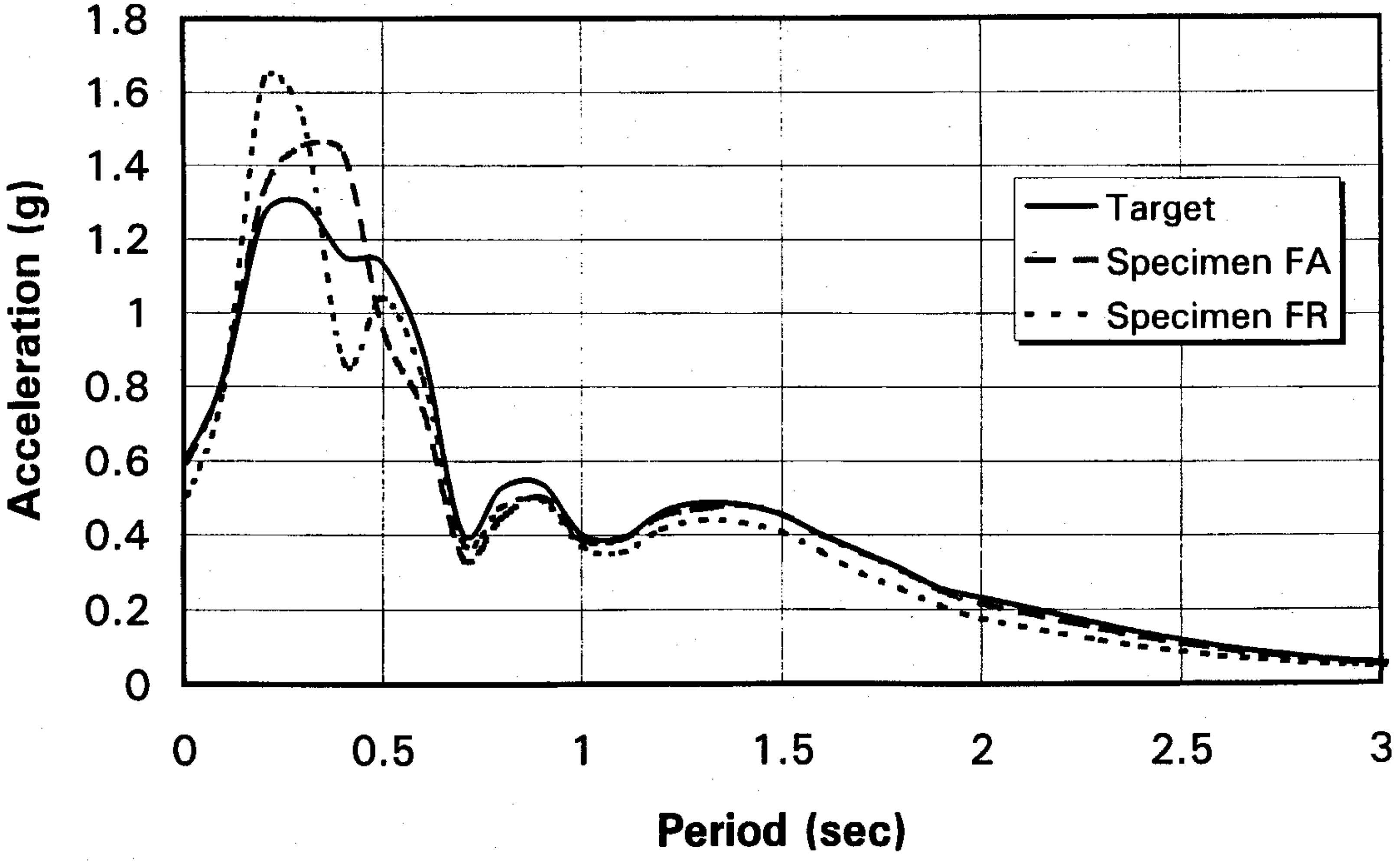

Fig. 3-7 Spectral Accelerations for Run 4

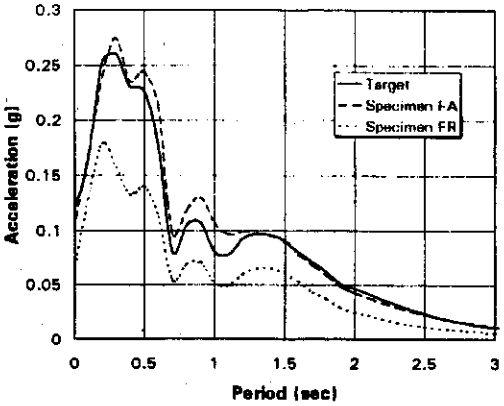

Spectral Accelerations
for Run 1

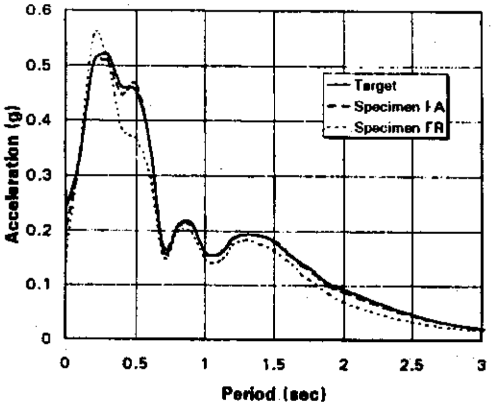

Spectral Accelerations
for Run 2

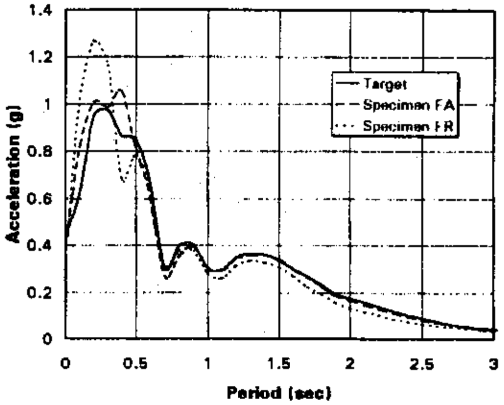

Spectral Accelerations
for Run 3

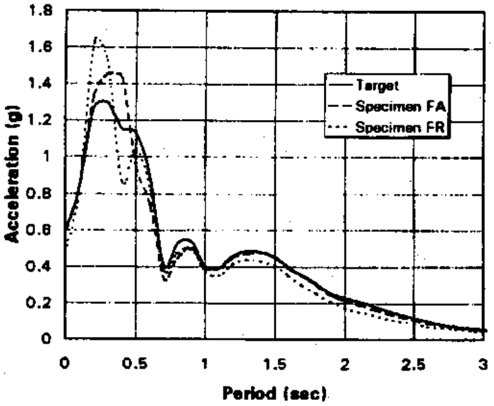

Spectral Accelerations
for Run 4

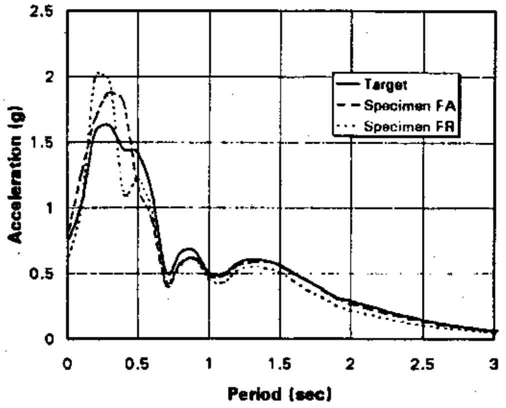

Spectral Accelerations
for Run 5

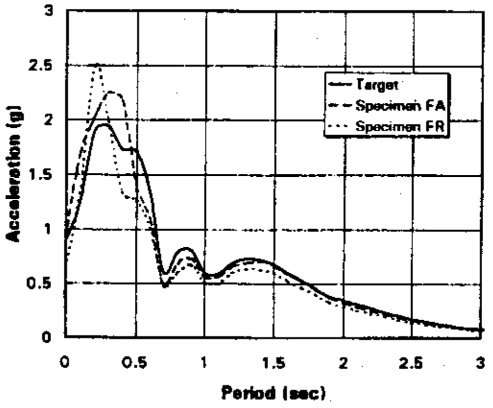

Spectral Accelerations
for Run 6

Fig. 3-8 Spectral Accelerations for Runs 1-6

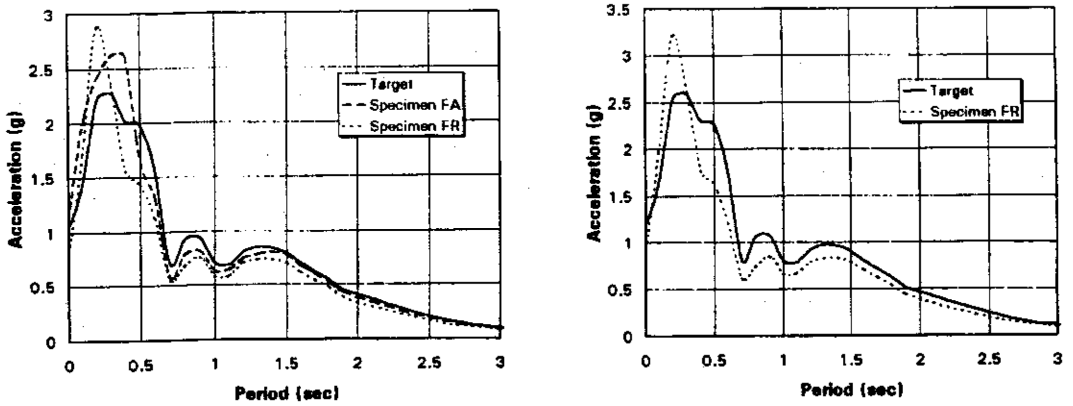

Spectral Accelerations
for Run 7

Spectral Accelerations
for Run 8

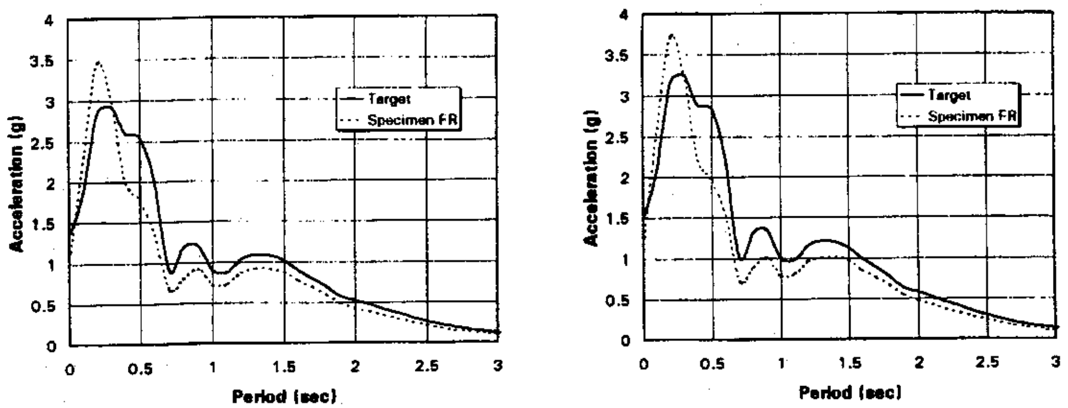

Spectral Accelerations
for Run 9

Spectral Accelerations
for Run 10

Fig. 3-9 Spectral Accelerations for Runs 7-10

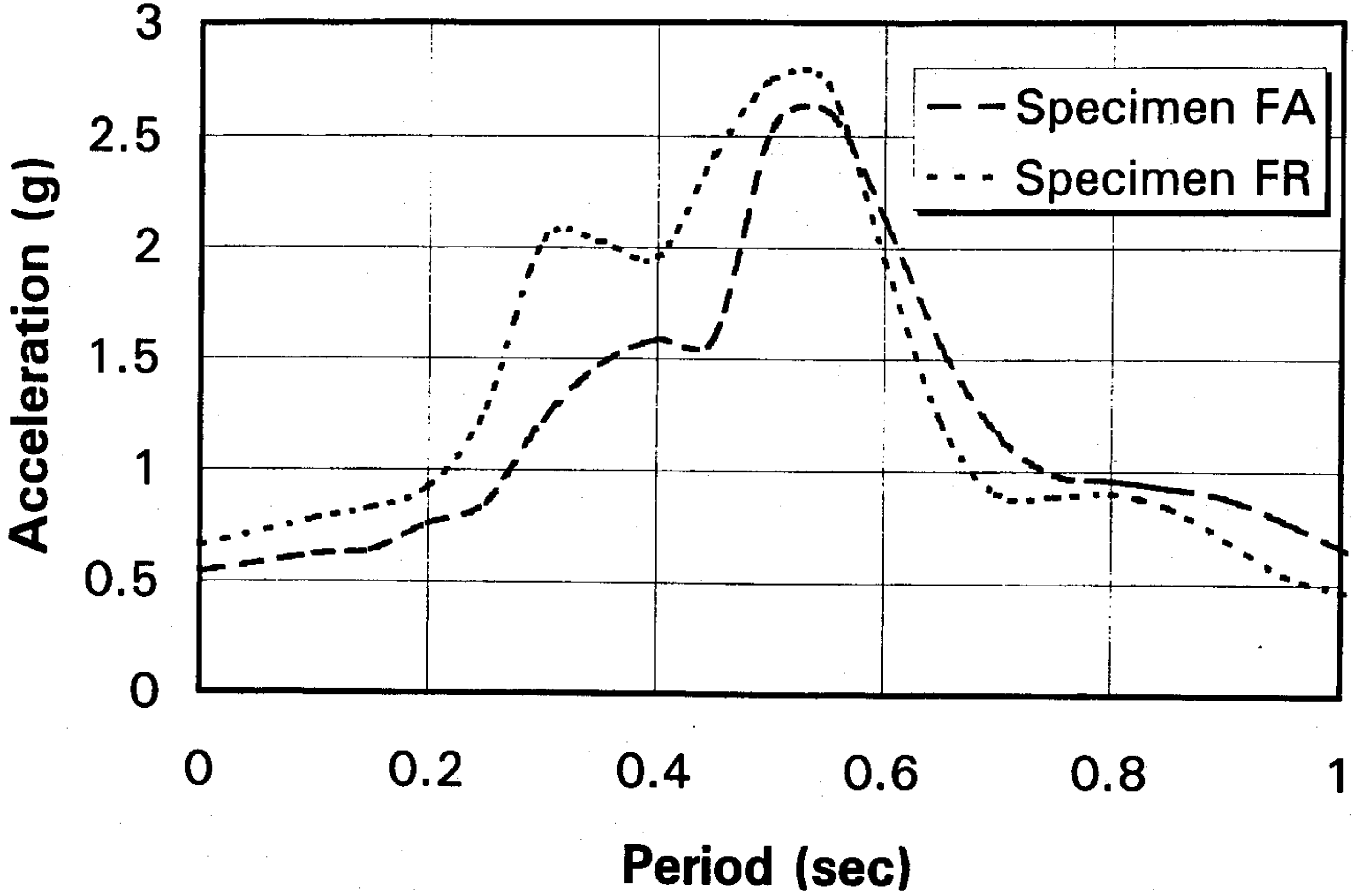

Fig. 3-10 Spectral Accelerations for Run 4, Link Accelerometer

Fig. 3-11 Specimen FA, Run 2, Cracking

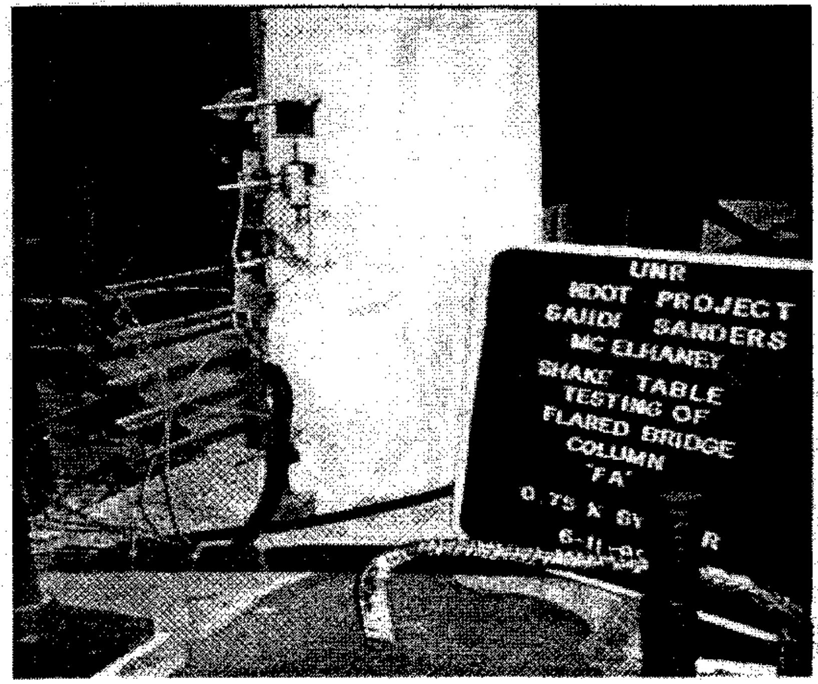

Fig. 3-12 Specimen FA, Run 3, Spalling

Fig. 3-13 Specimen FA, After Testing

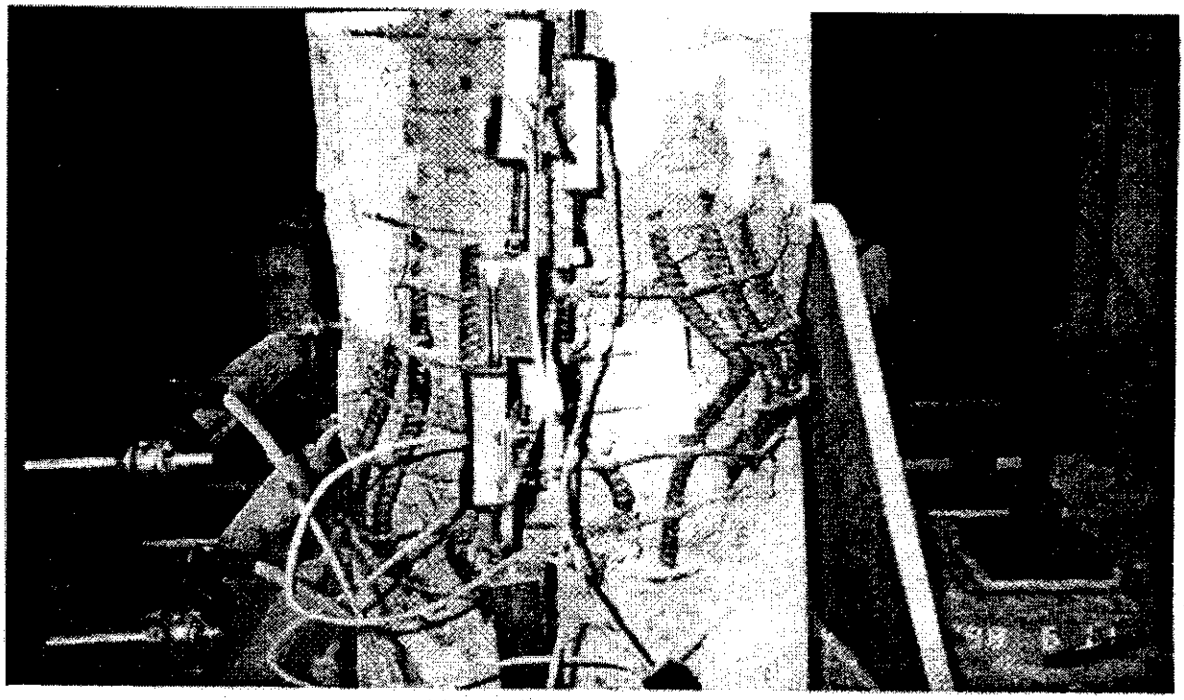

Fig. 3-14 Specimen FA, After Testing

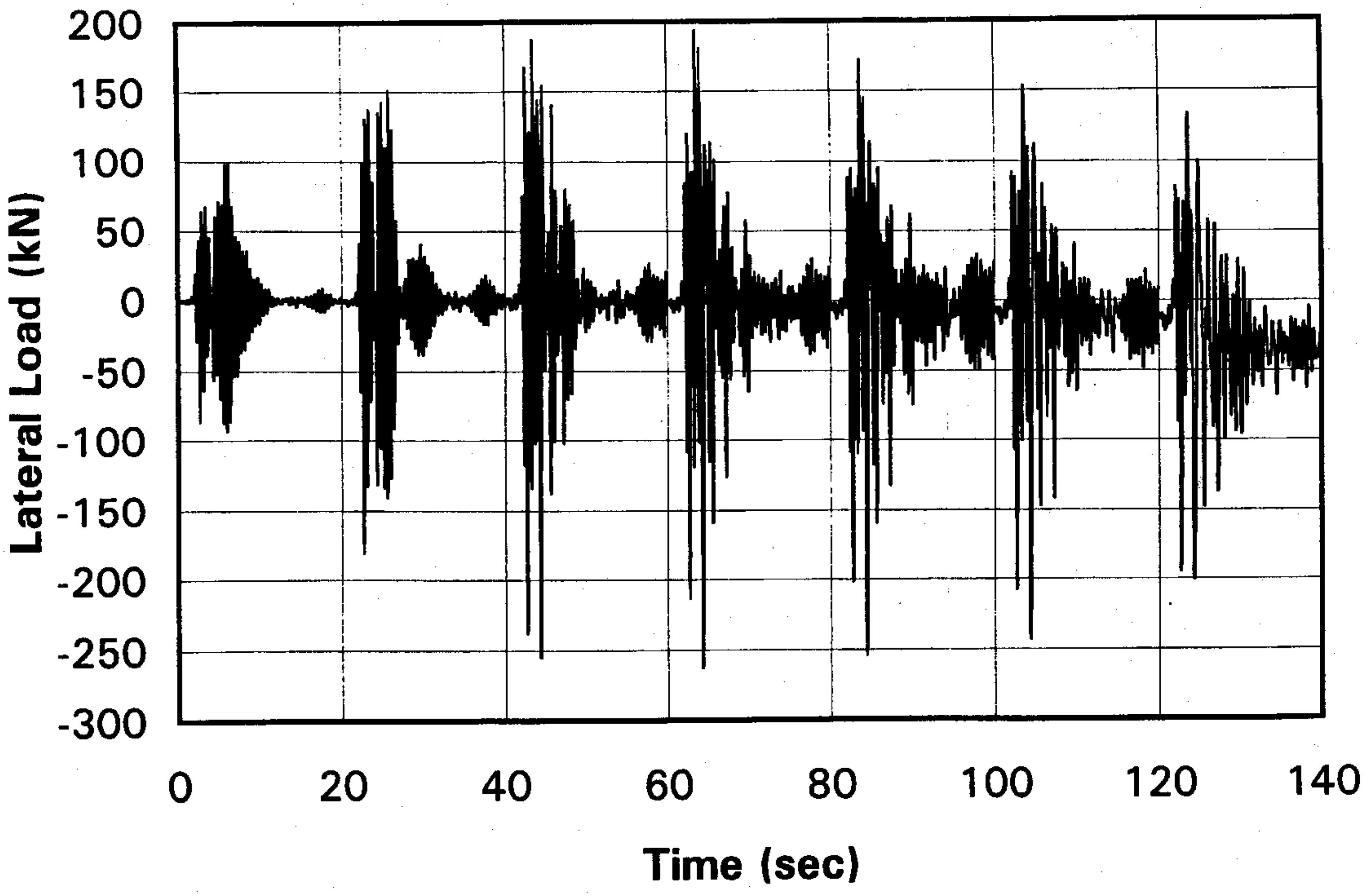

Fig. 3-15 Lateral Loading History for Specimen FA

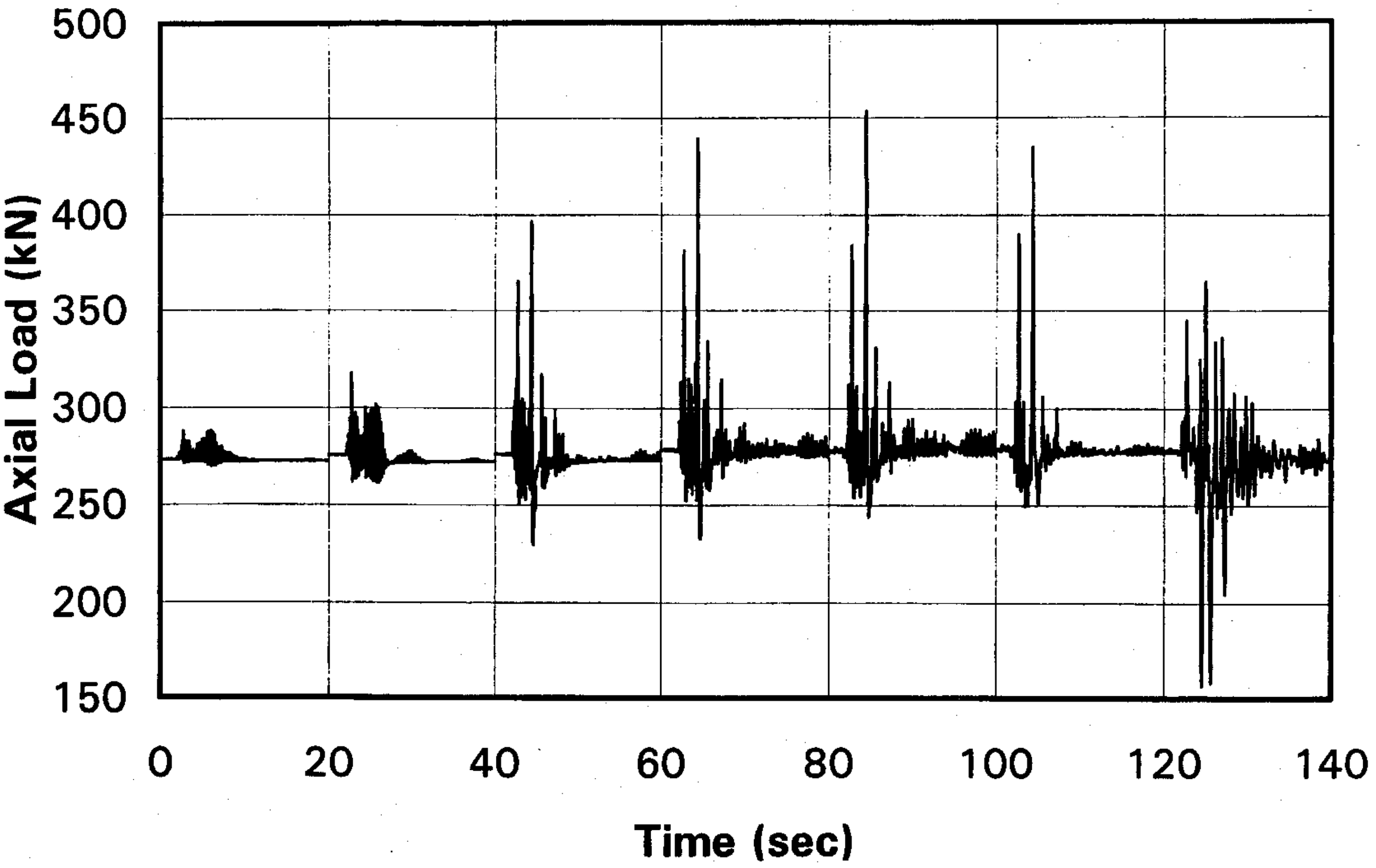

Fig. 3-16 Axial History for Specimen FA

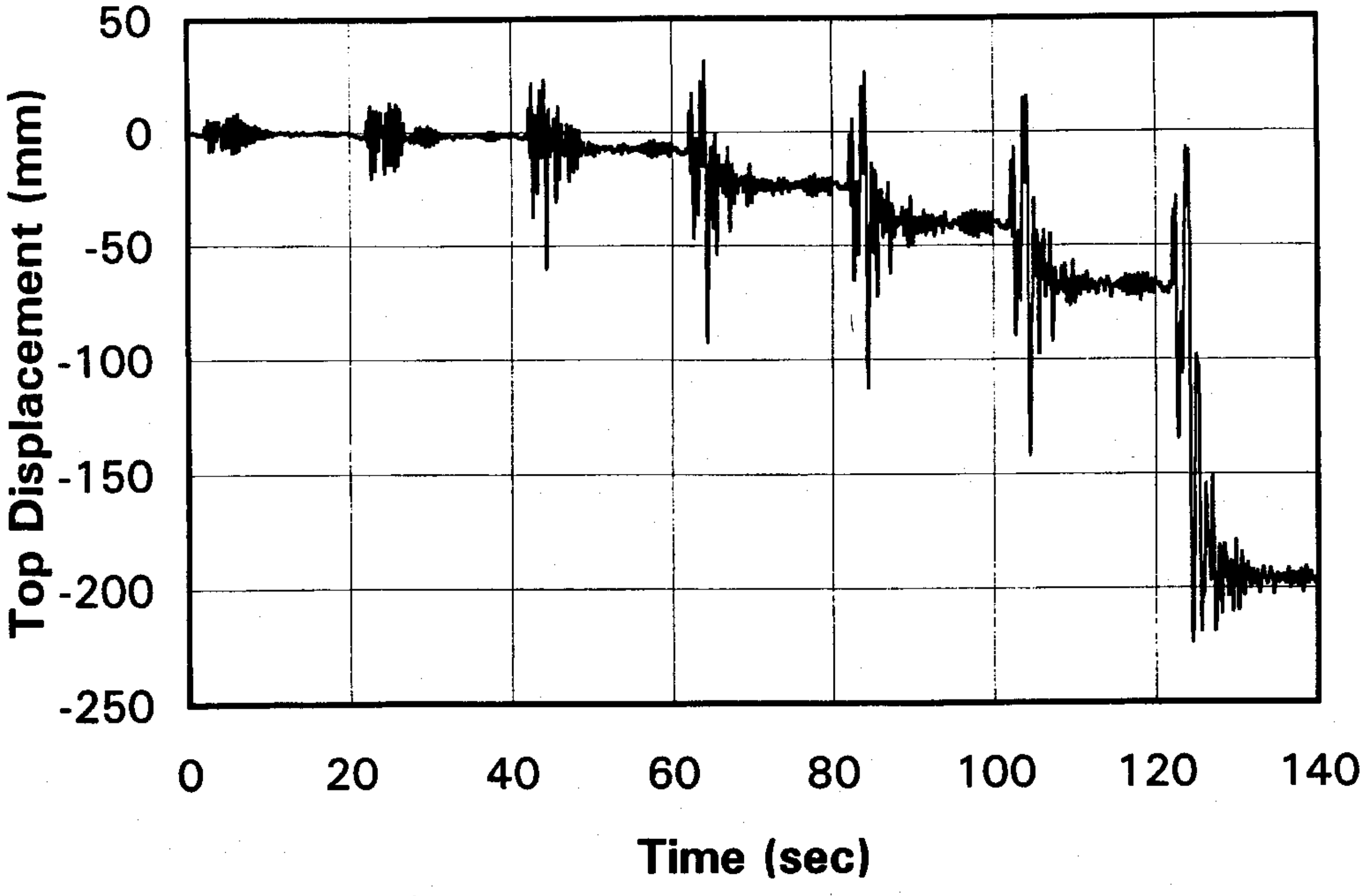

Fig. 3-17 Displacement History for Specimen FA, All Runs

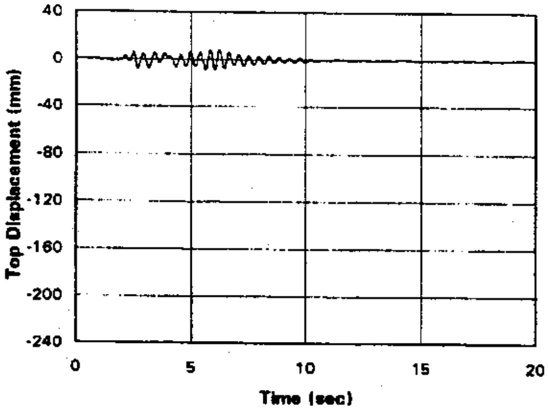

Displacement History for
Specimen FA, Run 1

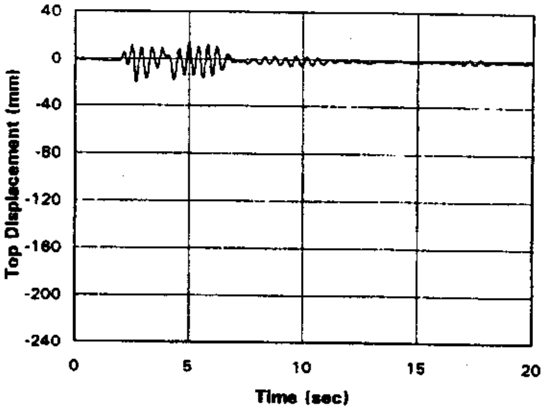

Displacement History for
Specimen FA, Run 2

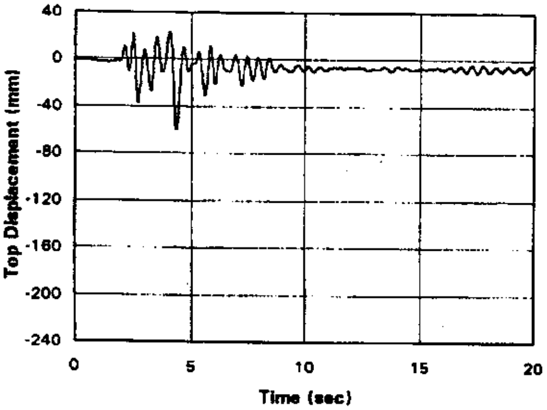

Displacement History for
Specimen FA, Run 3

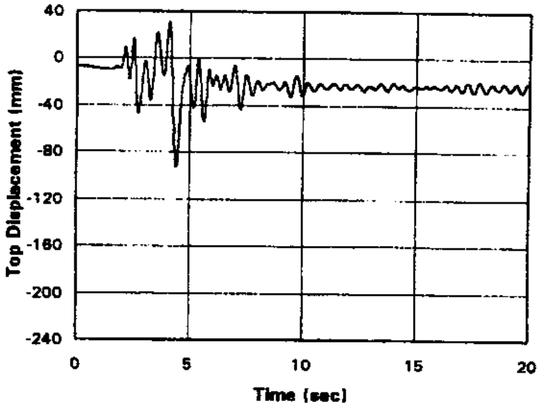

Displacement History for
Specimen FA, Run 4

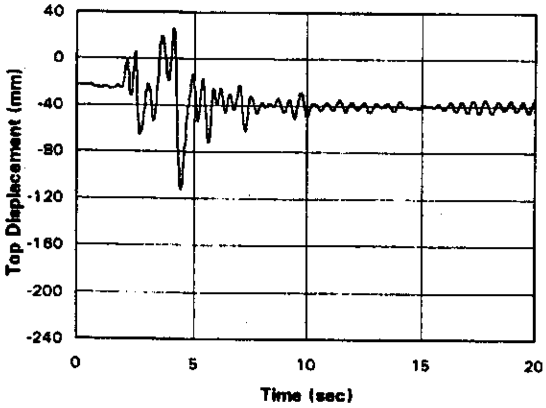

Displacement History for
Specimen FA, Run 5

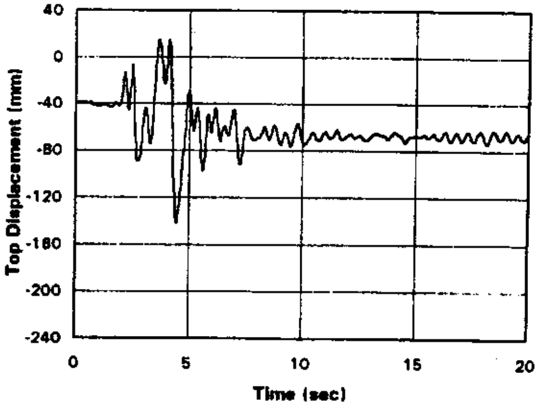

Displacement History for
Specimen FA, Run 6

Fig. 3-18 Displacement History, Specimen FA, Runs 1-6

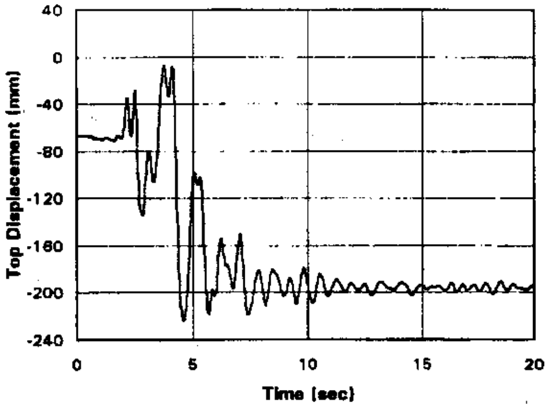

Displacement History for
Specimen FA, Run 7

Fig. 3-19 Displacement History, Specimen FA, Run 7

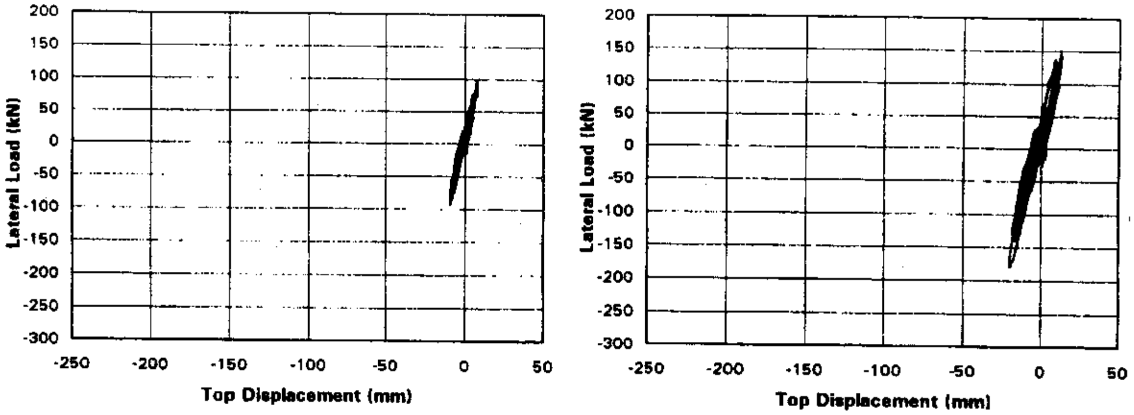

Hysteresis Loop for Specimen FA, Run 1

Hysteresis Loop for Specimen FA, Run 2

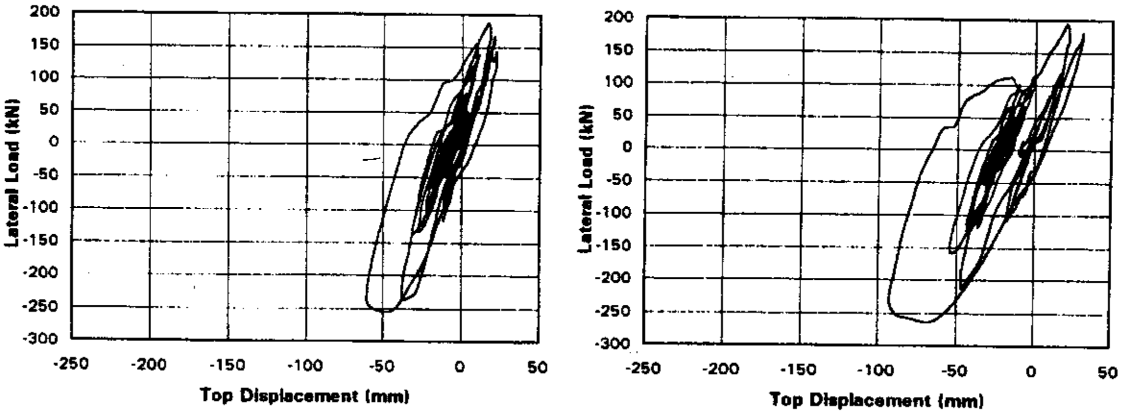

Hysteresis Loop for Specimen FA, Run 3

Hysteresis Loop for Specimen FA, Run 4

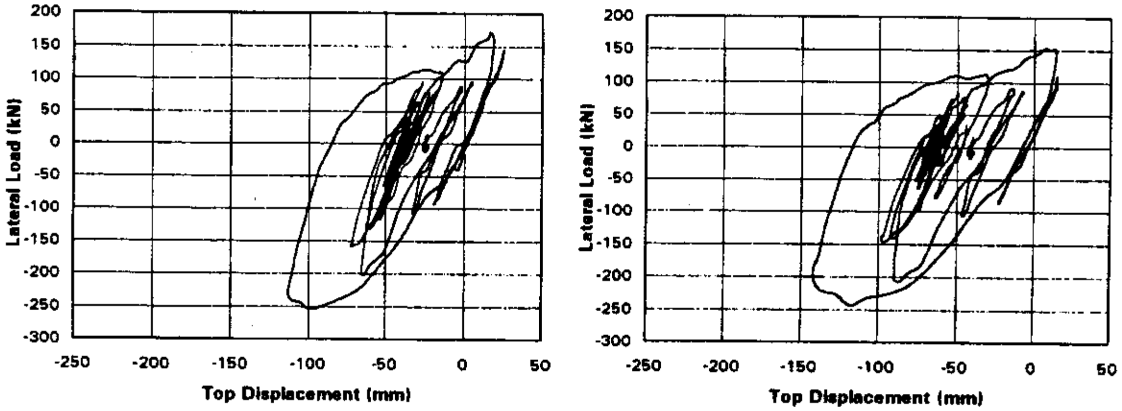

Hysteresis Loop for Specimen FA, Run 5

Hysteresis Loop for Specimen FA, Run 6

Fig. 3-20 Hysteresis Loops, Specimen FA, Runs 1-6

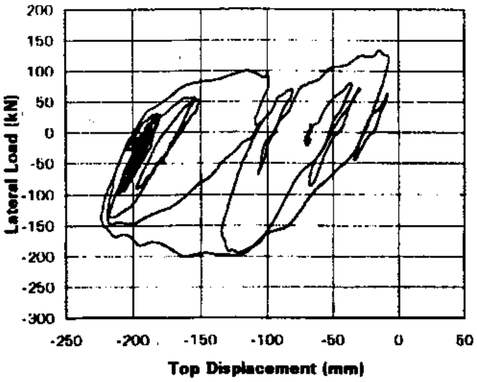

Hysteresis Loop for
Specimen FA, Run 7

Fig. 3-21 Hysteresis Loop, Specimen FA, Run 7

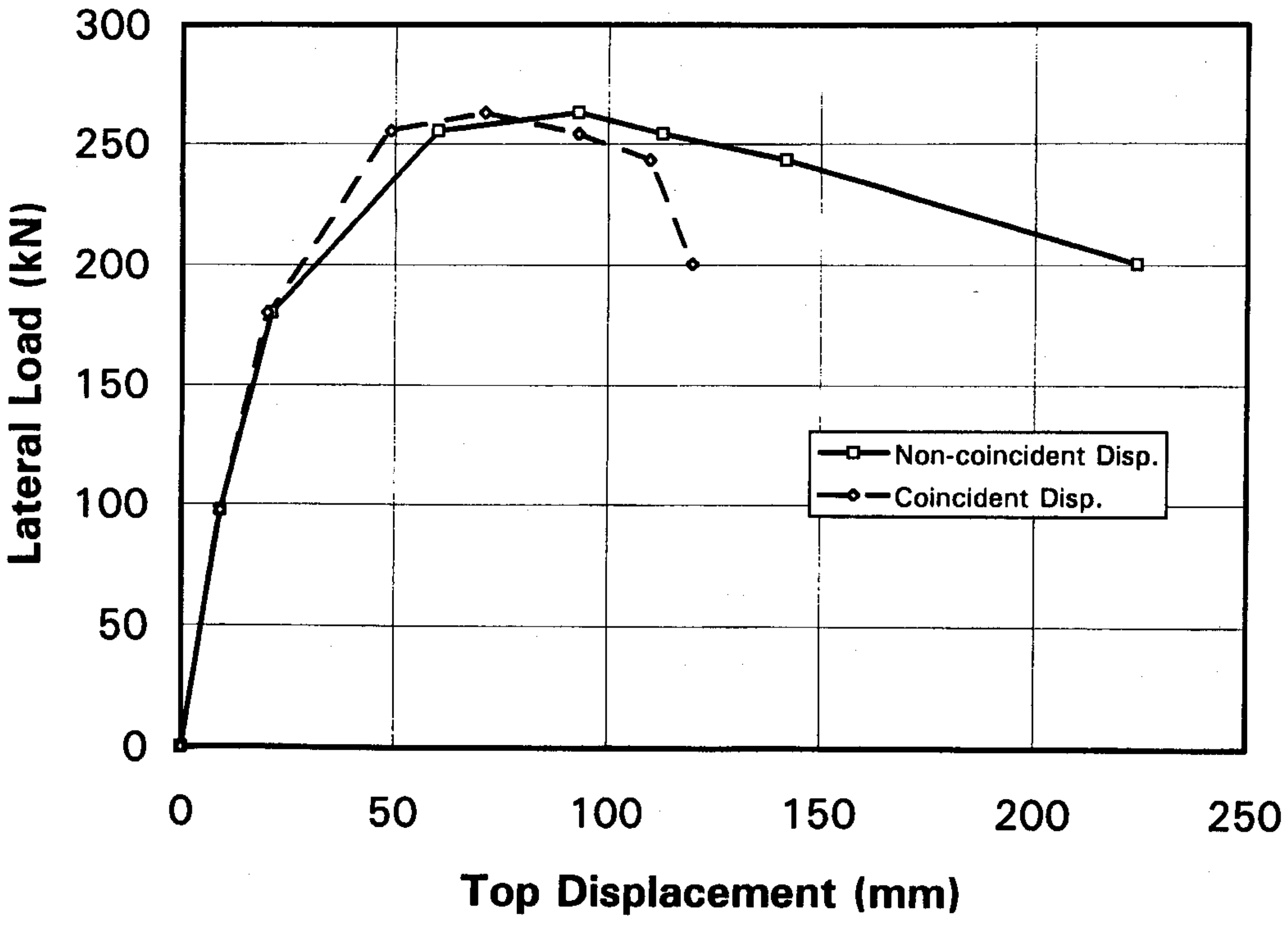

Fig. 3-22 Hysteresis Envelope for Specimen FA

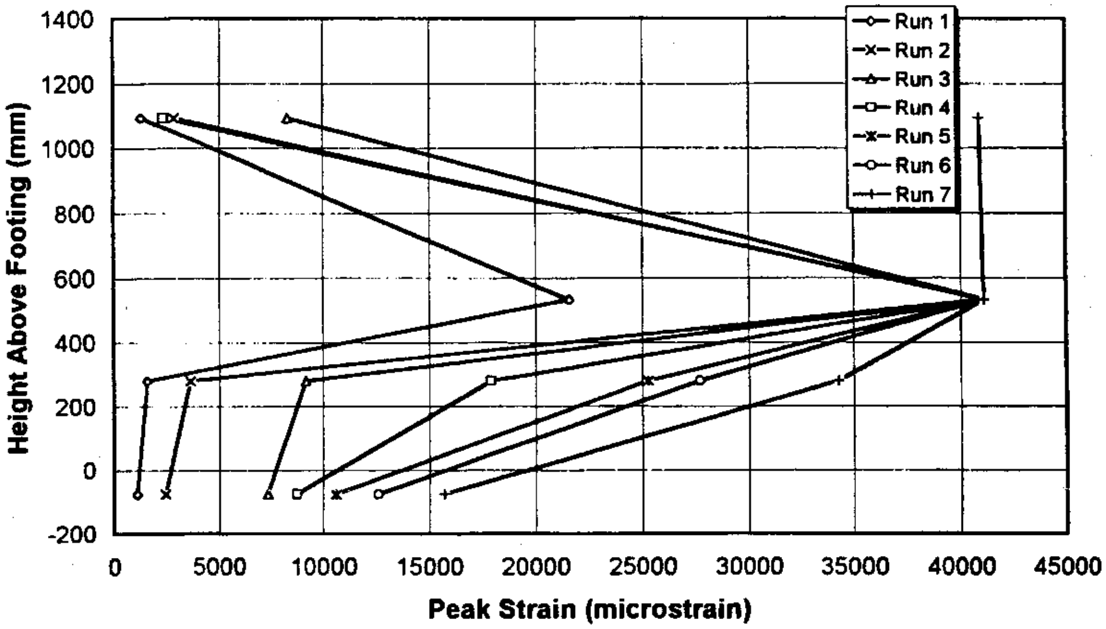

Fig. 3-23 Measured Tensile Strain Envelope for Extreme East Layer, Longitudinal Steel in FA

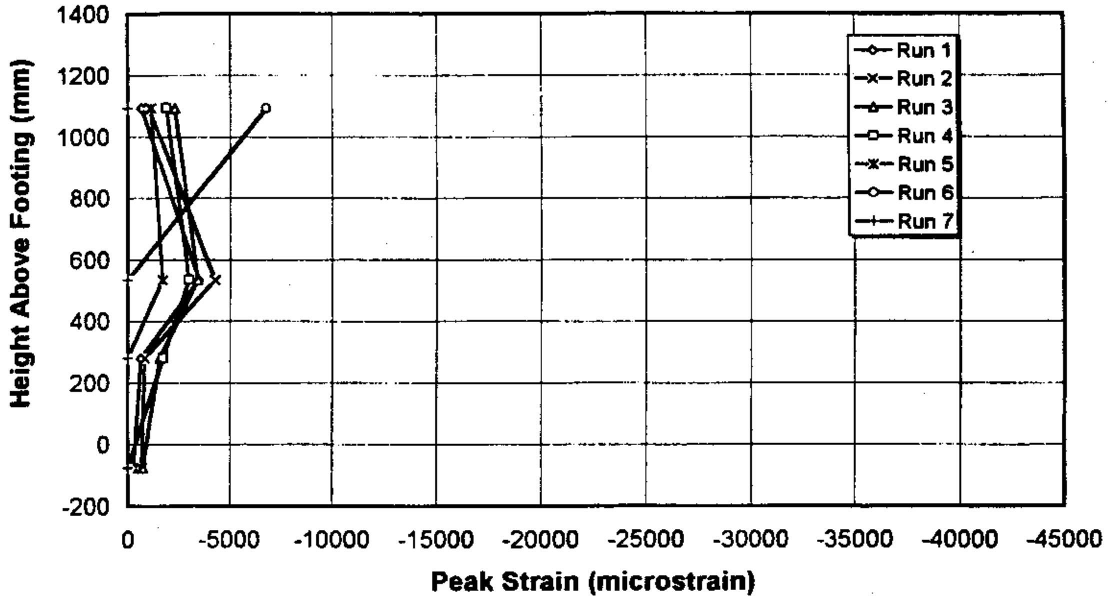

Fig. 3-24 Measured Compressive Strain Envelope for Extreme East Layer, Longitudinal Steel in FA

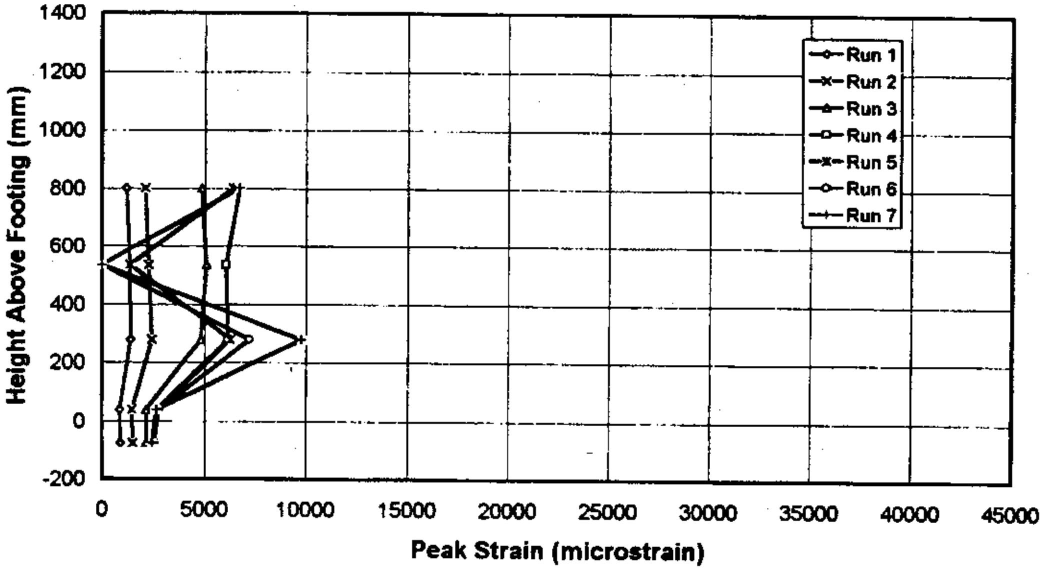

Fig. 3-25 Measured Tensile Strain Envelope for Extreme West Layer, Longitudinal Steel in FA

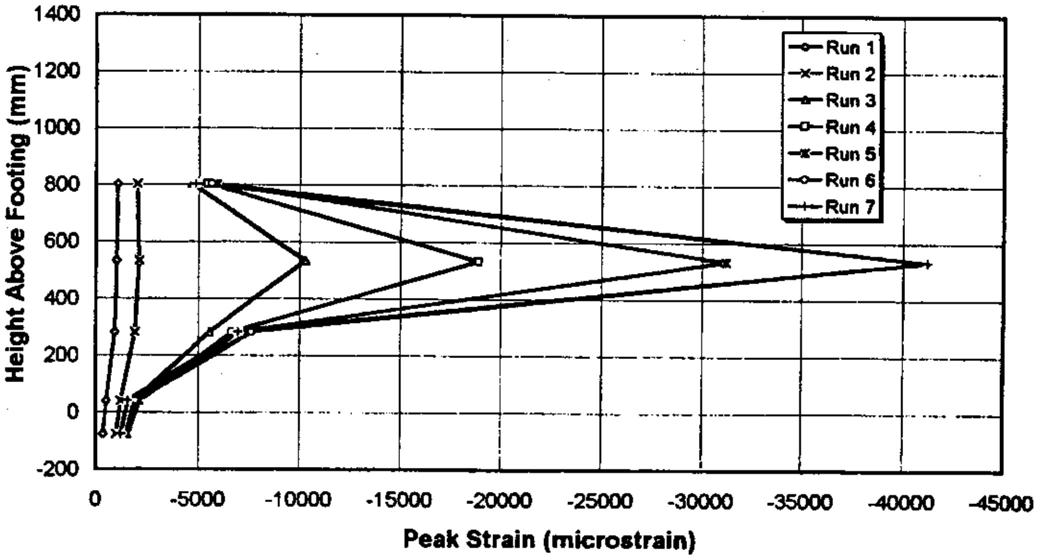

Fig. 3-26 Measured Compressive Strain Envelope for Extreme West Layer, Longitudinal Steel in FA

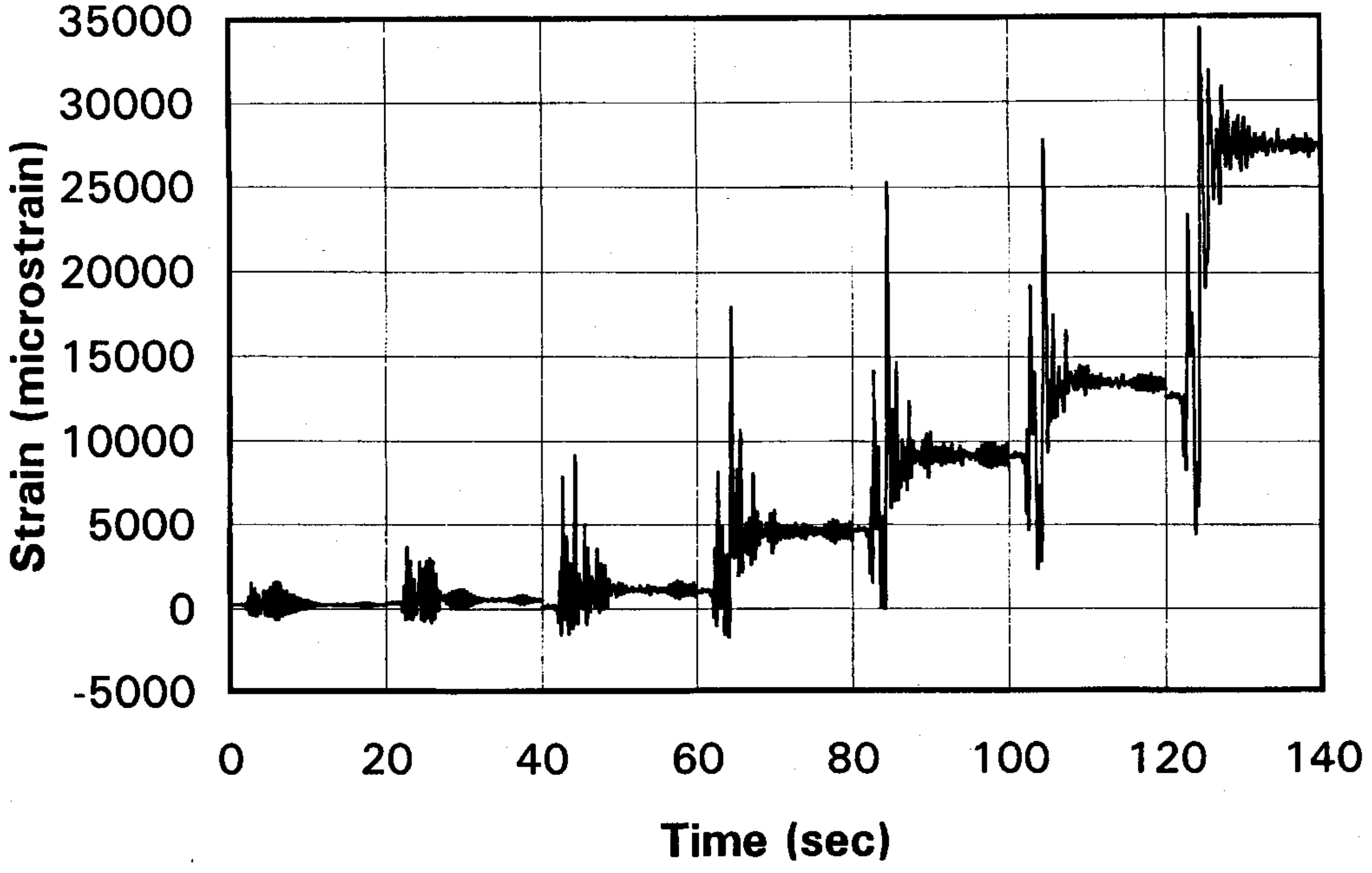

Fig. 3-27 Strain History for SG7, Extreme East Long. Bar, 279 mm Above Footing in FA

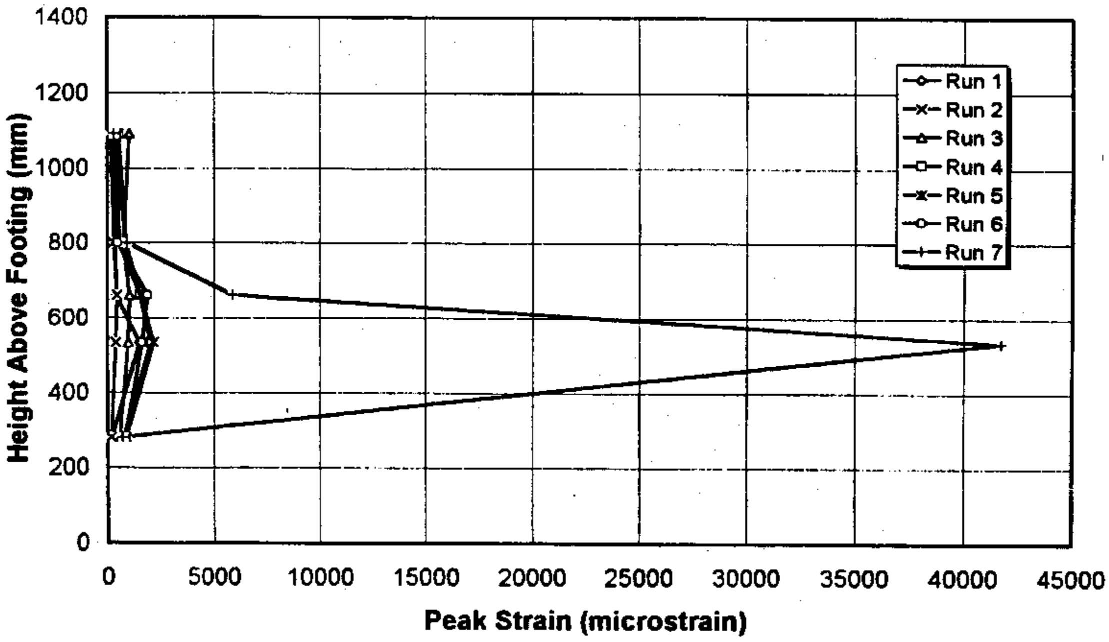

Fig. 3-28 Measured Tensile Strain Envelope for Crossties in FA

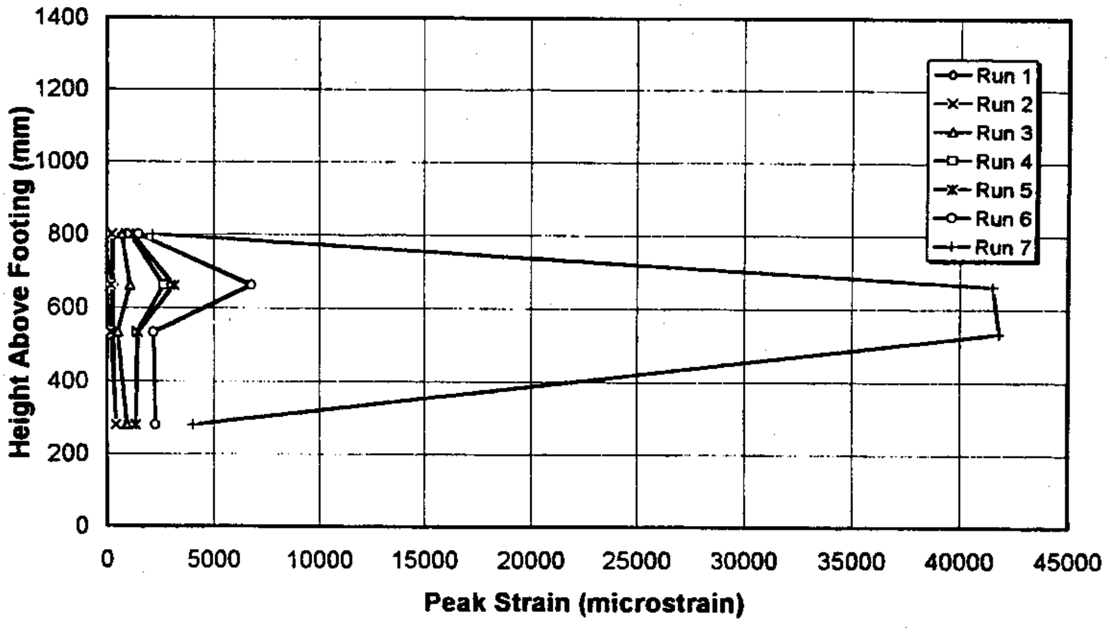

Fig. 3-29 Measured Tensile Strain Envelope for Perimeter Ties in FA

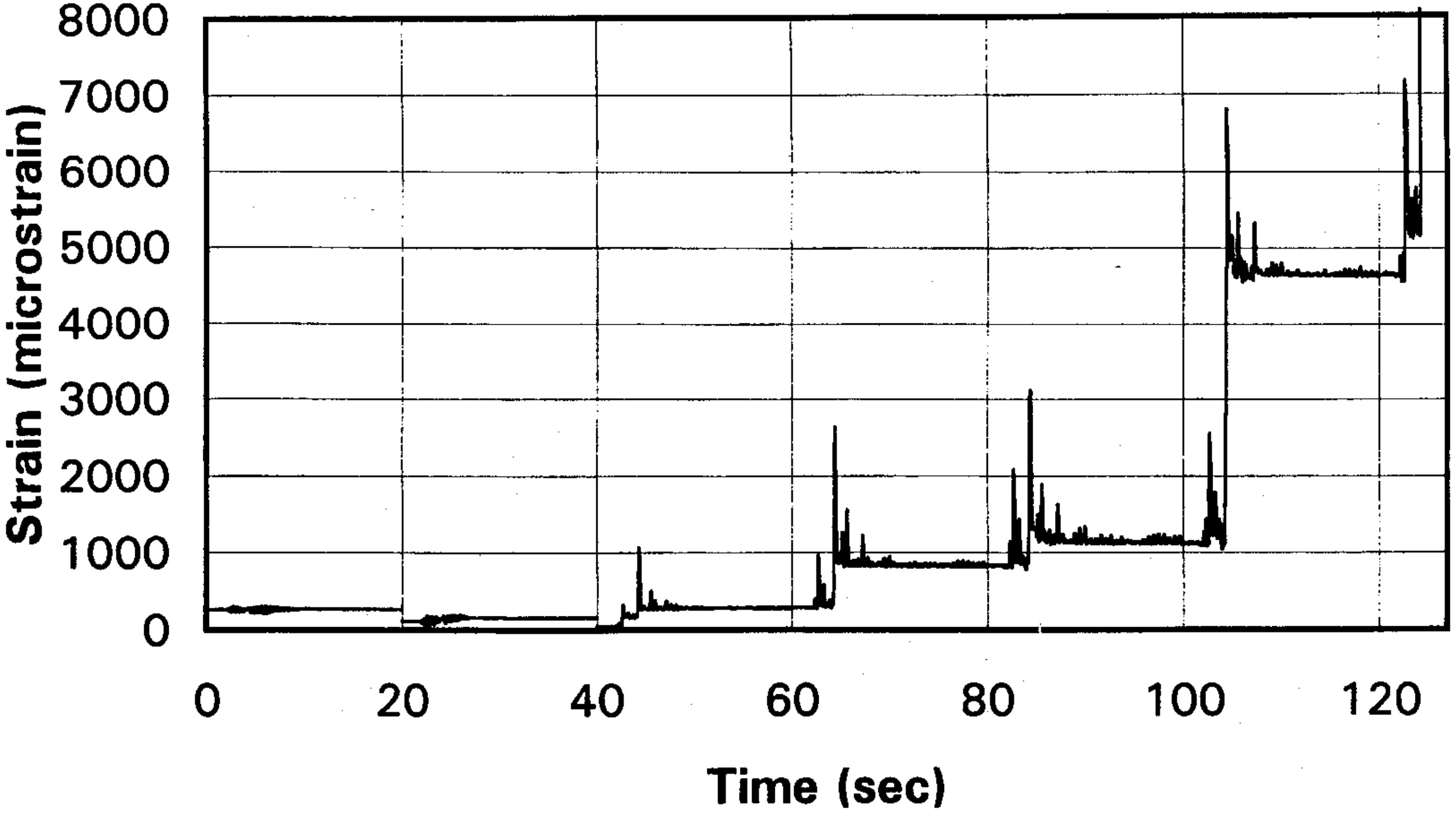

Fig. 3-30 Strain History for SG24, West Perimeter Tie, 660 mm Above Footing in FA

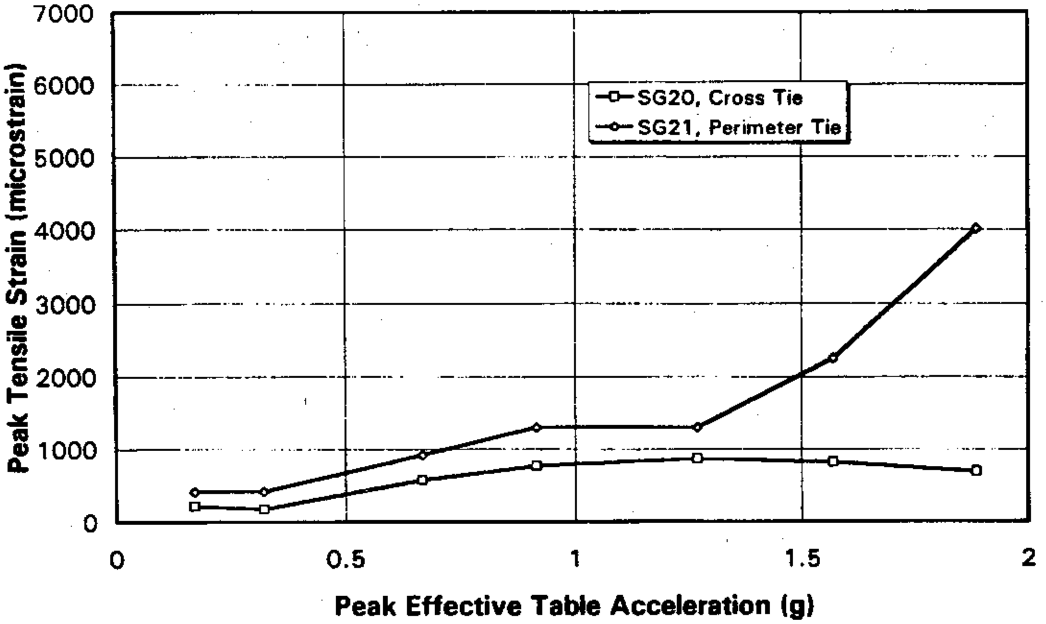

Fig. 3-31 Tie Bar Strains at 279 mm Above Footing in FA

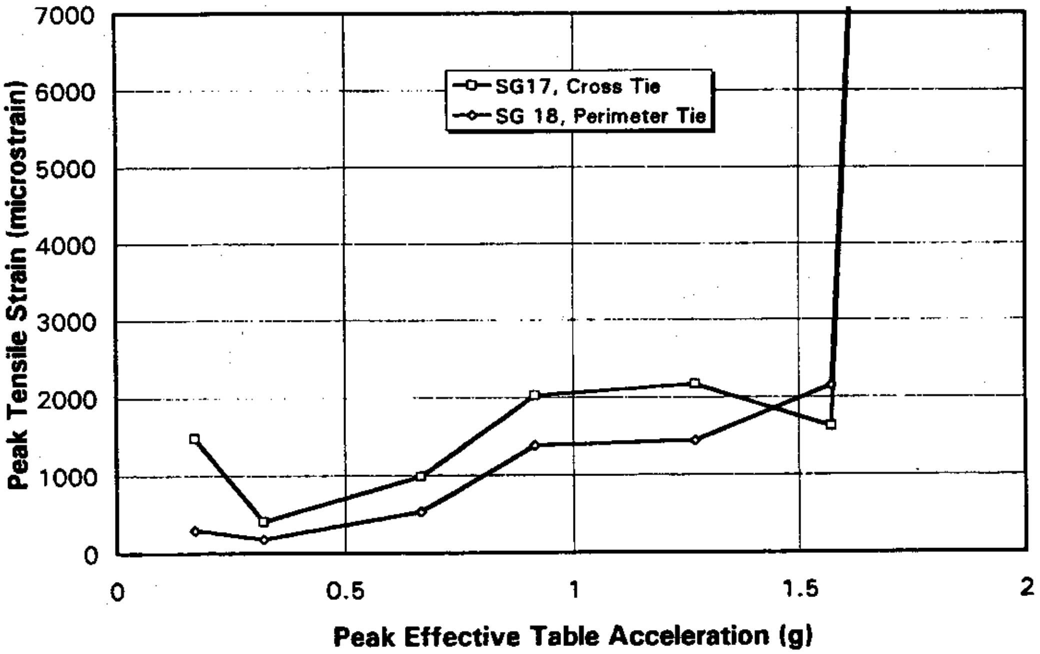

Fig. 3-32 Tie Bar Strains at 533 mm Above Footing in FA

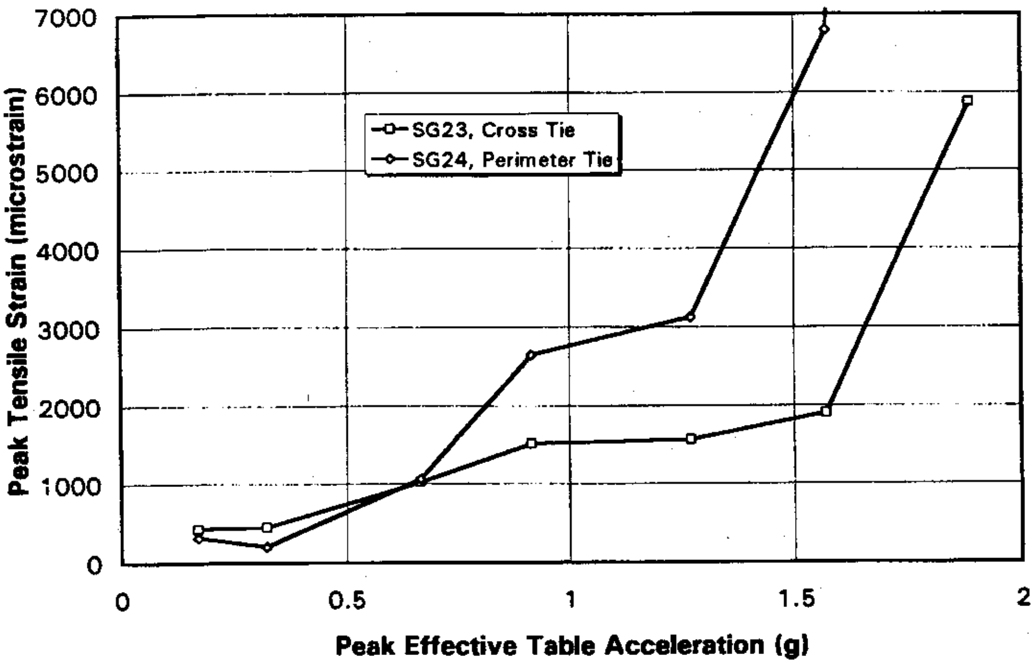

Fig. 3-33 Tie Bar Strains at 660 mm Above Footing in FA

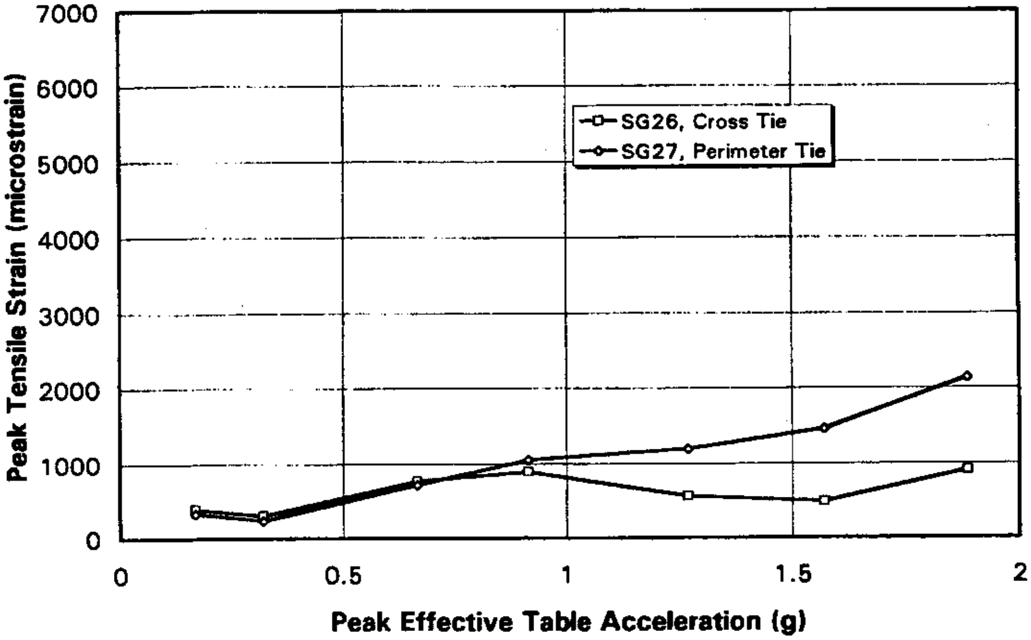

Fig. 3-34 Tie Bar Strains at 800 mm Above Footing in FA

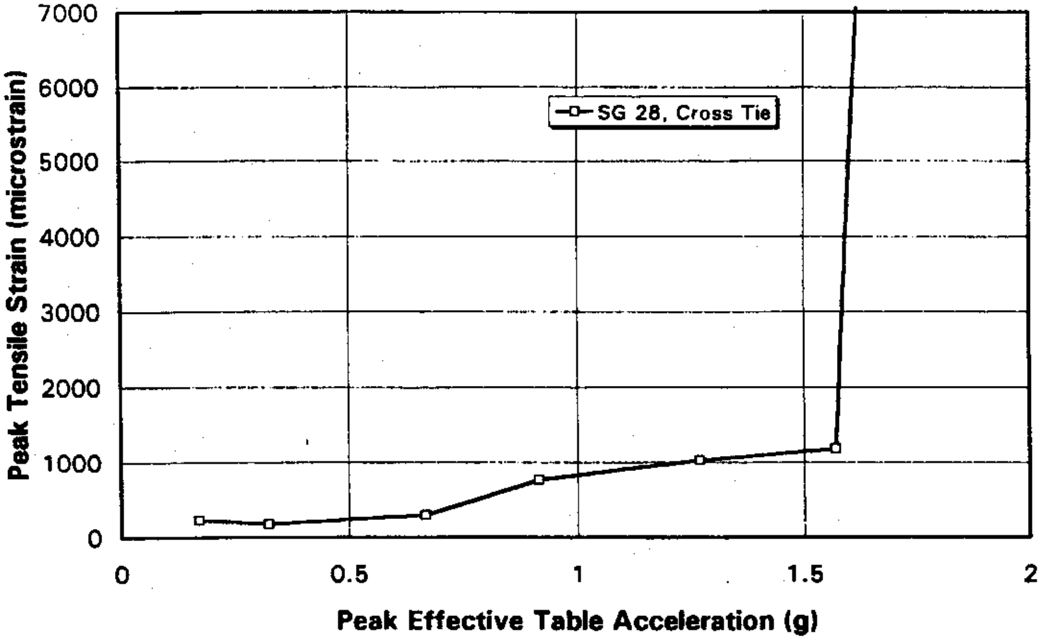

Fig. 3-35 Tie Bar Strains at 1092 mm Above Footing in FA

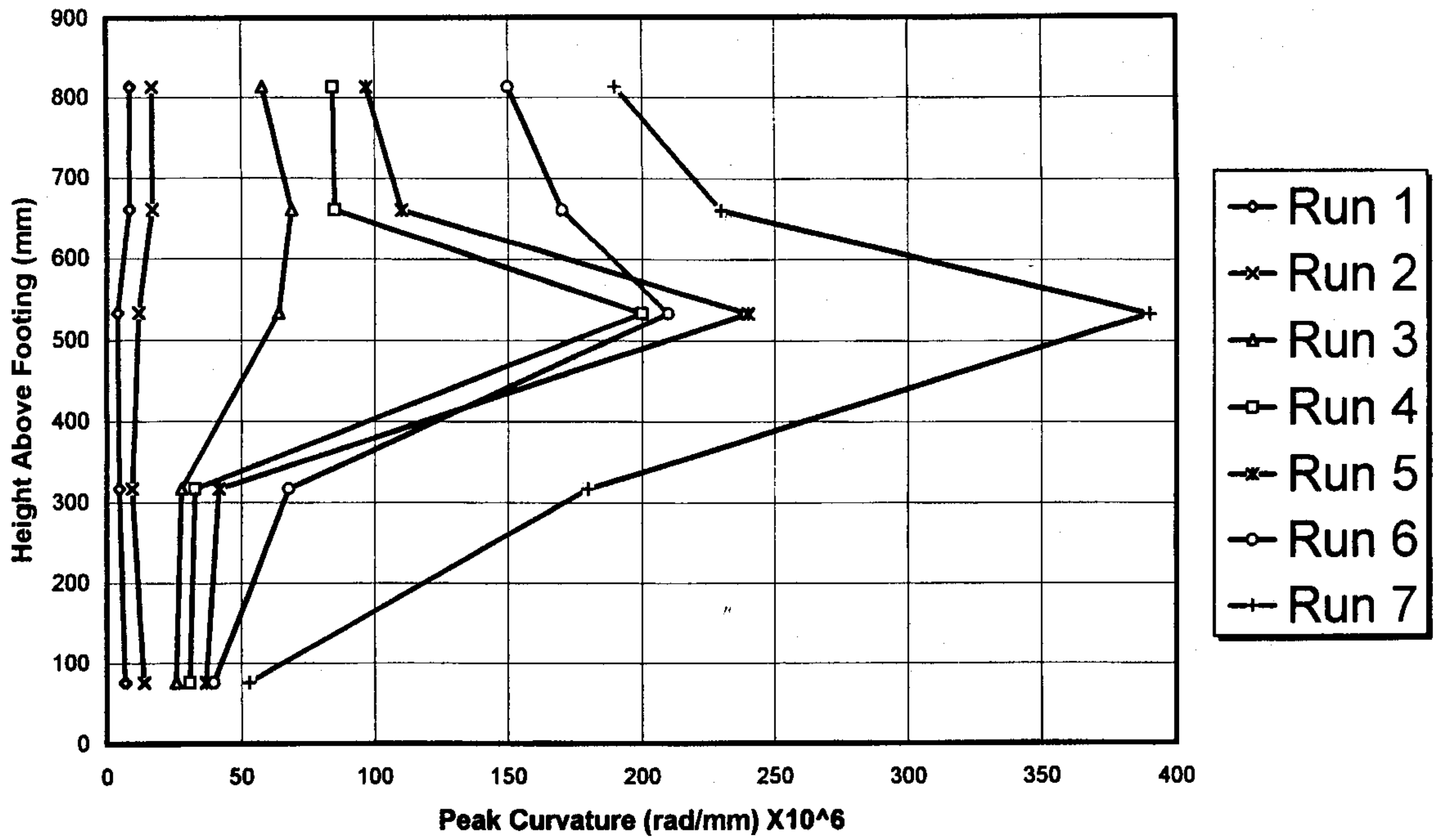

Fig. 3-36 Measured Curvature Envelope for Specimen FA

Fig. 3-37 Specimen FR, Run 8, Cracking

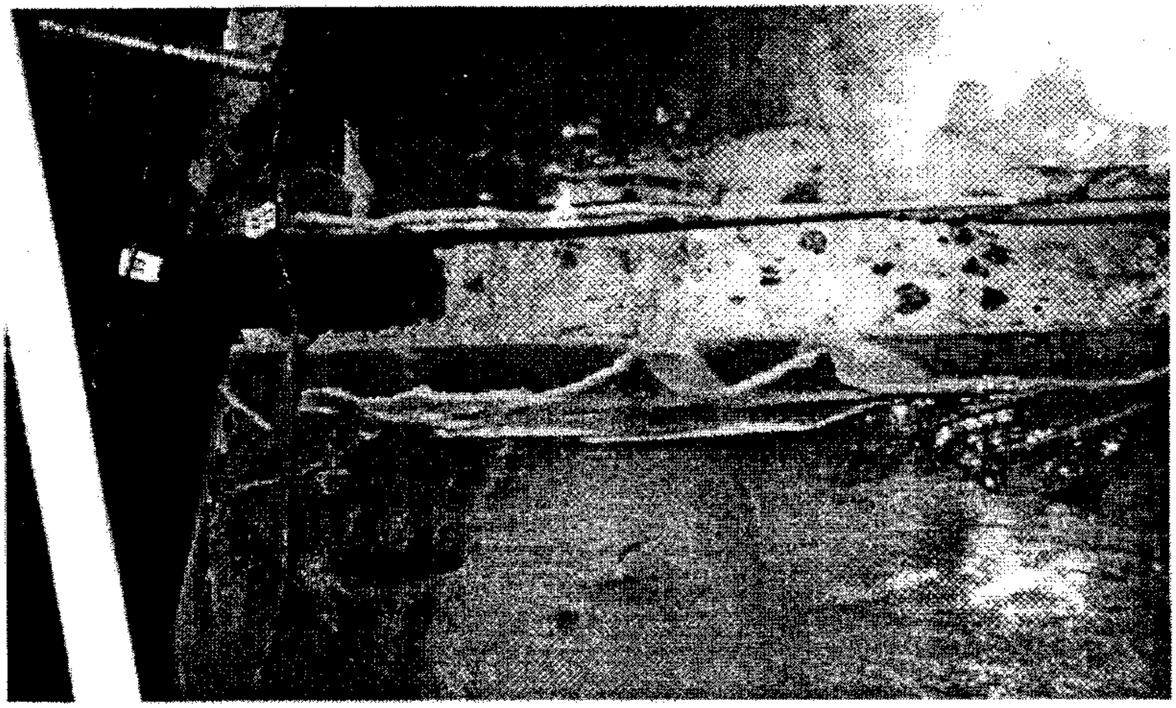

Fig. 3-38 Specimen FR, Run 8, Spalling

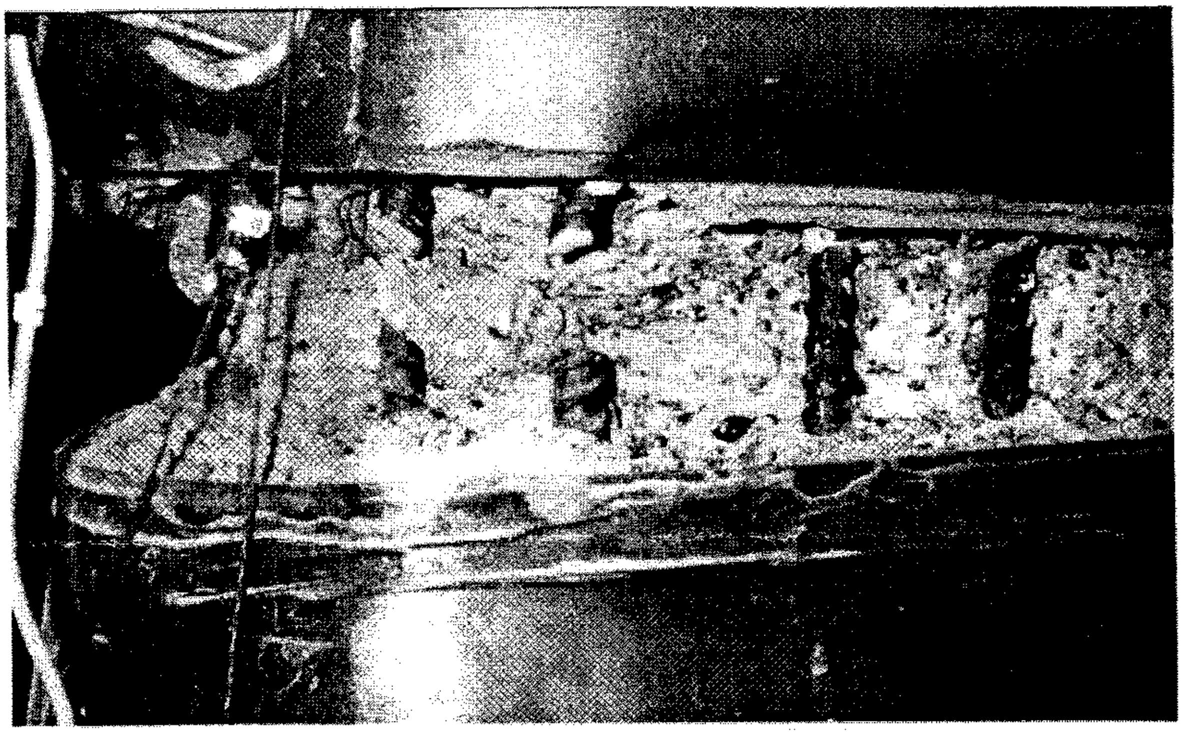

Fig. 3-39 Specimen FR, After Testing, Bar Fractures

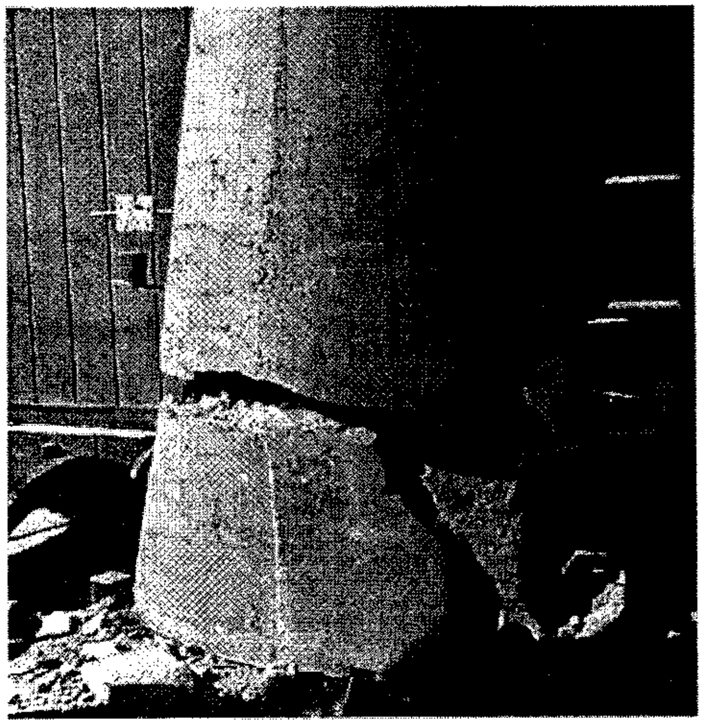

Fig. 3-40 Specimen FR, After Testing, Jacket Removed

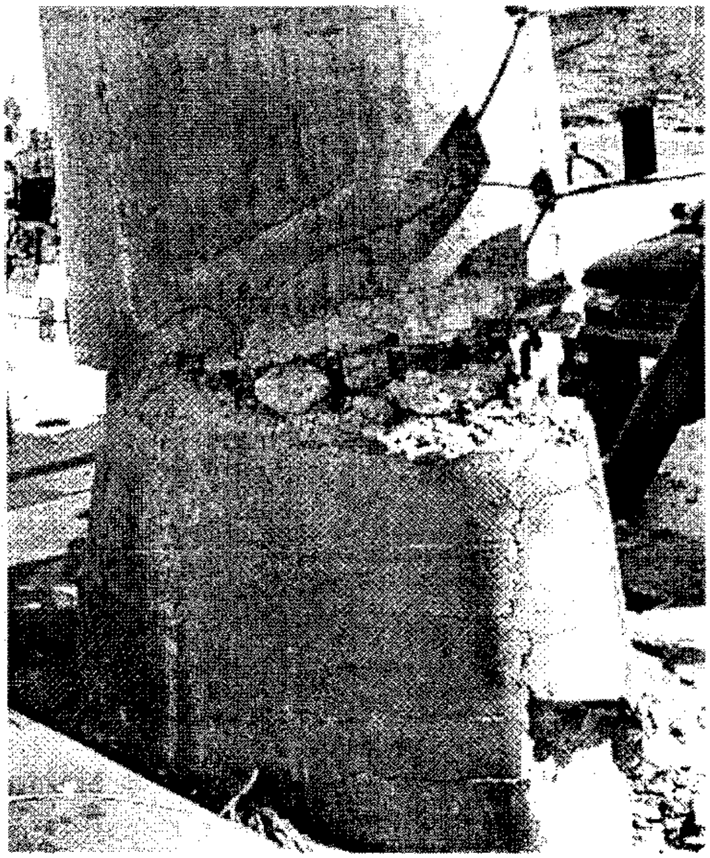

Fig. 3-41 Specimen FR, After Testing, Jacket Removed

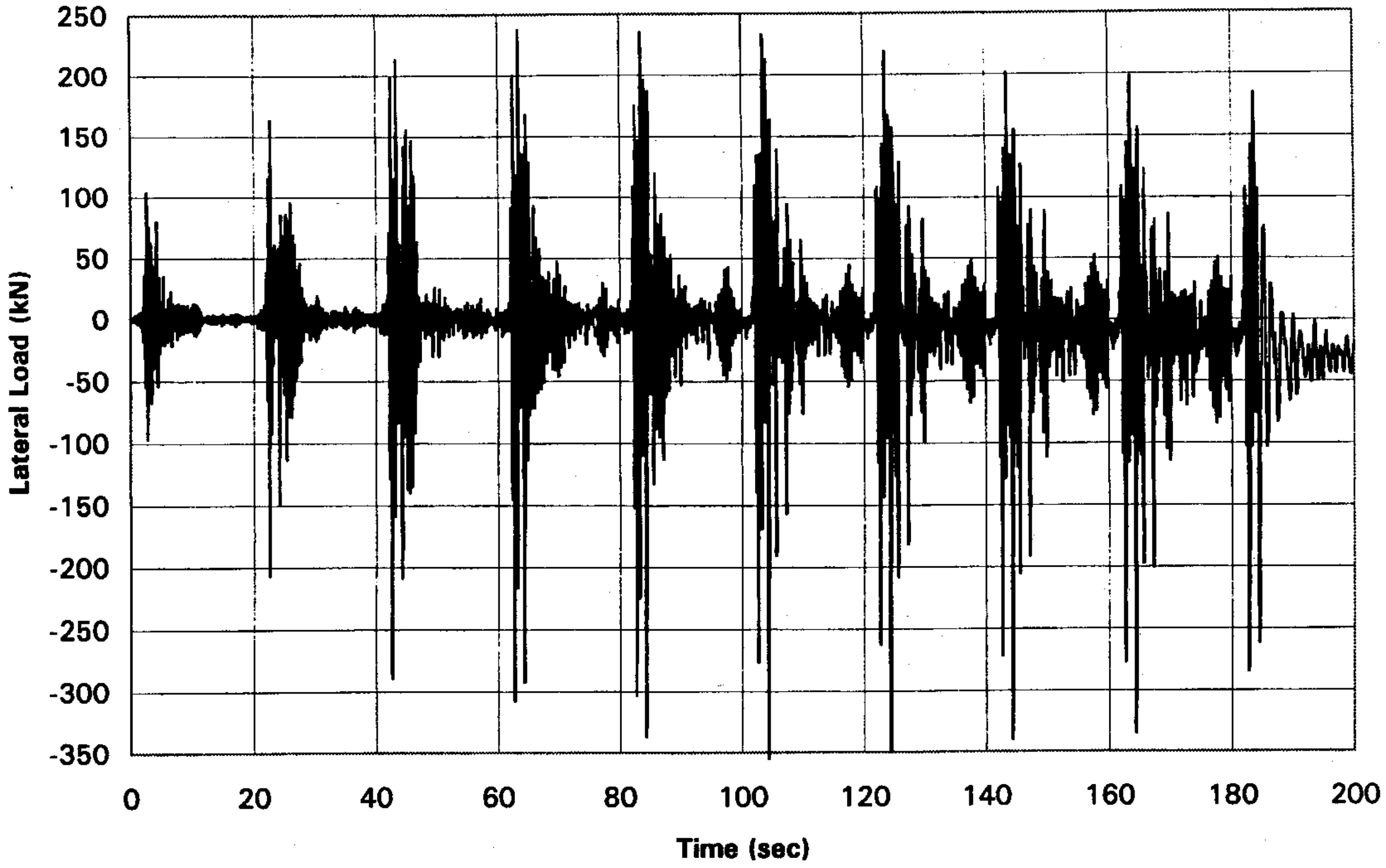

Fig. 3-42 Lateral Loading History for Specimen FR

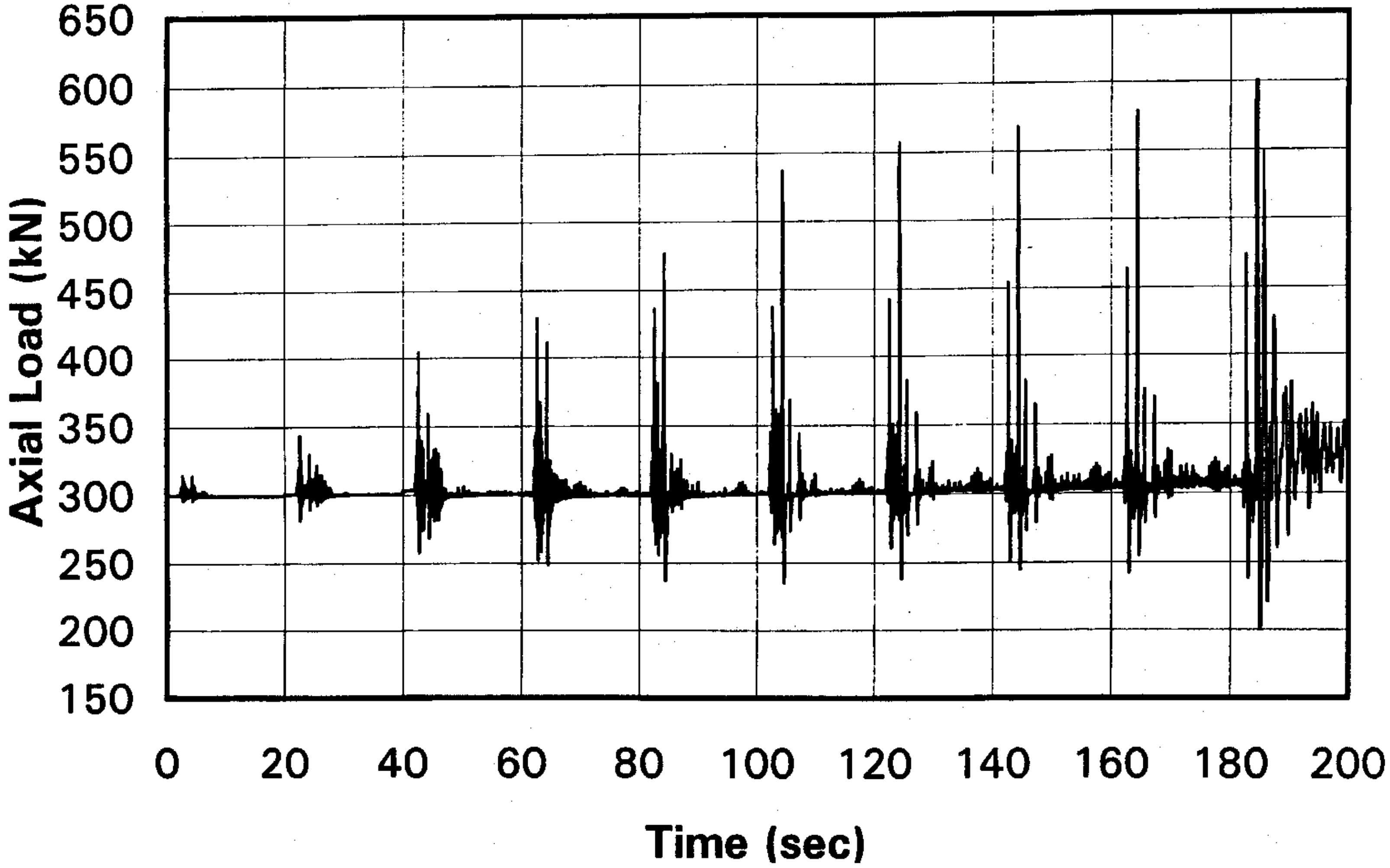

Fig. 3-43 Axial History for Specimen FR

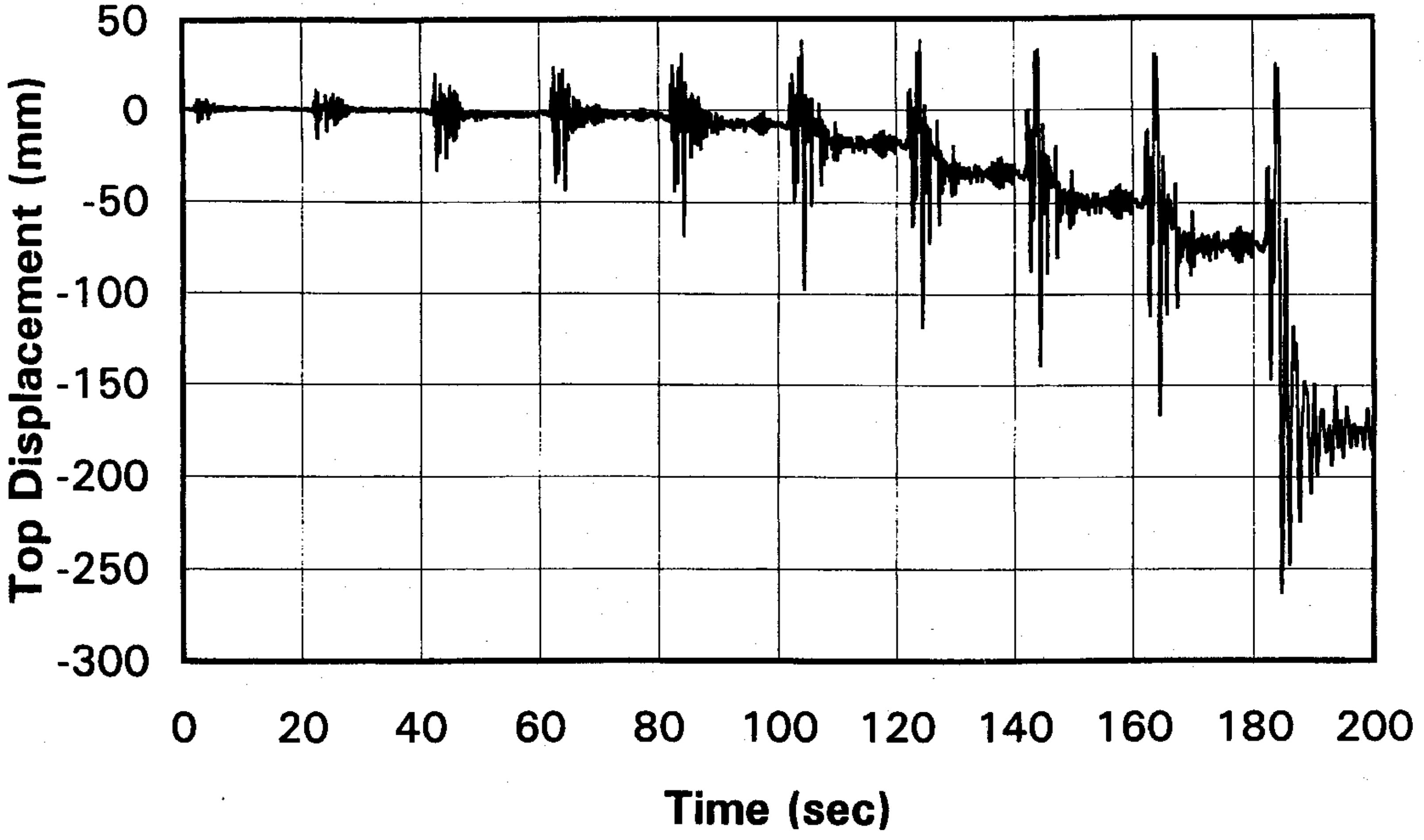

Fig. 3-44 Displacement History for Specimen FR, All Runs

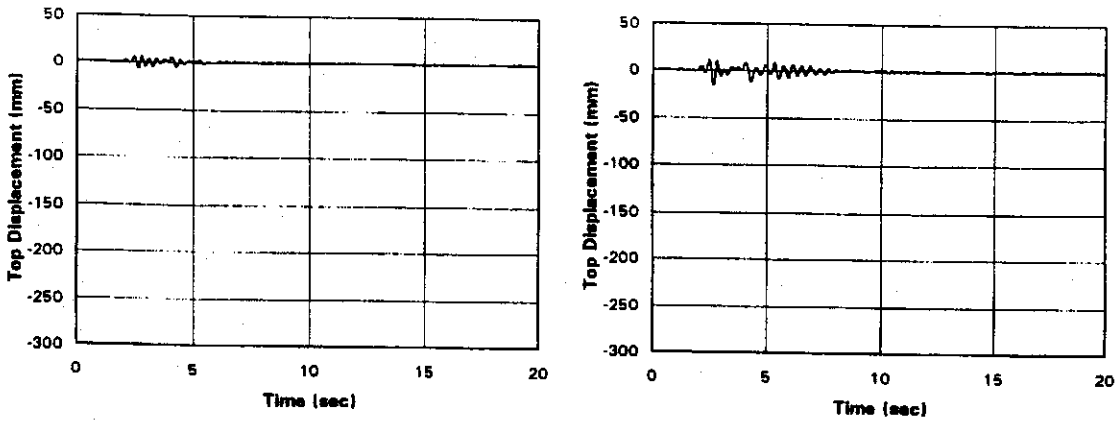

Displacement History for Specimen FR, Run 1

Displacement History for Specimen FR, Run 2

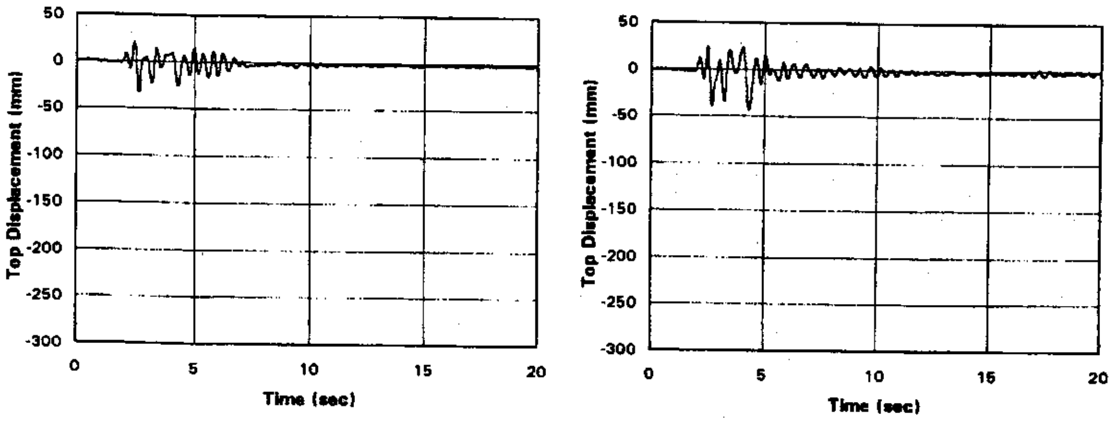

Displacement History for Specimen FR, Run 3

Displacement History for Specimen FR, Run 4

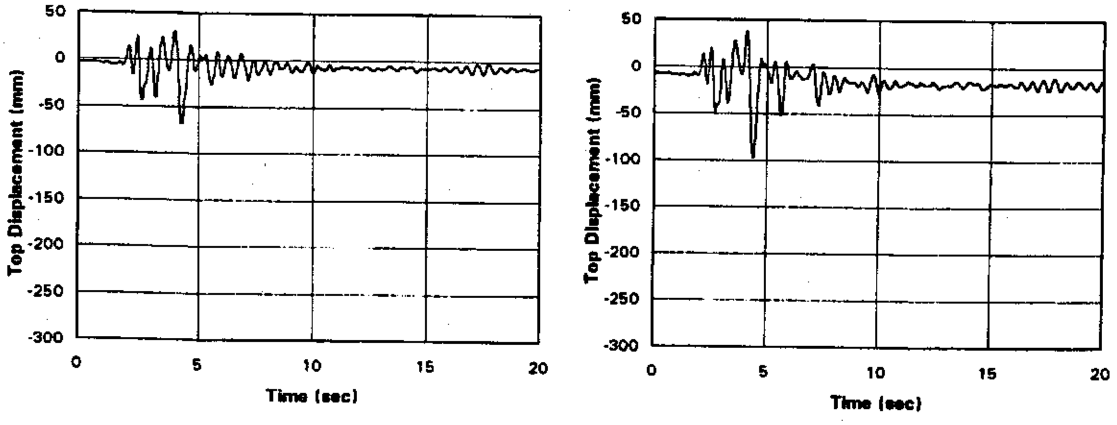

Displacement History for Specimen FR, Run 5

Displacement History for Specimen FR, Run 6

Fig. 3-45 Displacement History, Specimen FR, Runs 1-6

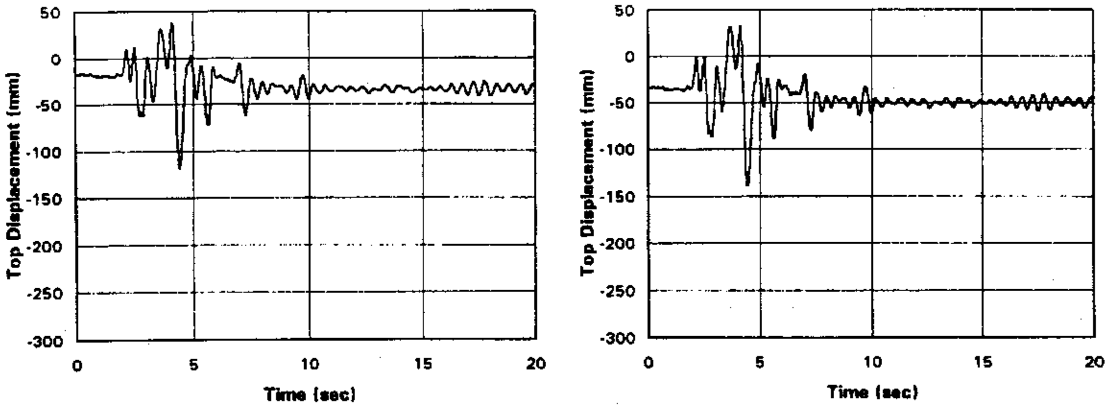

Displacement History for Specimen FR, Run 7

Displacement History for Specimen FR, Run 8

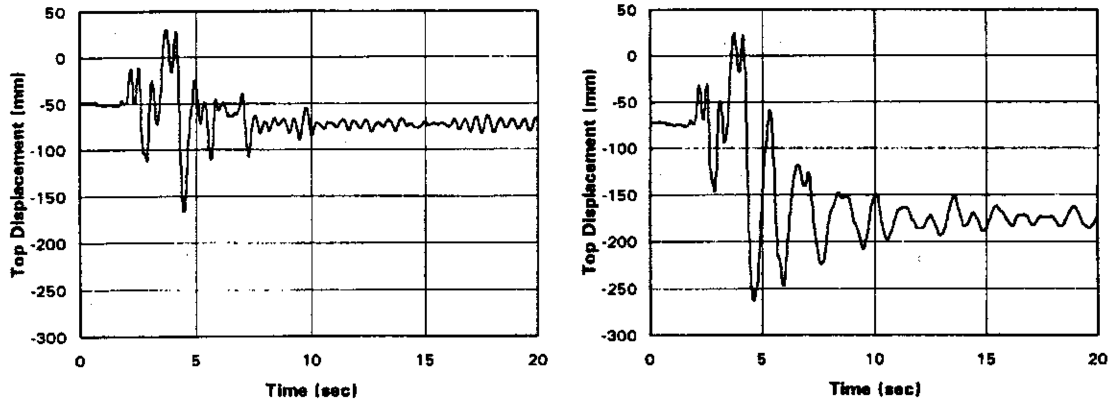

Displacement History for Specimen FR, Run 9

Displacement History for Specimen FR, Run 10

Fig. 3-46 Displacement History, Specimen FR, Runs 7-10

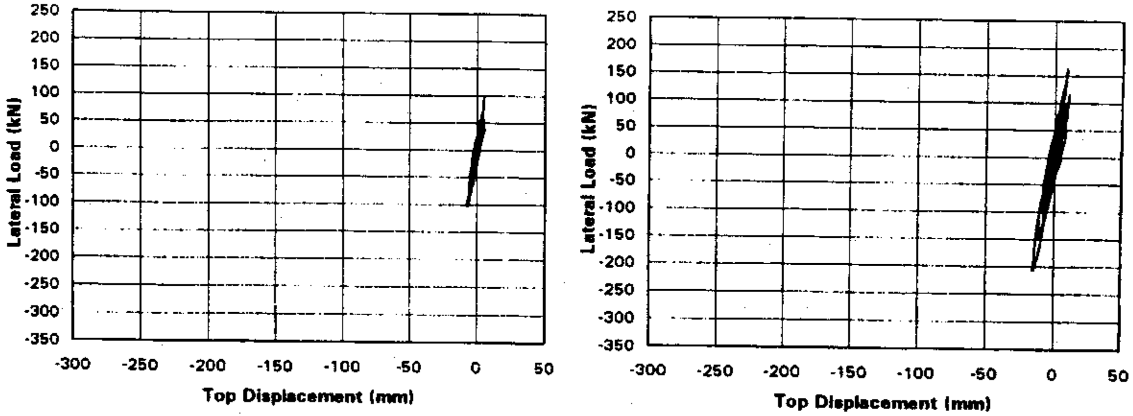

Hysteresis Loop for
Specimen FR, Run 1

Hysteresis Loop for
Specimen FR, Run 2

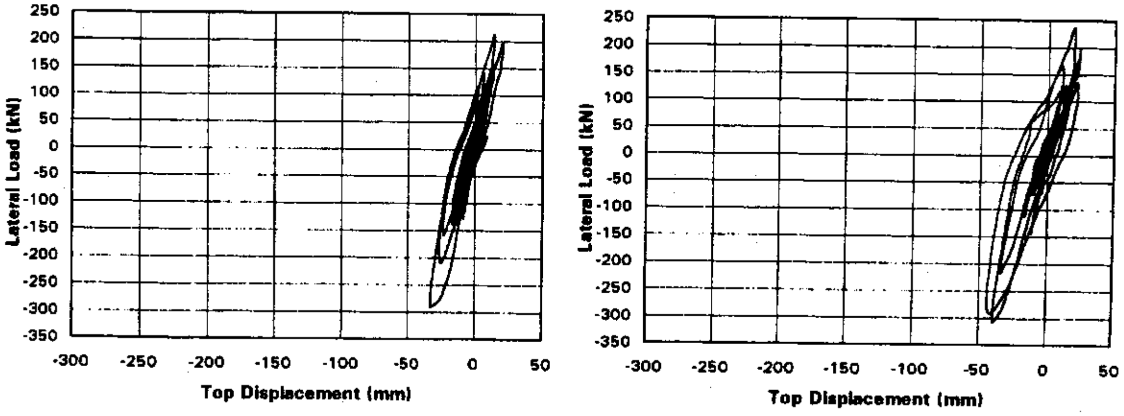

Hysteresis Loop for
Specimen FR, Run 3

Hysteresis Loop for
Specimen FR, Run 4

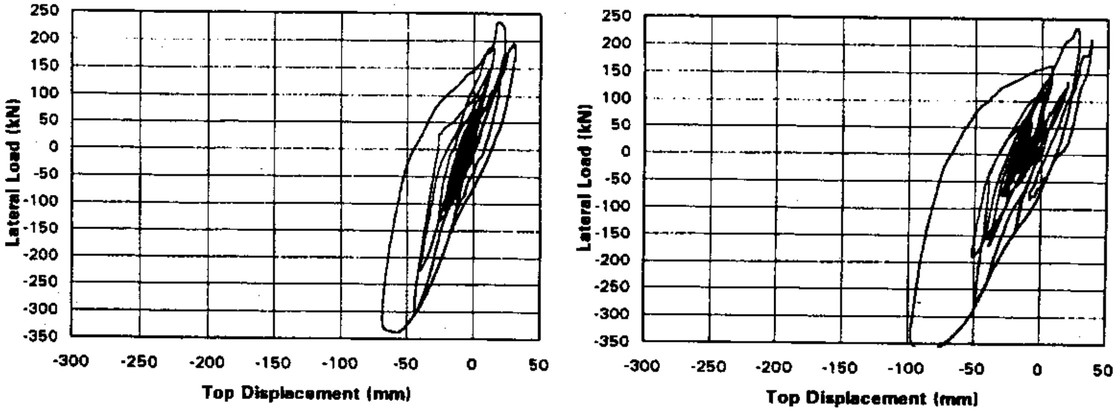

Hysteresis Loop for
Specimen FR, Run 5

Hysteresis Loop for
Specimen FR, Run 6

Fig. 3-47 Hysteresis Loops, Specimen FR, Runs 1-6

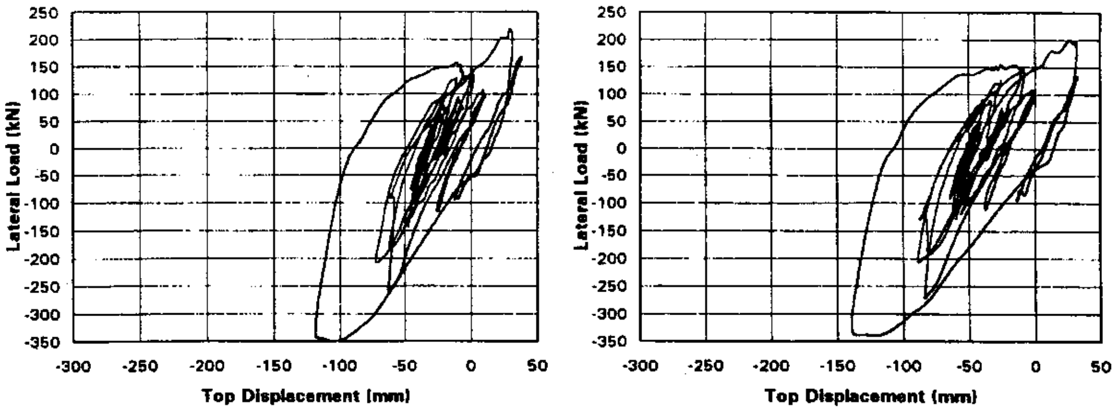

Hysteresis Loop for
Specimen FR, Run 7

Hysteresis Loop for
Specimen FR, Run 8

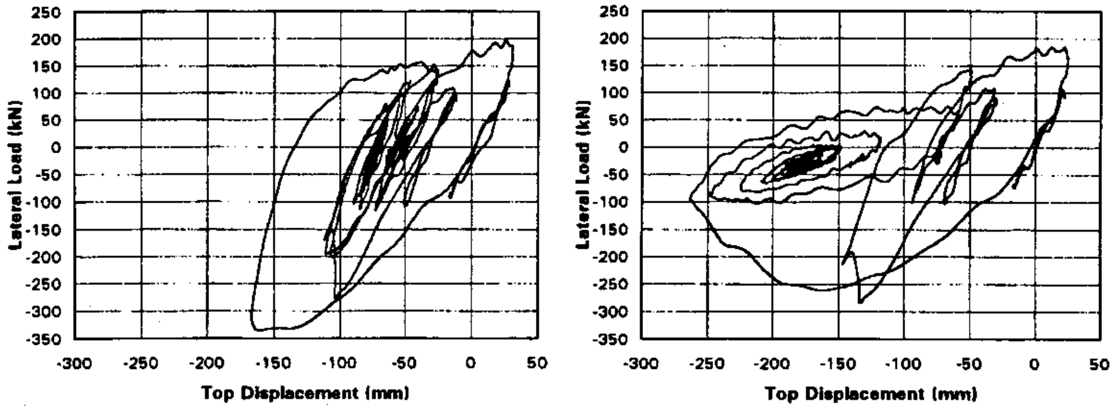

Hysteresis Loop for
Specimen FR, Run 9

Hysteresis Loop for
Specimen FR, Run 10

Fig. 3-48 Hysteresis Loops, Specimen FR, Runs 7-10

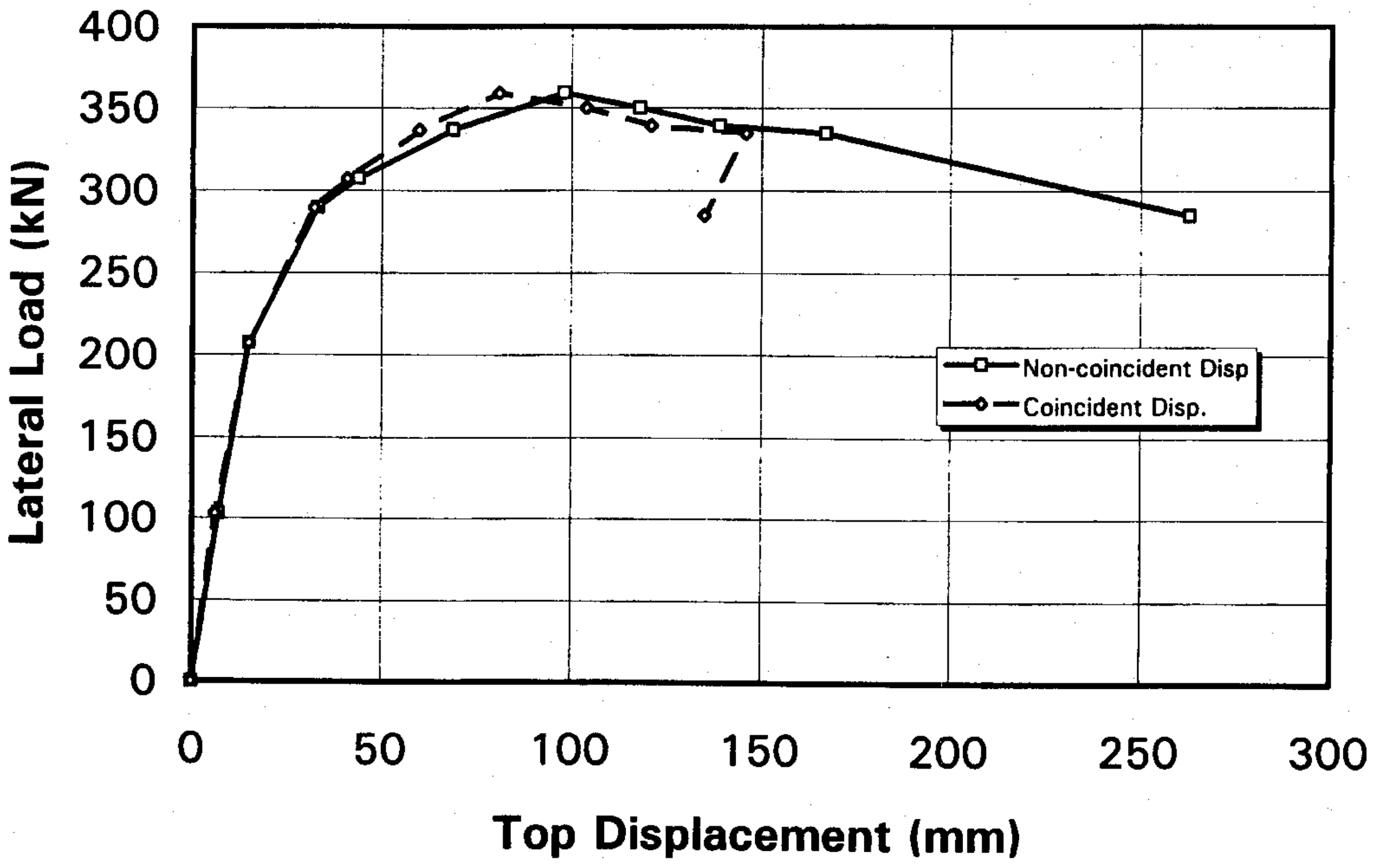

Fig. 3-49 Hysteresis Envelope for Specimen FR

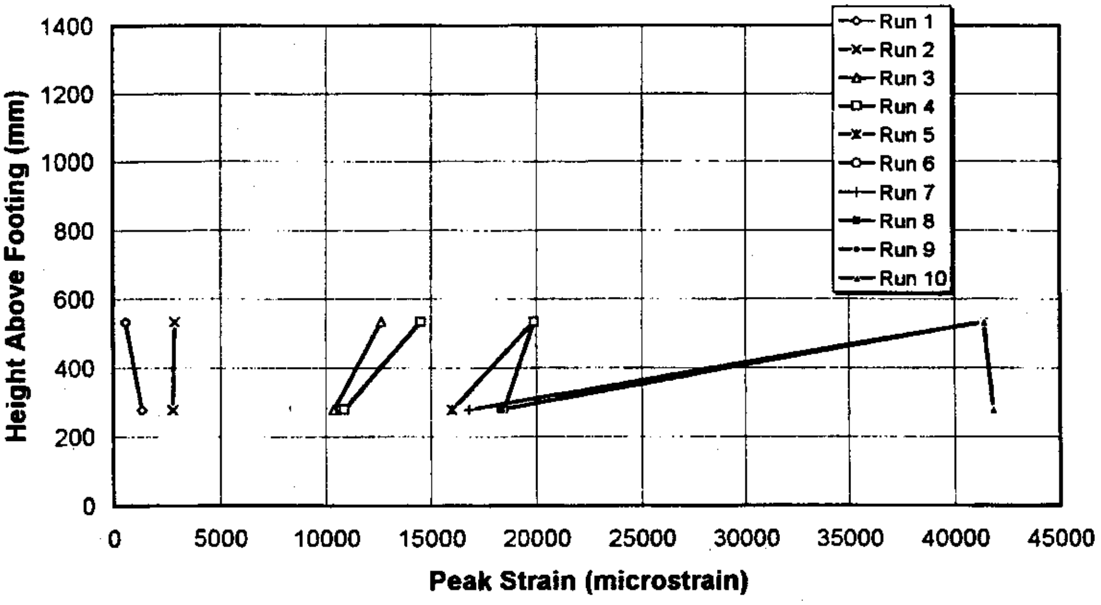

Fig. 3-50 Measured Tensile Strain Envelope for Extreme East Layer, Longitudinal Steel in FR

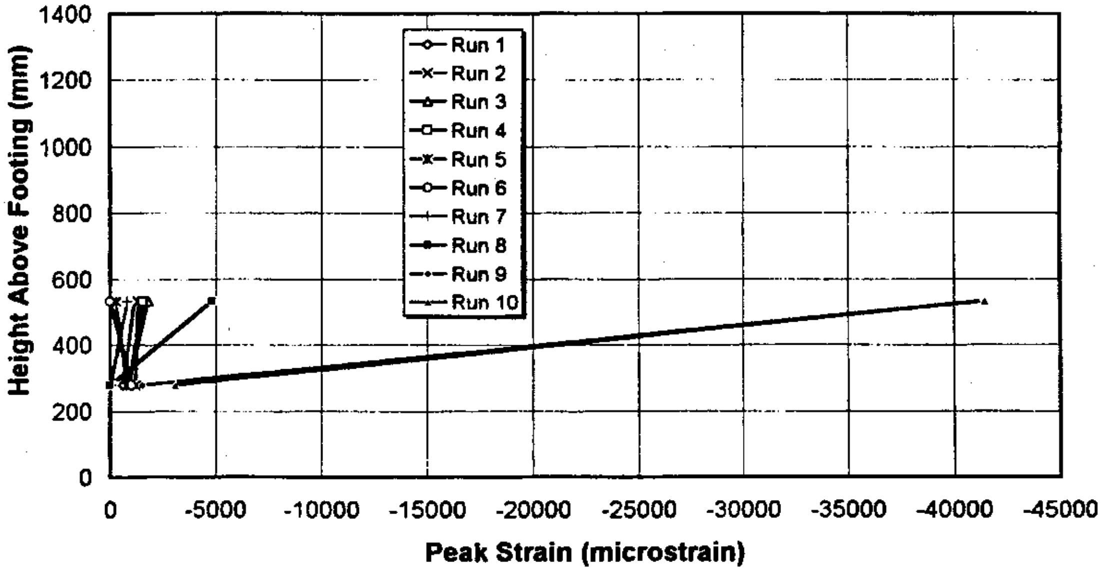

Fig. 3-51 Measured Compressive Strain Envelope for Extreme East Layer, Longitudinal Steel in FR

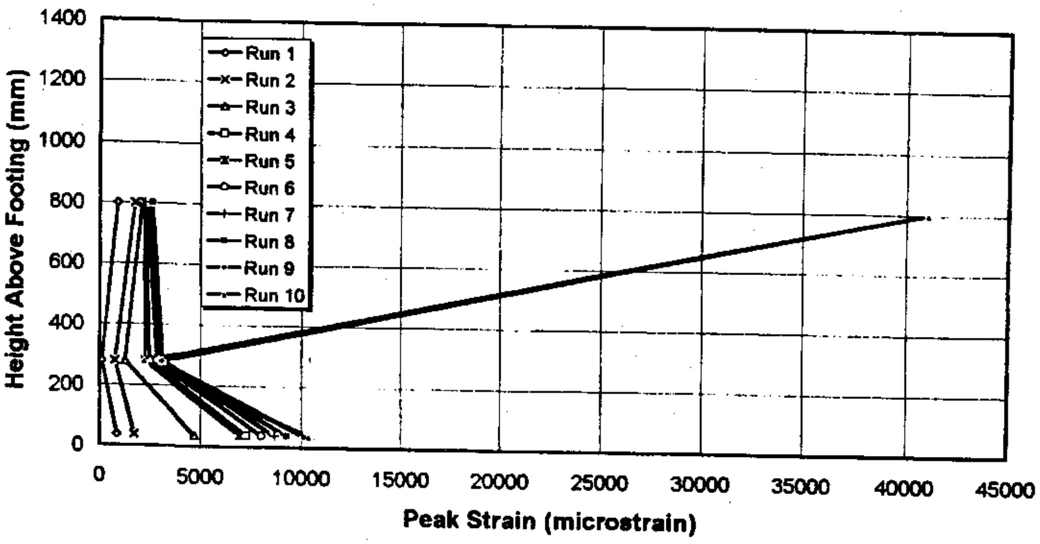

Fig. 3-52 Measured Tensile Strain Envelope for Extreme West Layer, Longitudinal Steel in FR

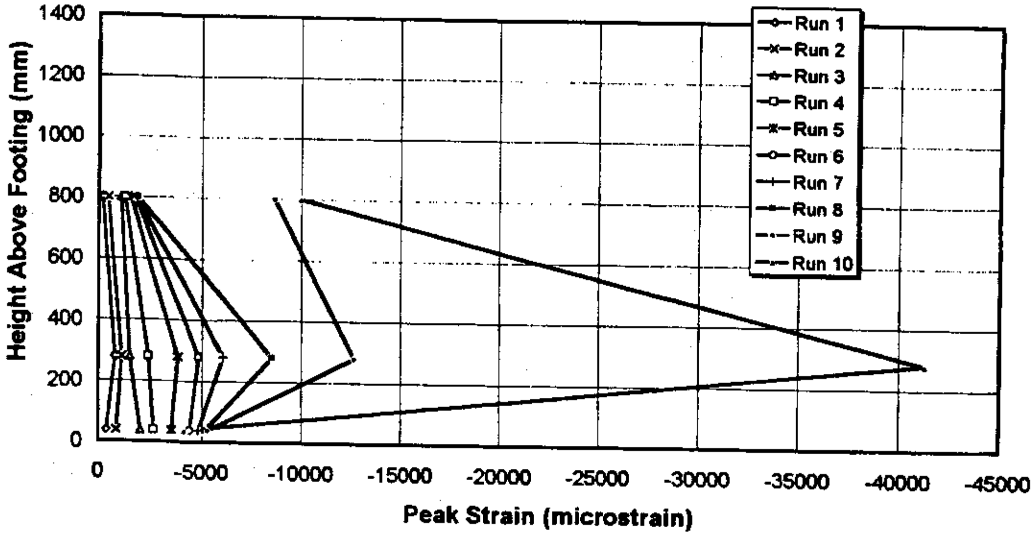

Fig. 3-53 Measured Compressive Strain Envelope for Extreme West Layer, Longitudinal Steel in FR

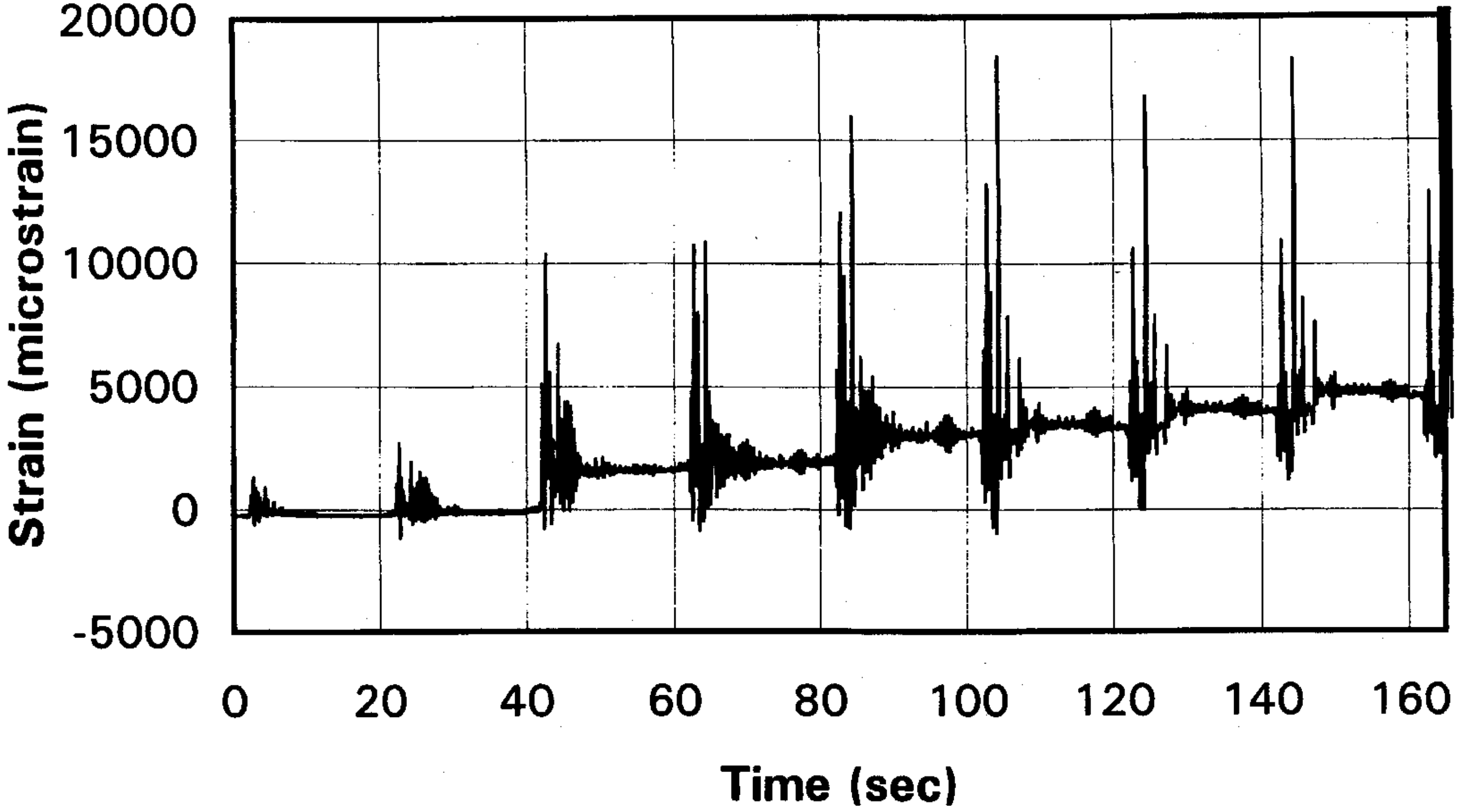

Fig. 3-54 Strain History for SG7, Extreme East Long. Bar, 279 mm Above Footing in FR

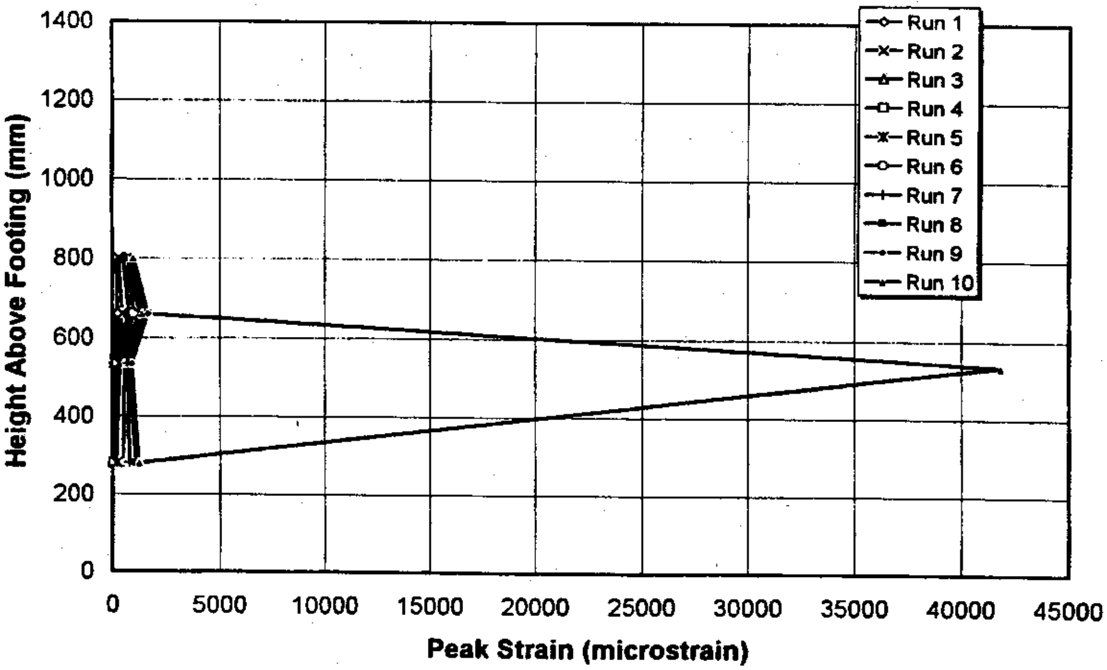

Fig. 3-55 Measured Tensile Strain Envelope for Crossties in FR

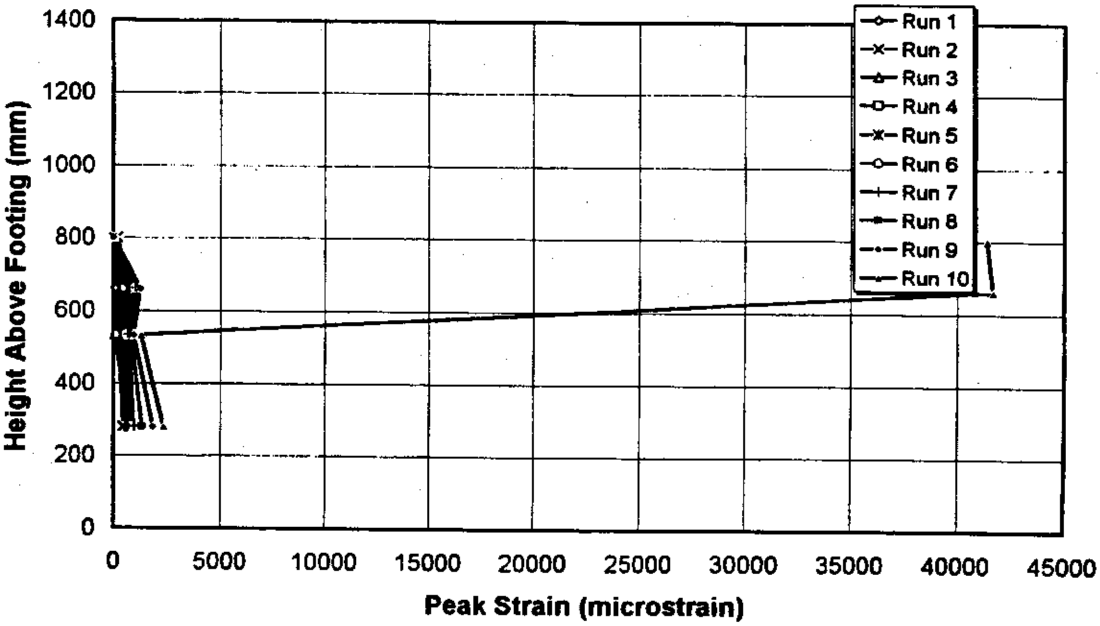

Fig. 3-56 Measured Tensile Strain Envelope for Perimeter Ties in FR

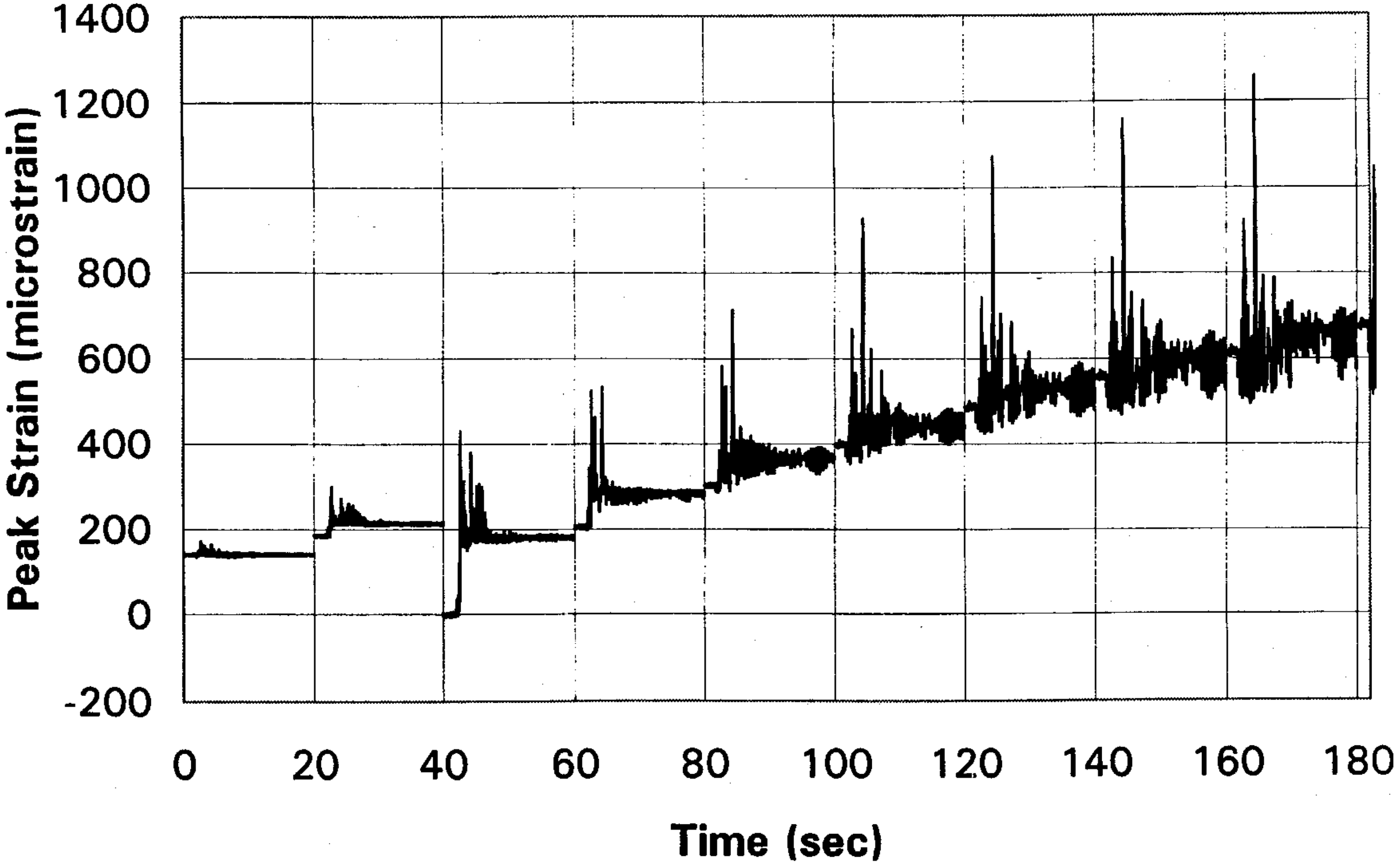

Fig. 3-57 Strain History for SG24, West Perimeter Tie, 660 mm Above Footing in FA

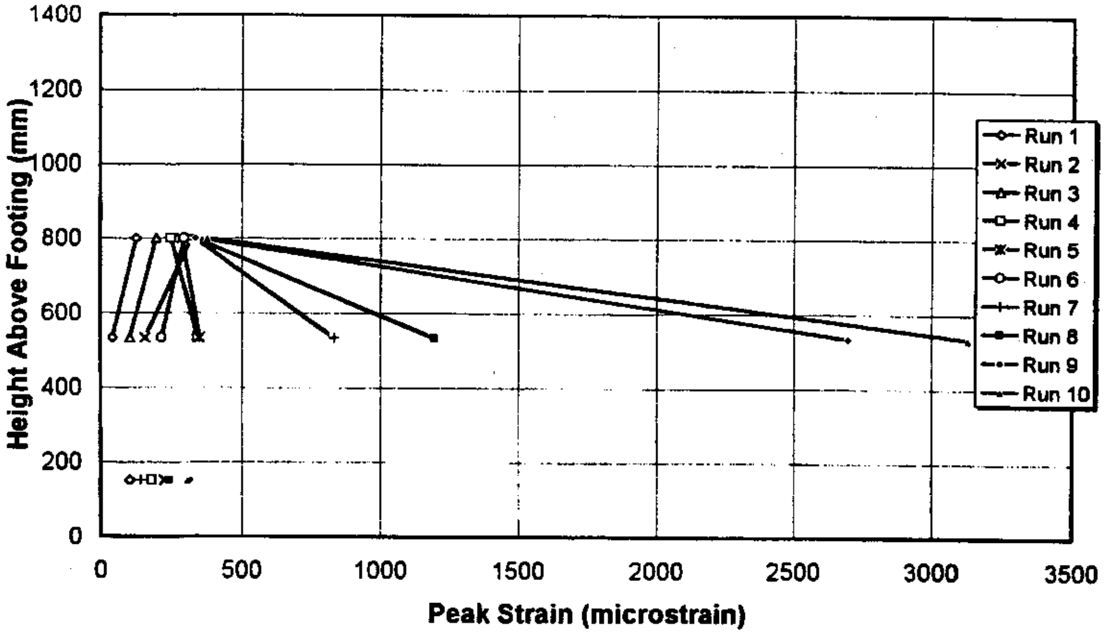

Fig. 3-62 Measured Horizontal Tensile Strain Envelope for East Side of Jacket

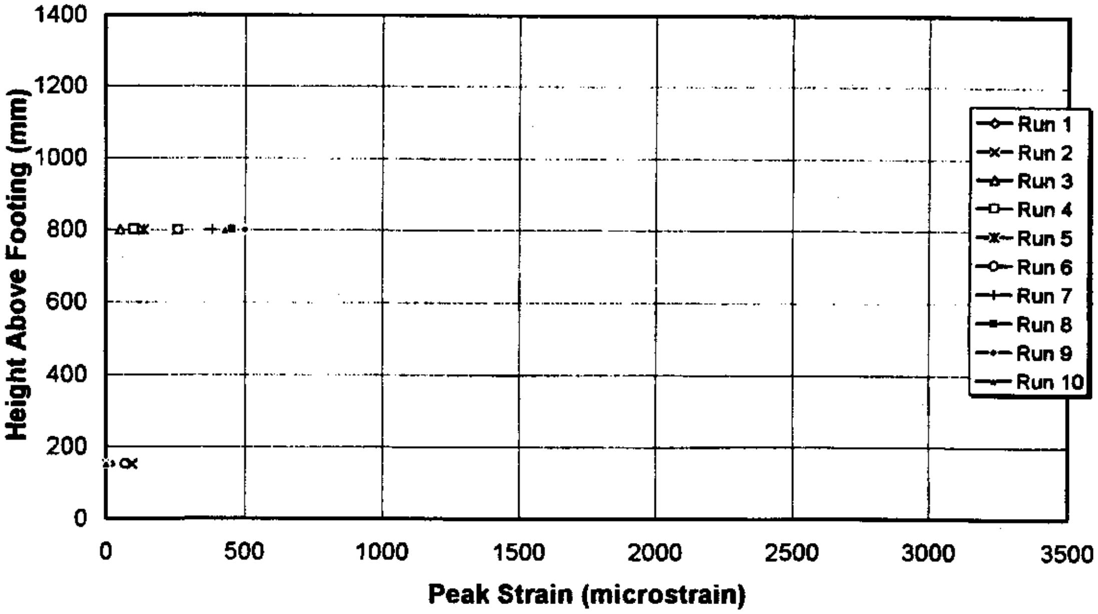

Fig. 3-63 Measured Horizontal Tensile Strain Envelope for West Side of Jacket

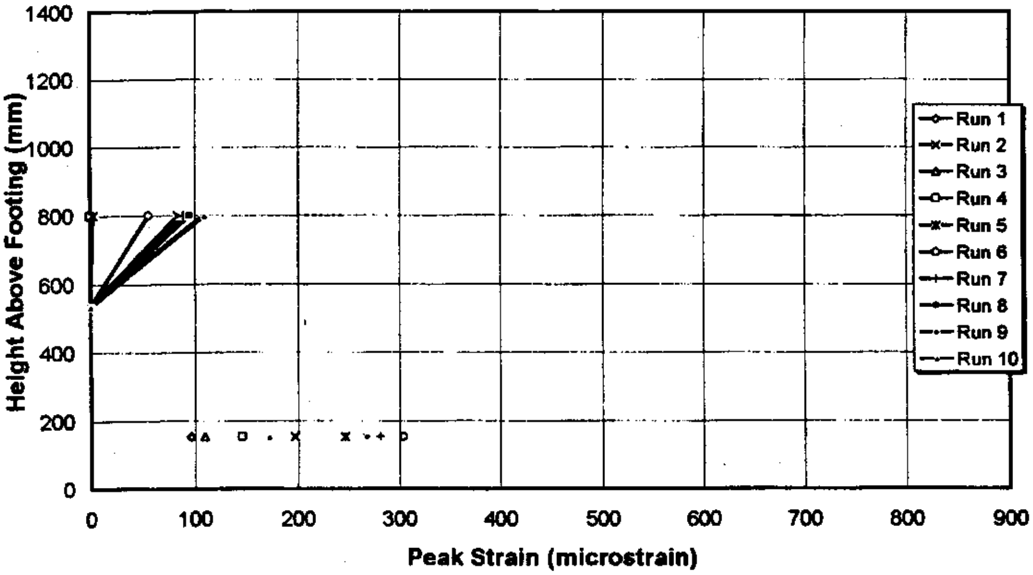

Fig. 3-64 Measured Horizontal Tensile Strain Envelope for North Side of Jacket

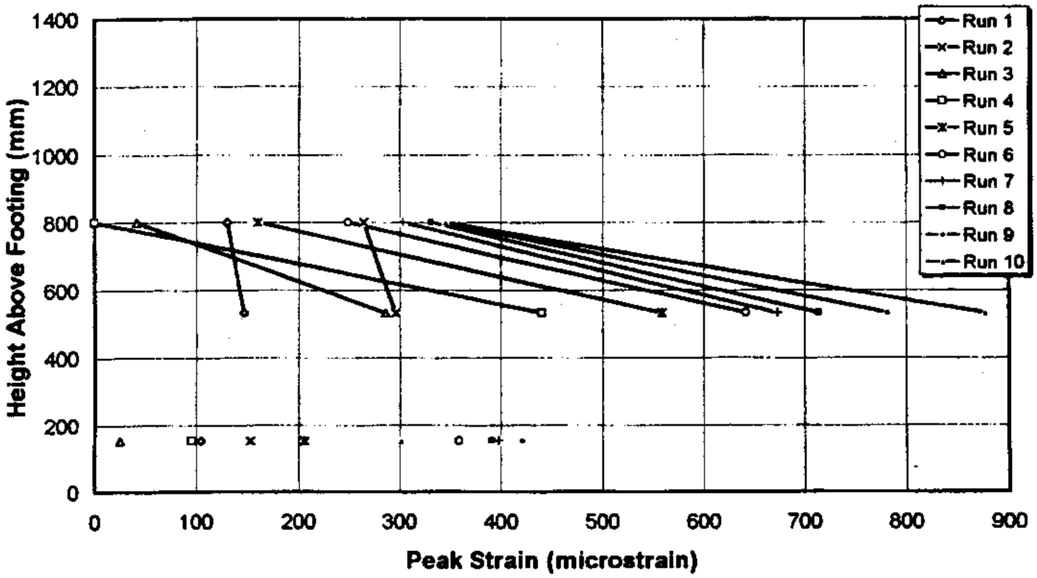

Fig. 3-65 Measured Horizontal Tensile Strain Envelope for South Side of Jacket

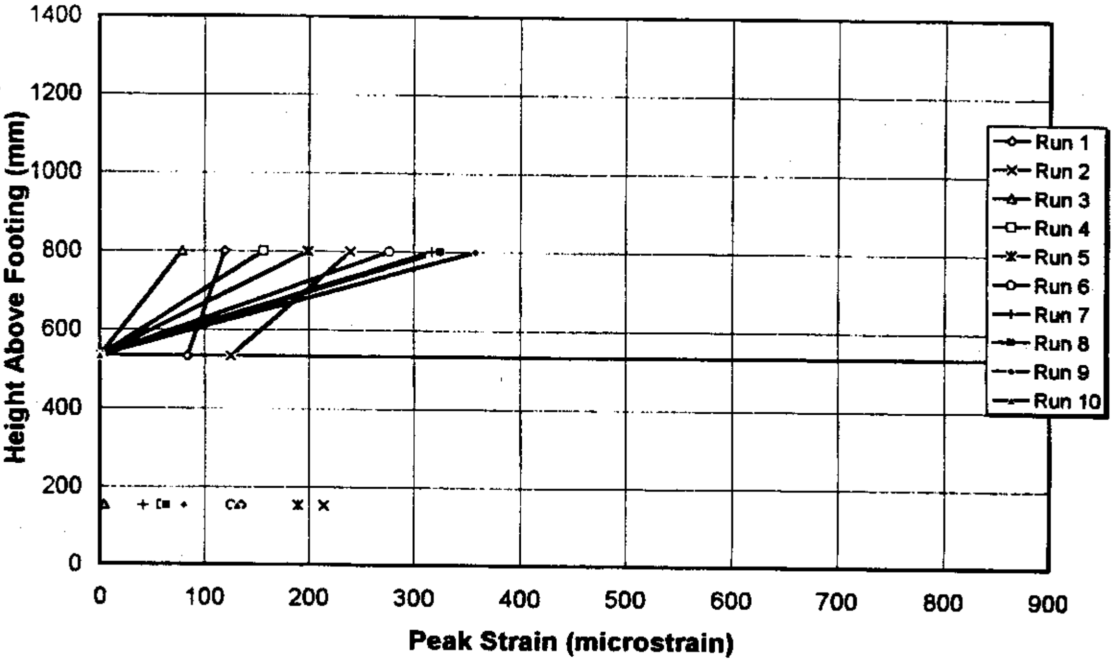

Fig. 3-66 Measured Vertical Tensile Strain Envelope for East Side of Jacket

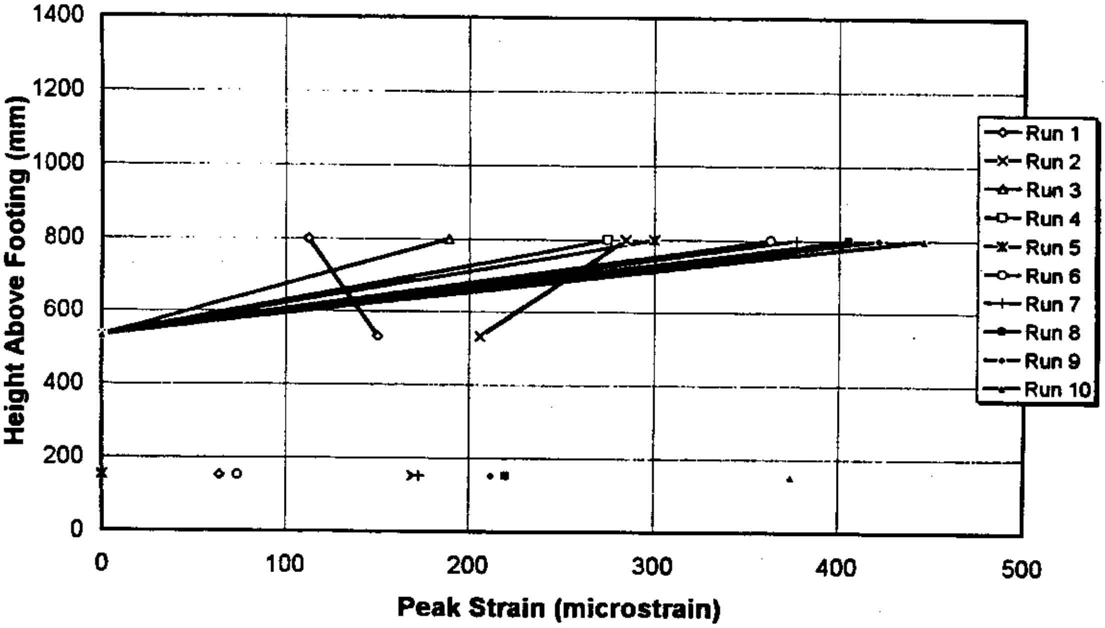

Fig. 3-67 Measured Vertical Tensile Strain Envelope for West Side of Jacket

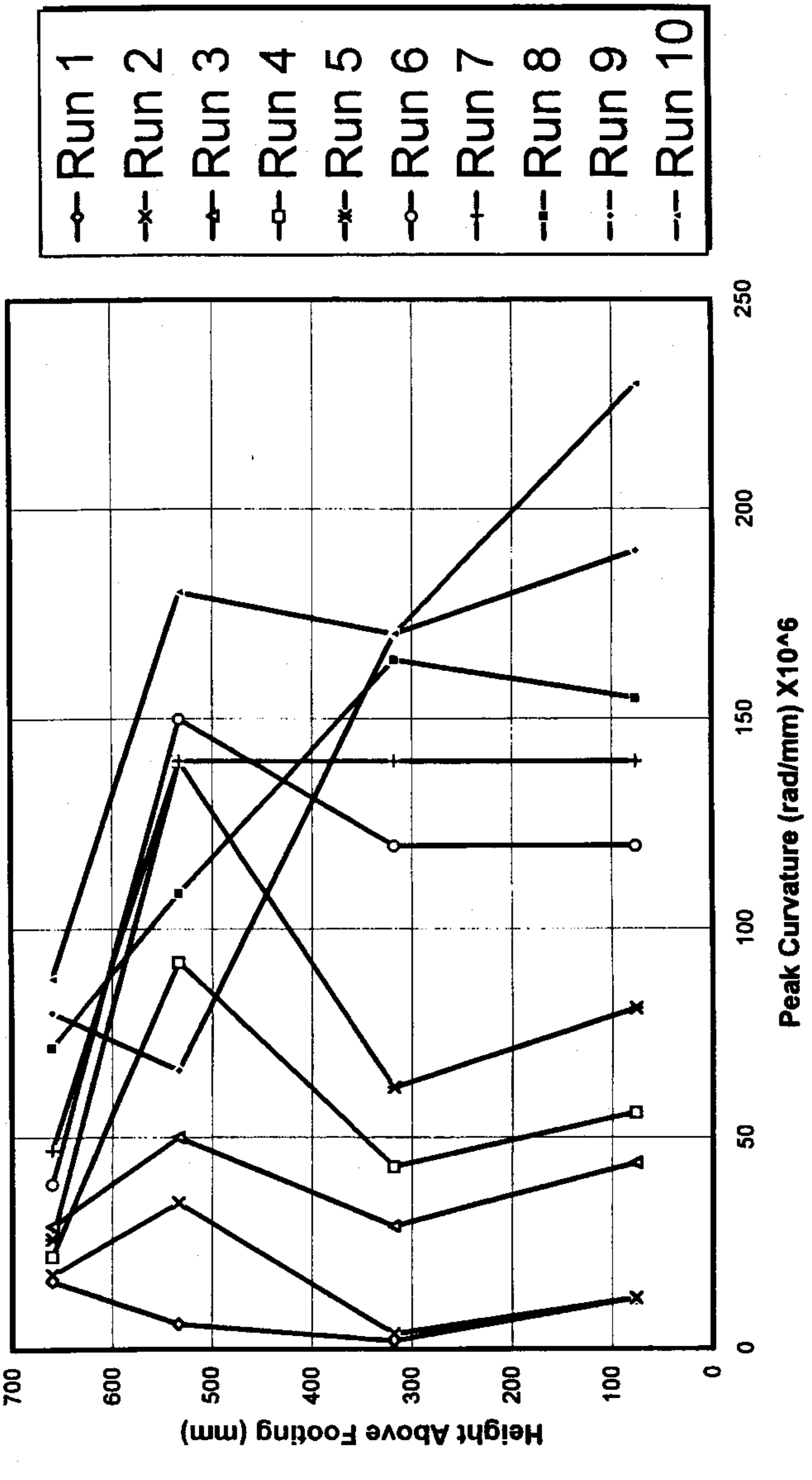

Fig. 3-68 Measured Curvature Envelope for Specimen FR

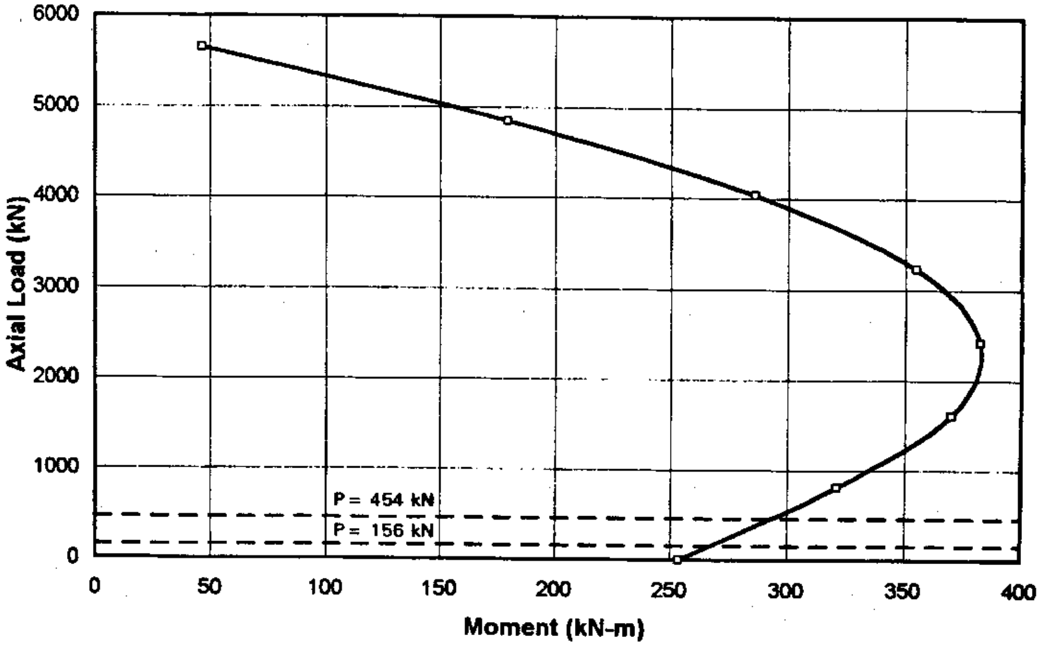

Fig. 4-1 Axial Load-Moment Interaction for FA

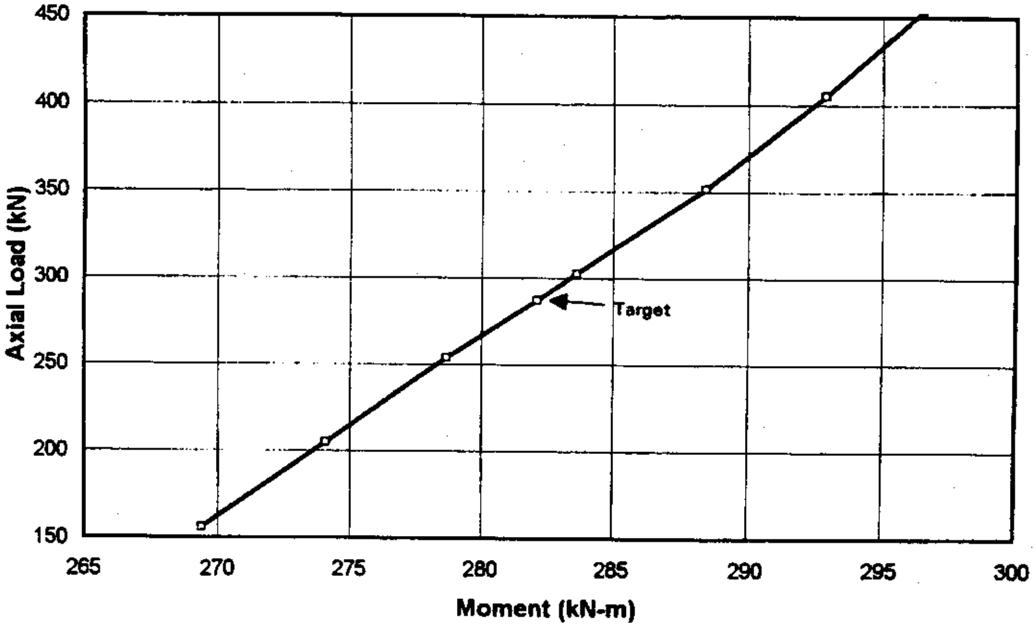

Fig. 4-2 Axial Load-Moment Interaction for FA

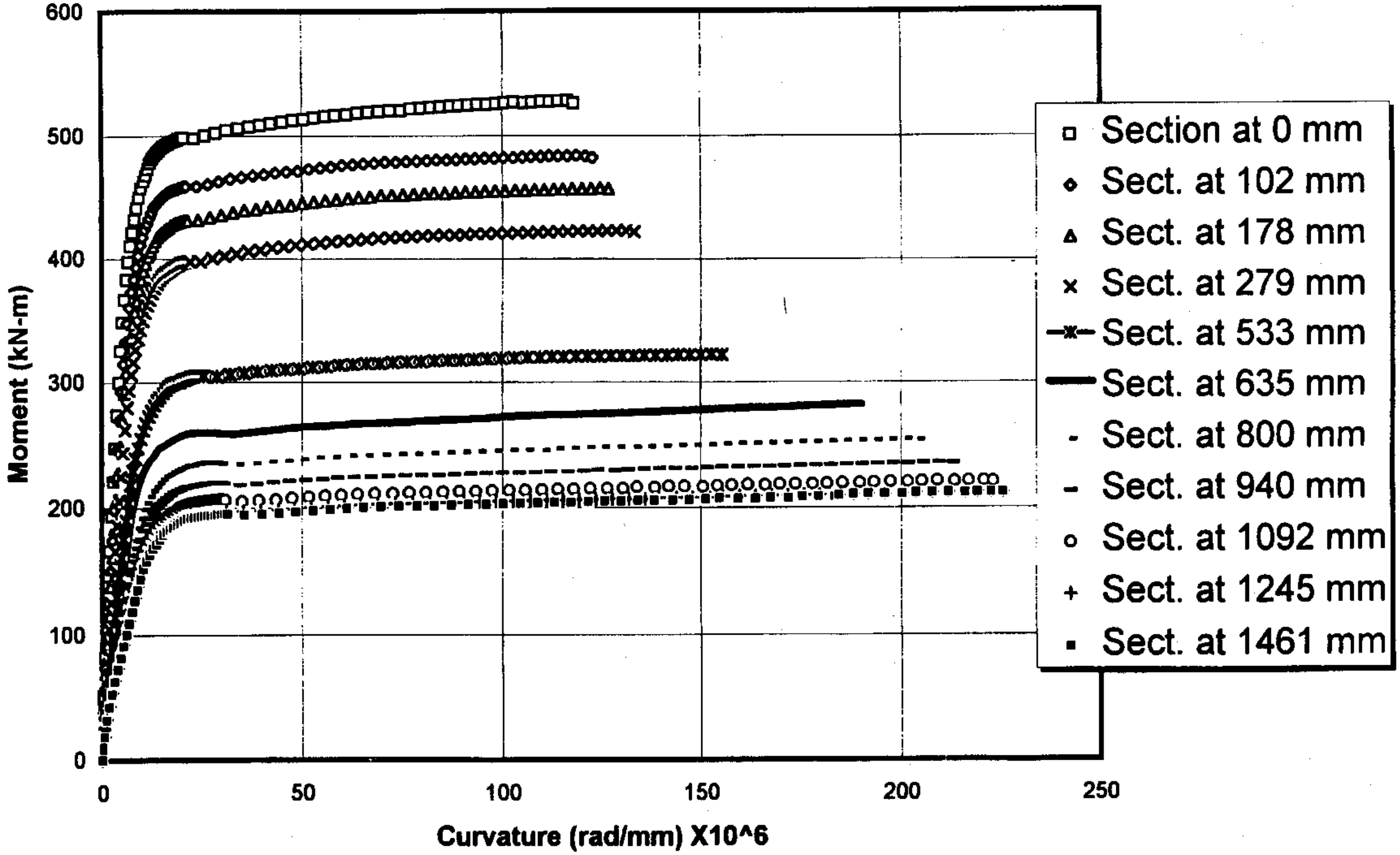

Fig. 4-3 Moment-Curvature Analysis for FA

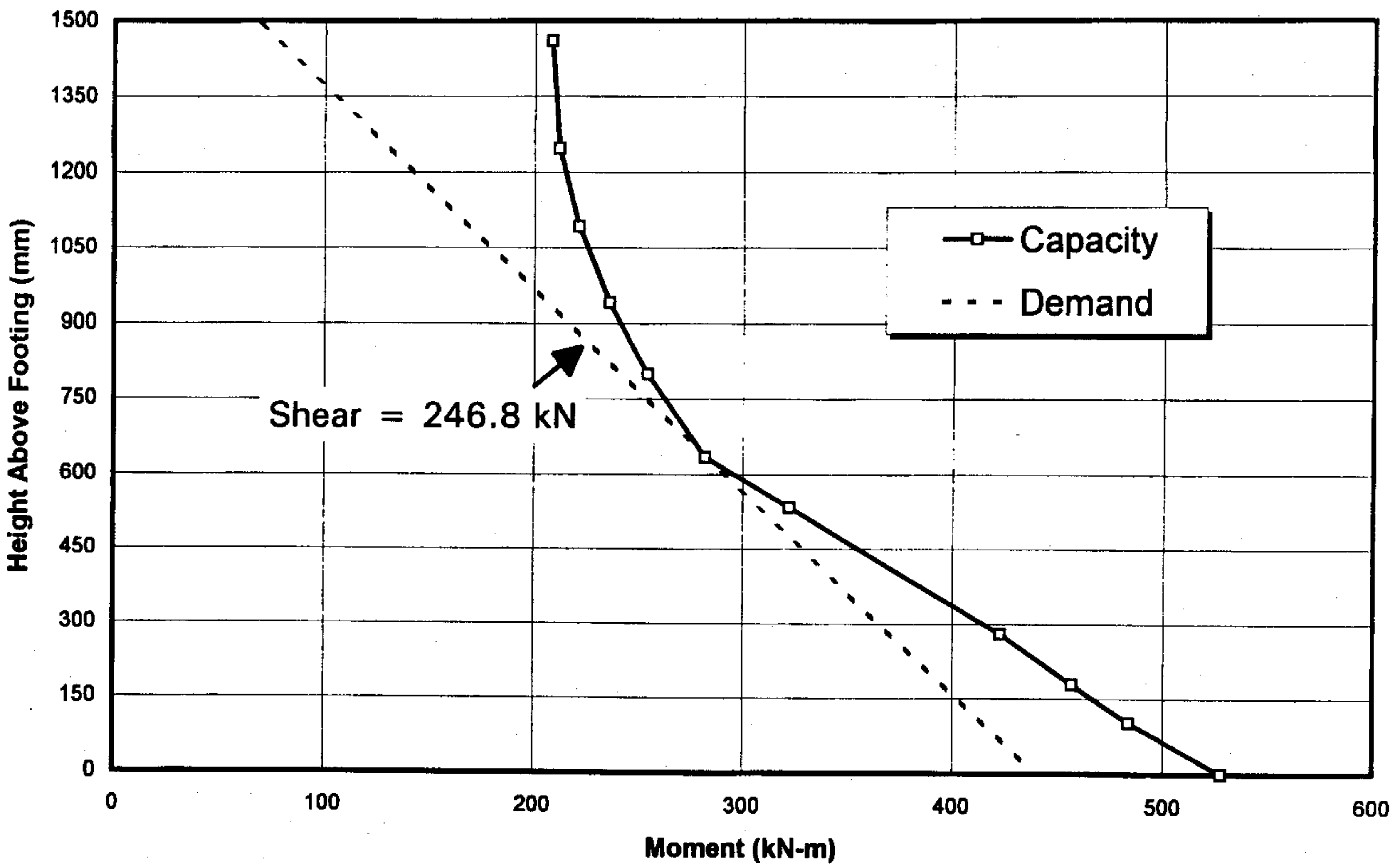

Fig. 4-4 Flexural Capacity for FA

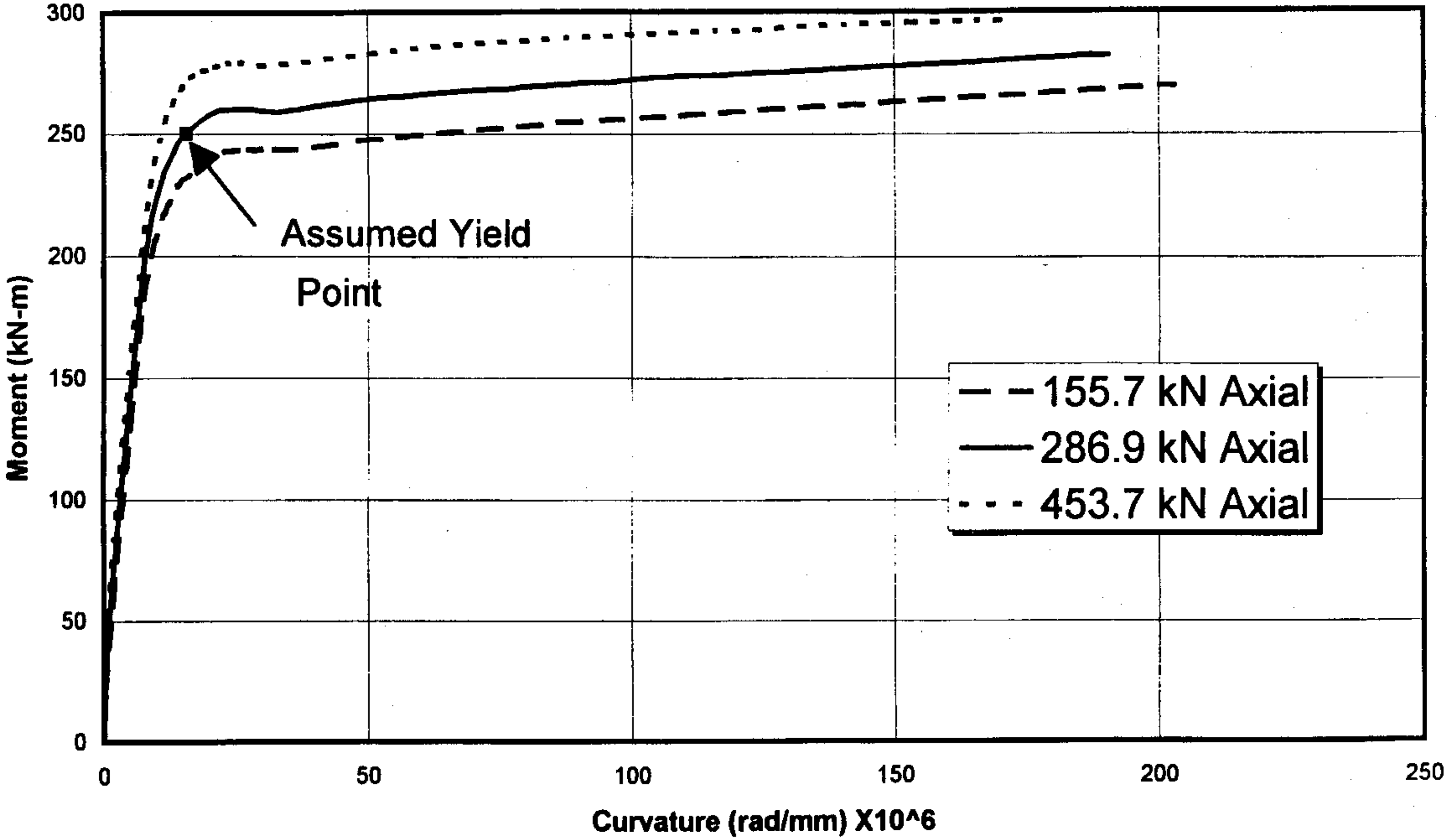

Fig. 4-5 Moment-Curvature Analysis at 635 mm for FA

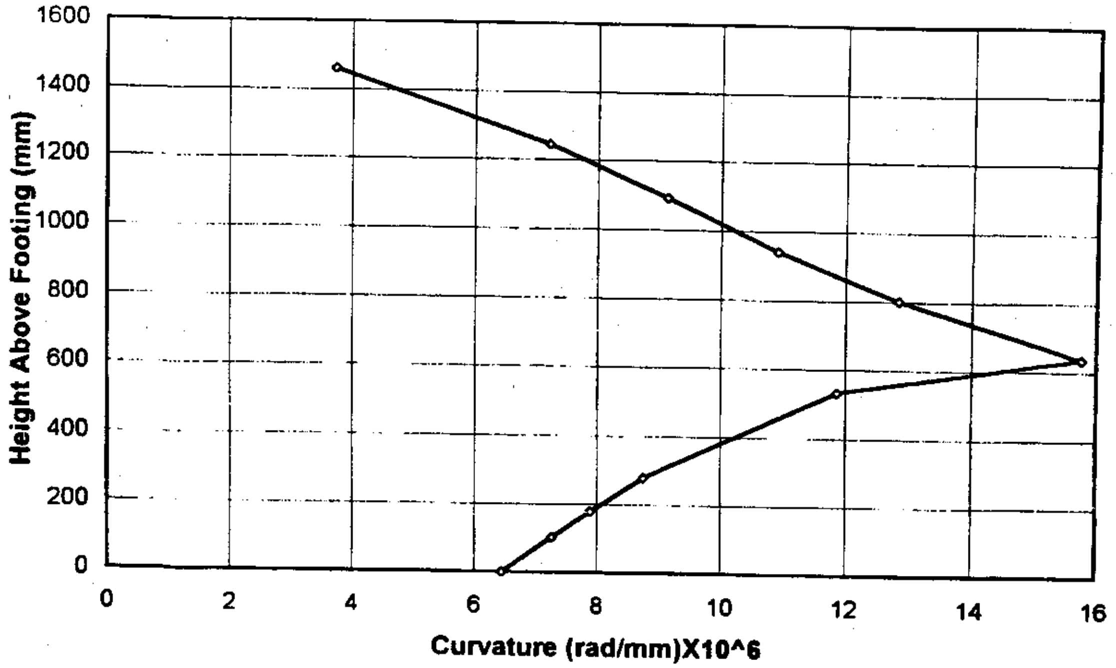

Fig. 4-6 Predicted Curvature Envelope for FA at Yield

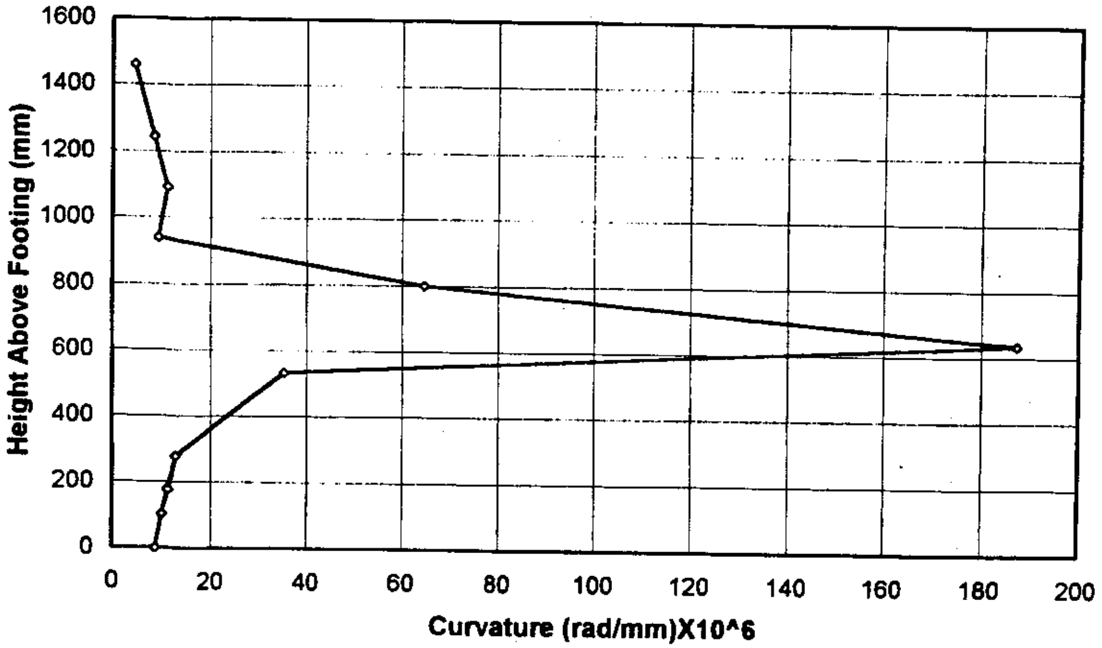

Fig. 4-7 Predicted Curvature Envelope for FA at Ultimate

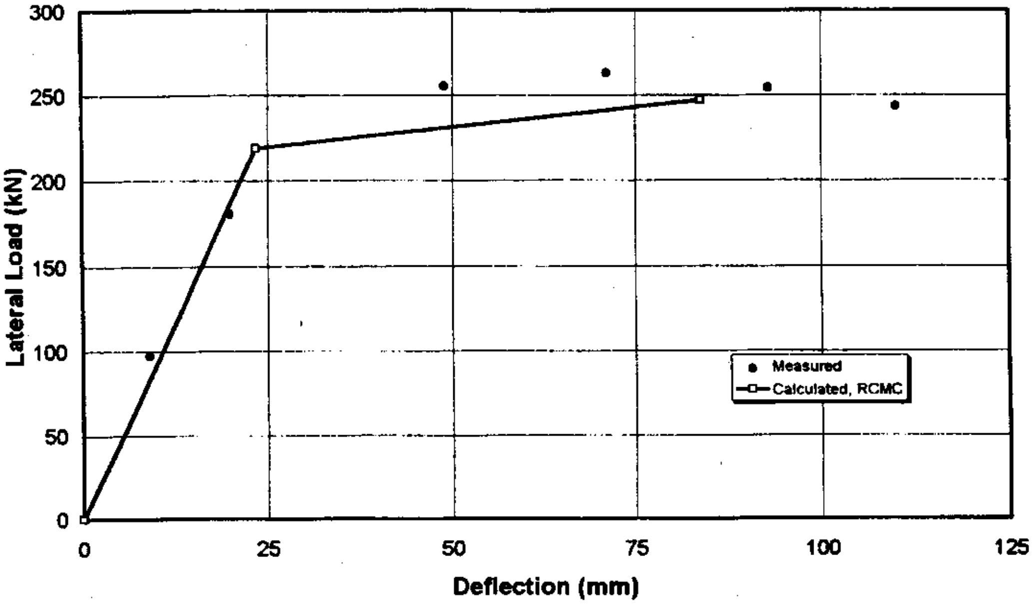

Fig. 4-8 Load-Deflection for FA

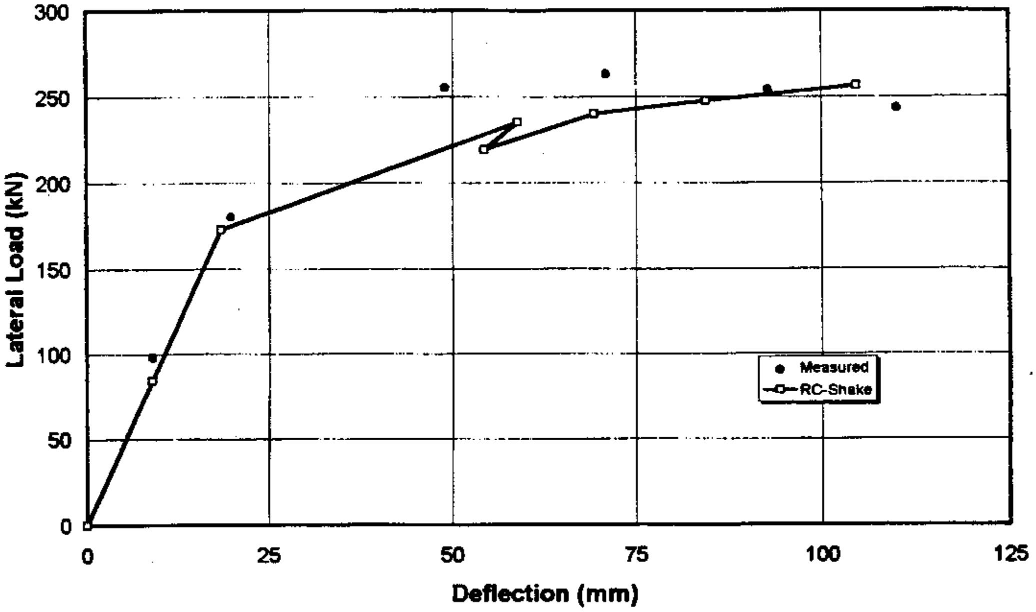

Fig. 4-9 Load Deflection for FA

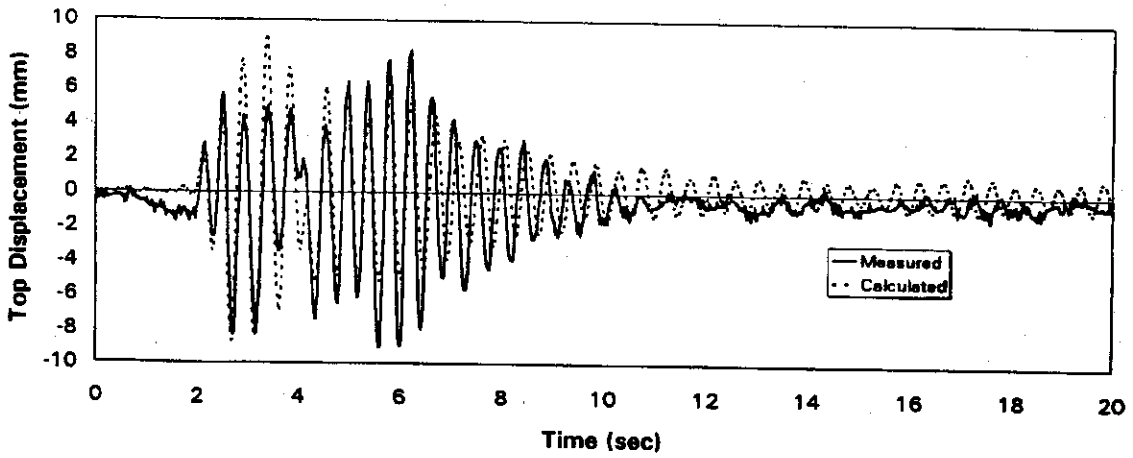

Run 1

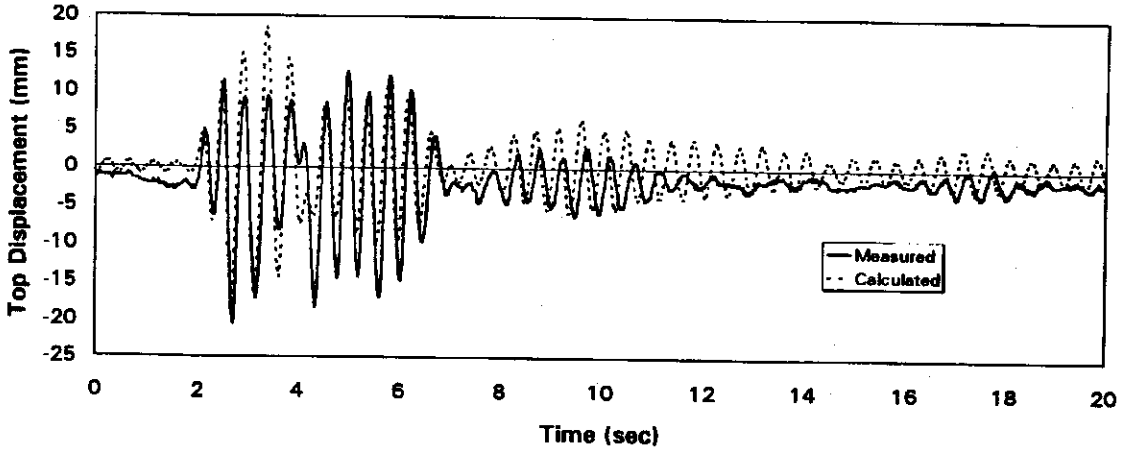

Run 2

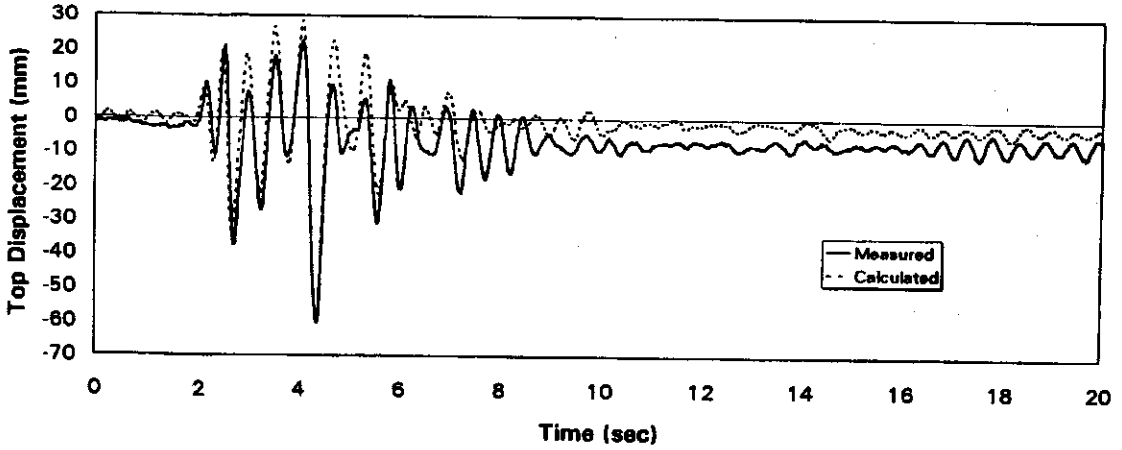

Run 3

Fig. 4-10 Displacement History for FA, Runs 1-3

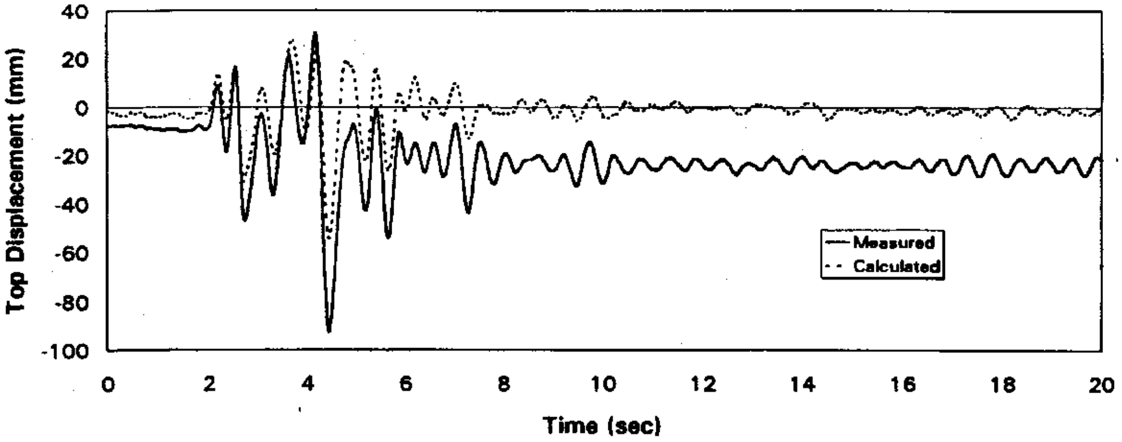

Run 4

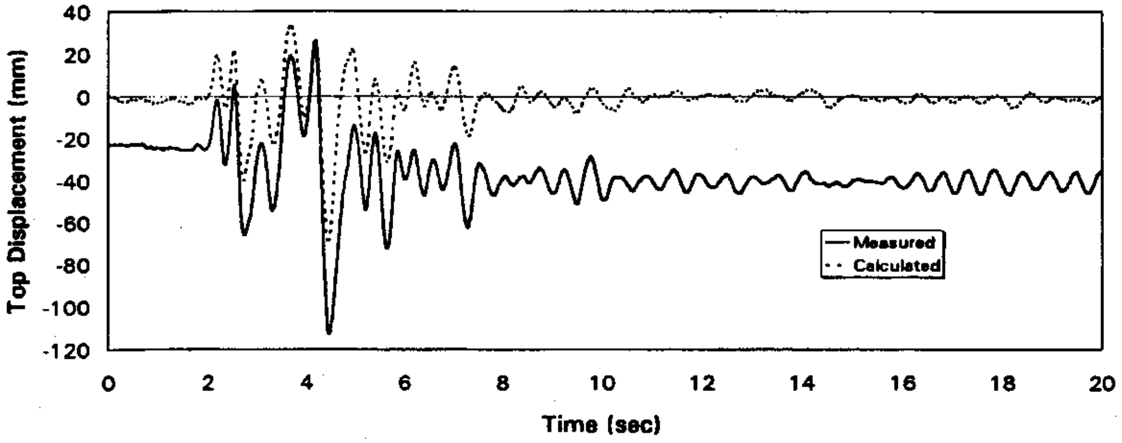

Run 5

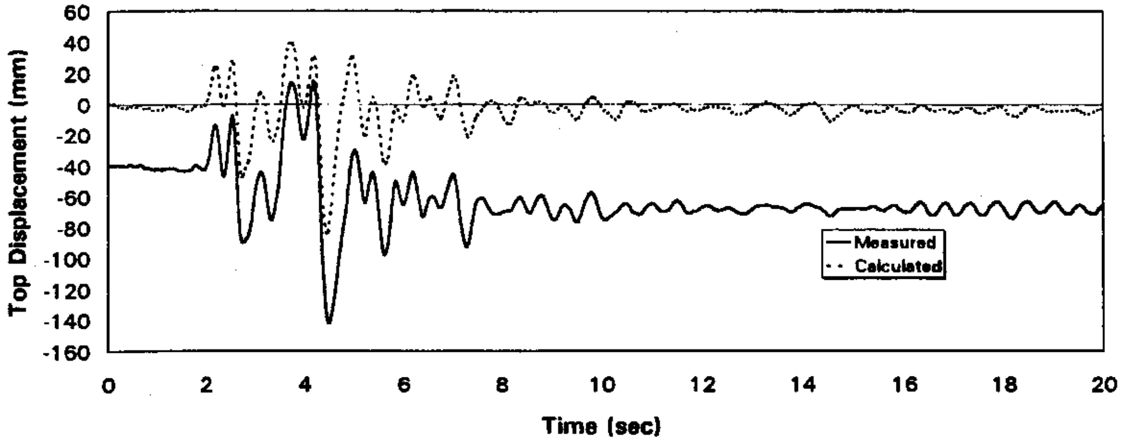

Run 6

Fig. 4-11 Displacement History for FA, Runs 4-6

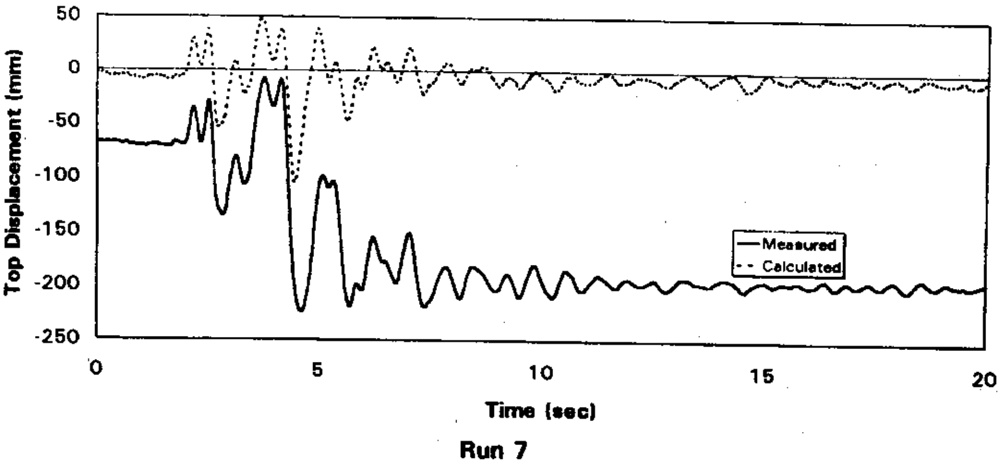

Fig. 4-12 Displacement History for FA, Run 7

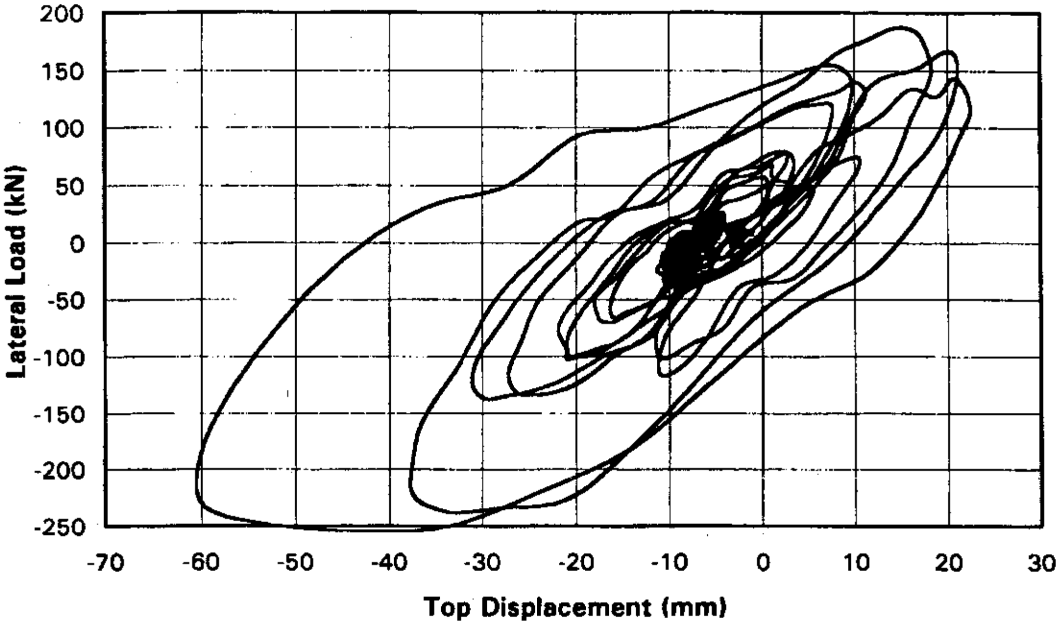

Fig. 4-13 Hysteresis Loop for FA, Run 3 (measured)

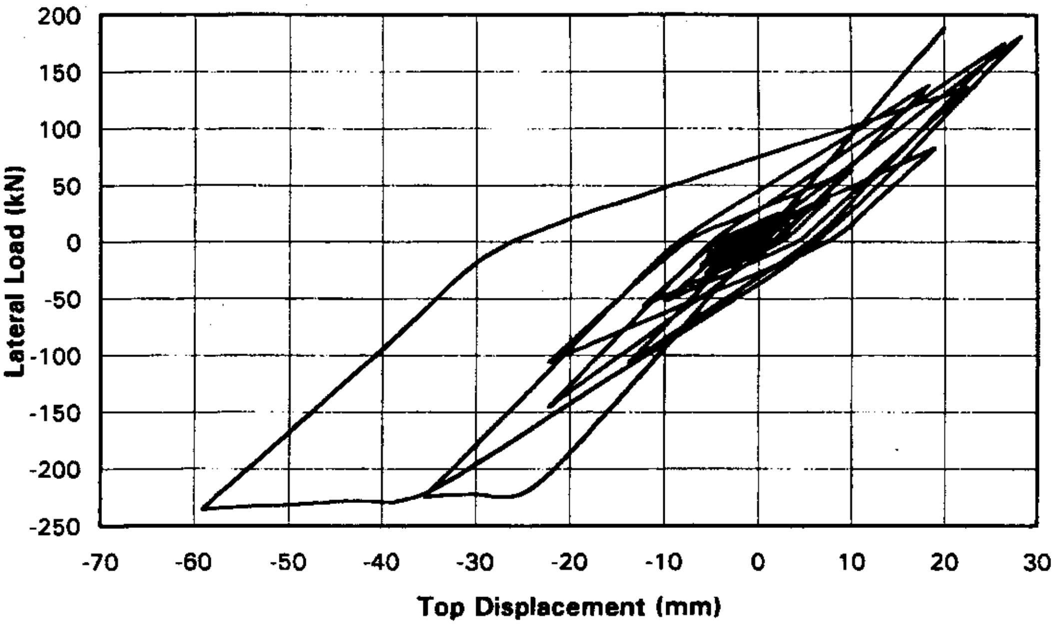

Fig. 4-14 Hysteresis Loop for FA, Run 3 (RC-Shake)

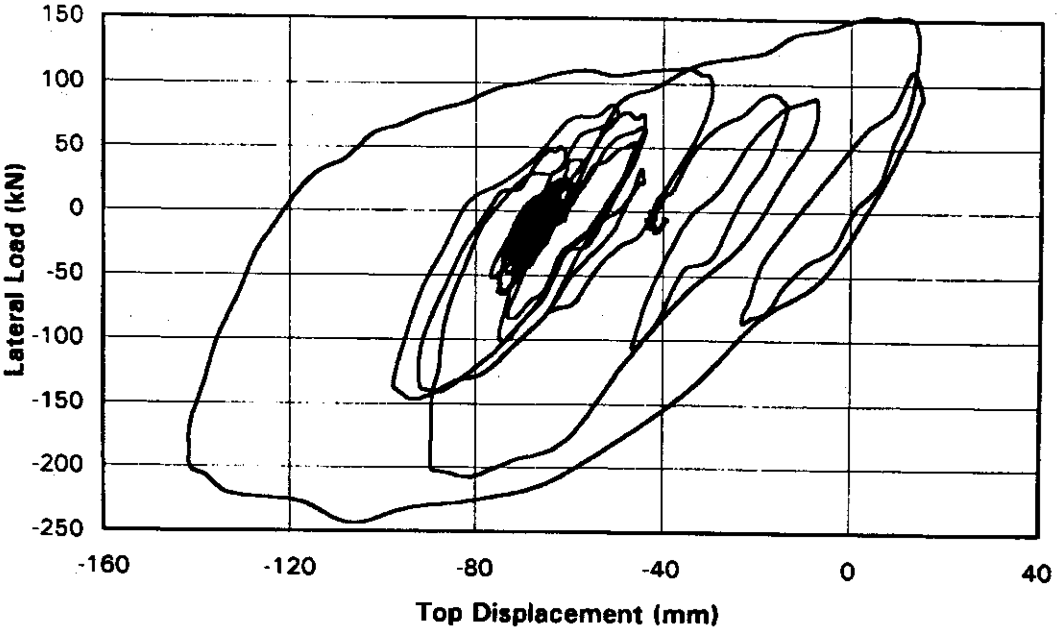

Fig. 4-15 Hysteresis Loop for FA, Run 6 (measured)

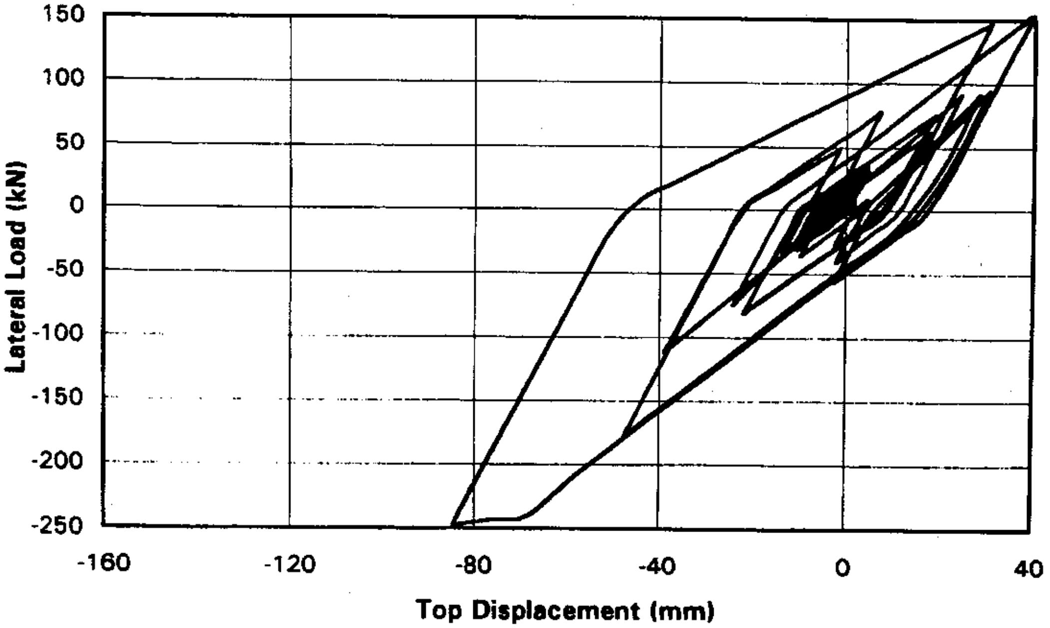

Fig. 4-16 Hysteresis Loop for FA, Run 6 (RC-Shake)

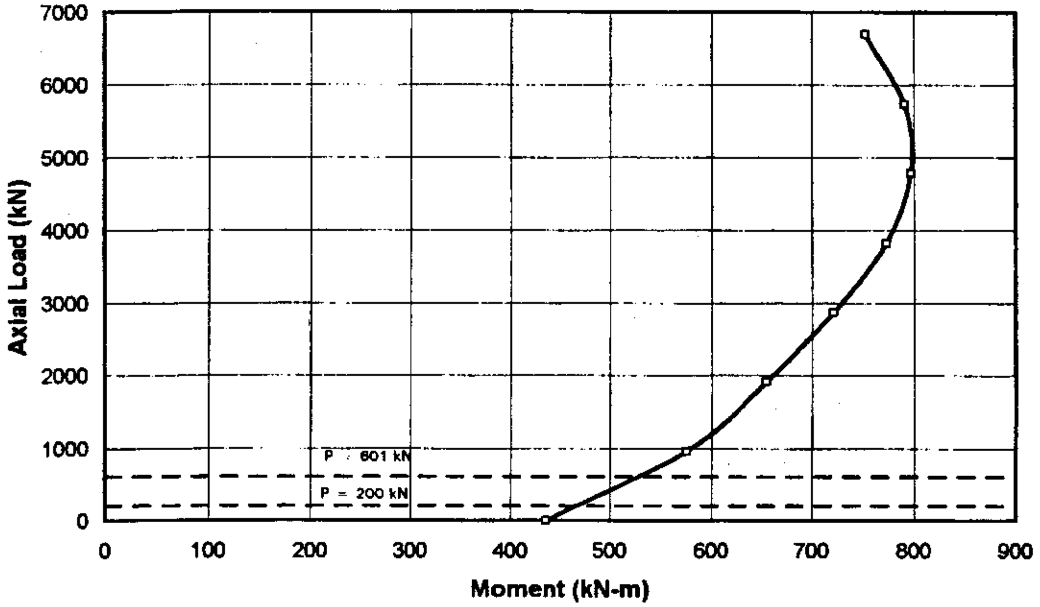

Fig. 4-17 Axial Load-Moment Interaction for FR

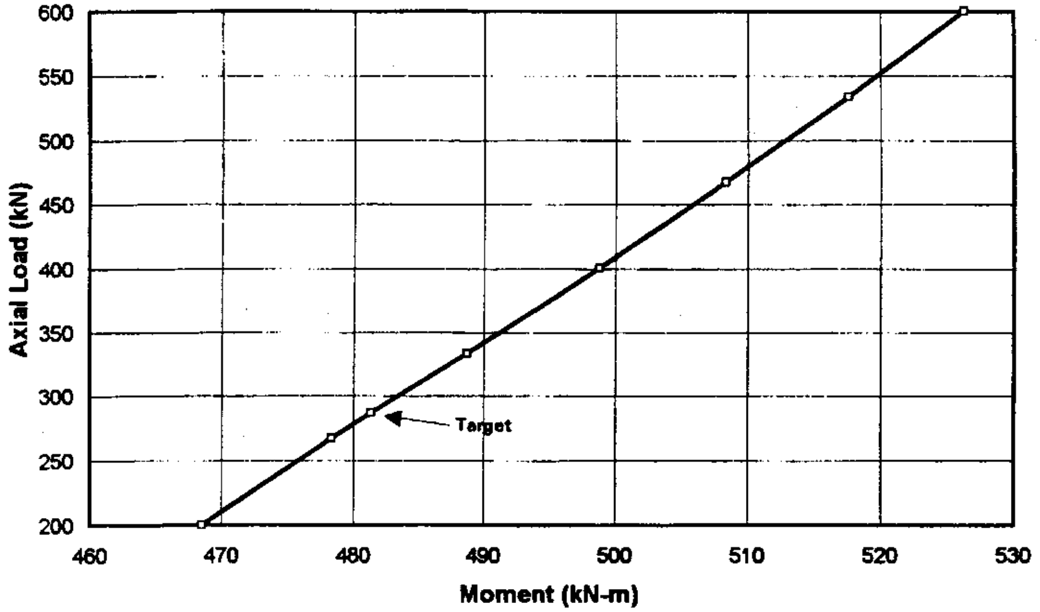

Fig. 4-18 Axial Load-Moment Interaction for FR

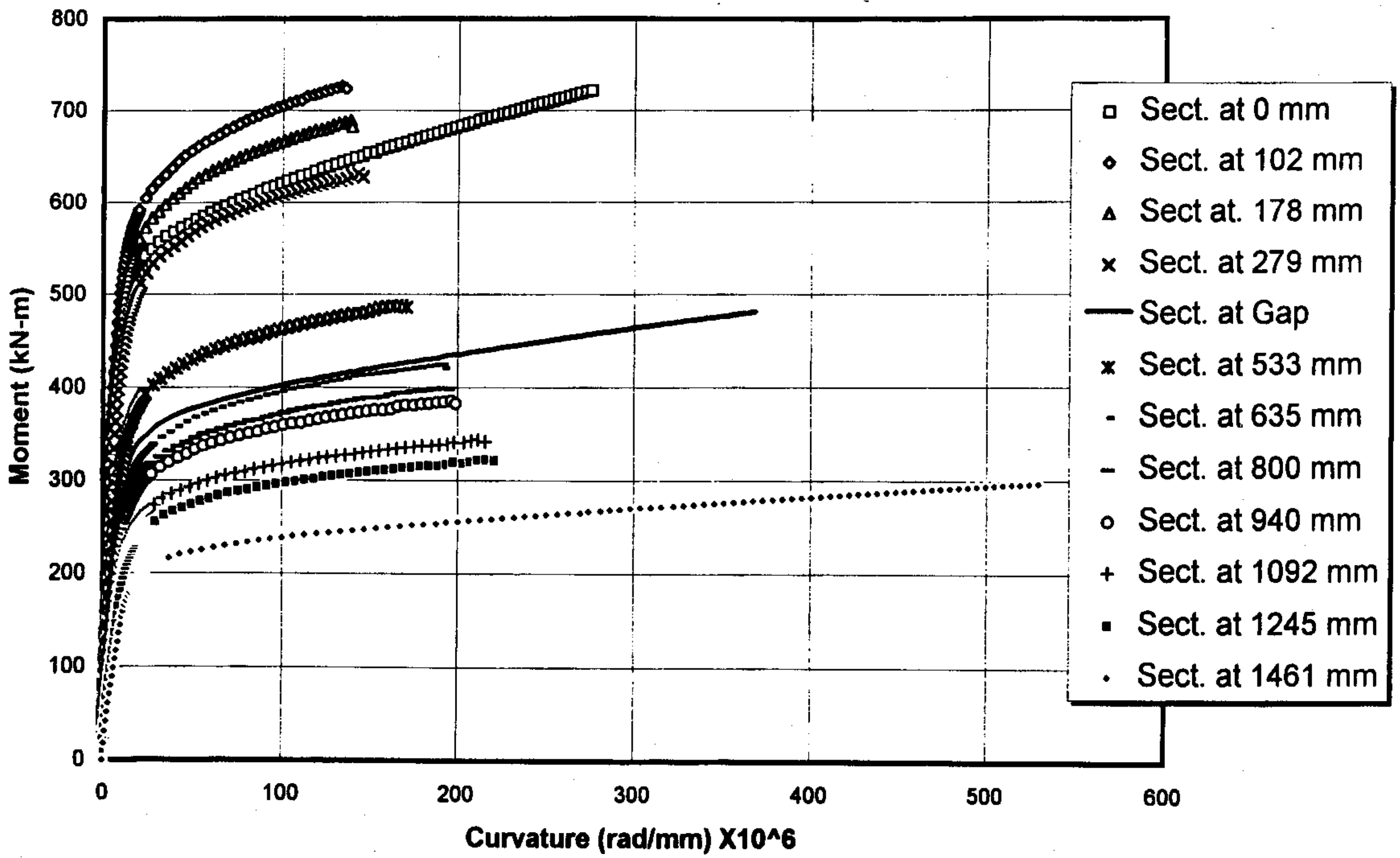

Fig. 4-19 Moment-Curvature Analysis for FR

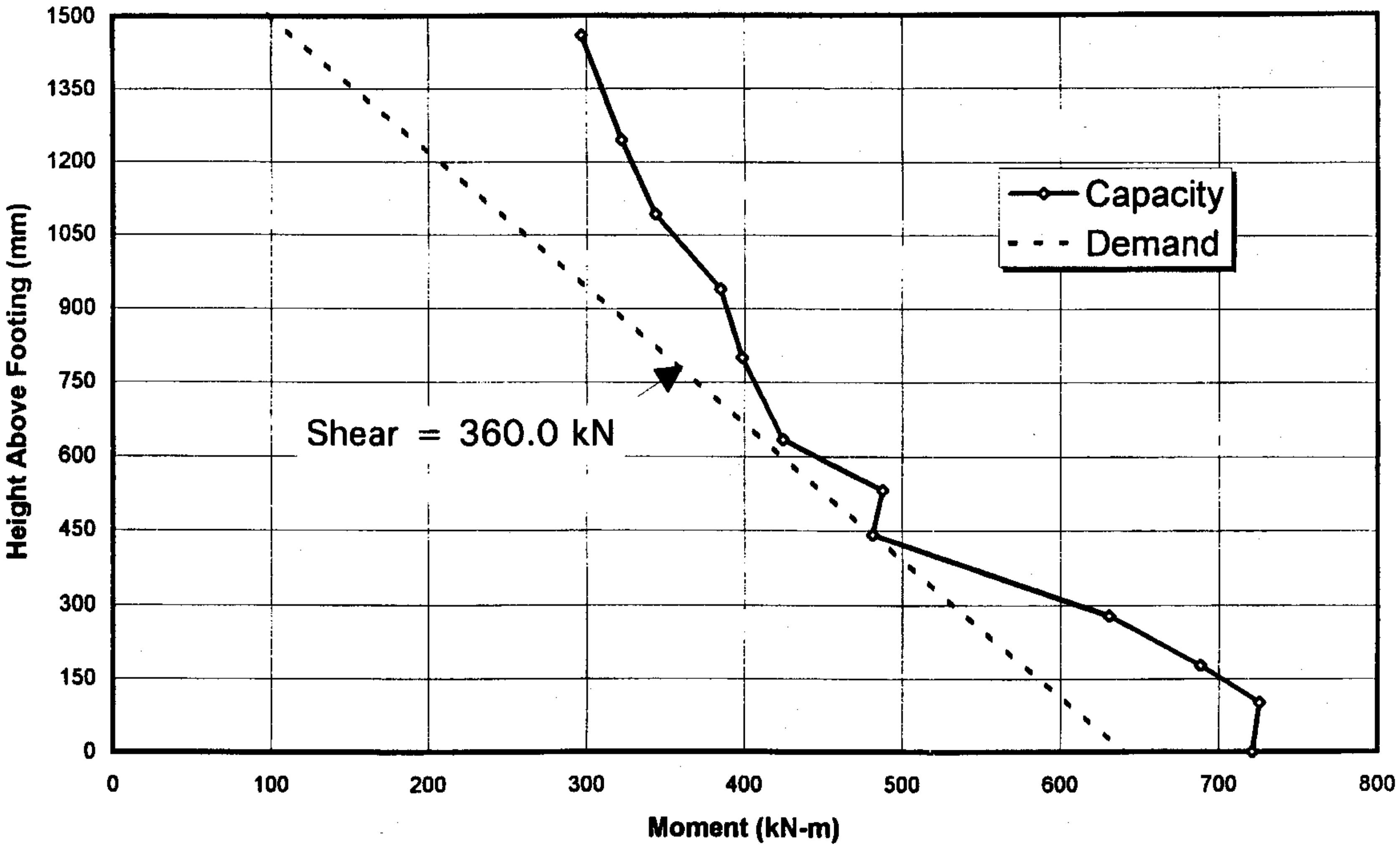

Fig. 4-20 Flexural Capacity for FR

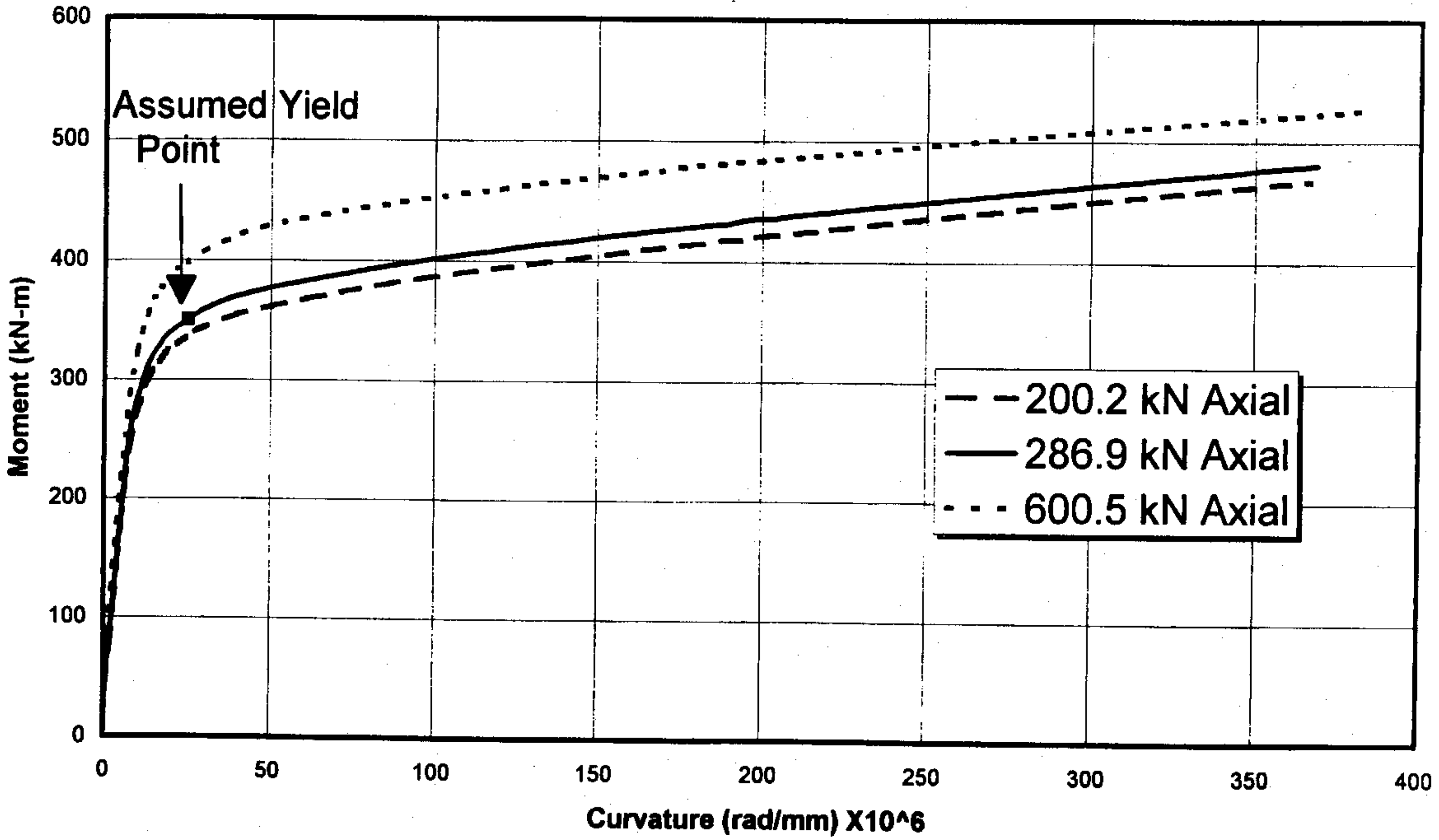

Fig. 4-21 Moment-Curvature Analysis at Gap for FR

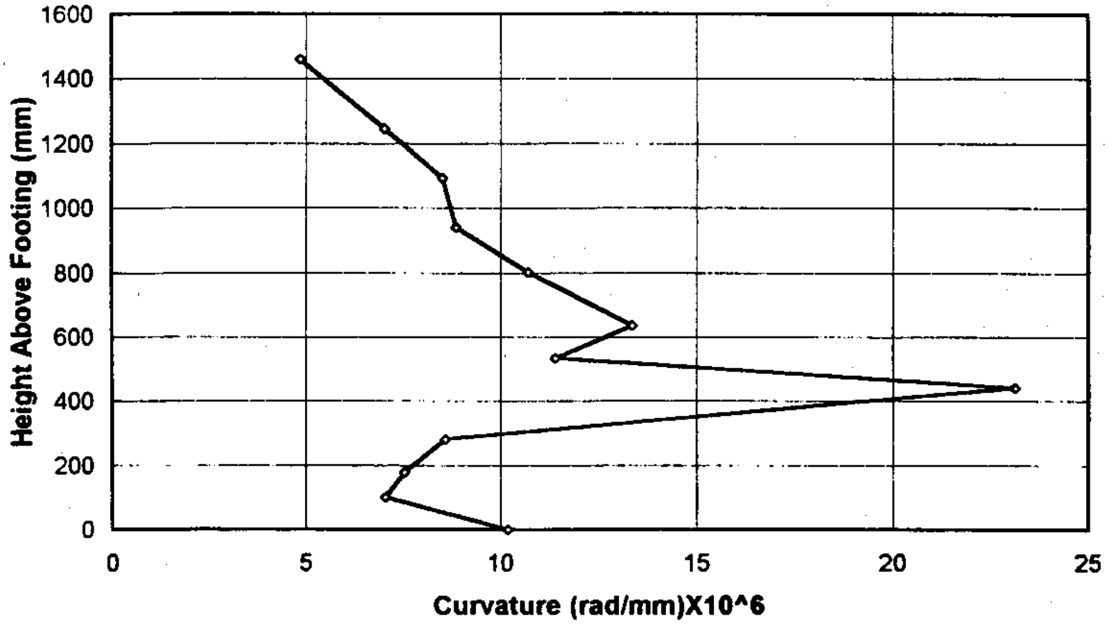

Fig. 4-22 Predicted Curvature Envelope for FR at Yield

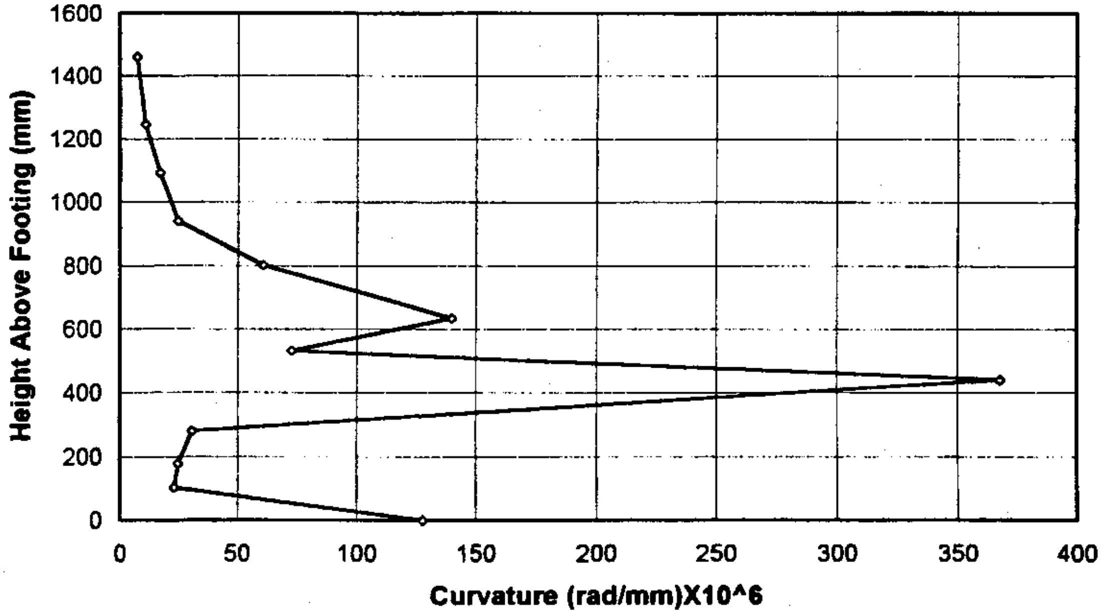

Fig. 4-23 Predicted Curvature Envelope for FR at Ultimate

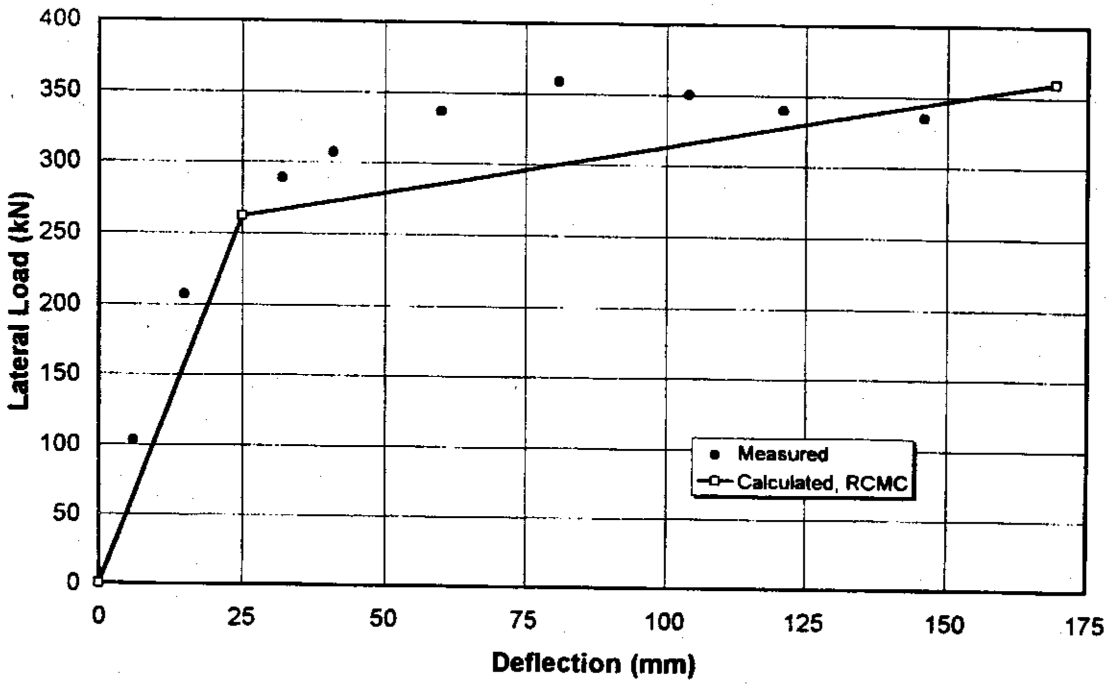

Fig. 4-24 Load-Deflection for FR

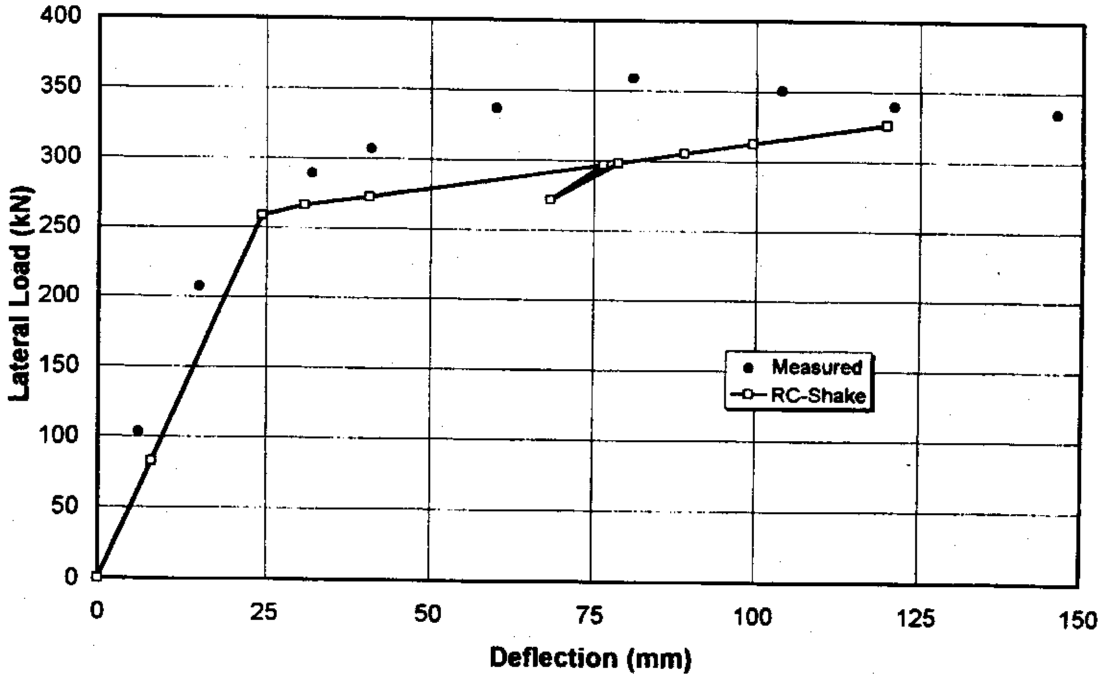

Fig. 4-25 Load-Deflection for FR

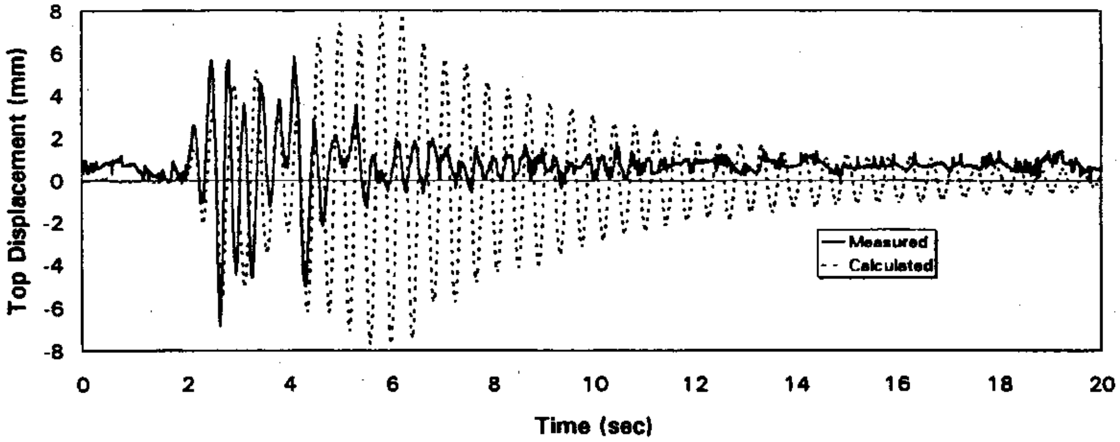

Run 1

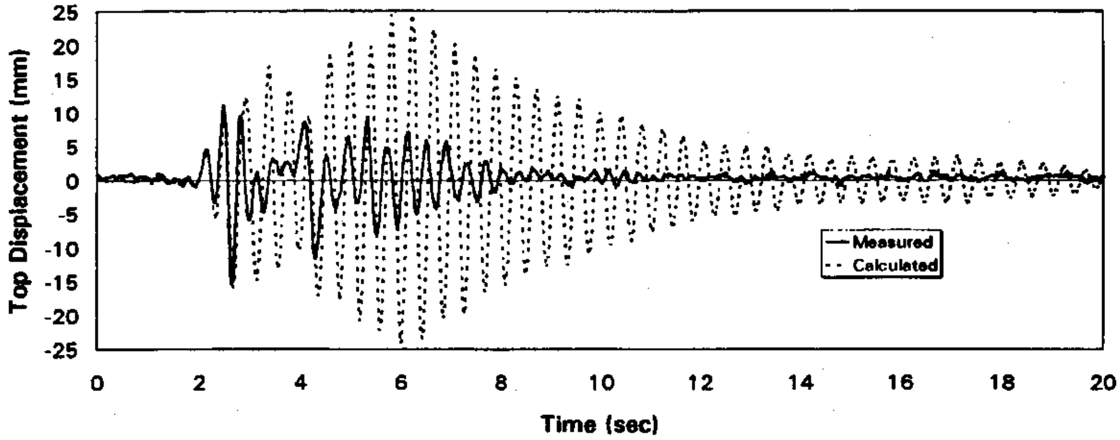

Run 2

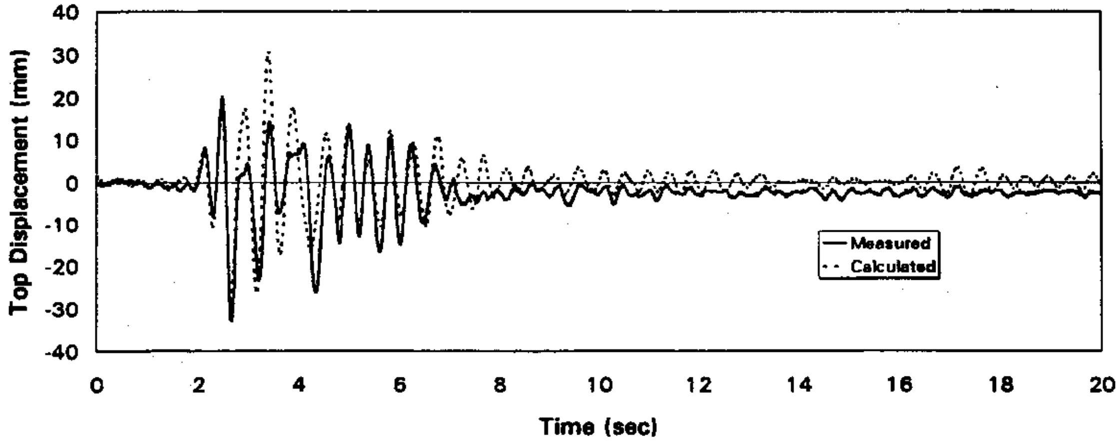

Run 3

Fig. 4-26 Displacement History for FR, Runs 1-3

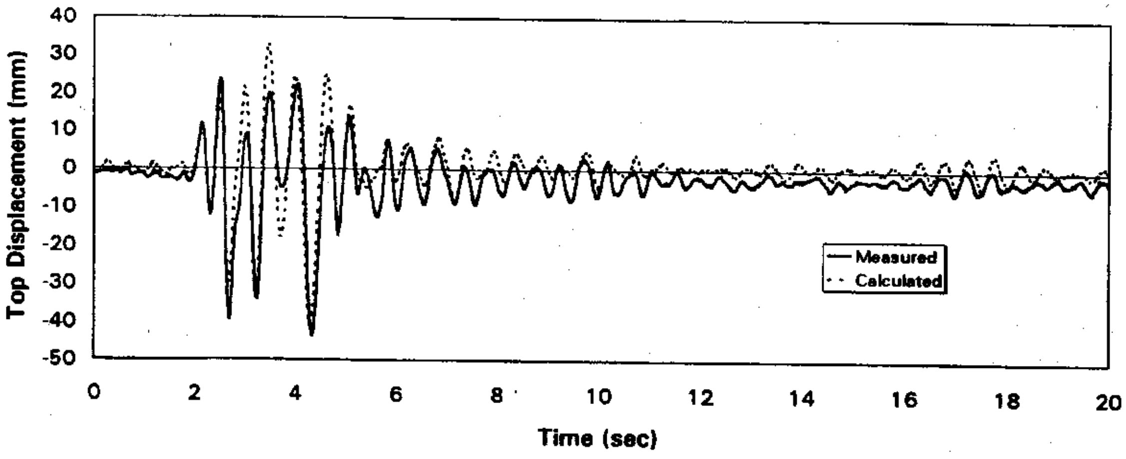

Run 4

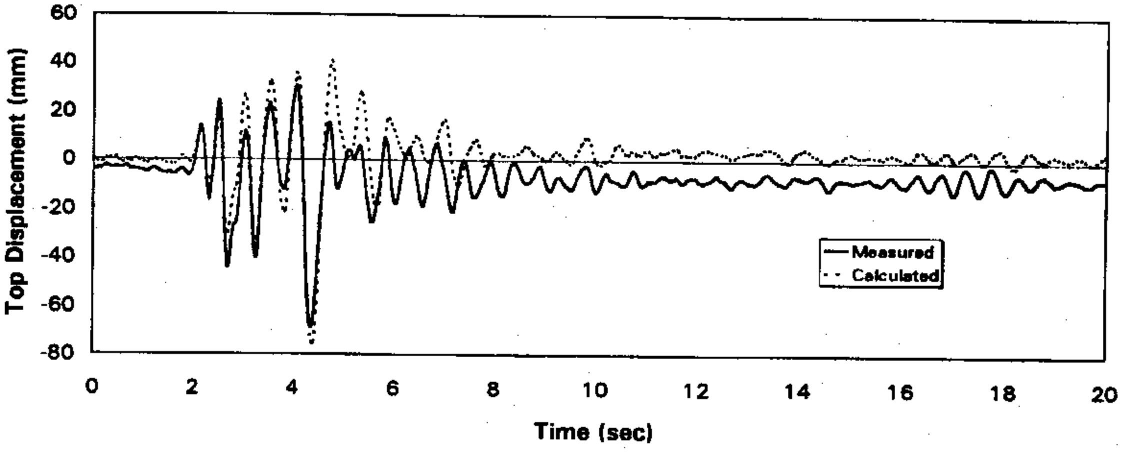

Run 5

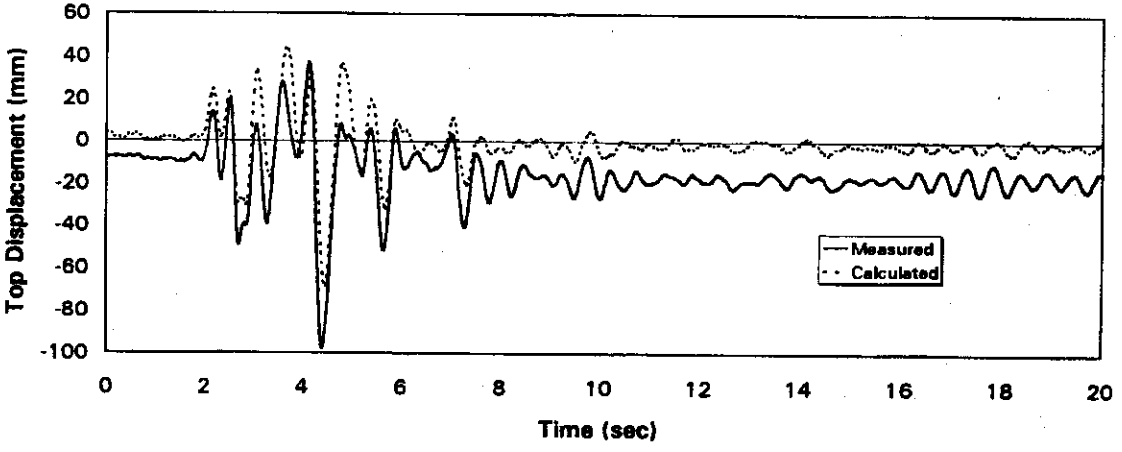

Run 6

Fig. 4-27 Displacement History for FR, Runs 4-6

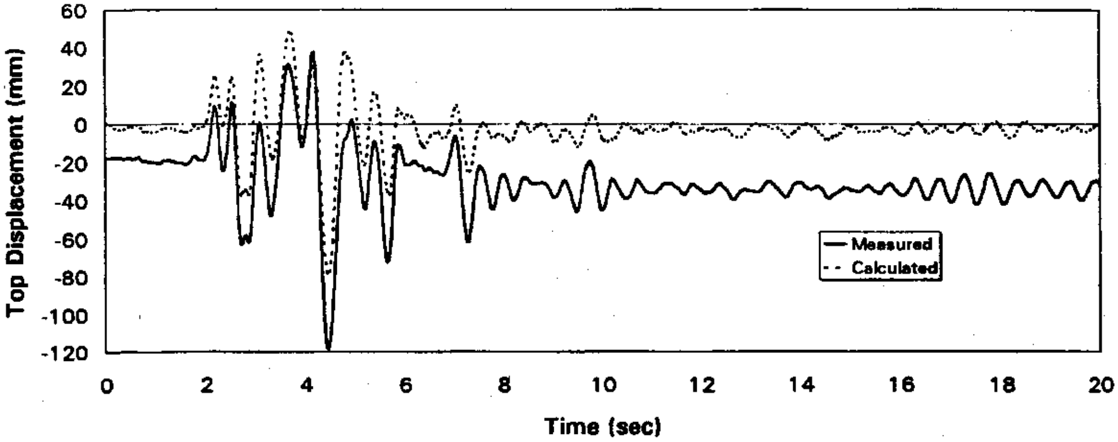

Run 7

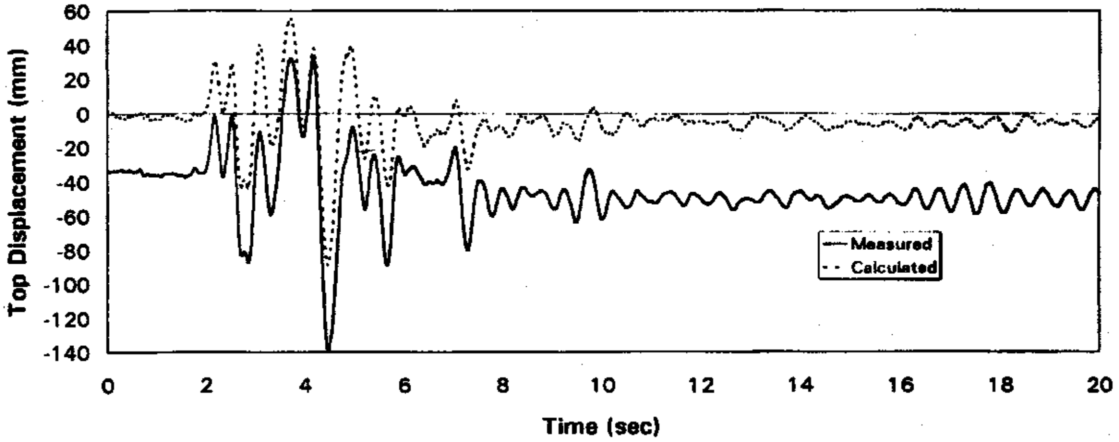

Run 8

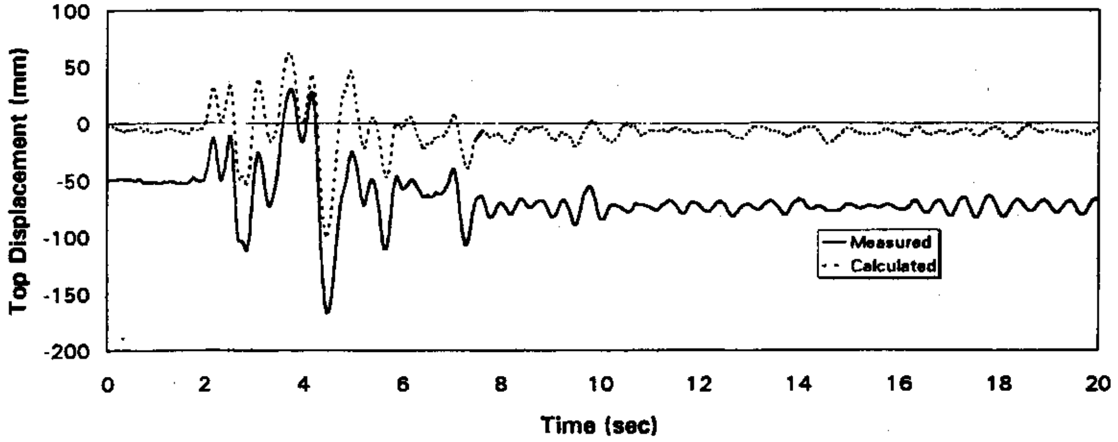

Run 9

Fig. 4-28 Displacement History for FR, Runs 7-9

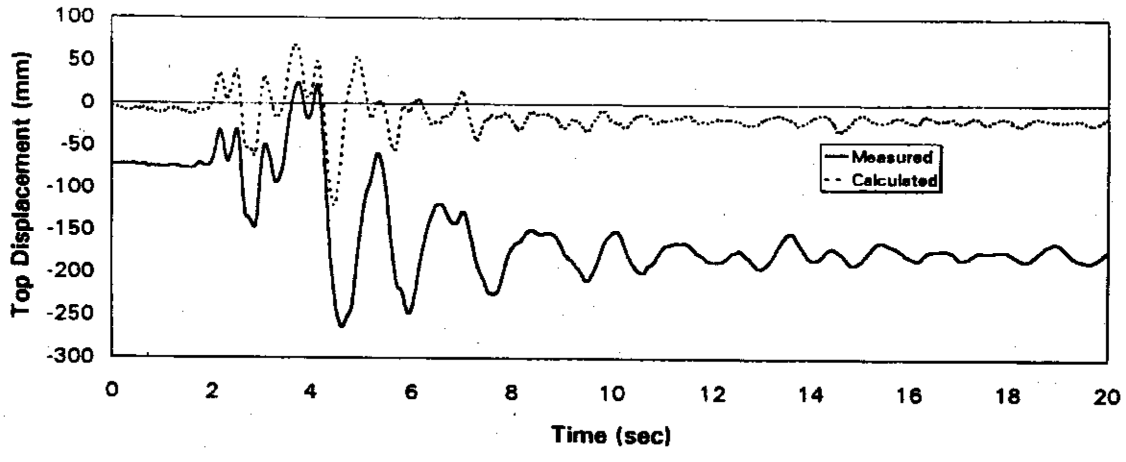

Run 10

Fig. 4-29 Displacement History for FR, Run 10

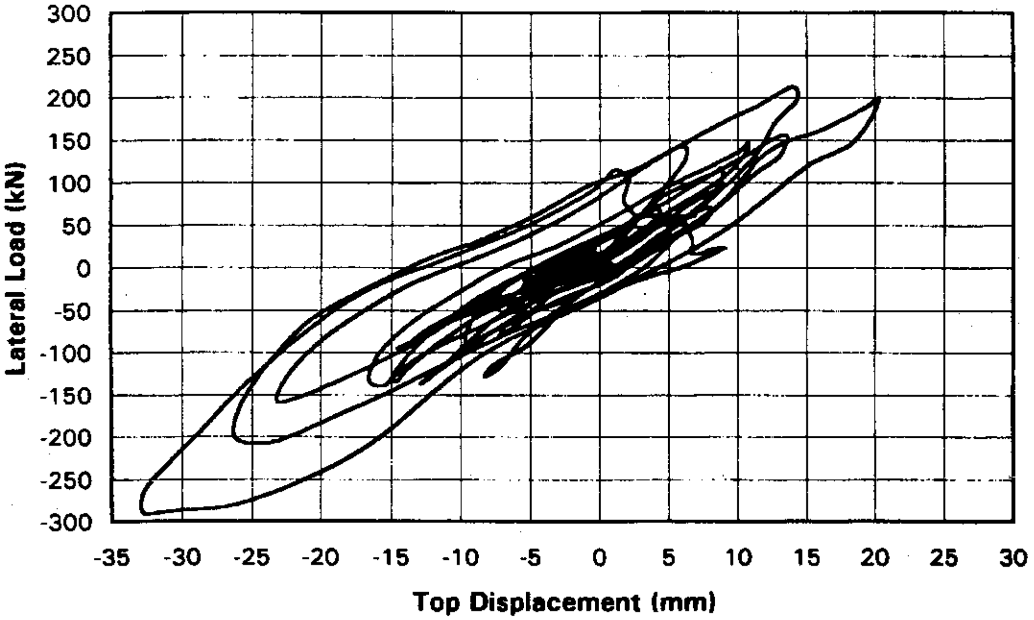

Fig. 4-30 Hysteresis Loop for FR, Run 3 (measured)

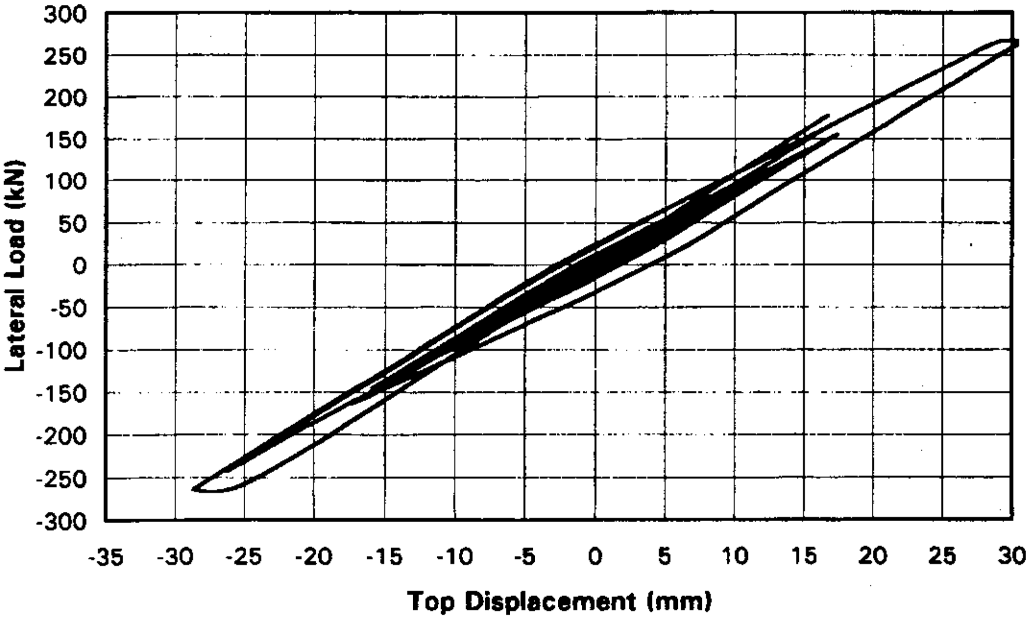

Fig. 4-31 Hysteresis Loop for FR, Run 3 (RC-Shake)

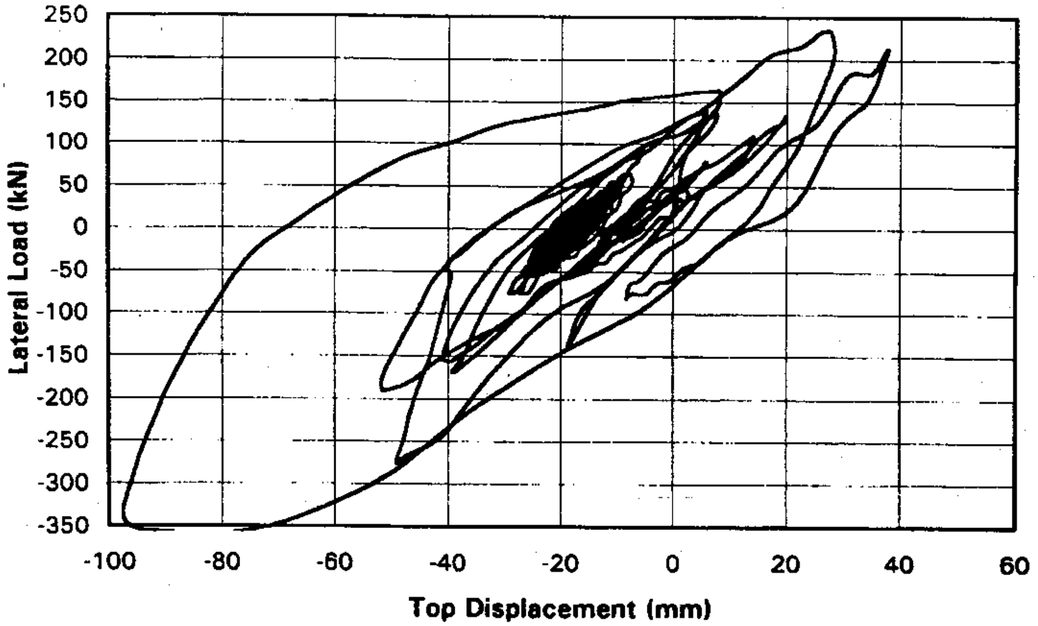

Fig. 4-32 Hysteresis Loop for FR, Run 6 (measured)

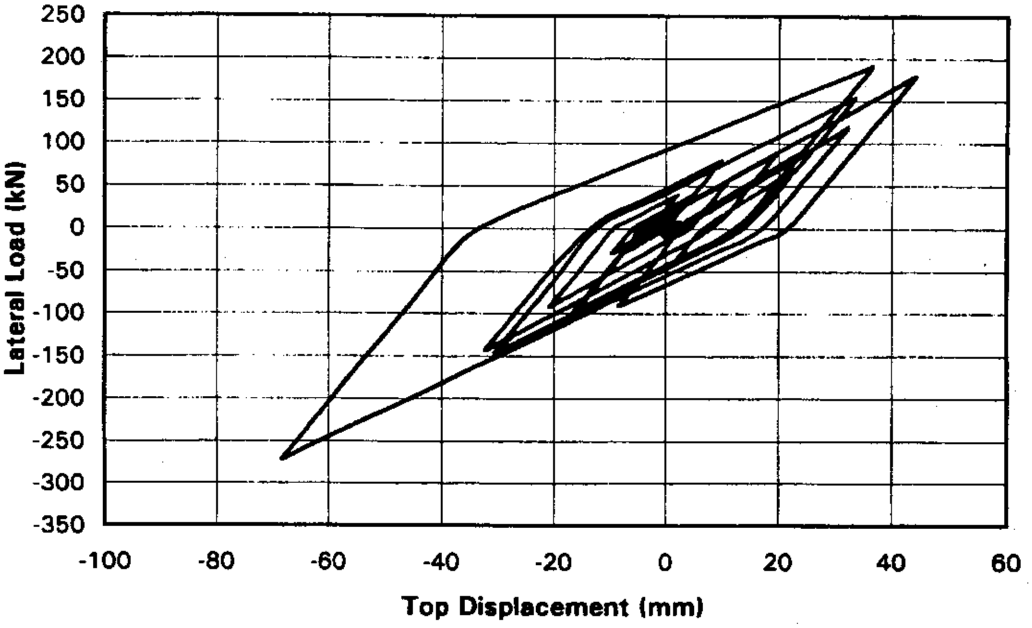

Fig. 4-33 Hysteresis Loop for FR, Run 6 (RC-Shake)

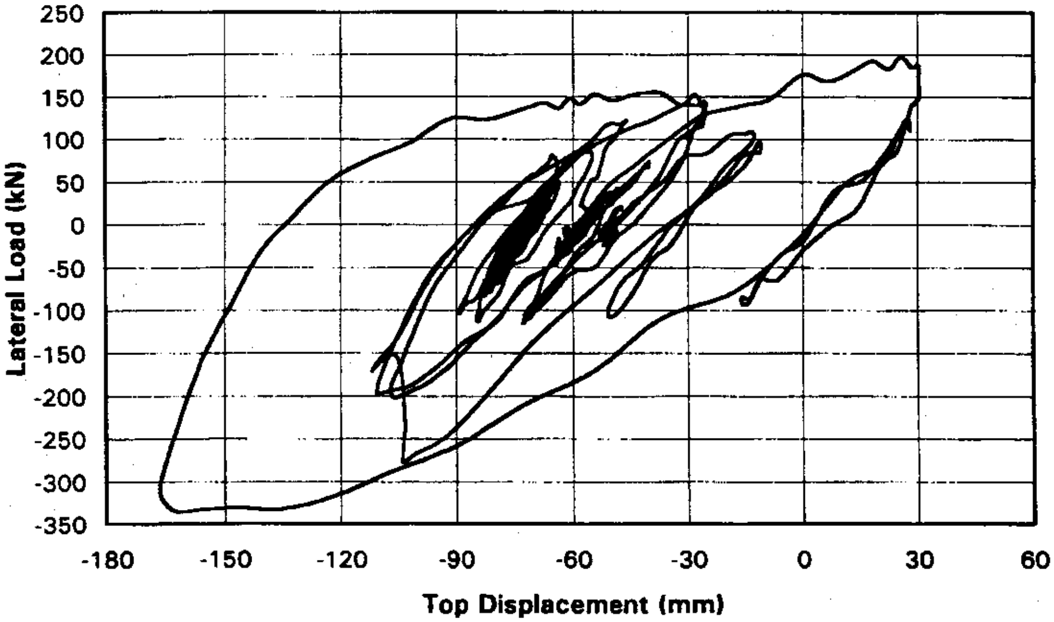

Fig. 4-34 Hysteresis Loop for FR, Run 9 (measured)

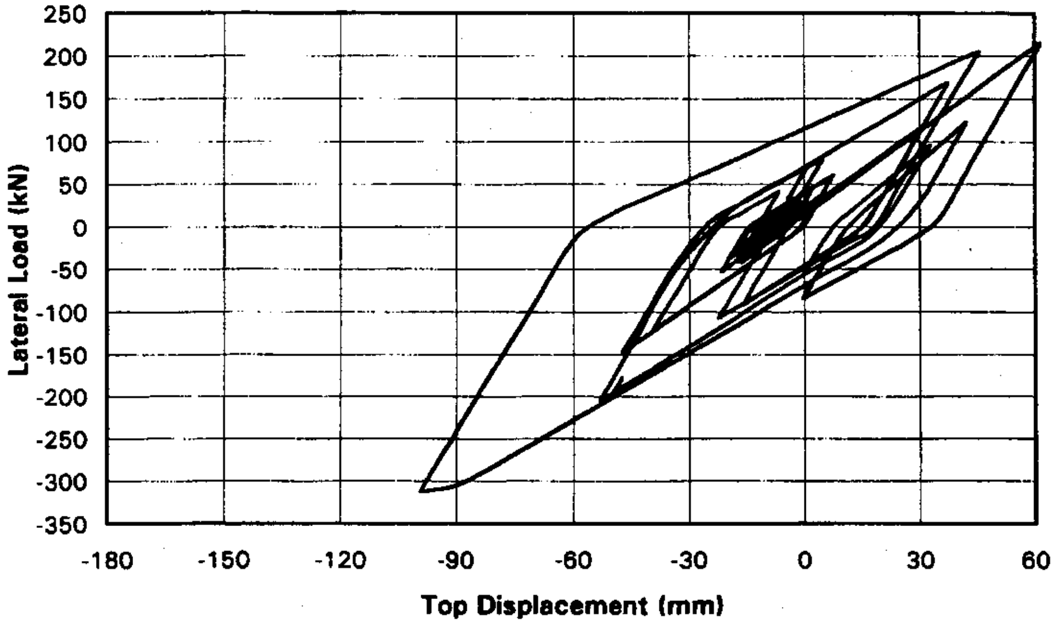

Fig. 4-35 Hysteresis Loop for FR, Run 9 (RC-Shake)

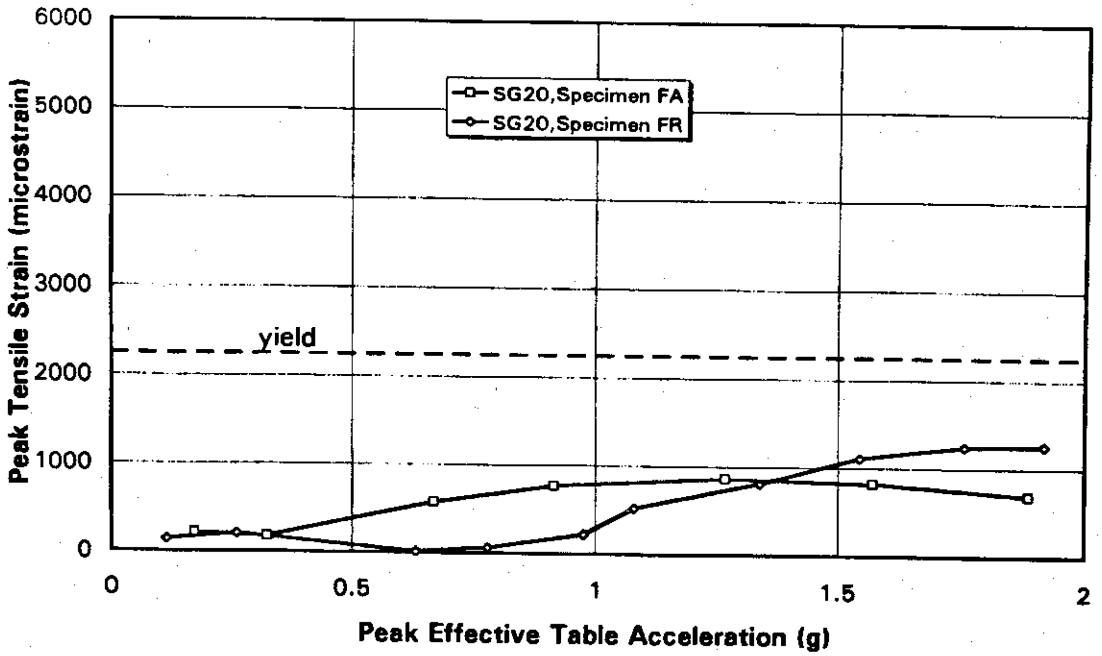

Fig. 4-36 Cross Tie Strains at 279 mm Above Footing

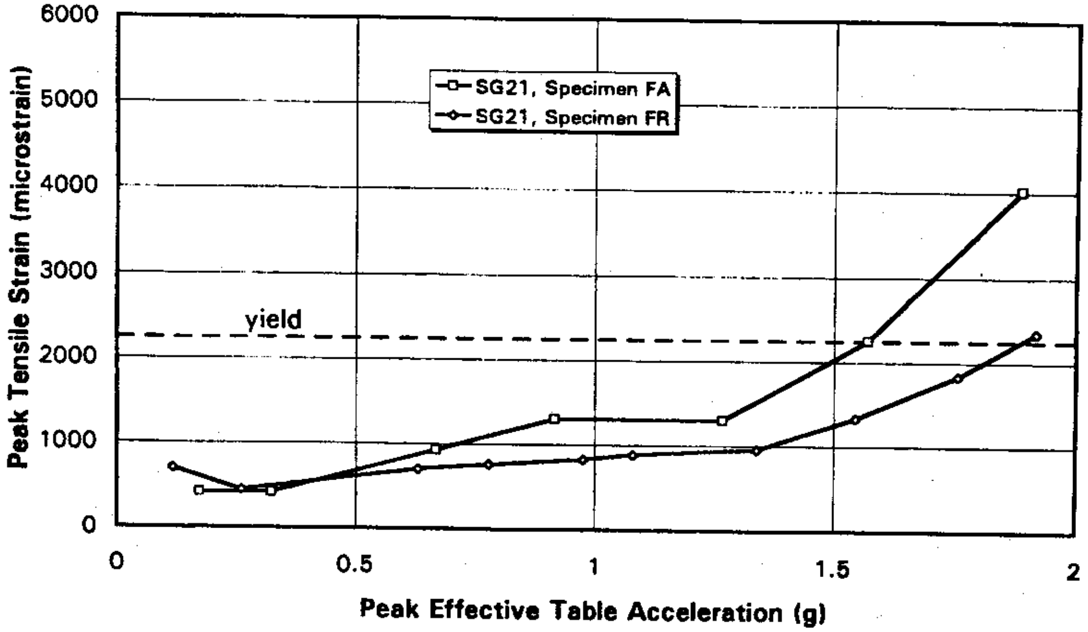

Fig. 4-37 Perimeter Tie Strains at 279 mm Above Footing

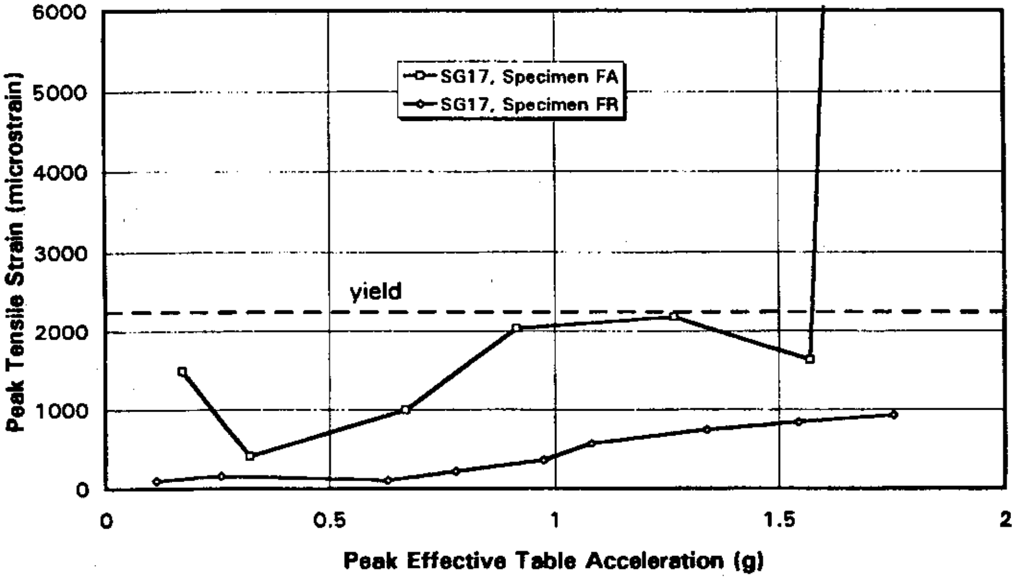

Fig. 4-38 Cross Tie Strains at 533 mm Above Footing

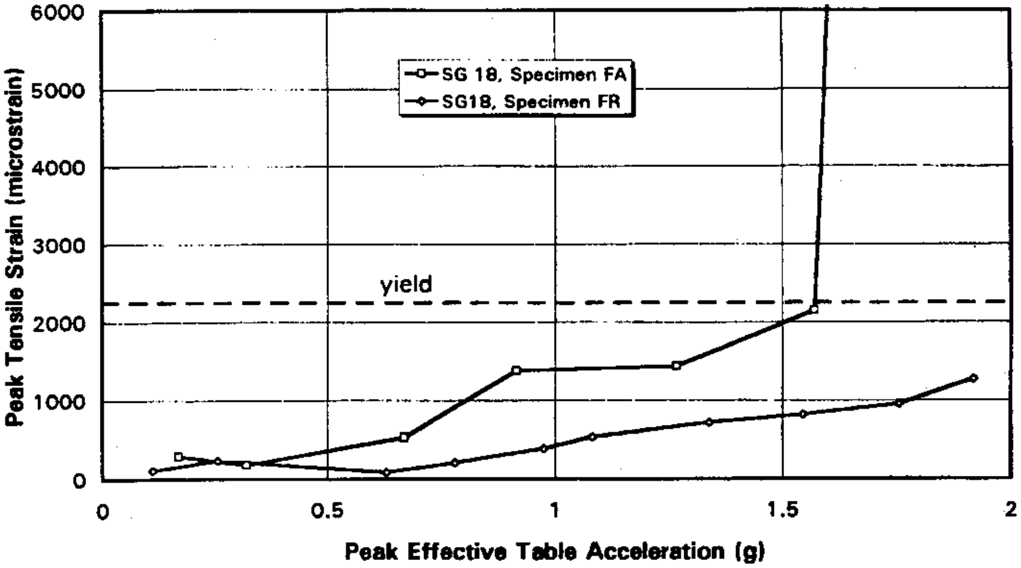

Fig. 4-39 Perimeter Tie Strains at 533 mm Above Footing

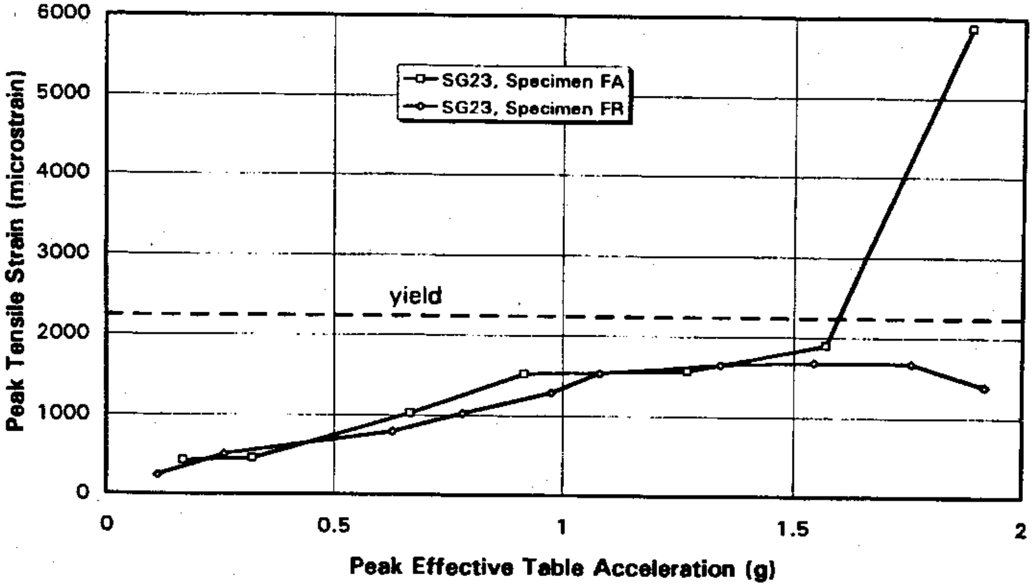

Fig. 4-40 Cross Tie Strains at 660 mm Above Footing

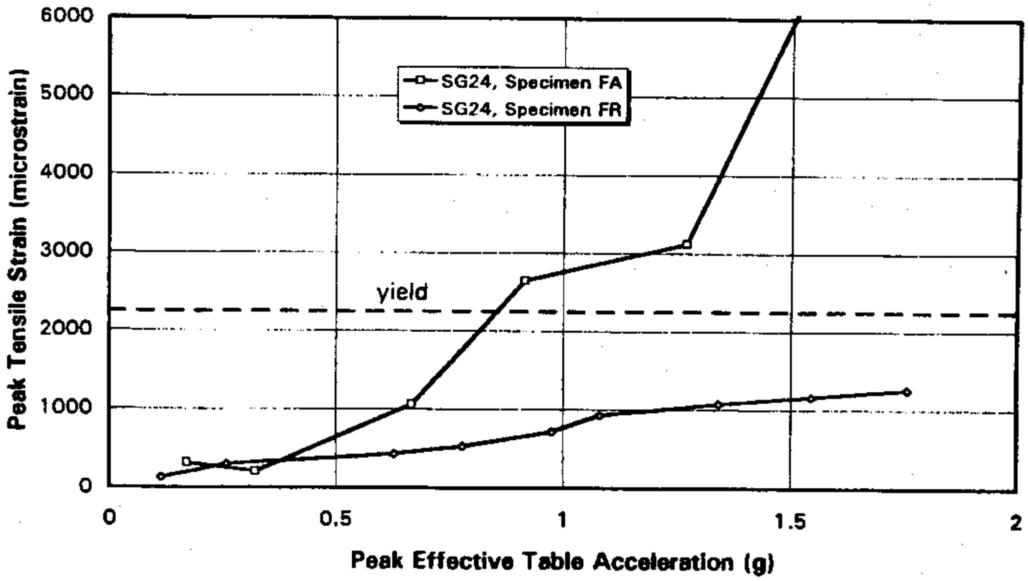

Fig. 4-41 Perimeter Tie Strains at 660 mm Above Footing

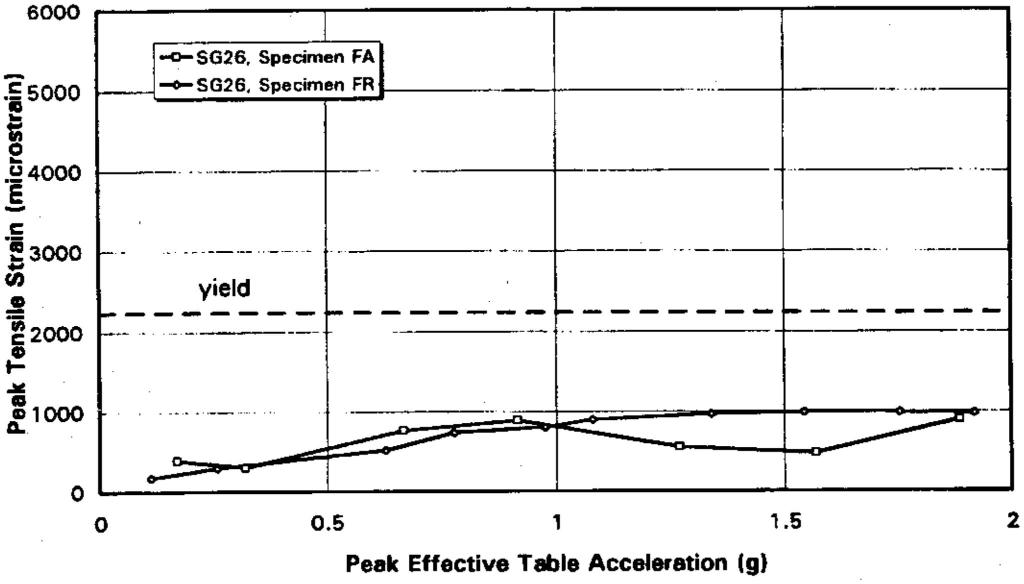

Fig. 4-42 Cross Tie Strains at 800 mm Above Footing

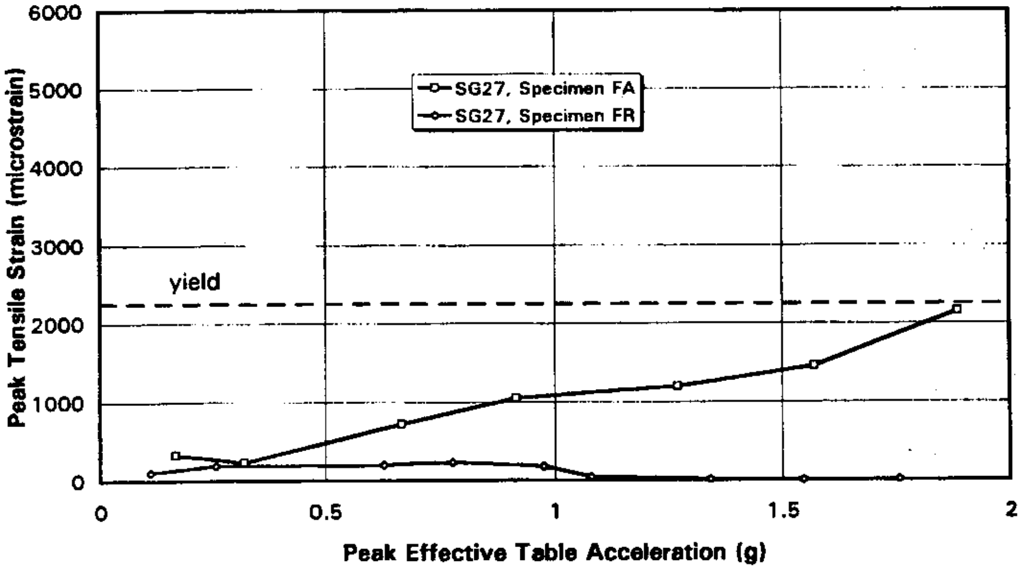

Fig. 4-43 Perimeter Tie Strains at 800 mm Above Footing

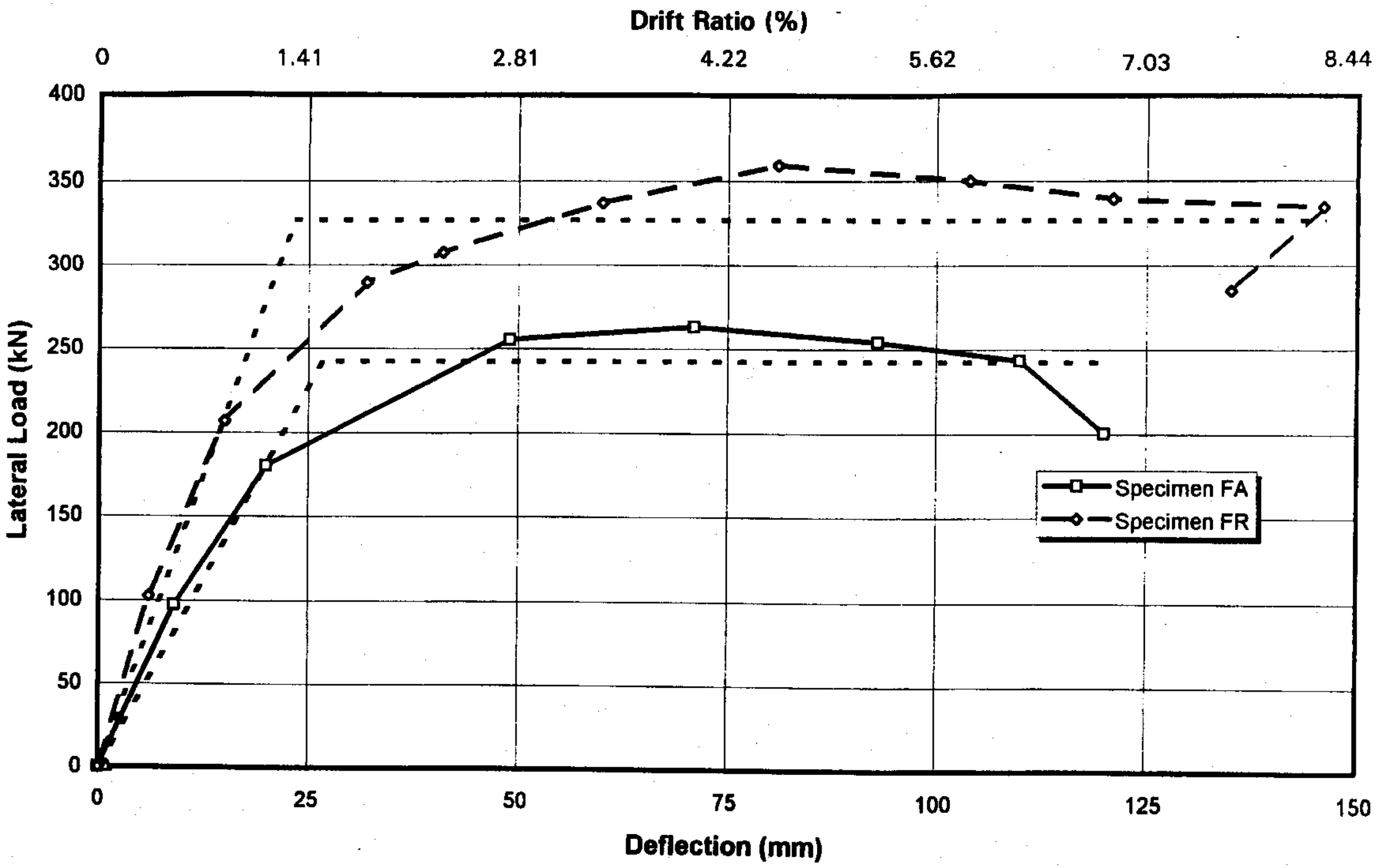

Fig. 4-44 Measured and Idealized Lateral Load-Deflection Envelopes

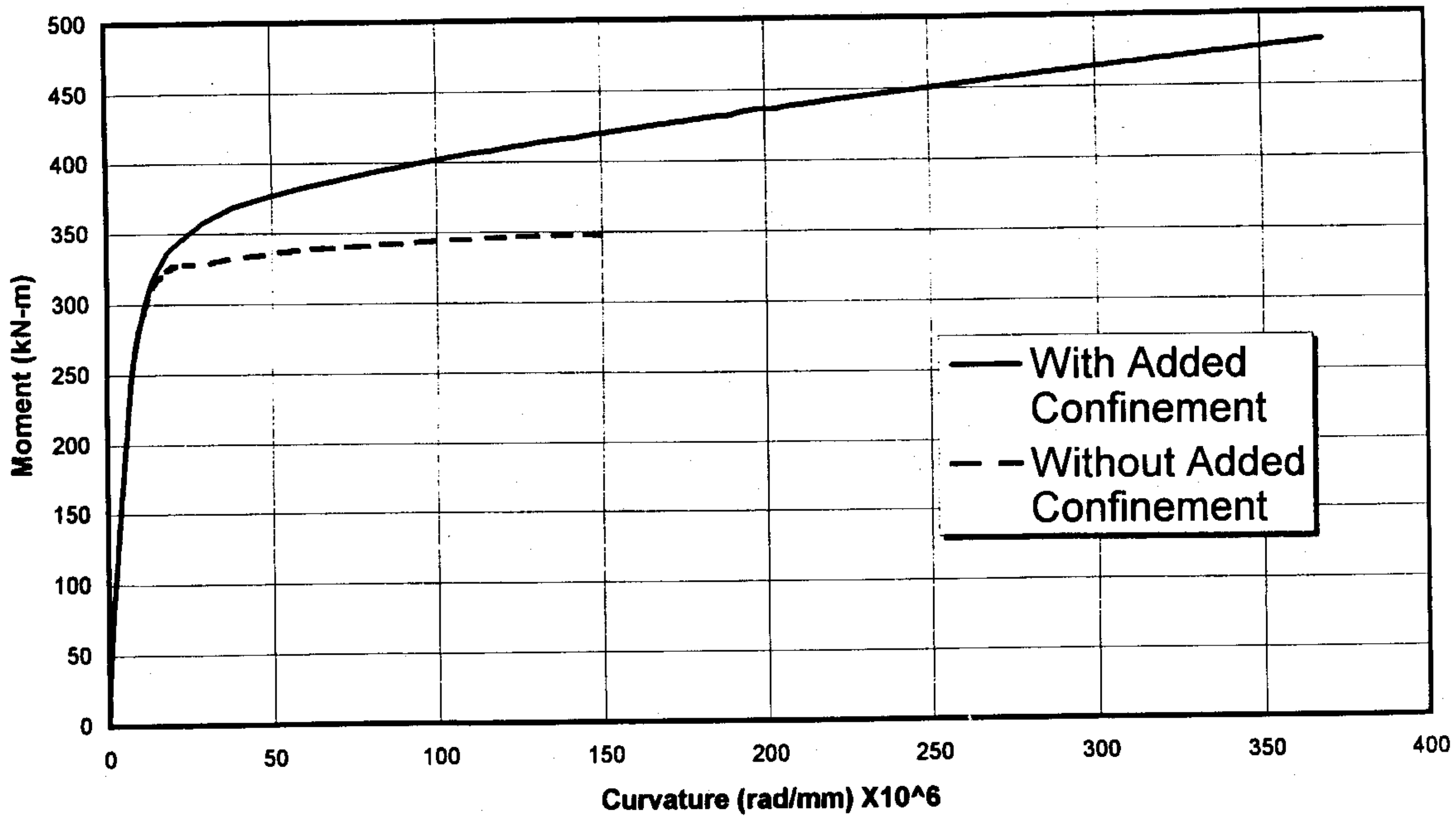

Fig. 4-45 Effect of Added Confinement of Jacket on Moment-Curvature Analysis at Gap for Specimen FR

LIST OF CENTER FOR CIVIL ENGINEERING EARTHQUAKE RESEARCH (CCEER) PUBLICATIONS

Report No.	Publication
CCEER-84-1	Saiidi, M., and R. Lawver, "User's Manual for LZAK-C64, A Computer Program to Implement the Q-Model on Commodore 64," Civil Engineering Department, Report No. CCEER-84-1, University of Nevada, Reno, January 1984.
CCEER-84-2	Douglas, B. and T. Iwasaki, "Proceedings of the First USA-Japan Bridge Engineering Workshop," held at the Public Works Research Institute, Tsukuba, Japan, Civil Engineering Department, Report No. CCEER-84-2, University of Nevada, Reno, April 1984.
CCEER-84-3	Saiidi, M., J. Hart, and B. Douglas, "Inelastic Static and Dynamic Analysis of Short R/C Bridges Subjected to Lateral Loads," Civil Engineering Department, Report No. CCEER-84-3, University of Nevada, Reno, July 1984.
CCEER-84-4	Douglas, B., "A Proposed Plan for a National Bridge Engineering Laboratory," Civil Engineering Department, Report No. CCEER-84-4, University of Nevada, Reno, December 1984.
CCEER-85-1	Norris, G. and P. Abdollaholiaee, "Laterally Loaded Pile Response: Studies with the Strain Wedge Model," Civil Engineering Department, Report No. CCEER-85-1, University of Nevada, Reno, April 1985.
CCEER-86-1	Ghusn, G. and M. Saiidi, "A Simple Hysteretic Element for Biaxial Bending of R/C Columns and Implementation in NEABS-86," Civil Engineering Department, Report No. CCEER-86-1, University of Nevada, Reno, July 1986.
CCEER-86-2	Saiidi, M., R. Lawver, and J. Hart, "User's Manual of ISADAB and SIBA, Computer Programs for Nonlinear Transverse Analysis of Highway Bridges Subjected to Static and Dynamic Lateral Loads," Civil Engineering Department, Report No. CCEER-86-2, University of Nevada, Reno, September 1986.
CCEER-87-1	Siddharthan, R., "Dynamic Effective Stress Response of Surface and Embedded Footings in Sand," Civil engineering Department, Report No. CCEER-86-2, University of Nevada, Reno, June 1987.
CCEER-87-2	Norris, G. and R. Sack, "Lateral and Rotational Stiffness of Pile Groups for Seismic Analysis of Highway Bridges," Civil Engineering Department, Report No. CCEER-87-2, University of Nevada, Reno, June 1987.
CCEER-88-1	Orie, J. and M. Saiidi, "A Preliminary Study of One-Way Reinforced Concrete Pier Hinges Subjected to Shear and Flexure," Civil Engineering Department, Report No. CCEER-88-1, University of Nevada, Reno, January 1988.
CCEER-88-2	Orie, D., M. Saiidi, and B. Douglas, "A Micro-CAD System for Seismic Design of Regular Highway Bridges," Civil Engineering Department, Report No. CCEER-88-2, University of Nevada, Reno, June 1988.
CCEER-88-3	Orie, D. and M. Saiidi, "User's Manual for Micro-SARB, a Microcomputer Program for Seismic Analysis of Regular Highway Bridges," Civil Engineering Department, Report No. CCEER-88-3, University of Nevada, Reno, October 1988.

CCEER-89-1	Douglas, B., M. Saiidi, R. Hayes, and G. Holcomb, "A Comprehensive Study of the Loads and Pressures Exerted on Wall Forms by the Placement of Concrete," Civil Engineering Department, Report No. CCEER-89-1, University of Nevada, Reno, February 1989.
CCEER-89-2	Richardson, J. and B. Douglas, "Dynamic Response Analysis of the Dominion Road Bridge Test Data," Civil Engineering Department, Report No. CCEER-89-2, University of Nevada, Reno, March 1989.
CCEER-89-2	Vrontinos, S., M. Saiidi, and B. Douglas, "A Simple Model to Predict the Ultimate Response of R/C Beams with Concrete Overlays," Civil Engineering Department, Report NO. CCEER-89-2, University of Nevada, Reno, June 1989.
CCEER-89-3	Ebrahimpour, A. and P. Jagadish, "Statistical Modeling of Bridge Traffic Loads - A Case Study," Civil Engineering Department, Report No. CCEER-89-3, University of Nevada, Reno, December 1989.
CCEER-89-4	Shields, J. and M. Saiidi, "Direct Field Measurement of Prestress Losses in Box Girder Bridges," Civil Engineering Department, Report No. CCEER-89-4, University of Nevada, Reno, December 1989.
CCEER-90-1	Saiidi, M., E. Maragakis, G. Ghusn, Y. Jiang, and D. Schwartz, "Survey and Evaluation of Nevada's Transportation Infrastructure, Task 7.2 - Highway Bridges, Final Report," Civil Engineering Department, Report No. CCEER 90-1, University of Nevada, Reno, October 1990.
CCEER-90-2	Abdel-Ghaffar, S., E. Maragakis, and M. Saiidi, "Analysis of the Response of Reinforced Concrete Structures During the Whittier Earthquake 1987," Civil Engineering Department, Report No. CCEER 90-2, University of Nevada, Reno, October 1990.
CCEER-91-1	Saiidi, M., E. Hwang, E. Maragakis, and B. Douglas, "Dynamic Testing and the Analysis of the Flamingo Road Interchange," Civil Engineering Department, Report No. CCEER-91-1, University of Nevada, Reno, February 1991.
CCEER-91-2	Norris, G., R. Siddharthan, Z. Zafir, S. Abdel-Ghaffar, and P. Gowda, "Soil-Foundation-Structure Behavior at the Oakland Outer Harbor Wharf," Civil Engineering Department, Report No. CCEER-91-2, University of Nevada, Reno, July 1991.
CCEER-91-3	Norris, G., "Seismic Lateral and Rotational Pile Foundation Stiffnesses at Cypress," Civil Engineering Department, Report No. CCEER-91-3, University of Nevada, Reno, August 1991.
CCEER-91-4	O'Connor, D. and M. Saiidi, "A Study of Protective Overlays for Highway Bridge Decks in Nevada, with Emphasis on Polyester-Styrene Polymer Concrete," Civil Engineering Department, Report No. CCEER-91-4, University of Nevada, Reno, October 1991.
CCEER-91-5	O'Connor, D.N. and M. Saiidi, "Laboratory Studies of Polyester-Styrene Polymer Concrete Engineering Properties," Civil Engineering Department, Report No. CCEER-91-5, University of Nevada, Reno, November 1991.
CCEER-92-1	Straw, D.L. and M. Saiidi, "Scale Model Testing of One-Way Reinforced Concrete Pier Hinges Subject to Combined Axial Force, Shear and Flexure," edited by D.N. O'Connor, Civil Engineering Department, Report No. CCEER-92-1, University of Nevada, Reno, March 1992.

CCEER-92-2 Wehbe, N., M. Saiidi, and F. Gordaninejad, "Basic Behavior of Composite Sections Made of Concrete Slabs and Graphite Epoxy Beams," Civil Engineering Department, Report No. CCEER-92-2, University of Nevada, Reno, August 1992.

CCEER-92-3 Saiidi, M. and E. Hutchens, "A Study of Prestress Changes in A Post-Tensioned Bridge During the First 30 Months," Civil Engineering Department, Report No. CCEER-92-3, University of Nevada, Reno, April 1992.

CCEER-92-4 Saiidi, M., B. Douglas, S. Feng, E. Hwang, and E. Maragakis, "Effects of Axial Force on Frequency of Prestressed Concrete Bridges," Civil Engineering Department, Report No. CCEER-92-4, University of Nevada, Reno, August 1992.

CCEER-92-5 Siddharthan, R., and Z. Zafir, "Response of Layered Deposits to Traveling Surface Pressure Waves," Civil Engineering Department, Report No. CCEER-92-5, University of Nevada, Reno, September 1992.

CCEER-92-6 Norris, G., and Z. Zafir, "Liquefaction and Residual Strength of Loose Sands from Drained Triaxial Tests," Civil Engineering Department, Report No. CCEER-92-6, University of Nevada, Reno, September 1992.

CCEER-92-7 Douglas, B., "Some Thoughts Regarding the Improvement of the University of Nevada, Reno's National Academic Standing," Civil Engineering Department, Report No. CCEER-92-7, University of Nevada, Reno, September 1992.

CCEER-92-8 Saiidi, M., E. Maragakis, and S. Feng, "An Evaluation of the Current Caltrans Seismic Restrainer Design Method," Civil Engineering Department, Report No. CCEER-92-8, University of Nevada, Reno, October 1992.

CCEER-92-9 O'Connor, D., M. Saiidi, and E. Maragakis, "Effect of Hinge Restrainers on the Response of the Madrone Drive Undercrossing During the Loma Prieta Earthquake," Civil Engineering Department, Report No. CCEER-92-9, University of Nevada, Reno, February 1993.

CCEER-92-10 O'Connor, D., and M. Saiidi, "Laboratory Studies of Polyester Concrete: Compressive Strength at Elevated Temperatures and Following Temperature Cycling, Bond Strength to Portland Cement Concrete, and Modulus of Elasticity," Civil Engineering Department, Report No. CCEER-92-10, University of Nevada, Reno, February 1993.

CCEER-92-11 Wehbe, N., M. Saiidi, and D. O'Connor, "Economic Impact of Passage of Spent Fuel Traffic on Two Bridges in Northeast Nevada," Civil Engineering Department, Report No. CCEER-92-11, University of Nevada, Reno, December 1992.

CCEER-93-1 Jiang, Y., and M. Saiidi, "Behavior, Design, and Retrofit of Reinforced Concrete One-way Bridge Column Hinges," edited by D. O'Connor, Civil Engineering Department, Report No. CCEER-93-1, University of Nevada, Reno, March 1993.

CCEER-93-2 Abdel-Ghaffar, S., E. Maragakis, and M. Saiidi, "Evaluation of the Response of the Aptos Creek Bridge During the 1989 Loma Prieta Earthquake," Civil Engineering Department, Report No. CCEER-93-2, University of Nevada, Reno, June 1993.

CCEER-93-3 Sanders, D.H., B.M. Douglas, and T.L. Martin, "Seismic Retrofit Prioritization of Nevada Bridges," Civil Engineering Department, Report No. CCEER-93-3, University of Nevada, Reno, July 1993.

CCEER-93-4 Abdel-Ghaffar, S., E. Maragakis, and M. Saiidi, "Performance of Hinge Restrainers in the Huntington Avenue Overhead During the 1989 Loma Prieta Earthquake," Civil Engineering Department, Report No. CCEER-93-4, University of Nevada, Reno, June 1993.

CCEER-93-5 Maragakis, E., M. Saiidi, S. Feng, and L. Flournoy, "Effects of Hinge Restrainers on the Response of the San Gregorio Bridge During the Loma Prieta Earthquake," (in final preparation) Civil Engineering Department, Report No. CCEER-93-5, University of Nevada, Reno.

CCEER-93-6 Saiidi, M., E. Maragakis, S. Abdel-Ghaffar, S. Feng, and D. O'Connor, "Response of Bridge Hinge Restrainers During Earthquakes -Field Performance, Analysis, and Design," Civil Engineering Department, Report No. CCEER-93-6, University of Nevada, Reno, May 1993.

CCEER-93-7 Wehbe, N., Saiidi, M., Maragakis, E., and Sanders, D., "Adequacy of Three Highway Structures in Southern Nevada for Spent Fuel Transportation, Civil Engineering Department, Report No. CCEER-93-7, University of Nevada, Reno, August 1993.

CCEER-93-8 Roybal, J., Sanders, D.H., and Maragakis, E., "Vulnerability Assessment of Masonry Public Buildings in the Reno-Carson City Urban Corridor," Civil Engineering Department, Report No. CCEER-93-8, University of Nevada, Reno, May 1993.

CCEER-93-9 Zafir, Z. and Siddharthan, R., "MOVLOAD: A Program to Determine the Behavior of Nonlinear Horizontally Layered Medium Under Moving Load," Civil Engineering Department, Report No. CCEER-93-9, University of Nevada, Reno, August 1993.

CCEER-93-10 O'Connor, D.N., Saiidi, M., and Maragakis, E.A., "A Study of Bridge Column Seismic Damage Susceptibility at the Interstate 80/U.S. 395 Interchange in Reno, Nevada," Civil Engineering Department, Report No. CCEER-93-10, University of Nevada, Reno, October 1993.

CCEER-94-1 Maragakis, E., B. Douglas, and E. Abdelwahed, "Preliminary Dynamic Analysis of a Railroad Bridge," Report CCEER-94-1, January 1994.

CCEER-94-2 Douglas, B.M., Maragakis, E.A., and Feng, S., "Stiffness Evaluation of Pile Foundation of Cazenovia Creek Overpass," Civil Engineering Department, Report No. CCEER-94-2, University of Nevada, Reno, March 1994.

CCEER-94-3 Douglas, B.M., Maragakis, E.A., and Feng, S., "Summary of Pretest Analysis of Cazenovia Creek Bridge," Civil Engineering Department, Report No. CCEER-94-3, University of Nevada, Reno, April 1994.

CCEER-94-4 Norris, G.M. and Madhu, R., "Liquefaction and Residual Strength of Sands from Drained Triaxial Tests, Report 2," Civil Engineering Department, CCEER-94-4, University of Nevada, Reno, August 1994.

CCEER-94-5 Saiidi, M., Hutchens, E., and Gardella, D., "Prestress Losses in a Post-Tensioned R/C Box Girder Bridge in Southern Nevada," Civil Engineering Department, CCEER-94-5, University of Nevada, Reno, August 1994.

CCEER-95-1 Siddharthan, R., El-Gamal, M., and Maragakis, E.A., "Nonlinear Bridge Abutment Stiffnesses:

Formulation, Verification, and Design Curves," Civil Engineering Department, CCEER-95-1, University of Nevada, Reno, January 1995.

CCEER-95-2 Norris, G.M., Madhu, R., Valceschini, R., and Ashour, M., "Liquefaction and Residual Strength of Loose Sands from Drained Triaxial Tests," Report 2, Civil Engineering Department, Report No. CCEER-95-2, University of Nevada, Reno, February 1995.

CCEER-95-3 Wehbe, N., Saiidi, M., Sanders, D., and Douglas, B., "Ductility of Rectangular Reinforced Concrete Bridge Columns with Moderate Confinement,"Civil Engineering Department, Report No. CCEER-95-3, University of Nevada, Reno, July 1995.

CCEER-95-4 Martin, T., Saiidi, M., and Sanders, D., "Seismic Retrofit of Column-Pier Cap Connections in Bridges in Northern Nevada," Civil Engineering Department, Report No. CCEER-95-4, University of Nevada, Reno, August 1995.

CCEER-95-5 Darwish, I., Saiidi, M., and Sanders, D., "Experimental Study of Seismic Susceptibility of Tapered Bridge Column-Footing Connections," Civil Engineering Department, Report No. CCEER-95-5, University of Nevada, Reno, September 1995.

CCEER-95-6 Griffin, G., Saiidi, M., and Maragakis, E., "Nonlinear Seismic Response of Isolated Bridges and Effects of Pier Ductility Demand," Civil Engineering Department, Report No. CCEER-95-6, University of Nevada, Reno, November 1995.

CCEER-95-7 Acharya, S., Saiidi, M., and Sanders, D., "Seismic Retrofit of Bridge Footings and Column-Footing Connections," Report for the Nevada Department of Transportation, Civil Engineering Department, Report No. CCEER-95-7, University of Nevada, Reno, November 1995.

CCEER-95-8 Maragakis, E., Douglas, B., and Sandirasegaram, U., "Full-Scale Field Resonance Tests of a Railway Bridge," A Report to the Association of American Railroads, Civil Engineering Department, Report No. CCEER-95-8, University of Nevada, Reno, December 1995.

CCEER-95-9 Douglas, B., Maragakis, E., and Feng, S., "System Identification Studies on Cazenovia Creek Overpass," Report for the National Center for Earthquake Engineering Research, Civil Engineering Department, Report No. CCEER-95-9, University of Nevada, Reno, October 1995.

CCEER-96-1 El-Gamal, M.E. and Siddharthan, R.V., "Programs to Computer Translational Stiffness of Seat-Type Bridge Abutment," Civil Engineering Department, Report No. CCEER-96-1, University of Nevada, Reno, March 1996.

CCEER-96-2 Labia, Y., Saiidi, M., and Douglas, B., "Evaluation and Repair of Full-Scale Prestressed Concrete Box Girders," A Report to the National Science Foundation, Research Grant CMS-9201908, Civil Engineering Department, Report No. CCEER-96-2, University of Nevada, Reno, May 1996.

CCEER-96-3 Darwish, I., Saiidi, M., and Sanders, D., "Seismic Retrofit of R/C Oblong Tapered Bridge Columns with Inadequate Bar Anchorage in Columns and Footings," A Report to the Nevada Department of Transportation, Civil Engineering Department, Report No. CCEER-96-3, University of Nevada, Reno, May 1996.

CCEER-96-4 Ashour, M., Pilling, P., Norris, G., and Perez, H., "The Prediction of Lateral Load Behavior of Single Piles and Pile Groups Using the Strain Wedge Model," A Report to the California Department of

Transportation, Civil Engineering Department, Report No. CCEER-96-4, University of Nevada, Reno, June, 1996.

CCEER-97-1 Maragakis, E., Douglas, B., and Sandirasegaram, U. "Full-Scale Field Resonance Tests of a Railway Bridge," A Report to the Association of American Railroads, Civil Engineering Department, University of Nevada, Reno, May, 1996.

CCEER-97-2 Wehbe, N., M. Saiidi, and D. Sanders, "Effects of Confinement and Flares on the Seismic Performance of Reinforced Concrete Bridge Columns," Civil Engineering Department, University of Nevada, Reno, Report No. CCEER-97-2, September, 1997.

CCEER-97-3 Darwish, I., M. Saiidi, G. Norris, and E. Maragakis, "Determination of In-Situ Footing Stiffness Using Full-Scale Dynamic Field Testing," A Report to the Nevada Department of Transportation, Structural Design Division, Carson City, Nevada, Report No. CCEER-97-3, University of Nevada, Reno, October, 1997.

CCEER-97-4 Not Published.

CCEER-97-5 Isakovic, T., M. Saiidi, and A. Itani, "Influence of new Bridge Configurations on Seismic Performance," Department of Civil Engineering, University of Nevada, Reno, Report No. CCEER-97-5, September, 1997.

CCEER-98-1 Itani, A., "Cyclic Behavior of "as Built" Laced Members With End Gusset Plates on the San Francisco Bay Bridge", Center for Civil Engineering Earthquake Research, Department of Civil Engineering, University of Nevada, Reno, Nevada, Report No. CCEER-98-1, March, 1998.

CCEER-98-2 Norris, G., and M. Ashour, "Liquefication and Undrained response evaluation of Sands from Drained Formulation", Center for Civil Engineering Earthquake Research, Department of Civil Engineering, University of Nevada, Reno, Nevada, Report No. CCEER-98-2, May, 1998.

CCEER-98-3 Qingbin, C., B.M. Douglas, E. Maragakis, and I.G. Buckle, "Extraction of Nonlinear Hysteretic Properties of Seismically Isolated Bridges from Quick-Release Field Tests", Center for Civil Engineering Earthquake Research, Department of Civil Engineering, University of Nevada, Reno, Nevada, Report No. CCEER-98-3, June, 1998.

CCEER-98-4 Maragakis, E., B.M. Douglas, and C. Qingbin, "Full-Scale Field Capacity Tests of a Railway Bridge", Center for Civil Engineering Earthquake Research, Department of Civil Engineering, University of Nevada, Reno, Nevada, Report No. CCEER-98-4, June, 1998.

CCEER 98-5 Itani, A., B. Douglas, and J. Woodgate, "Cyclic Behavior of Richmond-San Rafael Retrofitted Tower Leg", Center for Civil Engineering Earthquake Research, Department of Civil Engineering, University of Nevada, Reno, Nevada, Report No. CCEER-98-5, June, 1998.

CCEER 98-6 Moore, R., M. Saiidi, and A. Itani, "Seismic Behavior of New Bridges with Skew and Curvature", Center for Civil Engineering Earthquake Research, Department of Civil Engineering, University of Nevada, Reno, Nevada, Report No. CCEER-98-6, October, 1998.

CCEER 98-7 Itani, A., and A. Dietrich, "Cyclic Behavior of Double Gusset Plate connections", Center for Civil Engineering Earthquake Research, Department of Civil Engineering, University of Nevada, Reno, Nevada, Report No. CCEER-98-7, December, 1998.

CCEER 99-1 Caywood, C., M. Saiidi, and D. Sanders, "Seismic Retrofit of Flared Bridge Columns with Steel Jackets," Civil Engineering Department, University of Nevada, Reno, Report No. CCEER-99-1, February 1999.

CCEER 99-2 Mangoba, N., M. Mayberry, and M. Saiidi, "Prestress Loss in Four Box Girder Bridges in Northern Nevada," Civil Engineering Department, University of Nevada, Reno, Report No. CCEER-99-2, March 1999.

CCEER 99-3 Abo-Shadi, N., M. Saiidi, and D. Sanders, "Seismic Response of Bridge Pier Walls in the Weak Direction," Civil Engineering Department, University of Nevada, Reno, Report No. CCEER-99-3, April 1999.

CCEER 99-4 Buzick, A. and M. Saiidi, "Shear Strength and Shear Fatigue Behavior of Full-Scale Prestressed Concrete Box Girders," Civil Engineering Department, University of Nevada, Reno, Report No. CCEER-99-4, April 1999.

CCEER 99-5 Randall, M., M. Saiidi, E. Maragakis, and T. Isakovic, "Restrainer Design Procedures for Multi-Span Simply-Supported Bridges," Civil Engineering Department, University ofNevada, Reno, Report No. CCEER-99-5, April 1999.

CCEER 99-6 Wehbe, N., and M. Saiidi, "User's Manual for RCMC v 1.2- A Computer Program for Moment-Curvature Analysis of Confined and Unconfined Reinforced Concrete Sections," Civil Engineering Department, University of Nevada, Reno, Report No. CCEER-99-6, May 1999.

CCEER-99-7 Burda, J. and A. Itani, "Studies of Seismic Behavior of Steel Base Plates," Civil Engineering Department, University of Nevada, Reno, Report No. CCEER-99-7, May 1999.

CCEER-99-8 M. Ashour and G. Norris, "Refinement of the Strain Wedge Model Program," Civil Engineering Department, University of Nevada, Reno, Report No. CCEER-99-8, March 1999.

CCEER-99-9 Dietrich, A., and A. Itani, "Cyclic Behavior of Laced and Perforated Steel Members on the San Francisco-Oakland Bay Bridge," Civil Engineering Department, University ofNevada, Reno,. Reno, Report No. CCEER-99-9, December 1999.

CCEER 99-10 Itani, A., and A. Dietrich, "Cyclic Behavior of Built Up Steel Members and their Connections," Civil Engineering Department, University of Nevada, Reno, Report No. CCEER-99-10, December 1999.

CCEER 99-11 Itani, A., and J. Woodgate, "Axial and Rotational Ductility of BuiltUp Structural Steel Members," Civil Engineering Department, University of Nevada, Reno, Report No. CCEER-99-11, December 1999.

CCEER 99-12 Sgambelluri, M., Sanders, D.H., and Saiidi, M., "Behavior of One-Way Reinforced Concrete Bridge Column Hinges in the Weak Direction," Report No. 99-12, Department of Civil Engineering, University of Nevada, Reno, December 1999.

CCEER 99-13 Laplace, P., Sanders, D.H., Douglas, B, and Saiidi, M. "Shake Table Testing of Flexure Dominated Reinforced Concrete Bridge Columns," Report No. 99-13, Department of Civil Engineering, University of Nevada, Reno, December 1999.

CCEER 99-14 Itani, A., J. A. Zepeda, and E. A. Ware "Cyclic Behavior of Steel Moment Frame Connections for the Moscone Center Expansion," Civil Engineering Department, University of Nevada, Reno, Report No. CCEER-99-14, December 1999.

CCEER 00-1 Ashour, M., and Norris, G. "Undrained Lateral Pile and Pile Group Response in Saturated Sand", Civil Engineering Department, University of Nevada, Reno, Report No. CCEER-00-1, May 1999. January 2000.

CCEER 00-2 Saiidi, M. and Wehbe, N., "A Comparison of Confinement Requirements in Different Codes for Rectangular, Circular, and Double-Spiral RC Bridge Columns," Civil Engineering Department, University of Nevada, Reno, Report No. CCEER-00-2, January 2000.

CCEER 00-3 McElhaney, B., M. Saiidi, and D. Sanders, "Shake Table Testing of Flared Bridge Columns With Steel Jacket Retrofit," Civil Engineering Department, University of Nevada, Reno, Report No. CCEER-00-3, January 2000.

Kenny C. Guinn, Governor

Nevada Department of Transportation
Tom Stephens, P.E. Director
Prepared by Research Division
Alan Hilton, Research Division Chief
(775) 888-7803
ahilton@dot.state.nv.us
1263 South Stewart Street
Carson City, Nevada 89712